FLINDERS
UNIVERSITY
ADELAIDE
AUSTRALIA

Domain-Independent Multi-Physical Multiple-Field Systems Modeling Approach

A Novel Energy-Based Aero-Thermo-Visco-Elastic Modeling Framework by Bond Graph

by

Amir Zanj

MEng and BEng of Aerospace & Mechanical Engineering

School of Computer Science, Engineering & Mathematics

Faculty of Science and Engineering

Flinders University, Adelaide, Australia

September 2016

A thesis presented

in total fulfilment of the requirements for the degree of

Doctor of Philosophy (Engineering)

Adelaide, South Australia

Table of Content

ABSTRACT

After passing through several decades of the emergence of aerothermoelastic problems, these problems are still conveniently considered by many modelers as an extension of aeroelastic problems. There is no doubt that by means of numerous useful methodologies proposed in the area of aeroelasticity, there now exist a range of sound strategies that potentially possess certain capabilities in solving a diverse range of problems arising in this area. However, it is evident from the literature that in situations where heating impacts become significant, the well-established framework of classical aeroelasticity would be unable to explain the true causality of the ongoing aerothermoelastic phenomena.

It is known that the classical fundamentals of aeroelasticity are based on assumptions (such as separation principle or weak connectivity) that largely ignore the thermal connections between the various physical fields of a system within which aerothermoelastic phenomena exist. Although the impact of neglecting the thermal connections could be added into the solution of each filed of the system, the real interactive nature of the thermal connections between the various fields (that could have significantly changed the dynamics of the system if considered), has been completely lost in this process. As a result, the true physical links between the various fields measured by the universal principle of conservation of power transactions are no longer held. Reinstalling these physical links will require a reconstruction of the fundamental assumptions upon which the aerothermoelastic phenomena of the system can be truthfully reflected.

Indeed, the classical decomposition of aerothermoelasticity into aeroelastic, aerothermo, and thermoelastic behaviors lacks a generic means with which the overall dynamics of the system can be effectively decomposed into components whose (i) energetic interactions can obey the universal conservation rules, (ii) are tractable, (iii) and can uncover the hidden details of the system's physical insights. This is because the elements used to decompose the system in the classical approach stay at a level that is higher than the level expected for enabling the unveiling of the system dynamics in such detail. Currently, to compensate for this deficiency, modelers rely heavily on the use of mathematical constrains (such as filtration and stabilization) as well as powerful computers, which has led to the development of drastically high-order models valid only within a limited operational range. The desired elements that can reveal the hidden physical insights of such complex phenomena are evidently required to be at a level that can directly reflect the primary

energetic interactions of the system and physically link the fundamentals of each of the fields involved.

In this thesis, an energy-based aerothermoelastic framework resulting from a unique decomposition of each of the involving fields of a system into a set of physical subdomains (e.g., thermal, kinetic, potential subdomains) is suggested. Given that the physical subdomains are alike in any fields, by generating their isomorphic models regardless of the field (i.e., domain-independent modeling), the conservation of continuous power transactions within each of the fields and between the fields at their interface can then become realizable. This novel strategy leads to a complete conservative coupling between all fields involved.

In this study, physical system theory in terms of Bond Graphs (BG) is employed to generate the proposed energy-based framework including domain-independent isomorphic components. The dynamics of the system are constructed from the reversible and irreversible dynamic interactions of the energetic components of the existing subdomains. Given that the energetic components are similar in different subdomains and that the interactions between the energetic components in different subdomains follow a similar pattern, the BG implementation can produce not only isomorphic models of counterpart physical subdomains between different fields, but also isomorphic models of all physical subdomains involved in the coupled fields. As a result, not only is the continuity of both the intra-field and inter-field power transportation satisfied, but also the possibility of tracking power transformation is provided. The conservation of power transactions of the entire system is thus guaranteed. The proposed methodology provides the ensuing framework with an intrinsically physical ability to control the data transactions between the coupled fields. The resulting conservative energetic framework of the system also allows modelers to check the well-posedness of the system before extracting state equations – a desirable capability for complex system dynamic investigations.

To generate the proposed aerothermoelastic framework, (i) each field is first decomposed into its initial physical subdomains; (ii) the energetic components of each subdomain is then defined with respect to the geometrical and material properties of the field; (iii) the dynamics of each subdomain are generated from the energetic interactions of the present components; (iv) the dynamics of each field are generated from the reversible and irreversible interactions of the present physical subdomains; (v) finally, based on power continuity between coupled fields and possible connections between fields' energetic components at the interface, a unique conservative coupled-

aerothermoelastic model of the system is generated through connecting the corresponding pairs of physical subdomains of the coupled fields. For coupled fluid and solid fields, (v) can be done if and only if the compatibility between the fixed Eulerian frame of the fluid field and the moving Lagrangian frame of the solid field can be addressed satisfactorily. To address this issue, a Variable Interface Dynamic Adaptation (VIDA) technique is proposed where the likely motions of the Lagrangian solid frame is translated into a reversible volumetric flow of the fixed Eulerian fluid frame. The compatibility of the two frames is satisfied and the required information at contact surface is refined at any instant in time to keep the power transactions at the interface continuous.

Using the proposed aerothermoelastic framework, an energetic network of the system is generated that can illustrate continuous reversible and irreversible power transactions among various subdomains and between coupled fields, and offer details in relation to memory, physical characteristics, and well-posedness of the system. This unique feature is critical for analyzing the complex multi-physical multiple-field behaviors of the system. As the model is developed without employing the typical slow-thermal-dynamics and weak-connectivity assumptions and with no additional mathematical constrains, the model is principally valid in an extended range much wider than its conventional counterparts. Undoubtedly, the proposed energetic network of the system can be a useful tool for developing control strategies and for energy management of the system. The novel framework proposed and implemented in this thesis provides a unique integrated platform based on which the aeothermoelastic phenomena in multi-physical-domain multiple-field systems can be modeled univocally while reflecting the true physical nature of such complex phenomena.

DECLARATION

I certify that this thesis does not incorporate, without acknowledgement, any material previously submitted for a degree or diploma in any university; and that, to the best of my knowledge and belief, it does not contain any material previously published or written by another person except where due reference is made in the text.

As specified under Clause 15 of Appendix E of the Flinders University Research Higher Degrees Policies and Procedures, I hereby request that access to this thesis be restricted for a period of 18 months from the acceptance of the award of the degree.

Adelaide, 7 September 2016

Amir Zanj

ACKNOWLEDGEMENTS

After an intensive period of four years and two months, today is the day: writing this note of thanks is the finishing touch on my thesis. It has been a period of intense learning for me, not only in the scientific area, but also on a personal level. I would like to reflect on the people who have supported and helped me throughout this period.

I would first like to thank my parents for their wise counsel and sincere dedication. You sacrificed your life to make me able to stand in my current stage, and I know that, you are always there for me.

Next, I would like to thank Australia for its generosity and hospitality. You gave me the chance to continue my scientific life with your overwhelming support in a homelike atmosphere. I would particularly like to single out my supervisor Prof. Fangpo He, I want to thank you for your excellent cooperation and for all of the opportunities I was given to conduct my research and further my thesis at Flinders University. I will never forget what you taught me: “PhD is not all just about a problem to be solved, it is a way of thinking”.

In addition, I would like to thank Prof. Peter Breedveld, for his valuable guidance during my research visit at the University of Twente. You definitely provided me with the tools that I needed to choose the right direction and successfully complete my thesis.

Outside the academia, I would like to thank my Australian parents, Mr. and Ms. Graeme and Elaine Hall, for their endless kindness. You were always with me with your sympathetic ear and parental love, and I will never forget it.

And Finally, I would like to give a special thanks to my lady who supported me with her tenderness, patience, and trust. I would like to let you know that, your belief in my capabilities was my greatest incentive in accomplishing this dissertation. Thank you for being such lovely companion for me in this journey.

At the end, I dedicate my research to all the people around the world, no matter what color or gender they are, where they live, or which language they speak. I hope one day this research as well as all the other research be used to make this world a better place to breathe.

Regards,

Amir Zanj 7 September 2016

CHAPTER 1: INTRODUCTION

1. The emergence of Aero-thermo-elasticity

For several decades, it appeared that the growth of aeroelasticity science was a sufficient basis for the design of different kinds of moving structures; however, by the early 1950's, as higher speed for moving structures (e.g., high performance rotary machines) was demanded, entirely new aeroelastic problems were encountered [1]. After a decade of intense investigations, it was revealed in [2] that unpredicted structural vibrations resulting from weakened structures are the main cause for the majority of these problems.

Relevant research suggests that substantial unknown thermal impacts on elastic moduli might be to blame for the unpredicted aeroelastic behaviors of structures [3]. These impacts have been attributed to various internal dissipation mechanisms, of which inelastic effects appear to be predominant. The increased importance of residual stress, creep, and material deterioration

associated with thermal effects leads to a greater consideration of the cumulative effects of thermally entangled aeroelastic loads.

In addition to the undesirable effects of high temperatures on the modulus of elasticity, there is another effect of heat which can be very important even at moderate temperatures, i.e., the effect of internal thermal stresses [4]. Thermal stresses can arise from rapidly changing conditions of heat input where time lags are involved, or from equilibrium conditions where thermal gradients occur. Thermal gradients result in incremental tension and compression stresses in different regions of a structure. Commonly, but by no means inevitably, a thermally stressed structure has a lessened net stiffness available to resist both static loads and inertia loadings associated with vibrations.

The foregoing problems have exemplified the necessity of *Aerothermal* investigations along with *Aeroelastic* considerations in structural analysis. Thus, the purely scientific aspects aimed at the prediction and understanding of this area, as well as the engineering or technological aspects aimed at simplified criteria, reliability, safety, and structural efficiency and integrity, are required to be refined with respect to the aforementioned added complexities. Since these aspects intrinsically are connected, it is necessary to pursue both aspects via modeling, analysis, and controlled experiments, and through specific component testing, environmental studies, and large-scale investigations. This is why the "Aerothermoelastic field will be continuing to offer challenges for many years to come for both science and technology [4]".

1. Classical definition of Aero-thermo-elasticity

A classical definition of aerothermoelasticity was first defined via the inclusion of the effects of heat inputs, H, into the collar's aeroelastic triangle [4], known as the aerothermoelasticity tetrahedron – presented in Fig. 1-1. In this presentation, the aerothermoelasticity is dealt with by broad interdisciplinary aspects of four distinguished areas: aerodynamic (A), inertia (I), elasticity (E), and heat (H).

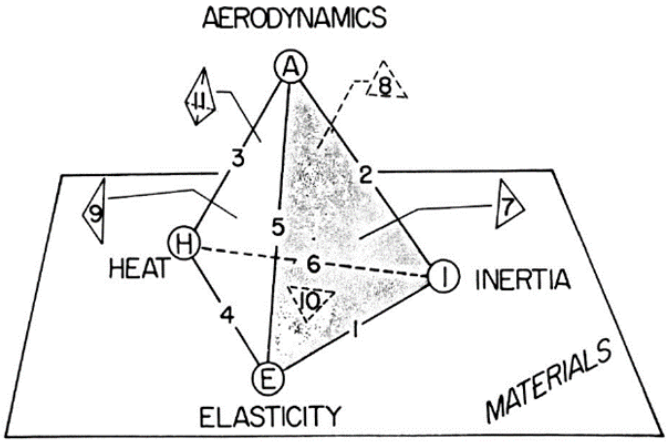

Fig. 1-1. Tetrahedron illustration the interrelationships of Aerothermoelasticity [4]

The six edges of the aerothermoelasticity tetrahedron present:

- E-I; Vibration, representing mechanical vibrations and structural dynamics with typical problem areas of determination of modes and frequencies of structures.
- I-A; Stability, including rigid-body aerodynamics as well as stability and control related problems.
- A-H; Aerothermodynamics, including problems relevant to shock waves and atmospheric heat inputs.
- H-E; Thermoelasticity, including calculations of thermal stresses, heat transfers within materials, and buckling phenomena.
- A-E; Static Aeroelasticity, including the classical field of static aeroelasticity due to deformation and air loads, including divergence and control reversal.
- H-I; Thermal Molecular Processes, including problems related to thermal shock phenomena. This is ordinarily a weak link on a macroscopic basis; however, it is a strong link for molecular processes in materials.

Along with the edges of the tetrahedron, the four triangular surfaces present the domains of interaction of the respective disciplines designated by their boundary links:

- A-E-I; Aeroelasticity, presenting the well-known Collar's aeroelastic triangle including problem areas such as dynamic aeroelasticity, flutter, buffet, and perhaps control feedback through aero-servo-elasticity.

• A-H-I; Stability and Heat, presenting the problems relative to stability and control, including the dynamics of shock waves and thermal shock in the fluid field.

• A-H-E; Static Aerothermoelasticity, presenting the effects of heat on static aeroelasticity, including the problems such as ablation, warping, and determination of associated aero loads.

• H-E-I; Vibration and Heat, presenting such effects as those of heat on vibration modes and frequencies, on moduli of materials, and on fatigue; including the problems relative to materials not only in the sense of determination of their properties for given engineering materials, but also in the more fundamental sense of development of the components of the desired properties.

• A-H-E-I; Aerothermoelaslicity, presenting dynamic aerothermoelasticity, including the interactions of the aforementioned ten fields.

2. Literature review

Aerothermoelasticity was a vibrant and active area of research in the late 1950's and during the 1960's. As is evident from [5] [6] [7], the solutions to problems in such a multidisciplinary area are mainly defined with respect to the following fundamental questions:

- whether to separate or combine the problem areas;
- whether the problems can be treated sequentially by aero-thermal, thermo-elastic, and aero-elastic methods;
- whether the problem can be regarded as static or a quasi-steady time-varying procedure, or by truly unsteady flow methods.

The answers, subsequently, will be strongly dependent on various time factors in the domains, as well as structural concepts and detail designs.

There exist several early publications, such as [5] [4] [8] [9] [10], providing insight into the salient aspects of aerothermoelasticity on the basis of its classical definition. The main achievement of these studies, upon which the solution strategies toward aerothermoelastic problems has been designed, is the illustration of the degree of coupling between the aerodynamic heating, aerodynamic forces, inertial forces, and elastic forces. As shown in Fig. 1-2, the impacts of elastic forces on aerodynamic heating is seen to be negligible, the inertial forces and aerodynamic heating are shown as uncoupled domains, and the aerodynamic heating is viewed to

have no impact on aeroacoustics inputs. Accordingly, by neglecting the mutual coupling between the elastic forces and heat transfer process, the aerothermoelastic problem was simplified to an aerothermal problem together with a separate aeroelastic problem [10].

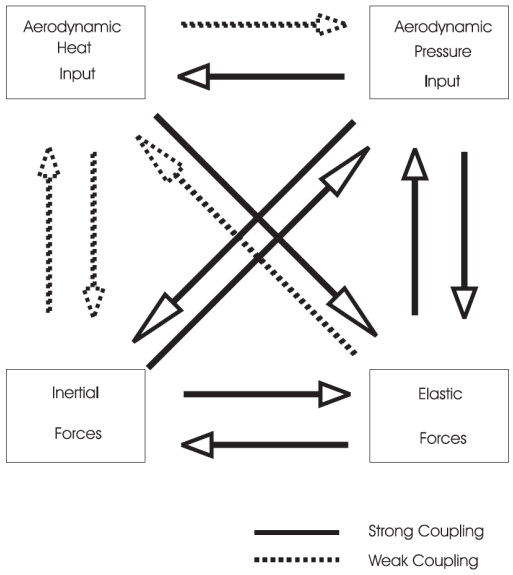

Fig. 1-2. Degree of coupling for the domain of Aerothermoelasticity [9]

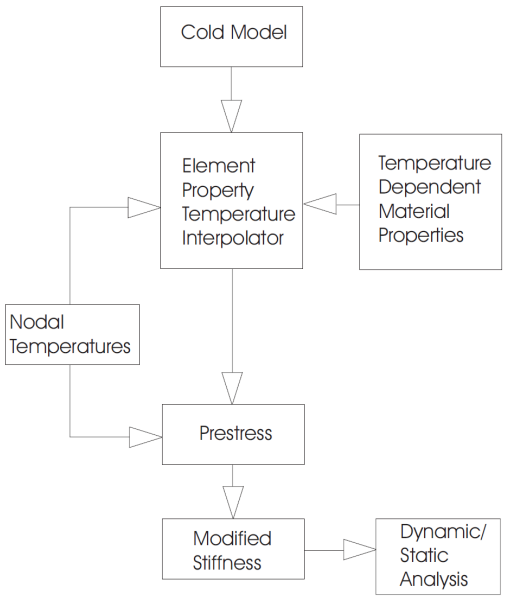

Fig. 1-3. Proposed process for including thermal effects into the finite element analysis of an aerodynamically heated structure [11]

The implementation of this terminology in finite element analysis (FEA) was first presented in [12] on the basis of the diagram depicted in Fig. 1-3. In this algorithm, the aerothermal solution is obtained first, and the aeroelastic analysis is then carried out on the updated structure. The main advantages of the implemented decomposition is the credibility of the already generated aeroelastic theories, methods, and tools to be directly applied to aerothermoelastic problems.

The most common aeroelastic theory reused for aerothermoelastic problems is the piston theory, which yields a point function relation between the unsteady pressure on the surface of the panel and its velocity normal to the surface. By implementing the piston theory, the aerodynamic loads are generated, and added as inputs for structural analysis. The accuracy of this simple aerodynamic theory is often considered appropriate for preliminary calculations. For low to moderate Mach numbers, i.e., $1.2 < M < 2$, the Van Dyke's version [13] [14] is often used. For moderate regime of $2 < M < 4$, the Lighthill's version [15] is employed commonly in first-order form. For higher Mach numbers, the Lighthill's nonlinear piston theory is preferred [16]. Although the implementation of this theory has helped to enhance the conceptual understanding of the phenomena, clarifying the valid range of the generated analysis in different situations remains to be an issue, as there is no direct interactive link to address the relationship between the considered components of the decomposed phenomena.

A fairly comprehensive survey of nonlinear aeroelastic studies which define the valid range of the piston theory can be found in [17] [18] [19] [20]. An important issue in these studies is the validity of the piston theory aerodynamics, widely used for $1.8 < M < 5.0$. While it is known that the piston theory is not valid for large Mach numbers [15], the actual upper bound is difficult to specify since it depends on the thickness of the geometry considered. Some researchers have suggested that the piston theory is generally valid for $3 < M < 10$ [21]. However, preliminary results presented in [22] indicate that this issue warrants further study.

In [10], the third-order piston theory, Euler, and Navier-Stokes aerodynamics were used to calculate the pressure on a typical panel in high Mach numbers. At $M = 10.0$, there was only a 5% difference between the unsteady pressure coefficient calculated using the third-order piston theory and that calculated using an exact solution to the Euler equations. However, there was approximately a 60% difference between the Euler solution and the pressure coefficient calculated using a numerical solution to the Navier-Stokes equations.

This result illustrates that at certain conditions, a solution to the Navier-Stokes equations may be needed for accurate prediction of the unsteady aerothermo loads. Since in higher Mach numbers the velocity perturbations are large as compared to the ambient speed of sound [23], the need to retain nonlinear aspects of the governing equations becomes significant. This makes the analysis of aerodynamic loading inherently more difficult than in other regimes. Furthermore, as the Mach number is increased, the shock, which is very strong, moves close to the body while the boundary layer grows rapidly. Therefore, viscous interactions between the outer inviscid flow, the shock, and the boundary layer become significant. Also, extreme temperatures are present in both the inviscid flow behind the shock and the boundary layer, due to significant flow compression and viscous dissipation. This intense aerodynamic heating can cause dissociation and ionization within the gas, resulting in chemically reacting boundary layers [24] [25] [26]. Thus, the proper solution to the aerodynamic problems within this regime can only be obtained by solving the unsteady Navier-Stokes equations which include high temperature effects, a task that presents a significant computational challenge.

To diminish the computational challenge while still providing a desirable solution, an improved method for calculating quasi-steady generalized forces using steady CFD calculations was proposed in [27]. Separate solutions for the real and imaginary portions of the pressure were obtained using carefully constructed boundary conditions reflecting the unsteadiness of the flow. It was observed, by comparing results with complete unsteady CFD calculations, that the CFD-based quasi-steady approach offered an improvement in accuracy over the linear piston theory [27]; however, the level of accuracy was not satisfactory for the desired range of applications.

Consequently, no solutions remained other than the implication of complete unsteady CFD calculations for the problem, along with reduced order models (ROMs). In [28], a CFD based aeroelastic analysis of X-43 configuration was performed, using system identification based on order reduction of the aerodynamic degrees of freedom. The system identification was carried out using an Auto-Regressive Moving Average (ARMA) model, which describes the modal response force of a system at a given time as a summation of scaled previous outputs and scaled values of modal displacement inputs. Surprisingly, it was shown that ARMA Euler calculations predicted somewhat similar results to high order piston theory. To verify this possibility, in [29] the unsteady aerodynamics results obtained from CFL3D solver and specified NASA CFD solver were

compared to those computed using a modified version of the third-order piston theory. It was concluded that a quasi-steady aerodynamic theory such as the third-order piston theory can be a valid approach to calculate the unsteady aerodynamic loads. The results indicate that in spite of employing more detailed solutions, the level of accuracy remains unchanged. This fact points the accusation at the level of data transaction between the fluid and solid fields.

Given that the incomplete understanding of the fluid-structure interactions may have been the cause of this problematic part of the aerothermoelastic studies, researchers were led to include more details in data transactions between the fields. However, since the combination of several different computational tools (CFD solver, structural solver, and heat transfer solver) is required for performing an aerothermoelastic analysis, significant data transfer between different computational tools becomes an issue to address. Several studies have focused on developing codes to efficiently combine these components. In [30], using the finite element method, the flow, thermal, and structural analyses were coupled into one integrated code. The aerodynamic pressure and heating were determined by solving the Navier-Stokes equations, and the internal dynamics of the structure were obtained by solving the Helmholtz free energy equations. Results indicated that at higher Mach numbers (M = 6.6), structural deformations due to aero-thermo loads introduce unforeseeable phenomena in the flow (such as shocks, expansions, and recirculation regions), and the heating rate distributions were altered significantly. As a result, the weak connectivity assumption (frequently used in former solutions for interface problems) seems to be no longer evident in aerothermoelastic analysis. Although this detailed approach revealed some hidden aspects of fluid-solid interactions, it brought new significant problems into the stage which limits the applications of such approaches. The problems are related to the different coordinate frames implemented for solid and fluid fields and, more importantly, to the control of data transactions between the solvers – the latter is associated with attaining dynamic data transfer between the fields and avoiding double counting of the physical impacts.

The application of dynamic meshing strategies was chosen to address the problem related to the incompatibility of the Eulerian-Lagrangian coordinate frame. In [31], an implicit/explicit upwind cell-centered finite element algorithm coupled with an adaptive unstructured finite element re-meshing technique was examined in order to study the fluid-thermal-structural interaction of aerodynamically heated leading edges. The analysis was validated with experimental results of a

cylinder in M = 8.0. A loose coupling of these codes was achieved by selecting a master surface for a specific variable, and interpolating/projecting that variable to the other codes at each time step. Although the algorithm provided a cost-effective means of using existing CFD (fluid solver), CSD (structural solver), and CTD (thermal solver) codes with minimal alterations, the mathematical based data transactions necessitate significant computational cost for more complex geometries.

In a recent study [32], an integrated CFD-CSD-CTD solver for aerodynamic heating analysis and aerothermoelastic stability analysis was developed to reduce the computational cost of the aforementioned data transactions. The fluid, structure, and mesh dynamics were solved separately in a serial manner, and the solutions from each of the computational domains were then transferred via the interface boundary to account for interaction effects. The proposed aerothermoelastic formulation was in principal an extension of a previous aeroelastic formulation developed in [33]. In the aerothermoelastic analysis, only one-way thermal coupling was considered. Furthermore, stress and deformations due to temperature changes were included; however feedback was neglected between the stress/deformations and the aerodynamic heating computations. It is therefore deduced that the reduction of the computational cost offered by the proposed formulation in that study is achieved at the cost of depleting the physical nature of the problem.

From the reviewed literature it can be concluded that the physical gap resulting from the initial assumptions (developed to permit a sequential solution) cannot be satisfactorily filled by merely increasing the computational costs, unless some aspects (such as those described above) of the phenomena become neglected. This fact can indicate the limiting role of the fundamental assumptions in defining the capacity of the existing solutions.

Overall, it is well known that aerothermoelastic phenomena is a multidisciplinary problem and has an influence over a wide range of operational conditions. This makes the study of this field severely challenging without the use of a varying degree of approximations to separate the different aspects of the phenomena. As stated by Bisplingoph in [5], “Since the time constants of the thermoelastic processes are usually considerably greater than those for the aerothermal and aeroelastic processes, indeed, there is very strong motivation for the structural designer to plan to separate as far as possible the severest regions of these three processes”. This permission has led to the establishment of highly operational methodologies and tools within this area of study.

However, from the literature, it can be concluded that the existing framework on the basis of the permission of separation has reached its maximum capacity in truly understanding the ongoing phenomena.

One should consider that the motivation of separation is acceptable so long as it does not become a barrier to improvement, even after establishing highly operational frameworks. The challenges revealed in the aforementioned studies highlight the amount of extra attempts (e.g., expensive computational cost in data transactions between the solvers) made to maintain the core assumptions underpinning the separation motivation [5] [4] [8] [9] [10]:

- Thermodynamic coupling between heat generation and elastic deformation is negligible;
- Dynamic aeroelastic coupling is small, i.e. the characteristic time of the aerothermal system is large relative to the time periods of the natural modes of the aeroelastic system;
- Static aeroelastic coupling is small, i.e. total elastic deflections are insufficient to alter the temperature distribution.

Although the understanding of aerothermoelasticity up until this current stage was almost unmanageable without making use of these fundamental assumptions, as stated in [34], “it is evident that the intricate interaction of aerodynamic heating on the oscillating structure, over a wide range of operating conditions, is yet far from well understood”. This fact indicates an existing gap in this area of knowledge. To address this knowledge gap, a rethink of the existing assumptions tomove towards bringing the neglected part of the phenomena back into consideration may be required.

3. Shortcoming of the current approaches

Considering the reviewed literature, it is clear that after passing through several decades of the emergence of aerothermoelastic problems, these problems are still conveniently considered by many modelers as an extension of aeroelastic problems. There is no doubt that by means of numerous useful methodologies proposed in the area of aeroelasticity, there now exist a range of sound strategies that potentially possess certain capabilities in solving a diverse range of problems arising in this area. However, it is evident from the literature that in situations where heating

impacts become significant, the well-established framework of classical aeroelasticity would be unable to explain the true causality of the ongoing aerothermoelastic phenomena. For instance, in [10], although the unsteady solution is employed for the flow, the data transformations between the generated component of the decomposed area has decreased the accuracy level of the total solution to a level that can also be generated via a quasi-steady method. This vicious circle can be an indicator of the shortcomings of the physical knowledge when defining the thermal interactions between the components in the classically decomposed aerothermoelastic area. Accordingly, one can see that the consideration of aerothermoelasticity as the extension of aeroelasticity has brought researchers to an undeniable limitation, which even with costly mathematical computational solutions cannot be improved.

It is known that the classical fundamentals of aeroelasticity are based on assumptions (such as separation principle or weak connectivity) that largely ignore the thermal connections between the various physical fields of a system within which aerothermoelastic phenomena exist. Although the impact of neglecting the thermal connections could be added into the solution of each filed of the system, the real interactive nature of the thermal connections between the various fields (that could have significantly changed the dynamics of the system if considered), has been completely lost in this process. As a result, the true physical links between the various fields measured by the universal principle of conservation of power transactions are no longer held. Reinstalling these physical links will require a reconstruction of the fundamental assumptions upon which the aerothermoelastic phenomena of the system can be truthfully reflected.

As just mentioned, by using the classical definition of aerothermoelasticity, the conservation of power transactions that can be a physical foundation for generating a universal controlling tool for data transactions between the solid and fluid fields, cannot be granted. Therefore, although each of the solvers can generate an accurate behavior of the field within the solver's valid range, the data transactions between the solvers by no means possess a physically-based dynamic nature. As concluded in the literature, the highest level of accuracies for the fluid and solid fields mainly belongs to the solutions of the Novier-Stokes [36] equations and the Helmholtz free energy [37] equations, respectively. Considering the different extensive variable choices in these approaches, the generated models for both the solid and fluid fields become domain-dependent [38] in nature, especially in their respective thermal subdomains. This feature makes the dynamic coupling of the

thermal subdomains of the two fields on the interface impossible to implement. Consequently, the entropic interactions between the two fields remain ambiguous. Although these interactions may be negligible [39] in comparison with mechanical interactions, the disregard for this factor will bring questions to the conservation of power transactions between the two fields. Accordingly, while the generated models are capable of providing a clear picture of the ongoing dynamics of the system, they are seen to be unsuitable for providing a useful and unbroken root upon which the physical memory of the system underpinning the energy conservation law can be firmly established. As a result, the remaining strategy for connecting the two models is to generate separate loads for the shared boundary at the interface, instead of following the power transactions (Fig. 1-4). This strategy on the one hand leaves no means for generating a conservative dynamic data transaction, and on the other hand leads to a tremendous computational cost.

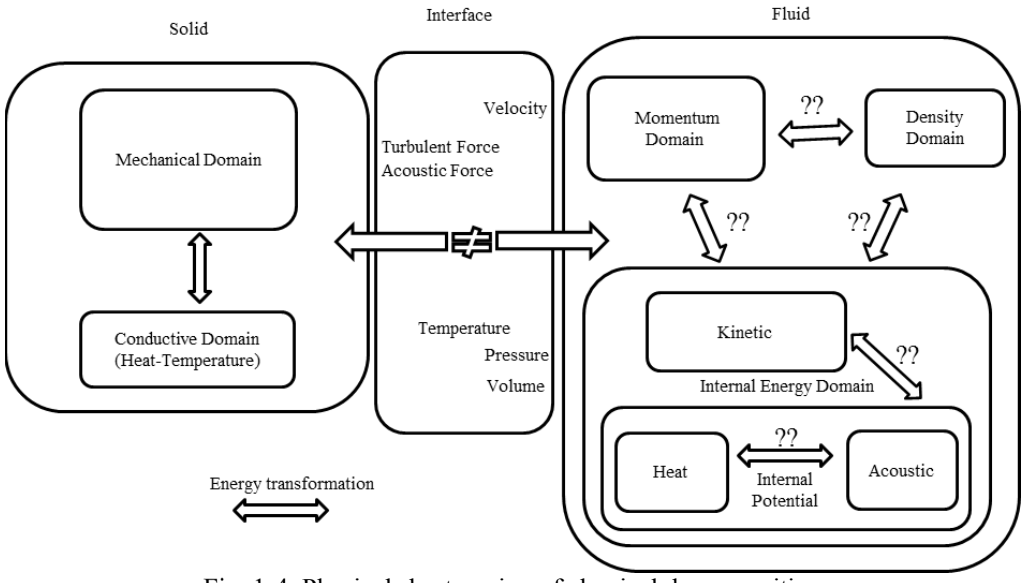

Fig. 1-4. Physical shortcoming of classical decomposition

On the basis of the physical system theory, to generate such conservative data transactions between the fields, the general dynamics of the system are required to be generated from the constructive elements that can connect the dynamics of the system to the energetic interactions of the existing subdomains [40]. However, in the classical aerothermoelasticity, the level of decomposition (which is mainly phenomenon based) is higher than the level in which the constructive elements of the dynamics of the system exist. This leaves no generic means for a component to relate the general behavior of the system to its constructive energetic interactions by means of which the conservation of data transactions could be tractable. Consequently, the

transactions of the information between the fields are not detailed enough to include the required level of the history of such transactions. Accordingly, the true dynamic coupling between the fields won't be achieved which can be problematic, especially when the two field are coupled via a combinatory dynamics with different time scales.

The attained modeling accuracy using the classical approach is seen to be heavily rely on mathematical constraints (filtration and stabilization [41]) and computational capacity, which leads to the development of drastically high-order models valid only within a limited operational range. There is therefore a need to rethink the modeling technique and to create a new methodology that can be based on the purely intrinsic physical constraints of the system, in order to generate valid models that naturally obey the energy conservation law and reveal the interconnected physical insights of the system dynamics truthfully.

4. Original contributions and the proposed solution

The conservation of power transactions on the interface can be satisfied if isomorphic models of both the fluid and solid fields can be generated (as demonstrated in Fig. 1-5). In isomorphic models, for each portion of the power transportation in one field (either physical such as thermal, acoustic, or kinetic), there exists a specific gate in the other field with which a tractable transaction between the fields is attainable. However, because of the fundamental differences between the two fields (namely the existence of mass flow in the fluid field), generating isomorphic models for each of the fields in a general form is not possible unless each field is decomposed into a set of alike subdomains where counterparts between the two fields become isomorphic.

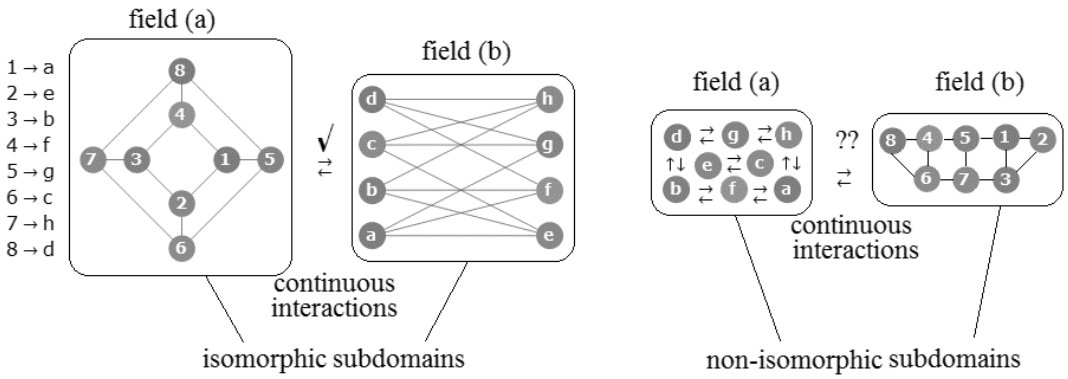

Fig. 1-5. Isomorphism between two counterpart subdomains of two different fields

Knowing that aerothermoelastic phenomena occur in multi-physical multiple-field (fluid and solid) systems, if a field-independent model can be generated (using physical states) for existing physical subdomains for each of the fields, the counterpart physical subdomains between the two fields (e.g., the thermal subdomain of the solid field and the thermal subdomain of the fluid field) will become isomorphic. Thus, the conservative power transactions including power transportation and power transformation among the physical subdomains will become tractable, regardless of the specific field.

4.1. The aim of the thesis

In the current study, in order to develop a framework for a conservative coupled-aero-thermo-elastic model, it is suggested that the physical decomposition of the system, as shown in Fig. 1-6, replace the phenomenon-based decomposition of the system. In doing so, since the physical (thermal, mass, kinetic, and potential) subdomains are alike in any fields [42], generating isomorphic models for the physical subdomains regardless of the field will make the conservative power transactions on the interface, and thus the complete dynamic coupling of the system, achievable.

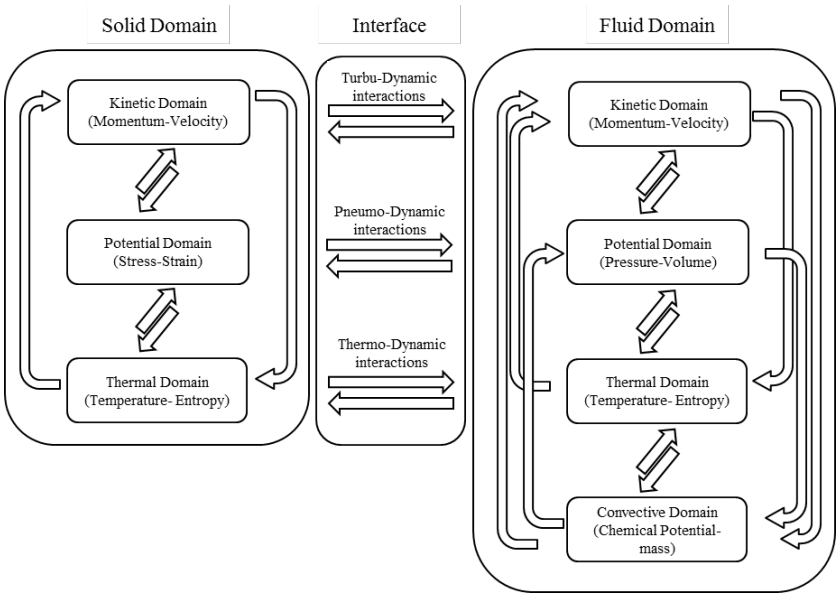

Fig. 1-6. Physical decomposition of aerothermoelastic problem

4.2. Suggested approach

Models of two subdomains become isomorphic *if and only if* the propagation of energy within

them becomes identical [43]. To generate such identical energetic models, in this study physical system theory in terms of the Bond Graphs (BG) methodology is employed [44] [45] [46] [47]. According to this theory, the dynamics of the system are generated from the reversible and irreversible dynamic interactions of the system's energetic components (namely, resistance, capacitance, and inertance). Given that the energetic components are similar in different subdomains and that the interactions between the energetic components in different subdomains follow a similar pattern (as shown in Fig. 1-7), the BG implementation can produce not only isomorphic models of counterpart physical subdomains between different fields, but also isomorphic models of all physical subdomains involved in the coupled fields. As a result, not only is the continuity of both the intra-field and inter-field power *transportation* satisfied, but also the possibility of tracking power *transformation* is provided. The conservation of power transactions of the entire system is thus guaranteed. The proposed methodology provides the ensuing framework with an intrinsically physical ability to control the data transactions between the coupled fields. The resulting conservative energetic framework of the system also allows modelers to check the well-posedness of the system before extracting state equations – a desirable capability for complex system dynamic investigations.

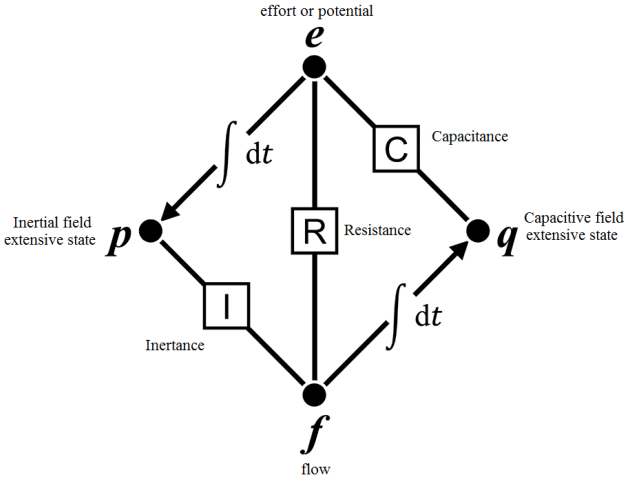

Fig. 1-7. Possible interactions of the energetic components in a system

4.3. Original contributions

Using the proposed concept, the following steps are sequentially taken to generate the fundamental structure of aerothermoelasticity. Each proposed step contains its own novel

methodologies. Together, the implementation of the proposed steps forms the overall original contributions of this thesis:

- Each field is first decomposed into its primitive physical subdomains (as shown in Fig. 1-8);

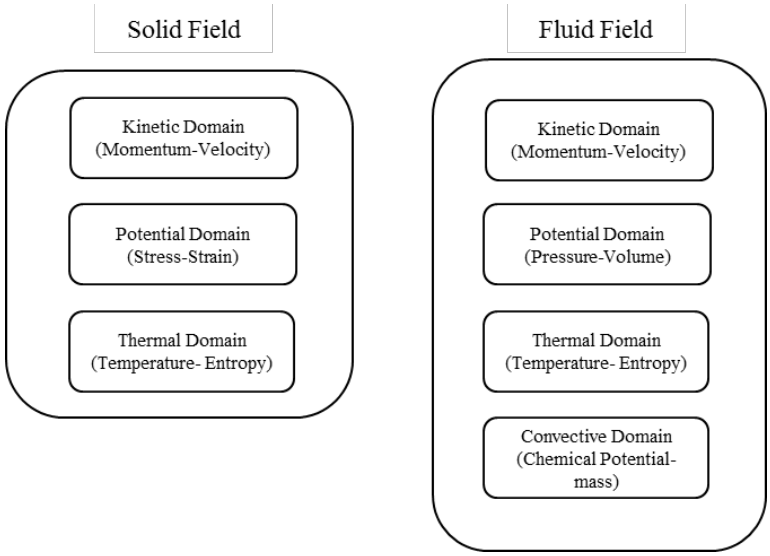

Fig. 1-8. Physical decomposition of the two fields

- The energetic components of each subdomain are then defined with respect to the geometrical and material properties of the field (as shown in Fig. 1-9);

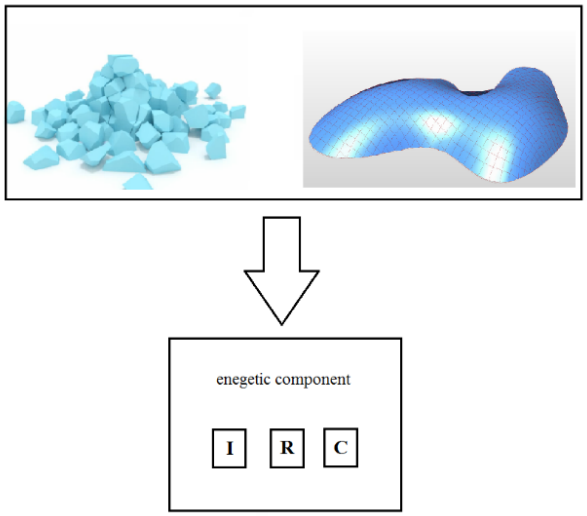

Fig. 1-9. Generating energetic components with respect to physical properties of the system

- The dynamics of each subdomain are generated from the energetic interactions of the present components (as shown in Fig. 1-10);

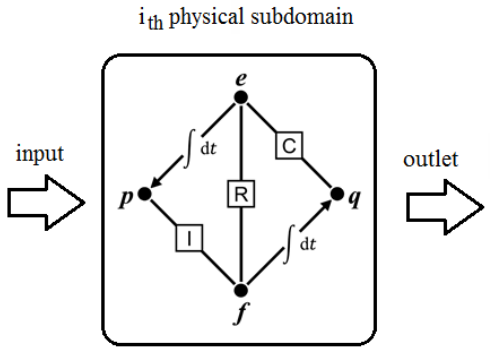

Fig. 1-10. Generating the dynamic of each subdomain with respect to the energetic component's interactions

- The dynamics of the field are then generated from the reversible and irreversible interactions of the present physical subdomains of each field (as shown in Fig. 1-11);

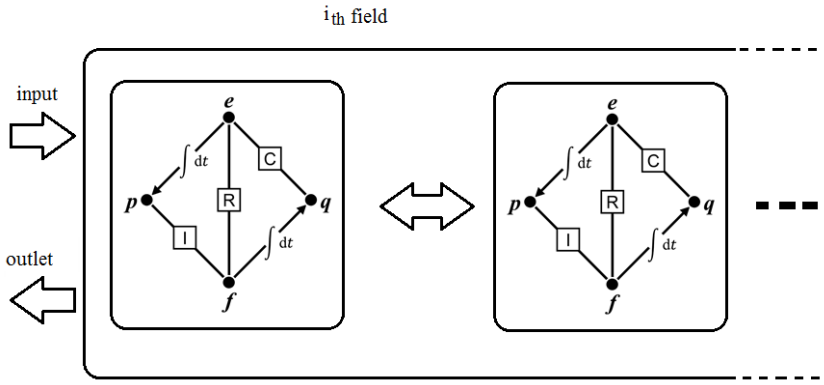

Fig. 1-11. Generating the dynamic of each field with respect its subdomains interactions

- Finally, based on the power continuity between the two fields, through connecting the counterpart pairs of the physical subdomains of the two fields with respect to the possible connections of their energetic components at the interface, the conservative uniform coupled-aerothermoelastic model of the system, as shown in Fig. 1-12, can be generated *if and only if* the compatibility issue between the fixed Eulerian frame of the fluid field and the moving Lagrangian frame of the solid field can be addressed satisfactorily.

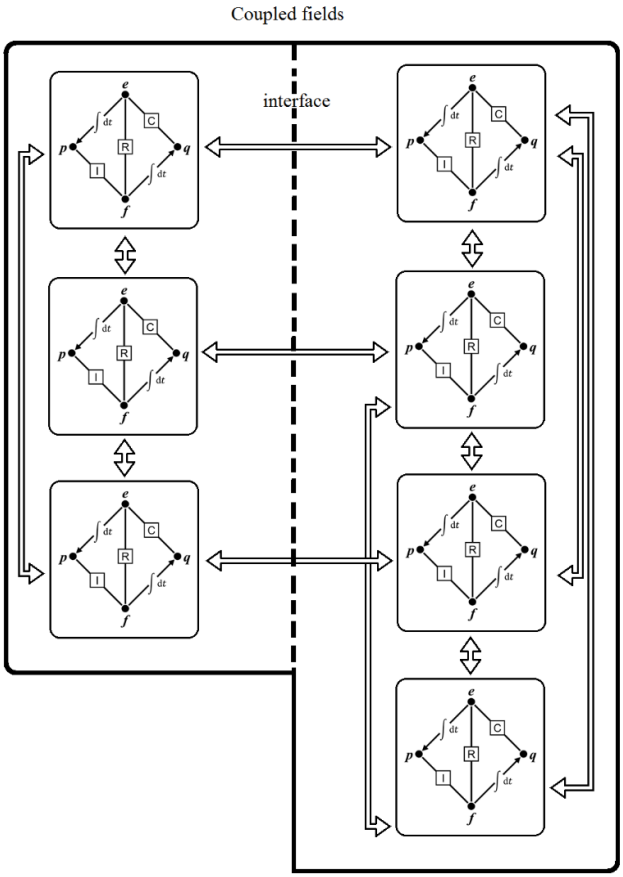

Fig. 1-12. Coupled aerothermoelastic framework

- To address the compatibility issue, a variable interface dynamic adaptation (VIDA) technique [48] is proposed. According to the VIDA technique, the likely motions of the Lagrangian solid frame is virtually translated into a reversible volumetric flow for the fixed Eulerian fluid frame. In doing so, the compatibility of the two frames is satisfied and the required information from the contact surface is refined at any instant in time to keep the power transactions at the interface continuous.

4.4. The outcome of this thesis

Overall, by using the proposed methodologies, an energetic network of the system will be generated that can illustrate continuous reversible and irreversible power transactions (including power transformation and power transportation) among the various subdomains and between the two fields. The dynamics obtained from such a model will include more details in relation to the

memory and physical characteristics of the system, which can in turn provide a well-posed model and a desirable basis for analyzing the complex multi-physical multiple-field behaviors of the system. As the model is developed without the slow-thermal-dynamics and weak-connectivity assumptions and with no additional mathematical constraints, the model is valid in an extended range, principally much wider than its conventional counterparts. Undoubtedly, the proposed energetic network of the system can be a useful tool for developing control strategies and energy management of the system.

5. Thesis outline

To illustrate the development of the proposed framework, the reminder of this thesis is organized as follows.

In Chapter 2, to form an introductory on implementing the BG method and to demonstrate the capability of this method in providing the dynamics of the system from the system's interactive energetic components, the nonlinear model of a multi-physical system is presented by which the combined transient behavior of the system is extracted from the conservative interactions of the present subdomains.

In Chapter 3, highlighting the thermoelastic phenomena and the related problems in the solid field, a domain-independent dynamic model of the existing physical subdomains of the solid field is generated. To achieve this, the energetic components of the elastic and thermal subdomains are defined for a simple geometry, and the general behavior of each subdomain is generated from the reversible and irreversible interactions of the energetic components sequentially. Accordingly, separate energy lines for the present subdomains of the solid field is generated by means of which a decomposed power distribution of the system is obtained with respect to each subdomain.

In Chapter 4, a reversible thermoelastic coupled model is generated. To achieve this, first a multi-dimensional capacitor is proposed by means of which reversible connections between the two present subdomains of the solid field is derived. By replacing the existing capacitance of each subdomain with the generated capacitive components, the dynamics of the existing subdomains of the solid field become reversibly coupled together.

In Chapter 5, to generate an energy-based thermoviscoelastic model, the irreversible coupling between the present subdomains of the solid field is generated. To achieve this, first an energy-based domain-independent model of the existing dissipative mechanism of the solid field is generated, which gives the physical interpretation of the anelastic behavior of the system. By adding the generated dissipative mechanism in the form of resistive components to the already-coupled model, the irreversible energetic interaction between the elastic and thermal subdomains is then generated, forming a thermoviscoelastic model. The proposed energy-based model is capable of generating the general dynamic behavior of the solid field from the reversible and irreversible interactions of the energetic components of the existing physical subdomains.

In Chapter 6, an energy-based model of the fluid field is developed. To achieve this, first a new decomposition of the fluid field is proposed by means of which an identical decomposition with the solid field is obtained. Next, similar to the solid field, the multi-dimensional energetic components of the fluid field are defined. Finally, by generating the reversible and irreversible interconnections between the components, the power structure of the fluid field is developed in which the general behavior of the field is created from the energetic interactions of the existing subdomains.

In Chapter 7, a comprehensive novel aerothermoviscoelastic model is generated via connecting the generated power structure of the fluid field with that of the solid field together. To satisfy the compatibility conditions raised from the implementation of different coordinate frames respectively for the solid and fluid fields, a novel VIDA technique is proposed to be implemented on the interface of the two fields. Since the decomposition of the two fields utilizes a similar terminology, the generated power structures of the two fields become connectable continuously, which demonstrates the continuous power interactions between the two fields.

In each chapter, the capability of the proposed model in capturing the ongoing dynamic behavior of the system, together with the suitability of the generated model for use in discrete system modeling, are examined via a sample geometry. The capability of the proposed model in capturing the complex behavior of the system using the energetic interactions of the physical subdomains described in a discrete configuration is concluded in Chapter 8.

Chapters 2 to 7 of this thesis are organized on the basis of the following peer reviewed papers submitted to the various journals:

Chapter 2:

- Non-Linear Analysis of Hydro-Mechanical Interactions in Control Device during the Transient Period: Bond Graph Approach
  Journal of Dynamic Systems, Measurement and Control

Chapter 3:

- Energy-based Thermo-Mechanical Discrete Model: Bond Graph Approach
  ISA Transactions
- Domain-Independent Conduction Discrete Model Compatible for Multi-Physical System Dynamic Investigations
  SIMULATION: Transactions of The Society for Modeling and Simulation International

Chapter 4:

- Domain-Independent Reversible Thermoelastic Coupling: a Bond Graph Approach
  Journal of Continuum Mechanics and Thermodynamics

Chapter 5:

- Energy-Based Viscoelastic Model: A Physical Approach for Material Anelastic Behavior
  Journal of Thermophysics and Heat Transfer (AIAA)
- Domain-Independent Thermoviscoelastic Model: A Bond Graph Approach
  Journal of Thermophysics and Heat Transfer (AIAA)

Chapter 6:

- Energy-Based Compressible Convective Model Proper for Aerothermoelastic Dynamic Investigation: A Bond Graph Approach on FSI Problems
  AIAA Journal

Chapter 7:

- A Novel Energy-Based Aerthermoviscoelastic Modeling Frame for Multiple-field System Dynamic Investigations, Bond Graph Approach
  AIAA Journal

It should be mentioned that the References of each chapter are presented at the end of the chapter, and the entire Bibliography summarizing all references of the thesis is given at the end of the thesis.

References

[1] L. E. Garrick, "Aeroelasticity-Frontiers and Beyond," *Journal of Aircraft,* vol. 13, no. 9, pp. 641-657, 1976.

[2] H. Försching, "Prediction of the unsteady airloads on oscillating lifting systems and bodies for aeroelastic analyses," *Progress in Aerospace Sciences,* vol. 18, pp. 211-269, 1978.

[3] F. L. Vosteen, "Effect of Temperature on Dynamic Modulus of Elasticity of Some Structural Alloys," NACA TN 4348, 1958.

[4] L.E. Garrick, "A survey of Aerothermoelasticity," FIAS, NASA, Langley Research Centre, 1963.

[5] R. L. Bisplinghoff, J. Dugundji, Influence of Aerodynamic Heating on Aeroelastic Phenomena, Pergamon Press, 1958, p. 288–312.

[6] J. Hedgepeth, E. Widmayer, "Dynamic and Aeroelastic Problems of Lifting Re-Entry Bodies," *Aerospace Engineering,* p. 148–153, 1963.

[7] W. R. Laidlaw, J. H. Wyker , "Potential Aerothermoelastic Problems Associated with Advanced Vehicle Design," *Aerospace Engineering,* p. 154–164, 1963.

[8] R.L. Bisplinghoff, "Some Structural and Aeroelastic Considerations of High- Speed Flight," *Journal of the Aerospace Sciences,* vol. 23, no. 4, p. 289–329, 1956.

[9] M. Rogers, "Aerothermoelasticity," *AeroSpace Engineering,* p. 34–43, 1958.

[10] J. J. McNamara, "Aeroalastic and Aerothermoelastic Behavior of Two and Three Dimentional Lifting Surfaces in Hypersonic Flow," The Univercity of Michigan, 2005.

[11] D. Raney, J. McMinn, A.Pototzky, C. Wooley, "Impact of Aeroelasticity on Propulsion and Longitudinal Flight Dynamics of an Air-Breathing Hypersonic Vehicle," in *34th AIAA/ASME/ASCE/AHS/ASC Structures, Structural Dynamics and Materials Conferences*, La Jolla, April, 1993.

[12] R. V. Doggett, R. H. Ricketts, T. E. Noll, J. B. Malone, "NASP Aeroservothermoelasticity Studies," NASA TM 104058, 1991.

[13] M. D. Van Dyke, "A Study of Second-Order Supersonic Flow Theory," Tech. Rep. 1081, NACA, 1951.

[14] H.G. Morgan, H.L. Runyan, V. Huckel, "Theoretical Considerations of Flutter at High Mach Numbers," *Journal of the Aeronautical Sciences,* vol. 25, no. 6, p. 371–381., 1958.

[15] M. Lighthill, "Oscillating Airfoils at High Mach Numbers," *Journal of the Aeronautical Sciences,* vol. 20, no. 6, 1953.

[16] C. Mei, C. Grey, "A Finite Element Method for Large-Amplitude, Two-Dimensional Panel Flutter at Hypersonic Speeds," in *30th AIAA/ASME/ASCE/AHS/ASC Structures, Structural Dynamics and Materials Conference* , April, 1989.

[17] D.Y. Xue, C. Mei, "Finite Element Two-Dimensional Panel Flutter at High Supersonic Speeds and Elevated Temperature," in *31st AIAA/ASME/ASCE/AHS/ASC Structures, Structural Dynamics and Materials Conference*, 1990.

[18] E.G. Gray, C. Mei "Large-Amplitude Finite Element Flutter Analysis of Composite Panels in Hypersonic Flow," in *33rd AIAA/ASME/ASCE/AHS/ASC Structures, Structural Dynamics and Materials Conference*, Dallas, TX, April 1992.

[19] J.F. Abbas, R.A. Ibrahim, "Nonlinear Flutter of Orthotropic Composite Panel Under Aerodynamic Heating," *AIAA Journal,* vol. 31, no. 8, p. 1478– 1488., 1993.

[20] C. Mei, K. Abdel-Motagly, R. Chen, "Review of Nonlinear Panel Flutter at Supersonic and Hypersonic Speeds," *Applied Mechanics Reviews,* 1988.

[21] R. Ricketts, T. Noll, W. Whitlow, L. Huttsell, "An Overview of Aeroelasticity Studies for the National Aerospace Plane," in *34th AIAA/ASME/ASCE/AHS/ASC Structures, Structural Dynamics and Materials Conference*, La Jolla, CA, April, 1993.

[22] I. Nydick, P. P. Friedmann, X. Zhong, "Hypersonic Panel Flutter Studies on Curved Panels," in *36th AIAA/ASME/ASCE/AHS/ASC Structures, Structural Dynamics and Materials Conference*, New Orleans, LA, April 1995.

[23] J. Anderson, Hypersonic and High Temperature Gas Dynamics, New York: McGraw-Hill, 1989.

[24] I. Nydick, "Studies in Hypersonic Aeroelasticity, Ph.D. thesis," University of California, Los Angeles, 2000.

[25] J. Bertin, "Hypersonic Aerothermodynamics," *AIAA,* 1994.

[26] M. Rasmussen, Hypersonic Flow,, New York: JohnWiley & Sons, 1994.

[27] R.C. Scott, A.S. Pototzky, "A Method of Predicting Quasi-Steady Aerodynamics for Flutter Analysis of High Speed Vehicles Using Steady CFD Calculations," in *34th AIAA/ASME/ASCE/AHS/ASC Structures, Structural Dynamics and Materials Conference* , La Jolla, CA, April, 1993.

[28] K.K. Gupta, L.S. Voelker, C. Bach, T. Doyle, E. Hahn, "CFD-Based Aeroelastic Analysis of the X-43 Hypersonic Flight Vehicle," in *39th Aerospace Sciences Meeting & Exhibit*, 2001, AIAA Paper No. 2001-0712..

[29] S.L. Krist, R.T. Biedron, C.L. Rumsey, "CFL3D User's Manual (Version 5.0)," NASA TM 1998-208444, 1997.

[30] E. Thornton, P. Dechaumphai, "Coupled Flow, Thermal, and Structural Analysis of Aerodynamically Heated Panels," *Journal of Aircraft,* vol. 25, no. 11, p. 1052 – 1058, 1988.

[31] P. Dechaumphai, A. Wieting, A. Pandey, "Fluid-Thermal-Structural Interaction of Aerodynamically Heated Leading Edges," in *30th AIAA/ASME/ASCE/AHS/ASC Structures, Structural Dynamics and Materials Conference*, April 1989.

[32] H. Tran, C. Farhat, "An Integrated Platform for the Simulation of Fluid-Structure-Thermal Interaction Problems," in *43rd AIAA/ASME/ASCE/AHS Structures, Structural Dynamics and Materials Conference*, Denver, CO, April 2002.

[33] C.Farhat, M. Lesoinne, N. Maman, "Mixed Explicit/Implicit Time Integration of Coupled Aeroelastic Problems: Three-field Formulation, Geometric Conservation and Distributed Solution," *International Journal for Numerical Methods in Fluids,* vol. 21, pp. 807-835, 1995.

[34] A. J. Culler, J. J. McNamara, "Fluid-Thermal-Structural Modeling and Analysis of Hypersonic Structures under Combined Loading," in *52nd AIAA/ASME/ASCE/AHS/ASC Structures, Structural Dynamics and Materials Conference*, Denver, Colorado, April 2011.

[35] N. J. Falkiewicz, S. G. V. Frendreis, C. E. S. Cesnik, "Effect of Control Surface-Fuselage Inertial Coupling on Hypersonic Vehicle Flight Dynamics," in *AIAA Atmospheric Flight Mechanics Conference*, Portland, Oregon, August 2011.

[36] L. Daun, M. M. Choudhari, M. Wu, "Numerical Study of Pressure Fluctuations due to High-Speed Turbulent Boundary Layers," in *42nd AIAA Fluid Dynamics Conference and Exhibit*, New Orleans, Louisiana, June, 2012.

[37] W. K. Nowacki, "Progress in Thermoelasticity," *Warszawa: European Mechanics Colloquium,* 1967.

[38] A. Zanj, P. C. Breedveld, F. He, "Domain-Independent Thermoelastic Coupling Suitable for Aerothermoelastic Modeling," in *23rd International Congress on Sound and Vibration*, Athens, Greece, July, 2016.

[39] W. R. Graham, "A comparison of models for the wavenumber–frequency spectrumof turbulent boundary layer pressures," *Journal of Sound and Vibration ,* vol. 206, p. 541–565, 1997.

[40] P. C. Breedveld, "Thermodynamic Bond Graphs and the Problem of Thermal Inertance," *Journal of the Franklin Institute,* vol. 314, no. 1, pp. 15-40, 1982.

[41] J. Balino, "BG-CFD methodology for multicomponent solutions. Part I: Multivelocity model," in *International Conference on Bond Graph Modeling and Simulation*, 2003.

[42] P. Breedveld, Physical System Theory In Therms of Bond graphs, Enschede, Netherland: Univercity of Twente, 1984.

[43] S. Awodey, Category Theory, New York: Oxford University Press, 2006.

[44] J. Thoma, Simulation by Bond graph, Verlag, Gemany: Springer, 1990.

[45] A. Mukherjee, R. Karmakar, Modeling and Simulation of Engineering Systems through Bon dgraph, New Delhi, India: Narosa Publishing House, 2000.

[46] H. Afshari, A. Zanj, "Dynamic Analysis of a Nonlinear Pressure Regulator Using Bondgraph Simulation Technique," *Journal of Simulation Modeling Practice and Theory,* 2010.

[47] A. Zanj, F. He, "A Thermomechnical Enhanced Elastic Model: Bond Graph," in *23rd International Congress on Sound & Vibration*, Athens, Greece, July, 2016.

[48] P. C. Breedveld, A. Zanj, "Bond Graph Representation of Convection by Fluid Flow Alonf an Elastic Surface," in *12th international Conference on Bond Graph Modeling and Simulation*, Montreal,Quebec, Canada, July, 2016.

CHAPTER 2: AN INTRODUCTION OF THE IMPLEMENTATION OF BG METHOD IN MULTIPLE-FILED DYNAMIC INVESTIGATIONS:

Aim

In this chapter, an introduction of the implementation of BG method on how to generate the nonlinear dynamics of multi-physical systems from the dynamic interactions of the existing energetic components is presented.

Description

To achieve this aim, for a chosen example, the procedure of decomposition of the system in terms of defining the energetic components of the system, developing the BG model for the system, and extracting the governing equations of the system from the BG model is demonstrated. For this purpose, a hydro-control device is chosen as a sample representative of a multi-physical multiple-field system for which the initial transient of the system is investigated according to the following outline:

Results

The original contribution made in this study is the development of a novel variable degree-of-freedom nonlinear model, by means of which the complex behavior of the system during the start procedure of such multiple field devices can be investigated. The obtained results clarify the capability of the chosen methodology (BG method) in defining such complex behavior of the

system in a way that can connect the system behavior to the physical root of the ongoing phenomena.

Conclusion

Overall, by means of the generated nonlinear model we show how the combined transient behavior of the system can be extracted from the conservative interactions of the involving subdomains.

NON-LINEAR ANALYSIS OF HYDRO-MECHANICAL INTERACTIONS IN CONTROL DEVICE DURING THE TRANSIENT PERIOD: BOND GRAPH APPROACH

A. Zanj* & F. He

Advanced Control Systems Research Group, School of Computer Science, Engineering & Mathematics, Flinders University, Adelaide, Australia, (e-mail: amir.zanj@flinders.edu.au)

***Abstract*—**In this paper, a feasibility study on modeling the multi-physical dynamic behaviors of the start period of hydro-mechanical control devices is presented. Using a novel multi-model Bond graph approach, a nonlinear, variable degree-of-freedom, state-space model is developed for a typical pressure regulator during its start period. Simulation studies demonstrate the essential physical behavior of the regulator during the transient, and confirm the integrity of the resulting nonlinear model of the system.

***Index Terms*:** Control systems, Multi-physical system, Fluid flow control, Hydrodynamics, Transient analysis, Dynamic interactions.

1. Introduction

START period is an unavoidable multi-physical dynamic process during which the internal moving components of a hydro-mechanical control device will experience unpredicted dynamics before settling in their required operating condition. Maintaining the safety of these components during this process is one of the key design issues of the device. Although a smooth start period is preferred for the internal components, a quick start is often demanded of the device to meet certain transient performance specifications. In this situation, the device will exhibit a degree of unpredicted and severe dynamic behavior during its start period. Lack of attention to this period can lead to a complete failure of the device. This is certainly true for a liquid propulsion system often found in a space vehicle, where hydro-mechanical valves such as regulators and stabilizers are responsible for regulating the engine transient behaviors [1, 2].

The start period of a hydro-mechanical control device, such as a regulator, is defined as the duration between the moment that the first fluid droplet enters into the valve and the moment that the internal moving components of the device are fully stabilized. During the early transient of the start period, fluid fills different chambers of the valve, forming the filling process of the period. Since the valve's boundary visited by the fluid is varying, the geometry of the system with respect to the input energy flow will be a variable. One can thus consider the filling process as several consecutive early stages of the start period; each having its own way of distributing the power in

the system. Modeling of the filling process is then a task of revealing the dynamics of the varying power distributions as a function of the varying geometry of the system touched by the fluid during this transient. In the late stages of the start period, hydraulic pressures move the valve's internal components, instigating additional interactive hydro-mechanical phenomena between the fluid acceleration and the components' movement. These complex multi-physical dynamic interactions, if not modelled properly in the device's design phase, may result in severe damages to the system. The modeling of the entire start period therefore requires a valid analytical representation of the system that can accurately describe the internal power transfer and geometry change during the transient phase and truly reveal the coupled dynamic behavior in a multi-physical domain setting. Many techniques for modeling hydro-mechanical control devices in the literature have not yet touched on this issue.

Early studies on the modeling of pressure control valves [1-3] only concentrated on the flow visualization of the system, and completely neglected the internal interactions between the fluid and the moving mechanical parts. The resultant models are useless in revealing the multi-physical dynamics existed in such systems. The transfer function technique used in [4] provided a conventional solution for the nonlinear dynamics of a pressure relief valve by linearizing the system about one operating point. The resulting linear model is unable to capture the nonlinear dynamic details and removes the true physical phenomena during the transient. These modeling techniques are deemed to be unsuitable for the start period, as the system dynamics within this period is highly nonlinear and physical.

To adequately model the start period in a multi-physical domain setting, a physical approach that can truly reveal the nonlinear interactions between each domain of concern thus providing the required dynamic details of the system during this transient, is preferred. The Bond graph (BG) technique which works on the basis of power exchange inside a dynamic system [5-6] is deemed to be ideal, as the method is capable of keeping the integrity of the power flow within a system while extracting the physical model of the system as a set of nonlinear governing equations. It interpretes different physical domains in a unique terminology, reserves the true physical meaning of the system by conforming to the underlying governing laws, and provides an analytical representation of the system without linearization.

Some studies on hydro-mechanical devices' modeling using the BG technique have been reported in the literature. Borutzky [7] analyzed the hydro-mechanical dynamics of a spool valve for the control of orifices. Dasgupta and Watton [8] studied the performance of a multiple-input multiple-output pilot relief valve with parameter variations; the system was then modelled using measured parameters [9] and analyzed in the transient and steady state [10]. Zanj *et al*. developed nonlinear BG models of direct and indirect pressure control valves [11-12], and investigated a range of dynamic behaviors of an indirect valve including nonlinear effects of flow forces, coulomb friction, hydraulic resistances, and fluid chamber compressibility [13]; the model was validated in experiment. None of these studies has attempted to model the start period, as the traditional single-model BG approach used can only describe fixed degree-of-freedom (DoF) dynamics, whereas the dynamics of the start period are varying DoF in nature. This is because the geometry of the system in contact with the hydraulic energy grows with time during the filling process, which requires the number of the state variables for each of the filling stages to be increased in order to describe the hydro-mechanical dynamic interactions within that stage properly. To reflect this graduate increase of DoF using the usual single-model BG approach will violate the energy conservation law underpinning the BG concept.

A multi-model BG approach is thus proposed in this paper, where a growing-DoF structure is used to describe the dynamic behaviors of different filling stages while the energy conservation law within each of the stages is tightly upheld. By using a volumetric state whose dimension varies according to the energy conservation of the stage of concern, a variable energy distribution observable in the physical system during the start period can be captured and truthfully represented.

The rest of this paper is organized as follows. In Section 2, the start period of a chosen hydro-mechanical control devise is described. A multi-model BG approach is proposed in Section 3, where the state equation for each of the stages of the start period is extracted from the related BG. In Section 4, the multi-model structure of the start period for the chosen device is evaluated via simulation, and the significant impact of inclusion of the start period on the dynamic behaviors of the system internal components is revealed. The modeling effect of the proposed multi-model BG approach on the system safety and operation are concluded in Section 5.

2. Physical model

A pressure regulator shown in Figs. 1 and 2 is chosen for the start period modeling. The control valve is composed of four major parts: (a) Control Part – including inlet (1), outlet (2), and control orifice (5) the size of which is changed by the movement of control spool (3); (b) Amplifying Part (where the pilot signal is regulated and amplified) – including control piston (4) and damping orifice which connects piston front zone (ppf) (17) and piston back zone (ppb) (18); (c) Adjusting Part (which regulates and sends the hydro-control signal to (a)) – including adjusting spool (9), flexible elements (16), feedback pipe (7), and adjusting orifice (15); (d) Pre-adjusting Part (where initial adjustment of the valve is imposed) – including adjusting screw (13), noise canceler (11), and adjusting spring (12).

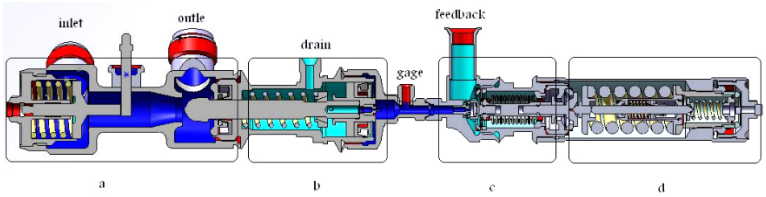

Fig. 1 A pressure control regulator valve [13]

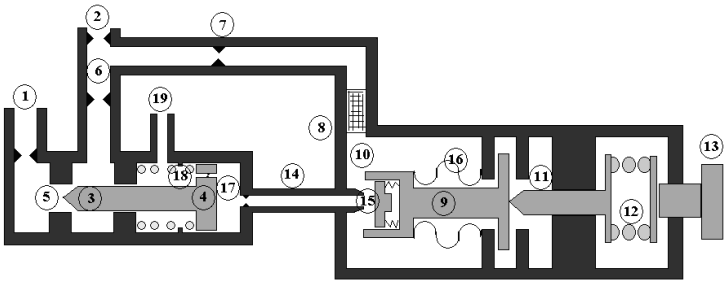

Fig. 2 Scheme of the chosen valve [13]

The main goal of the control valve is to regulate the outlet pressure. In a nominal operating condition after the start period, the dynamic behavior of the valve can be described as follows. By increasing the inlet pressure, the pressures of the feedback pipe and adjusting zone (10) are increased, which will open the adjusting orifice resulting in a corresponding pressure rise in the ppf that will move the control spool to narrow the control orifice. As the cross section area of the passing flow decreases, the total pressure loss of the valve increases. The pressure rise in the outlet

flow is consequently compensated. This standard dynamic behavior cannot be applied to the start period, as the valve will experience entirely different transient interactions between multi-physical domains during this period. In fact, the internal components of the valve when moving from their initial positions (shown in Fig. 3) to their nominal operating positions during the start period will go through five consecutive stages. Initially (see Fig. 3), the control piston stays at the bottom of amplified cylinder (b), so control orifice (a) is fully open. The adjusting spring force pushes the adjusting spool to its upper seat (d), so the tip of the adjusting spool and plate (c) closes the adjusting orifice completely. Since the valve is initially placed empty of fluid, the first four stages of the start period will constitute the filling process where the fluid progressively fills different zones of the valve and the resultant hydraulic pressure moves the internal components of the valve. Using Figs. 1-3, the chosen valve's internal dynamics of the five stages during the entire start period can be described as follows.

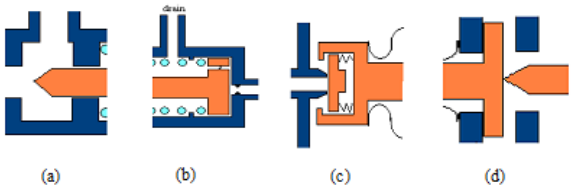

Fig. 3 Initial positions of valve's moving components, before start [13]

Stage 1 – Filling part (a) of Fig. 1. Upon receiving the start signal, fluid starts to fill the inlet, control orifice, and sense zone (6). Other parts of the valve are untouched. No hydro-mechanical interactions occur in the valve, thus no inside mechanical movement is anticipated.

Stage 2 – Filling zones (7) and (10) of Fig. 2. After filling the sense zone, the feedback pipe and adjusting zone are filled. The hydraulic pressure is increasing in the control area while staying at the atmospheric level in the adjusting zone. The hydro-mechanical interactions are about to occur on the control spool while currently pressuring it to stay at its seating position (b) of Fig. 3. Hence, no mechanical movement is yet to be anticipated.

Stage 3 – Opening zone (15) and filling zone (17) of Fig. 2. After filling the adjusting zone, the hydraulic pressure starts to accumulate. The resultant hydraulic force pushes the adjusting spool and lifts it from its initial position (c) of Fig. 3. But, the plate inside the tip of the adjusting spool keeps the adjusting orifice closed until the hook of the adjusting spool reaches the plate. Mechanical motions are observed in the adjusting part, but not yet in the control part as the

hydraulic pressure is still forcing the control spool to remain at its seating position. Since the adjusting orifice is opened, the fluid fills the ppf up.

Stage 4 – Filling zone (18) of Fig. 2. As the hydraulic force in the ppf increases, it pushes the control spool to narrow the control orifice, so the valve begins to control the pressure from this point on. Meanwhile, the feedback flow finds its way via the damping orifice located in the control piston to fill the ppb whose dimension is a variable depending on the location of the control piston. Filling the ppb works as a break for the moving control spool. At the end, all internal mechanical components are fully engaged in the dynamics behavior of the system.

Stage 5 – Regulating the operating outlet pressure. After filling the ppb, the outlet pressure is continuously controlled by the movements of the internal components that attempt to stabilize the system until the required operating condition is achieved.

The above 5-stage procedure is common to almost all hydro-mechanical automatic control devices of liquid engines. This highly-nonlinear multi-physical dynamic behavior, if ignored, may result in fatal collisions between the internal components and the body of the system. This is particularly true for engines that involve a fast start command. Modeling of the start period is thus a necessary step that can facilitate the proper selection of a suitable start command for a successful system operation.

3. Mathematical model

As can be seen, during the start period, the rate and location of the simultaneous interactions between the hydraulic power and mechanical movement within the system vary according to the different filling stages that the system is in. This makes the geometry of the energy domain of the system vary during the start period. To describe this effectively, the concept of a dynamic system with varying DoF is developed. A multi-model BG approach is proposed in which each BG model represents a corresponding stage of the start period. An exact energy distribution of the system for the corresponding filled geometry of the system is accurately defined for each of the filling stages. The system's DoF is fixed for one filling stage, but varying for different filling stages. As the fluid is gradually filling the sequential chambers of the valve, the filled geometry of the system is growing and so does the DoF of the system. This varying DoF ceases when the filling process completes.

Consider the fluid inertia. Without loss of generality, six assumptions are adopted here: (i) the valve's initial pressure be atmospheric; (ii) the flow stream inside the chambers be 1D; (iii) fluid be incompressible and Newtonian; (iv) resistive and capacitive effects be lumped when appropriate; (v) temperature effects be neglected; (vi) all solid elements be rigid.

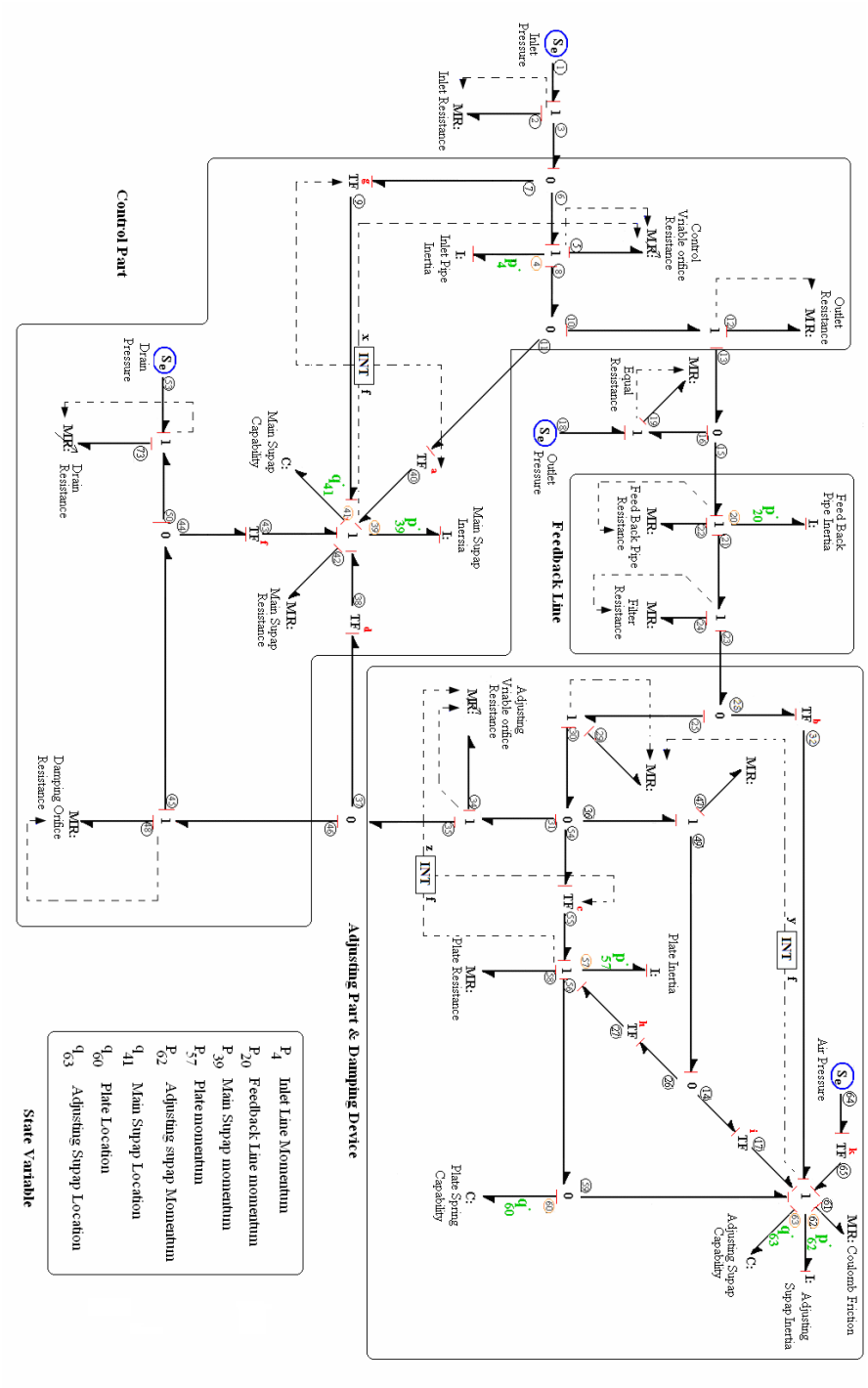

Fig. 4 BG model of the valve at Stage 5 of start period

Fig. 4 shows the overall BG model of the entire energy domain of the system at the final stage of the start period. Element S_{e1} represents the inlet pressure supplied to the valve from a stable source. Elements S_{e18}, S_{e53}, and S_{e64} denote, respectively, the stable sources of pressures in the valve outlet, drain outlet (19), and ambient pressure; all of which are equal to the atmospheric pressure P_{atm}. Bonds 39 and 41 denote the momentum p_{39} and position q_{41} of the control spool. By the same token, bonds 62 and 63 denote those, p_{62} and q_{63}, for the adjusting spool, and bonds 57 and 60, p_{57} and q_{60}, for the plate. Considering the causality of the extracted BG model, a total of eight state variables are defined for the entire system dynamics during the start period. These state variables will be gradually added into the system model as the energy domain of the system grows with the advancement of the filling stages.

Four intermediate BG models that lead to the evolvement of Fig. 4 are derived as follows. Each intermediate BG model describes one corresponding filling stage of the start period. Collectively, the five BG models form the overall analytical model of the system for the entire start period, and reveal the very essence of the system's internal dynamics when the system is progressing through the five stages defined in Section II.

A. Model of Stage 1:

Only the control part is being filled like a container while the other parts remain untouched. The energy distribution of this stage is shown in Fig. 5 with S_{e8} being P_{atm}. The one-DoF state equation with a single state variable, p_4 indicating the iterance flow momentum, for this stage is extracted from Fig. 5 as:

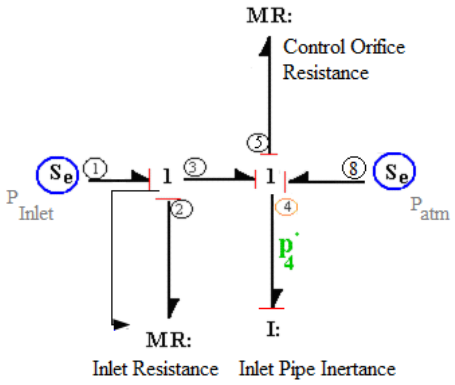

Fig. 5 BG model of the valve at Stage 1 of start period

$$\dot{p}_4 = S_{e1} - \frac{1}{I_4}(R_2 + R_5)p_4 - S_{e8} \tag{1}$$

B. Model of Stage 2:

As the pressure of the control part increases, a new state variable, p_{20} indicating the feedback flow momentum, is added to demonstrate the inertial behavior of the flow in the feedback pipe. The energy distribution of this stage is shown in Fig. 6 with S_{e25} being P_{atm}. The two-DoF state equation describing the system dynamics in this stage is derived from Fig. 6 as:

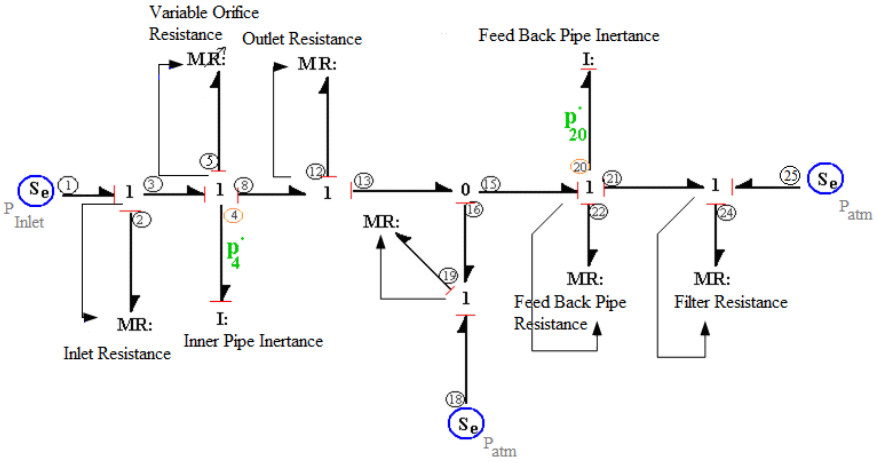

Fig. 6 BG model of the valve at Stage 2 of start period

$$\dot{p}_4 = S_{e1} - \frac{1}{I_4}(R_2 + R_5 + R_{12} - R_{19})p_4 - R_{19}\frac{p_{20}}{I_{20}} - S_{e18} \tag{2}$$

$$\dot{p}_{20} = R_{19}\left(\frac{p_4}{I_4} - \frac{p_{20}}{I_{20}}\right) - S_{e18} - (R_{22} + R_{24})\frac{p_{20}}{I_{20}} - S_{e25} \tag{3}$$

C. Model of Stage 3:

The hydraulic pressure in the filled adjusting zone increases and pushes the adjusting spool, while the plate located inside the adjusting spool keeps the adjusting orifice close. Three state variables, the momentum p_{62} and location q_{63} of the adjusting spool and the plate's location q_{60}, are added to represent the dynamics of the adjusting components. The energy distribution of this stage is shown in Fig. 7 with S_{e35} being P_{atm} and S_{f56} 0. Keeping Eq. (2) unchanged, the state equation of the system grows to five-DoF and is extracted from Fig. 7 as:

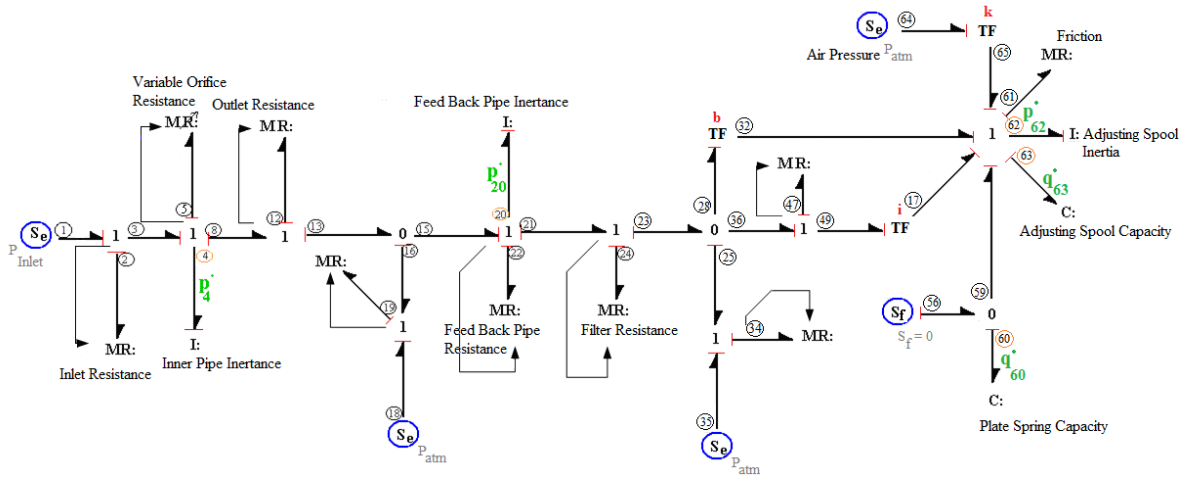

Fig. 7 BG model of the valve at Stage 3 of start period

$$\dot{p}_{20} = R_{19}\frac{p_4}{I_4} - S_{e18} + (R_{19} - R_{22} - R_{24} - R_{34})\frac{p_{20}}{I_{20}} - R_{34}(b+i)\frac{p_{62}}{I_{62}} - S_{e35} \tag{4}$$

$$\dot{p}_{62} = kS_{e64} + b\left(R_{34}\left(\frac{p_{20}}{I_{20}} - (b+i)\frac{p_{62}}{I_{62}}\right) - S_{e35}\right) + i\left(R_{34}\left(\frac{p_{20}}{I_{20}} - (b+i)\frac{p_{62}}{I_{62}}\right) - S_{e35} - R_{47}i\frac{p_{62}}{I_{62}}\right) + \frac{q_{60}}{C_{60}} - \frac{q_{63}}{C_{63}} \tag{5}$$

$$\dot{q}_{60} = S_{f56} - \frac{p_{62}}{I_{62}} \tag{6}$$

$$\dot{q}_{63} = \frac{p_{62}}{I_{62}} \tag{7}$$

D. Model of Stage 4:

The fluid fills the ppb, while the control spool is moving and creating a substantial effect on the valve dynamic performance via altering the dynamics of the adjusting area. The added state variables are p_{39}, q_{41}, and p_{57} which represent respectively the momentum and location of the control spool and the momentum of the plate. The energy distribution of this stage is shown in Fig. 8 with S_{e45} being P_{atm}. Keeping Eqs. (2) and (7) unchanged, the state equation of the system grows to eight-DoF and is derived from Fig. 8 as:

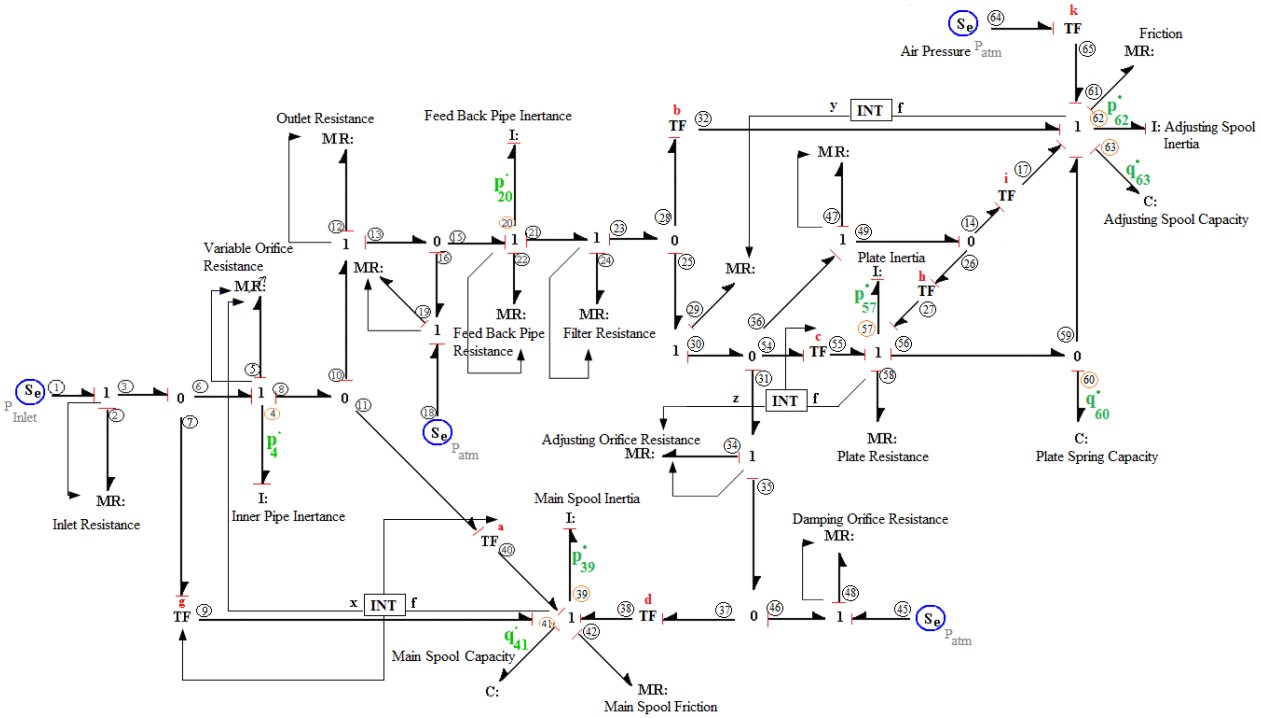

Fig. 8 BG model of the valve at Stage 4 of start period

$$\dot{p}_{20} = R_{19}\left(\frac{p_4}{I_4} - \frac{p_{20}}{I_{20}}\right) - S_{e18} - (R_{22} + R_{24})\frac{p_{20}}{I_{20}} + R_{29}\left(\frac{p_{20}}{I_{20}} - b\frac{p_{62}}{I_{62}}\right) + R_{34}\left(\frac{p_{20}}{I_{20}} - b\frac{p_{62}}{I_{62}} - c\frac{p_{57}}{I_{57}}\right) + R_{48}\left(\frac{p_{20}}{I_{20}} - b\frac{p_{62}}{I_{62}} - c\frac{p_{57}}{I_{57}} - d\frac{p_{39}}{I_{39}}\right) - S_{e45} \tag{8}$$

$$\dot{p}_{39} = a\left(R_{12}\left(\frac{p_4}{I_4} - a\frac{p_{39}}{I_{39}}\right) + R_{19}\left(\frac{p_4}{I_4} - a\frac{p_{39}}{I_{39}} - \frac{p_{20}}{I_{20}}\right) - S_{e18} + g\left(S_{e18} - R_2\left(g\frac{p_{39}}{I_{39}} + \frac{p_4}{I_4}\right)\right) + d\left(R_{48}\left(\frac{p_{20}}{I_{20}} - b\frac{p_{62}}{I_{62}} - c\frac{p_{57}}{I_{57}} - d\frac{p_{39}}{I_{39}}\right) - S_{e45}\right) - \frac{q_{41}}{C_{41}}\right) \tag{9}$$

$$\dot{p}_{57} = c\left(R_{34}\left(\frac{p_{20}}{I_{20}} - b\frac{p_{62}}{I_{62}} - c\frac{p_{57}}{I_{57}}\right) + R_{48}\left(\frac{p_{20}}{I_{20}} - b\frac{p_{62}}{I_{62}} - c\frac{p_{57}}{I_{57}} - d\frac{p_{39}}{I_{39}}\right) - S_{e45}\right) + h\left(R_{47}\left(i\frac{p_{62}}{I_{62}} + h\frac{p_{57}}{I_{57}}\right) + R_{34}\left(\frac{p_{20}}{I_{20}} - b\frac{p_{62}}{I_{62}} - c\frac{p_{57}}{I_{57}}\right) + R_{48}\left(\frac{p_{20}}{I_{20}} - b\frac{p_{62}}{I_{62}} - c\frac{p_{57}}{I_{57}} - d\frac{p_{39}}{I_{39}}\right) - S_{e45}\right) - \frac{q_{60}}{C_{60}}\right) \tag{10}$$

$$\dot{p}_{62} = kS_{e64} + b\left(R_{29}\left(\frac{p_{20}}{I_{20}} - b\frac{p_{62}}{I_{62}}\right) + R_{34}\left(\frac{p_{20}}{I_{20}} - b\frac{p_{62}}{I_{62}} - c\frac{p_{57}}{I_{57}}\right) + R_{48}\left(\frac{p_{20}}{I_{20}} - b\frac{p_{62}}{I_{62}} - c\frac{p_{57}}{I_{57}} - d\frac{p_{39}}{I_{39}}\right) - S_{e45}\right) + i\left(R_{47}\left(i\frac{p_{62}}{I_{62}} + h\frac{p_{57}}{I_{57}}\right) + R_{34}\left(\frac{p_{20}}{I_{20}} - b\frac{p_{62}}{I_{62}} - c\frac{p_{57}}{I_{57}}\right) + R_{48}\left(\frac{p_{20}}{I_{20}} - b\frac{p_{62}}{I_{62}} - c\frac{p_{57}}{I_{57}} - d\frac{p_{39}}{I_{39}}\right) - S_{e45}\right) + \frac{q_{60}}{C_{60}} - \frac{q_{63}}{C_{63}} \tag{11}$$

$$\dot{q}_{41} = \frac{p_{39}}{I_{39}} \tag{12}$$

$$\dot{q}_{60} = \frac{p_{57}}{I_{57}} - \frac{p_{62}}{I_{62}} \tag{13}$$

E. Model of Stage 5:

Upon filling the ppb, for the first time, the energy can be in contact with the entire geometry of valve at any instant of time. Fig. 4 demonstrates the energy distribution of this final stage. Although remaining as eight-DoF, the state equation is changed to include the effect of the stopping force on the control piston and the impact of the drain orifice on the internal flow of the adjusting part. Keeping Eqs. (2), (7), and (12)-(13) unchanged, a set of eight governing equations describing the system dynamics from this stage onwards is extracted from Fig. 4 as:

$$\dot{p}_{20} = R_{19}\left(\frac{p_4}{I_4} - \frac{p_{20}}{I_{20}}\right) - S_{e18} - (R_{22} + R_{24})\frac{p_{20}}{I_{20}} + R_{29}\left(\frac{p_{20}}{I_{20}} - b\frac{p_{62}}{I_{62}}\right) + R_{34}\left(\frac{p_{20}}{I_{20}} - b\frac{p_{62}}{I_{62}} - c\frac{p_{57}}{I_{57}}\right) + \tag{14}$$
$$R_{48}\left(\frac{p_{20}}{I_{20}} - b\frac{p_{62}}{I_{62}} - c\frac{p_{57}}{I_{57}} - d\frac{p_{39}}{I_{39}}\right) + R_{73}\left(\frac{p_{20}}{I_{20}} - b\frac{p_{62}}{I_{62}} - c\frac{p_{57}}{I_{57}} - d\frac{p_{39}}{I_{39}} - f\frac{p_{39}}{I_{39}}\right) - S_{e53}$$

$$\dot{p}_{39} = a(R_{12}\left(\frac{p_4}{I_4} - a\frac{p_{39}}{I_{39}}\right) + R_{19}\left(\frac{p_4}{I_4} - a\frac{p_{39}}{I_{39}} - \frac{p_{20}}{I_{20}}\right) - S_{e18} + g\left(S_{e18} - R_2\left(g\frac{p_{39}}{I_{39}} + \frac{p_4}{I_4}\right)\right) + \tag{15}$$
$$d\left(R_{48}\left(\frac{p_{20}}{I_{20}} - b\frac{p_{62}}{I_{62}} - c\frac{p_{57}}{I_{57}} - d\frac{p_{39}}{I_{39}}\right) + R_{73}\left(\frac{p_{20}}{I_{20}} - b\frac{p_{62}}{I_{62}} - c\frac{p_{57}}{I_{57}} - d\frac{p_{39}}{I_{39}} - f\frac{p_{39}}{I_{39}}\right) - S_{e53}\right) - \frac{q_{41}}{C_{41}}$$

$$\dot{p}_{57} = c\left(R_{34}\left(\frac{p_{20}}{I_{20}} - b\frac{p_{62}}{I_{62}} - c\frac{p_{57}}{I_{57}}\right) + R_{48}\left(\frac{p_{20}}{I_{20}} - b\frac{p_{62}}{I_{62}} - c\frac{p_{57}}{I_{57}} - d\frac{p_{39}}{I_{39}}\right) + R_{73}\left(\frac{p_{20}}{I_{20}} - b\frac{p_{62}}{I_{62}} - c\frac{p_{57}}{I_{57}} - \right.\right. \tag{16}$$
$$\left.\left. d\frac{p_{39}}{I_{39}} - f\frac{p_{39}}{I_{39}}\right) - S_{e53}\right) + h\left(R_{47}\left(i\frac{p_{62}}{I_{62}} + h\frac{p_{57}}{I_{57}}\right) + R_{34}\left(\frac{p_{20}}{I_{20}} - b\frac{p_{62}}{I_{62}} - c\frac{p_{57}}{I_{57}}\right) + R_{48}\left(\frac{p_{20}}{I_{20}} - b\frac{p_{62}}{I_{62}} - c\frac{p_{57}}{I_{57}} - \right.\right.$$
$$\left.\left. d\frac{p_{39}}{I_{39}}\right) + R_{73}\left(\frac{p_{20}}{I_{20}} - b\frac{p_{62}}{I_{62}} - c\frac{p_{57}}{I_{57}} - d\frac{p_{39}}{I_{39}} - f\frac{p_{39}}{I_{39}}\right) - S_{e53}\right) + f(R_{73}\left(\frac{p_{20}}{I_{20}} - b\frac{p_{62}}{I_{62}} - c\frac{p_{57}}{I_{57}} - d\frac{p_{39}}{I_{39}} - \right.$$
$$\left. f\frac{p_{39}}{I_{39}}\right) - S_{e53}) - \frac{q_{60}}{C_{60}}$$

$$\dot{p}_{62} = kS_{e64} + b\left(R_{29}\left(\frac{p_{20}}{I_{20}} - b\frac{p_{62}}{I_{62}}\right) + R_{34}\left(\frac{p_{20}}{I_{20}} - b\frac{p_{62}}{I_{62}} - c\frac{p_{57}}{I_{57}}\right) + R_{48}\left(\frac{p_{20}}{I_{20}} - b\frac{p_{62}}{I_{62}} - c\frac{p_{57}}{I_{57}} - d\frac{p_{39}}{I_{39}}\right) + \tag{17}$$
$$R_{73}\left(\frac{p_{20}}{I_{20}} - b\frac{p_{62}}{I_{62}} - c\frac{p_{57}}{I_{57}} - d\frac{p_{39}}{I_{39}} - f\frac{p_{39}}{I_{39}}\right) - S_{e53}\right) + i\left(R_{47}\left(i\frac{p_{62}}{I_{62}} + h\frac{p_{57}}{I_{57}}\right) + R_{34}\left(\frac{p_{20}}{I_{20}} - b\frac{p_{62}}{I_{62}} - c\frac{p_{57}}{I_{57}}\right) + \right.$$
$$\left. R_{48}\left(\frac{p_{20}}{I_{20}} - b\frac{p_{62}}{I_{62}} - c\frac{p_{57}}{I_{57}} - d\frac{p_{39}}{I_{39}}\right) + R_{73}\left(\frac{p_{20}}{I_{20}} - b\frac{p_{62}}{I_{62}} - c\frac{p_{57}}{I_{57}} - d\frac{p_{39}}{I_{39}} - f\frac{p_{39}}{I_{39}}\right) - S_{e53}\right) + \frac{q_{60}}{C_{60}} - \frac{q_{63}}{C_{63}}$$

F. System Parameters:

Although the governing equations derived for each of the five stages have been shown in a linear format, the nature of the physical system is in fact nonlinear and represented by the so-called parameters of the equations that are typical energy elements: R_i, C_i, and I_i, representing

respectively the resistivity, capacity, and inertia of the system. For the chosen valve, although all C_i and I_i are constant and pre-determined (assuming incompressibility of the fluid and rigidity of the internal components), many R_i are time-varying and need to be updated at each time step. This is because the main nonlinearity of the system is related to the energy dissipation. Since the calculation of dissipated energy for a resistive element does not depend on the energy distribution history of the system, the values of R_i at each time step can be updated via the known values of the state variables and the boundary inputs of the system at that step. The updated R_i are then used in the governing equations to calculate the values of the state variables at the next time step. This way of presenting the state-space models of the system keeps the simplicity of the model structure while preserving the true physical meaning of the system during the entire solution process.

Apart from R_{42}, R_{61}, and R_{58} that represent respectively the constant frictions of the control spool, adjusting spool, and plate, the rest of the dissipative elements are hydraulic and can be obtained as follows:

$$R_i = \rho\left|\dot{Q}_i\right|\xi(A_{hi}) \quad (i = 2, 5, 12, 19, 22, 24, 29, 34, 48, 57, 73) \tag{18}$$

$$\xi\left(A_{h_i}\right) = \frac{\sum \zeta_{l_i} + \zeta_{f_i}}{2{A_{h_i}}^2} \tag{19}$$

where ρ, $\dot{Q}_i$, A_{h_i}, ζ_{l_i}, and ζ_{f_i} denote respectively the fluid density, volumetric flow rate, hydraulic cross section area, pre-determined local pressure loss coefficient, and pre-determined friction coefficient of the element. All volumetric flow rates, $\dot{Q}_i$, are algebraically calculated at each time step using the current values of the state variables in the related BG model, and the calculations are not included here for brevity.

The hydraulic cross section area, A_{h_i}, in (18) depends on the wet boundary of the corresponding cavities. For fixed cavities, it is a pre-determined constant parameter. For variable cavities, it must be calculated as:

$$A_{hms} = \frac{\pi}{4sin\alpha}({D^2}_{inms} - {X^2}_h sin^2 2\alpha), \;\; X_h = \acute{X} + x \tag{20}$$

$$A_{hcs} = \frac{\pi}{8sin\beta}({D^2}_{incs} - {Y^2}_h sin^2 2\beta), \;\; Y_h = \acute{Y} - y \tag{21}$$

$$A_{hcp} = \pi D_{hcp} z \tag{22}$$

where A_{hms}, A_{hcs}, and A_{hcp} are respectively the hydraulic cross section areas of R_5, R_{29}, and R_{34}. Constants α and β are the angles of attack of the control spool and adjusting spool, respectively. Constants D_{inms}, D_{incs}, and D_{hcp} are the internal diameters of the control spool, adjusting spool, and plate, respectively. Variables X_h and Y_h are the geometrical parameters attainable from the geometry of the orifice and the angle of attack of the spool with respect to the positions of the control spool and adjusting spool, respectively, with X' and Y' being the offsets obtained from the initial locations of the corresponding spools. The instantaneous locations of the control spool, adjusting spool, and plate are expressed by x, y, and z, respectively, and are calculated from the state variables as:

$$x(t) = \frac{1}{I_{39}} \int p_{39} dt \,;\; y(t) = \frac{1}{I_{39}} \int p_{62} dt \,;\; z(t) = \frac{1}{I_{39}} \int p_{57} dt \tag{23}$$

Parameters a, b, …, and i shown in the governing equations are the energy transformer coefficients indicating the pressure surfaces by which the hydraulic energy can be transferred into the mechanical domain and vice versa. For fixed cavities, these coefficients are equal to their respective known contact areas. For variable cavities, a and g will need to be derived as follows:

$$a = \frac{\pi}{4}\left(D_{tms}^2 - D_{ms}^2 - D_{fms}^2\right);\; g = \frac{\pi}{4} D_{fms}^2; D_{fms} = \sqrt{X_h^2 \sin^2(2\alpha)} \tag{24}$$

where D_{tms} and D_{ms} are the diameters of the control spool tip and beam, respectively.

G. Switching Functions:

To allow automatic switch of the five models from one stage to the next, switching functions are developed. A volumetric threshold, $V_i(t)$, representing the filled volume of the respective zone (signified by index, i) at each time step, is thus considered for each of the filling stages. Given the incompressibility of the fluid, for the fixed-geometry (control and adjusting) zones, $V_i(t)$ is calculated from the integration of the respective volumetric flow rate during the corresponding stage. For the variable-geometry (ppb) zone, the calculation of $V_i(t)$ takes the movement of the internal component into account in addition to the integration of the volumetric flow rate. The definitions of $V_i(t)$ for each of the considered zones are then expressed as:

$$\dot{V}_{Control\ Zone} = \frac{1}{I_4} p_4 \tag{25}$$

$$\dot{V}_{Adjusting\ Zone} = \frac{1}{I_{20}} p_{20} \tag{26}$$

$$\dot{V}_{ppb} = \frac{p_{20}}{I_{20}} - (b+i)\frac{p_{62}}{I_{62}} - (c+h)\frac{p_{57}}{I_{57}} - d\frac{p_{39}}{I_{39}} \tag{27}$$

Accordingly, four switching functions are formulated as:

$$Stage\ 1\ Switch = \begin{cases} 0 & \int \dot{V}(t)_{Control\ Zone} dt < V_{CZ} \\ 1 & else \end{cases} \tag{28}$$

$$Stage\ 2\ Switch = \begin{cases} 0 & \int \dot{V}(t)_{Adjusting\ Zone} dt < V_{AZ} \\ 1 & else \end{cases} \tag{29}$$

$$Stage\ 3\ Switch = \begin{cases} 0 & \int \dot{z}(t) dt < z_{ini} \\ 1 & else \end{cases} \tag{30}$$

$$Stage\ 4\ Switch = \begin{cases} 0 & \int \dot{V}(t)_{ppb} dt < (V_{PZ} - x(t)d) \\ 1 & else \end{cases} \tag{31}$$

where V_{CZ}, V_{AZ}, and V_{PZ} are the pre-determined geometrical volumes of the control zone, adjusting zone, and ppb, respectively, and $\dot{z}(t)$ and z_{ini} are the velocity and initial location of the plate, respectively.

4. Simulation results

The BG models developed for the chosen valve are validated via simulation. Physical constraints, such as component inter-domain barriers and coulomb friction, are added to the software using subprograms that include the calculation of the various parameter auxiliary equations. The subprograms regenerate the component accelerations with respect to their frictional forces obtained from R_{42}, R_{61}, and R_{58} at each time step, using the amplitude and direction of the force and velocity of the spools alongside the spools' locations. They predict possible collisions between the spools and the body using the moving components' locations and accelerations, and transmit a signal to the integral part of the main program to reset the initial condition when a possible collision is detected. The main program can thus determine when and where a possible collision may occur.

A simplified inlet pressure profile shown in Fig. 9 is used to mimic the valve input pressure change during field tests. The corresponding system dynamics for the entire start period are

presented in Figs. 10-20, where some of the curves are shown in dimensionless form as the range of the pressure difference for the chosen valve is too large. The designated five time intervals in seconds that correspond to the five stages of the start period are found to be: [0 0.0445), (0.0445 0.1265), (0.1265 0.1763), (0.1763 0.749), and (0.749 1.5]. After 1.5 s, the system completes its start period and enters into the nominal operation.

As shown in Fig. 9, after receiving the start signal, the inlet pressure starts to increase, and the flow begins to fill the control part. Fig. 10 shows the effect of the flow inertia during Stage 1. Continuously, the flow finds its way to the feedback pipe and adjusting zone. In Fig. 11, when the adjusting zone is completely filled, the flow rate in the feedback pipe suddenly stops as the adjusting orifice is still closed. Fig. 12 shows the pressure changes inside the valve during Stage 2, where the pressure jumps in P_{out} and P_{adj} are due to the fluid inertia inside the feedback pipe when the flow faces the closed end.

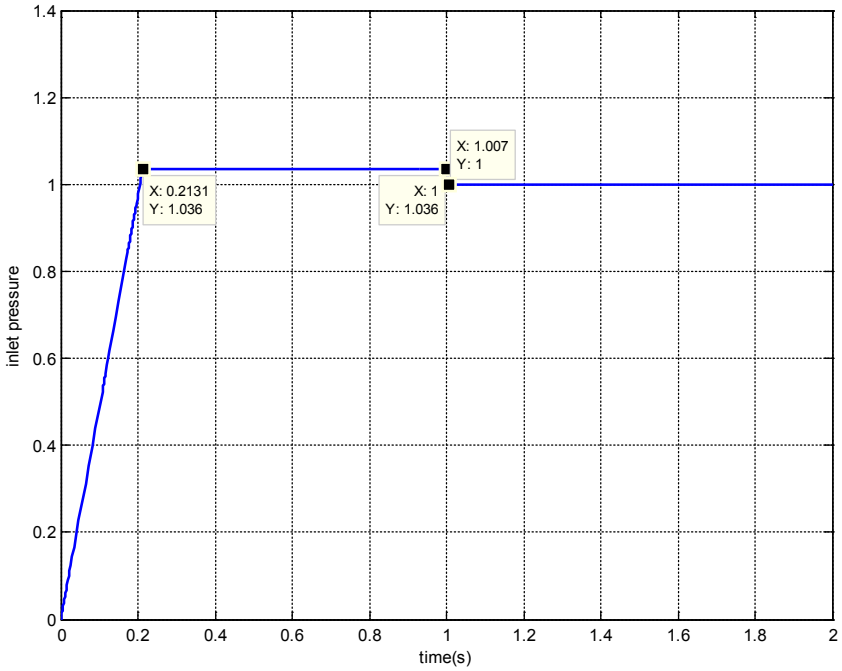

Fig. 9 Suggested inlet flow pressure during entire start period

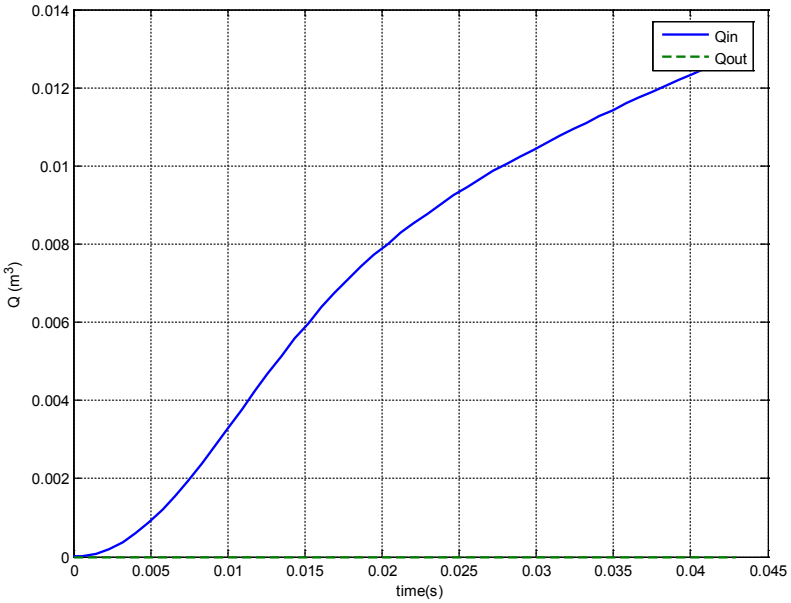

Fig. 10 Inlet and outlet flows to and from the valve at Stage 1

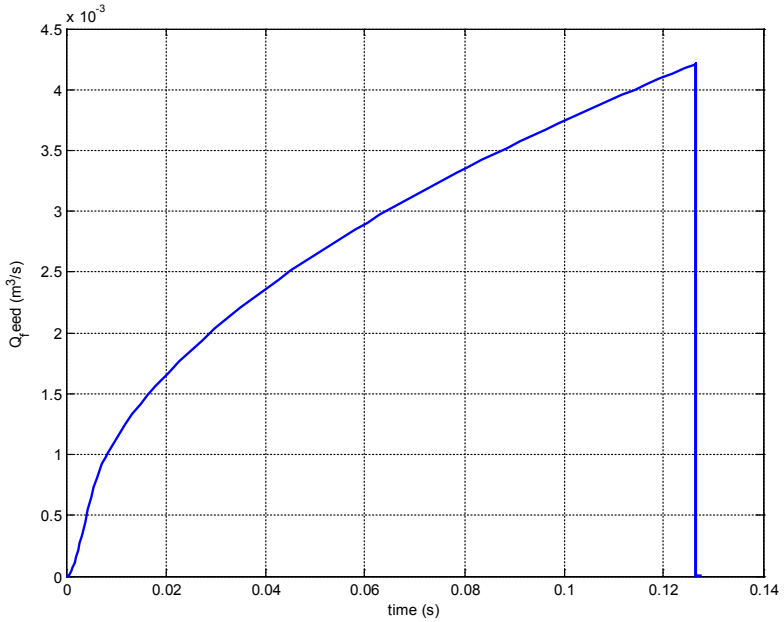

Fig. 11 Feedback flow rate at Stage 2 of start period

In Fig. 13, increasing the pressure in the adjusting zone leads to the increase of the hydraulic force on the tip of the adjusting spool. Fig. 14 shows that when the hydraulic force meets the pre-adjusting force, the adjusting spool starts to move to open the adjusting orifice (y). But, the pre-pressurization of the plate via springs under the plate still pushes the plate to the adjusting orifice

to keep the passageway blocked. As the pressure rise continues, the hooks of the tip of the adjusting spool take the plate up from its seating potion (z) to allow the flow to fill the ppf and to increase the ppf pressure in Stage 3.

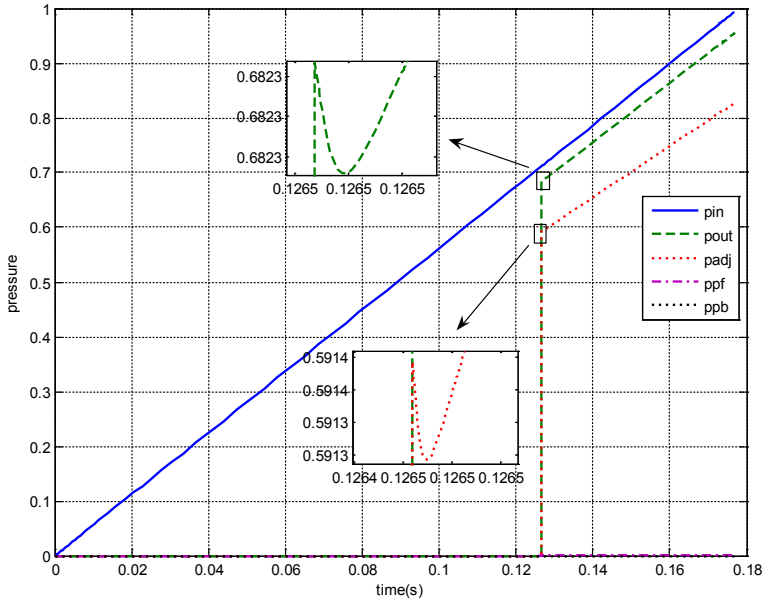

Fig. 12 Variations of internal pressures of the valve at Stage 2

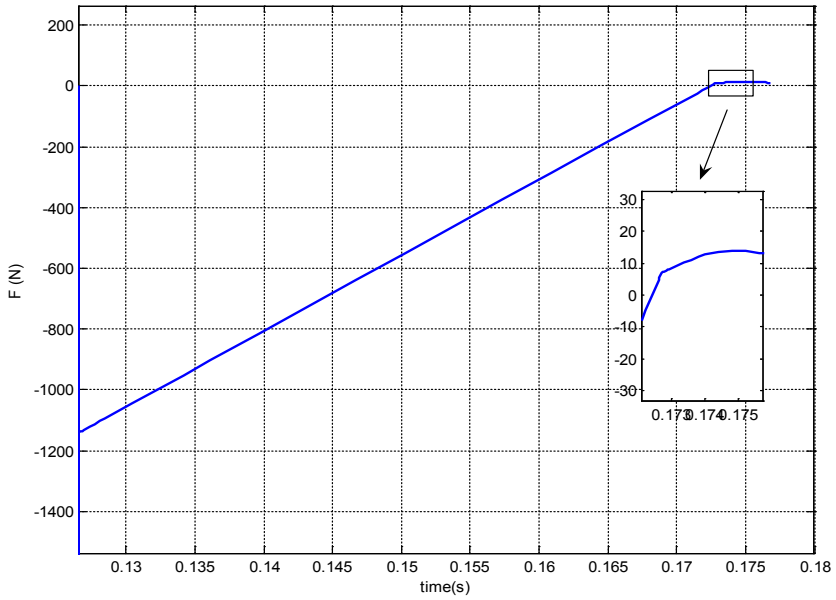

Fig. 13 Variation of force on adjusting spool in Stage 3

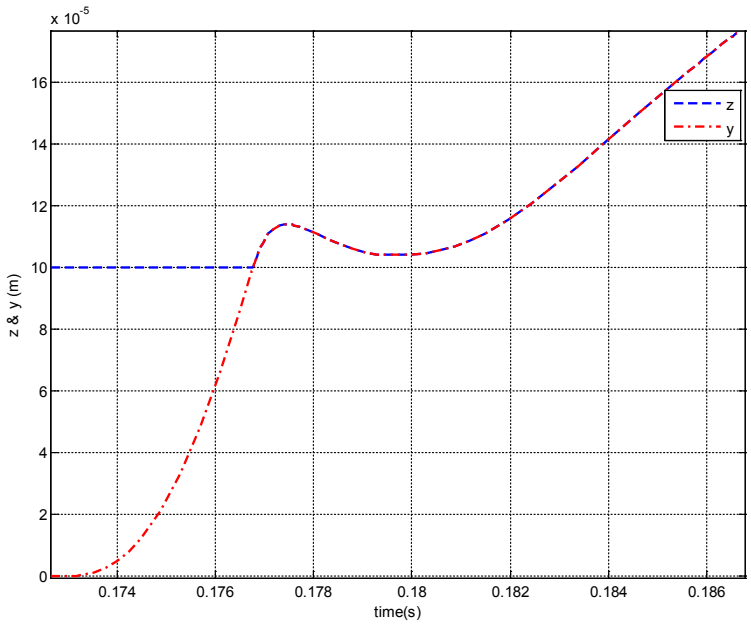

Fig. 14 Movements of adjusting spool (y) and placid (z) in Stage 3

Fig. 15 shows that the pressure accumulation in the ppf causes the control spool to move through to narrow the control orifice (x). In Fig. 16, the movement of the control piston decreases the volume of the ppb while the flow passing the piston's damping orifice keeps filling the variable volume of the ppb.

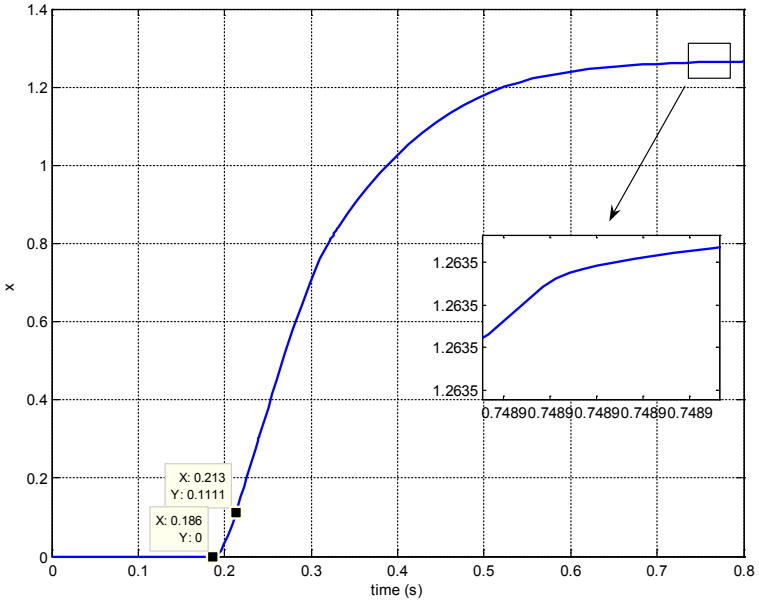

Fig. 15 Control spool movement in Stage 4

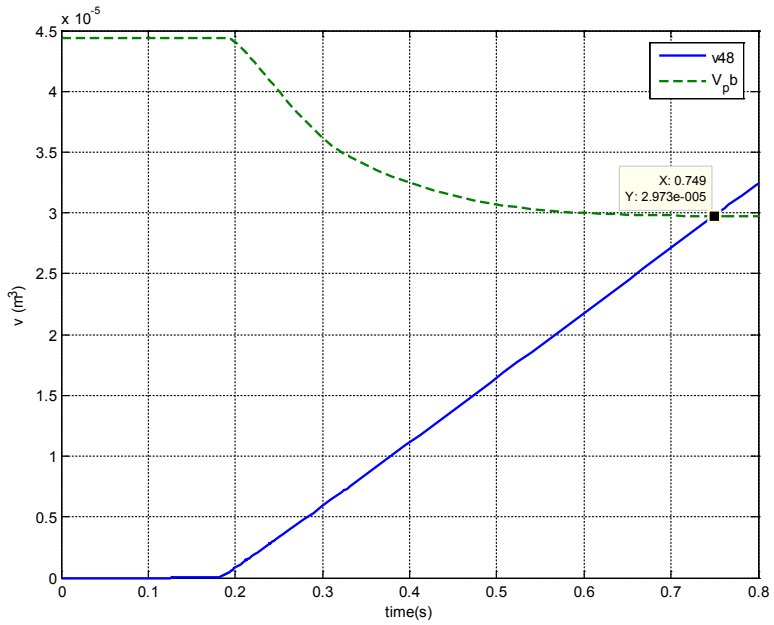

Fig. 16 Filling of ppb in Stage 4 of start period

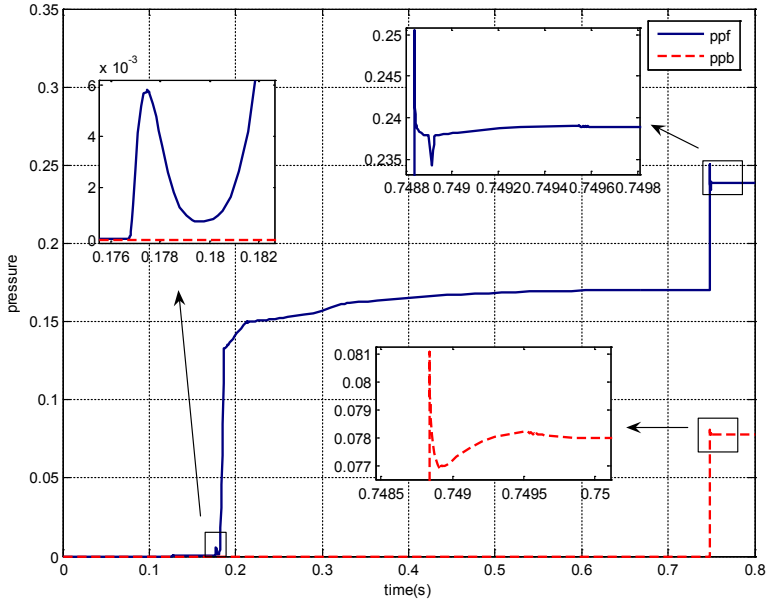

Fig. 17 Pressure changes in ppf and ppb in Stage 4 of start period

Fig. 17 illustrates the pressure changes for both sides of the control piston up to Stage 4. It shows that after opening the adjusting orifice, the ppf pressure increases, resulting in the movement of the control spool that in turn decreases the ppf pressure rise. Finally, sudden pressure rises in

both the ppf and the ppb occur when the last empty part of the valve is filled, which symbolizes the end of the filling process.

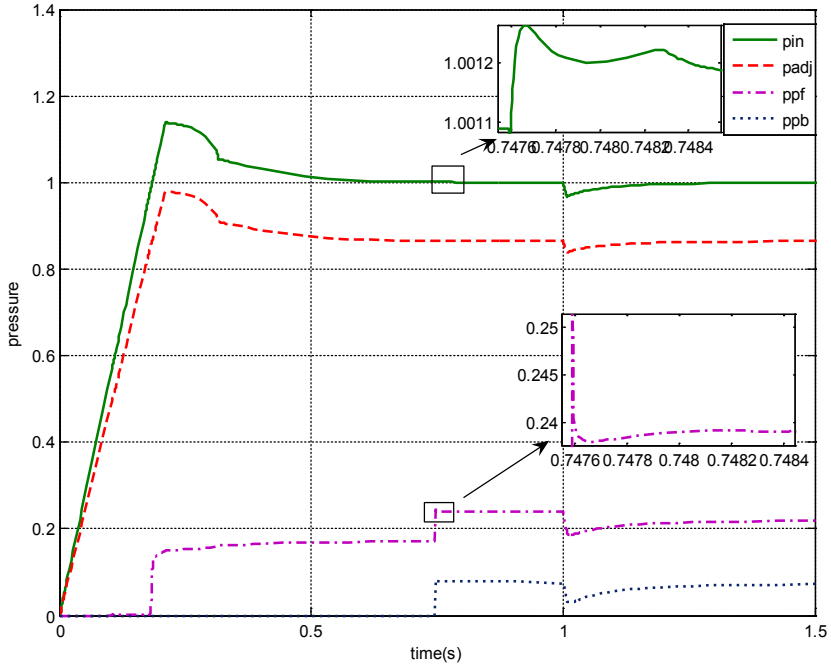

Fig. 18 Pressure behavior of the system during entire start period

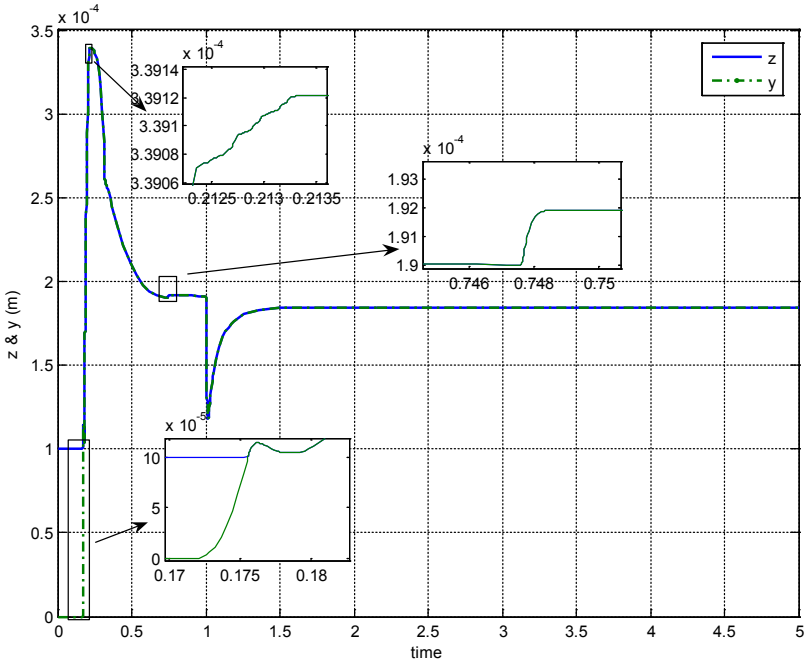

Fig. 19 Movement of adjusting part during entire start period

As shown in Fig. 18, by moving the control spool, the system starts to regulate the outlet pressure in Stage 5. The pressure drop in P_{adj} is a direct result of the control spool movement. The

effect of the ppb filling completion is observed at 0.749 s where the pressure of the control zone faces a minor jump.

Fig. 19 shows the movements of the adjusting spool and plate during the entire start period. At the beginning, these elements move to nearly the end of their stroke at 0.35 mm resulting in a pressure loss inside the adjusting zone. The adjusting spool then comes back to the middle stroke. The effect of the ppb filling completion is visible from the adjusting element's performance which at t = 1 s corresponds to the negative step change in Fig. 9. The pressure drop due to the negative step change is sensed via the adjusting element, causing the adjusting spool to move towards narrowing the adjusting orifice. The pressure loss then increases, and the ppf pressure decreases (Fig. 18). This makes the control spool moving backward to open the control orifice. As shown in Fig. 19, the pressure loss of the valve is decreased, which leads to the compensation of the inlet pressure drop.

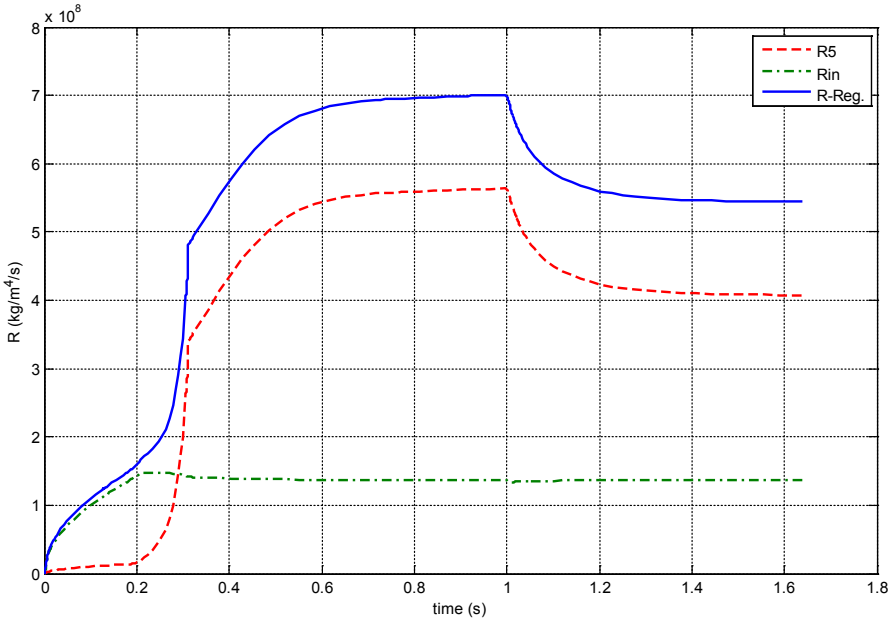

Fig. 20 Regulator hydraulic resistance during entire start period

Fig. 20 shows the profile of the regulator hydraulic resistance during the entire start period. The amount of this resistance is the control signal for the entire engine. Clearly, during the start period, the controller can change the dynamics of the system in a way that may not be desirable. A special attention can thus be drawn from this finding if the valve needs to be redesigned.

5. Conclusion

The modeling of the start period for hydro-mechanical control devices is investigated in this study. A new multi-model BG approach that can provide essential insights into the multi-physical dynamic behaviors of the control devices during the start period is proposed. A nonlinear, varying-DoF, state-space model is developed for a typical pressure regulator during its start period, and tested using a standard start command. The simulation results reveal a high-degree of complexity of the system's physical behaviors during the start period, which may otherwise be overlooked by other conventional modeling methods. The revealed physical behaviors are fully agreeable with the fundamental physics underpinning the multi-physical dynamics of the system during this period, which confirms the integrity of the resulting nonlinear model of the system.

From the insight provided by the proposed model, possible internal collisions or sever performance degradations of the system components during the start period can be predicted, and measures of preventions can be taken. The proposed modeling technique is thus seen to enable a better design of the system components and a safer operation of the system.

The essential feature of the proposed multi-model BG approach lies in its ability to vividly reveal, through the use of a growing number of state variables in the system governing equations, the physical details of the system while the system progressively completes its initial transient towards a nominal operation. It is this distinctive feature of the proposed approach that makes the modeling of the complex start period of the system feasible. The proposed approach can be applied to other similar control devices to enhance the reliability of the systems.

References

[1] H. karimi, A. Nassirharand, A. Zanj, Integration of modeling and simulation of warm pressurization and feed systems of liquid propulsion systems, Acta Astronautica J., 69(5–6), 2011, 258–265.

[2] A. Zanj, A. Kalabkhani,M.A. Abdous, and H. Karimi, Modeling, simulation, and optimization of a hot pressurization system for a liquid propellant space engine and comparing with experimental results, IMechE, Part G, J. of Aerospace Engineering, 224(10), 2010, 1141-1150.

[3] J. Watton, The design of a single-stage relief valve with directional damping, J. of Fluid Control Including Fluidics, 18(2), 1988, 22–35.

[4] C.Y. Chin, Static and dynamic characteristics of a two stage pilot relief valve, ASME Dyn. Sys. Measurements and Controls, 113, 1991, 280–288.

[5] D.C. Karnopp, R.C. Rosenburg, System Dynamics: A Unified Approach, Wiley Inter sciences, 1975.

[6] D.C. Karnopp, D.L. Margolis, R.C. Rosenburg, System Dynamics–Modeling and Simulation of Mechatronic Systems, John Wiley & Sons, 2000.

[7] W. Borutzky, A dynamic Bond graph model of the fluid mechanical interaction in spool valve control orifice, in: Bond graphs for Engineers, North Holland, 1992, 229–236.

[8] K. Dasgupta, J. Watton, Dynamic analysis of proportional solenoid controlled piloted relief valve by Bondgraph, J. of Simulation, Modeling, Practice and Theory, 13, 2005, 21–38.

[9] P.S. Zung, M.H. Perng, Nonlinear dynamic model of a two-stage pressure relief valve for designers, ASME, Dynamic, Systems, Measurements and Controls, 124, 2002, 62–66.

[10] R. Maiti, R. Saha, J. Watton, The static and dynamic characteristics of a pressure relief valve with a proportional solenoid-controlled pilot stage, IMechE, Part I, J. of System and Control Engineering, 216, 2002, 143–156.

[11] H. Afshari, A. Zanj, A. B. Noninzadeh, Dynamic Analysis of a Nonlinear Pressure Regulator Using Bondgraph Simulation Technique, J. of Simulation Modeling Practice and Theory, 18(2), 2010, 240-252.

[12] A. zanj, H. Afshari, Dynamic Analysis of a Complex Pneumatic Valve Using Pseudo-Bond Graph Modeling Technique, J. of Dynamic Systems, Measurement, and Control, 135(3), 2013, 250-259.

[13] A. Zanj, H. Karimi, A.J. Gholi, M. Shafiee, Dynamic Modeling of Indirect Hydro-Control Valve - Bondgraph Approach, J. of Simulation, Modeling, Practice and Theory, 28, 2012, 65-80.

CHAPTER 3: DOMAIN-INDEPENDENT MODELING OF SOLID FIELD'S SUBDOMAINS

Aim

The aim of this chapter is to generate a domain-independent nonlinear model of the involving physical subdomains of the solid field using the presented method in Chapter 2.

Description

To achieve this aim, sequentially, the energetic components of the elastic and thermal subdomains are defined for a simple geometry, the general behavior of each subdomain is generated from the reversible and irreversible interactions of the energetic components. The outcomes of this procedure are released in two papers:

In the first paper, highlighting the thermoelastic phenomena and the related problems in the solid field, the energy-based model of the elastic domain (which includes potential and kinetic subdomains) is first developed for a simple geometry. Then, a unique thermal effort and a novel modulated capacitor are derived for use in the proposed model to address the true physical causality behind the dilation behavior and the temperature dependency of material stiffness. The outline of this paper is organized as follows:

In the second paper, to model the thermal subdomain a novel domain-independent conduction model compatible for multi-physical system dynamic investigations is suggested. By means of BG method, a classical nonlinear conduction model containing physical states is first represented. A compatible discrete configuration of the thermal domain in line with the generated elastic domain is then developed through the enhancement of the configuration of the conventional thermal element. The outline of this paper is organized as follows:

Results

The obtained results from the above two papers indicate that the proposed models can effectively fill the gap between the conventional modeling techniques and the physical nature of the thermomechanical phenomena via the use of the BG methodology.

Conclusion

Overall, by means of the generated models, separate energy lines for the involving subdomains of the solid field (elastic and thermal subdomain) are generated with which a decomposed power distribution of the system with respect to each of the subdomains becomes obtainable.

ENERGY-BASED THERMO-MECHANICAL DISCRETE MODEL: BOND GRAPH APPROACH

Amir Zanj* & Fangpo He
Advanced Control Systems Research Group, School of Computer Science, Engineering & Mathematics, Flinders University, Adelaide, Australia, (e-mail: amir.zanj@flinders.edu.au)

Abstract

Thermomechanical phenomena in control devices if not addressed properly can be a source of inaccuracy. The resultant entangled dynamic behavior in pneumo-hydro-control systems has always been a challenging issue for the design of such devices. This indicates a gap between the conventional modeling techniques and the physical nature of the thermomechanical phenomena. In this paper, an enhanced thermomechanical model is proposed for a spool valve that can effectively fill this gap via the use of the Bond graph methodology. A unique thermal effort and a novel modulated capacitor are derived for use in the proposed model to address the true physics behind the dilation behavior and the temperature dependency of material stiffness. The obtained results demonstrate the ability of the proposed model to dynamically capture the thermomechanical phenomena, and indicate the significance of these undesired dynamics in affecting the performance of the system.

Keywords- Control device, thermoelastic phenomena, noise detection, Bond graph modeling, dynamic analysis, lumped modeling.

1. Introduction

Hydraulic and pneumatic control devices are such systems in which lack of attention to the internal thermomechanical phenomena may lead to an irreparable destiny of the devices. Thermal expansion may change the operational set-points of these devices on the one hand, and on the other hand material softening induced by temperature rise may alter the response modes of the systems. These thermomechanical behaviors in a typical liquid engine system can be fatal, as they may cause the propagation of a harmful disturbance in the engine's hydraulic circuit and put the system into an unstable situation leading to a deadly failure [1] [2].

Frequently, it is observed that during the operation of a control valve, thermal dilation of the valve's internal components (spools) can add an entangled dynamic to the total behavior of the system. Depending on the magnitude of the temperature and the velocity of the internal flow, the heat exchange occurring between the flow and the valve internal spools can result in shrinking or

expanding of these components. This entangled thermomechanical dynamic can cause the alteration of the control parameters especially the set-point of the system by changing the size of the control cavity inside the control valve. Furthermore, it is observed that heating or cooling can change the behavior of the valve under cyclic loading. Dilation of a structure often coexists with alteration of the structure material properties including stiffness. In this circumstance, depending on the level of the existing aero-hydro load on the internal spools, the existing turbulent frequency of the internal flow can be transmitted into the spool structure. This unpredicted internal noise can cause an inevitable fatal effect especially on the transient performance of the system, which may make the system unstable and destine to an unwanted failure. It is therefore important to understand the internal thermomechanical phenomena of the system and to model the multi-physical interactive structural-dilation and property-alternation behaviors as a part of the essential dynamics of the system for a successful operation of the system.

The common approach to investigate the thermomechanical phenomena inside a structure is via the Finite Element Methods (FEM). Odon and Kross [3] presented a complete review of the general concept on solving coupled thermoelasticity problems using FEM. In these methods, the main aim is to capture the phenomena as accurate as possible, however, in doing so, the time cost for generating the models is tremendously high. In addition, the models thus generated may not be desirable for control aspects, as they are fundamentally numerical and extremely higher-order in nature. A desirable modeling technique for use in control context is often required to be able to produce analytical and lower-order models within realistic timeframes (particularly if the models are used in real-time circumstances), and the ensuing models, apart from being able to catch the inherent dynamic behaviors of the systems of concern, must be easy to be used for the derivation of the control laws. The FEM results, however, naturally fail in these respects.

The transfer function approach [4] [5] has been seen to be able to generate likable models for control aspects. Although this approach is capable of capturing the dynamic behavior of a system to a certain degree within a narrow operating point, the inherent linearization process of the approach makes it unsuitable for highly-nonlinear systems that possess integrative dynamics in multi-physical domain settings. In particular, this approach is unable to produce models that can reflect the true physical meaning of the underlining thermomechanical phenomena when, for example, the subsequent thermal expansion behavior is a result of the interactions between the

elastic and thermal subdomains. To represent such dynamics, the model of the system is required to be closely related to the system's subdomain structures and parameters, as well as the nonlinear interactions between the various subdomains of concern.

The Bond graph (BG) technique that is based on energy flow exchange [6] [7] [8] is, subsequently, considered to be a suitable approach for modeling interactive dynamics in multi-physical domain settings. Using a diagram-based tool, the BG approach directly describes a physical system in the system's subdomain settings and predicts the corresponding dynamic behavior of the system across all subdomains of concern [9] [10]. In this approach, the model of the entire system is constructed from its subdomain models that are interconnected according to the conservation of energy and power exchange [11]. Models obtained in such a way are proven to be reusable, extendible, and physical in describing complex multiple-domain interactive dynamics of the systems [12].

Several studies on using the BG technique to model control valves' dynamics have been reported in the literature [13] [14] [15]. In these studies, to avoid the complications in revealing the valves' thermomechanical phenomena, a rigid-spool assumption is adopted. Although the resultant analytical nonlinear models can cover a wide range of dynamics of the multi-physical systems, the models are inherently invalid when the rigid-spool assumption is violated in real-life scenarios where thermomechanical interactions have direct effects on the rigidity of the spools. Using these models to design the control valves under (especially, high-frequency) thermomechanical loadings will inevitably make the devices vulnerable in passing through the operational frequencies and, thus, unreliable in real-time operations. The rigid-spool assumption must therefore be abolished.

In this paper, an elasto-expansive model of the spools is proposed to be incorporated into the existing BG models of the valves to make them capable of controlling the thermomechanical phenomena of the systems. The new thermoelstic model of the spool will address the coupled effects of structural expansion and material softening inside the spool, and provide desirable physical insights into the interactive dynamics that would, otherwise, be overlooked by existing comparable counterparts. The remainder of the paper is organized as follows. In Section 2, by means of the BG methodology, a distributed elastic model of the spool structure is first generated, and possible additions or alterations to the model for capturing the fundamental thermomechanical

phenomena of the spool are identified. In Section 3, to capture the effect of structural expansion, a thermal effort that represents the dynamics of dilations is proposed and added to the elastic model as an equivalent thermal load. In Section 4, to capture the effect of material softening, a new modulated storage element that reflects temperature-induced elasticity changes is developed and used to replace the tradition constant storage element in the elastic model. A new thermoelastic BG model of the spool, together with a new set of governing equations that takes the overall thermomechanical phenomena of the spool into account, is then presented in Section 5. The validity of the proposed spool model is assessed via simulation in Section 6. Concluding remarks regarding the model's usefulness in fault detection and control strategy development are given in Section 7.

2. Elastic spool Bond graph modeling

According to the geometry of the spool in a control device, the spool can be considered in the category of beam members. To investigate their internal dynamics, these beam members can be presented as distributed parameter systems governed by partial differential equations and lumped in space for finite approximations [16]. This discrete-lumped configuration is deemed to be suitable for deriving the thermoelastic model of the spool, as the internal interactions between the thermal and elastic subdomains of the spool are indeed distributed while the overall structure of the spool can be discretely formed by lumped elements. The resulting model of the spool will possess both numerical and analytical characteristics in describing the inherent multi-physical dynamics of the system. The BG method that can effectively describe both lumped and distributed parameter systems is chosen as the modeling tool for the beam-like axial spool structure. Unlike the other numerical methods, the BG method does not impose any approximations in the lumping techniques, and can fully represent the discrete numerical structure of the spool in a systematic way [7].

Fig. 1 shows a simplified Rayleigh reticulation of a simple beam structure. In this discrete space, using the acoustic assumption [17], each configured element is represented by two types of storage components, capacitor and inertia, that can store the potential energy and kinetic energy, respectively. Within each configured element of Fig. 1, the inertia component is considered to be distributed at both ends of the element on the boundary, whereas the capacitor component is assumed to be at the center of the element. This simply means that the potential energy of the

reticulated space can be stored at the center of each element, whereas the kinetic energy of the reticulated space is stored at the boundary of each element. Since the presented reticulated space is indeed continuous, the boundaries of any two adjacent elements are bonded to move together. Therefore, one can consider the discrete configuration of Fig. 1 as a junction-element chain in which the parameters of a junction between two adjacent elements are expressed as weighted functions of the related parameters of these two elements.

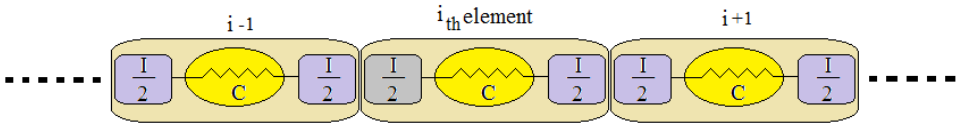

Fig. 1. 1D beam reticulation

The resultant BG model of the discrete beam of Fig. 1 is shown in Fig. 2. The state variables for the i_{th} element and the j_{th} junction are q_i and p_j which denote the deformation of the i_{th} element and the momentum of the j_{th} junction, respectively. According to the conservation of energy, the state equation for each junction-element is derived from Fig. 2 as:

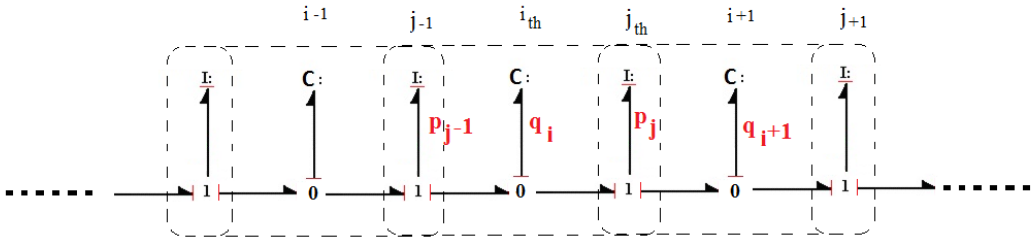

Fig. 2. Elastic beam Bond graph model

$$\dot{p}_j = \frac{q_i}{C_i} - \frac{q_{i+1}}{C_{i+1}} \tag{1}$$

$$\dot{q}_i = \frac{p_{j-1}}{I_{j-1}} - \frac{p_j}{I_j} \tag{2}$$

$$I_j = \frac{m_i}{2} + \frac{m_{i+1}}{2} \tag{3}$$

where the boundary inertance, I_j, is a function of the two adjacent elements' masses, and the element capacitance, C_i, is a function of the geometry and material parameters of the i_{th} element. For the left-end and right-end elements, since they receive external mechanical loading to the structure, Equation (1) will accordingly be re-written as:

$$\dot{p}_j = F_l - \frac{q_{i+1}}{C_{i+1}} \tag{4}$$

$$\dot{p}_j = \frac{q_i}{C_i} - F_r \tag{5}$$

where F_l and F_r are left and right external mechanical forces, respectively. Using Equations (1)-(3), a distributed elastic model of the spool that describes the dynamics of the spool in a pure elastic nature is formed. This model combines the feature of analytically-generated governing equations with the feature of numerically-distributed space elements, and provides a platform within which possible input addition and parameter alternation can be implemented to address desirable multi-physical dynamics as long as the energy within the domain is conserved. The model in its current shape is not yet able to describe the internal thermomechanical phenomena of the spool.

To include the thermomechanical interactions in the model of the spool, additions or alternations that can adequately represent the spool's structural expansion and material softening phenomena must be incorporated into the current pure elastic model in ways that are consistent with the BG methodology. An equivalent source of effort that can mimic the influence of dilation dynamics is thus proposed to be inserted into the boundary junction of each element to model the structural expansion phenomenon, while a modulated capacitance that can reflect the impact of temperature dependency of material properties is proposed to replace the existing constant capacitance inside each element to model the material softening phenomenon. Together, these changes will lead to the development of an enhanced elastic-structural model of the spool in which the underlining thermomechanical phenomena can be fully captured and revealed.

3. Consideration of structural expansion in elastic spool Bond graph model

To add a source to the existing pure elastic BG to mimic the influence of dilation dynamics, questions regarding the type of injected energy port and the location of injection must be answered first. For this reason, internal expansion behavior of materials due to temperature rise is examined.

It is well known that transferring thermal energy into or from most materials causes deformation. Assume that the transferred energy is stored inside the system as elastic energy. Based on the BG terminology, one can represent this accumulated energy as a product of a temperature dependent elastic effort and the existing deformation. The mechanism of the dilation can then be introduced to the elastic domain in the form of a causal relation in which the introduced

temperature-dependent effort will cause the dilation. This sequence simply means that a certain amount of internal effort inside an elastic element is needed to stand against the elasticity of the material to allow the element to be deformed. Consequently, as the temperature of the element decreases, the saved elastic energy of the element is released to settle the system back to its initial equilibrium condition. According to this terminology, the dynamics of the thermal dilation will be added into the system if the suggested temperature-dependent effort is implemented in the elastic domain. An effort-based energy port, named the thermal effort, can then be chosen as the added energy port to the system.

The suggested thermal effort can be identified by comparing the Hook's law expression with Eq. (1). To avoid the unnecessary complexity in calculating the suggested thermal effort, let's consider the well-known 1-D Hook's strain stress expression:

$$\sigma = E\varepsilon - E\alpha\Delta T \tag{6}$$

where σ, ε, α, E, and ΔT are the axial stress, strain, expansion coefficient, elasticity modulus, and temperature gradient, respectively. For a simple axial spool, one can rewrite the Hook's law for each junction that relates to two adjacent elements as:

$$F = \frac{AE}{L}\Delta q - AE\alpha\Delta T \tag{7}$$

where F is the collective force applied to the junction, Δq is the difference in deformation between the two adjacent elements, and A and L are the cross section area and length of each element. For a homogenous and uniformly-distributed beam structure, Eq. (1) from the pure elastic BG model can be reformed as:

$$F = \frac{AE}{L}\Delta q \tag{8}$$

where $C_i = C_{i+1} = AE/L$ and $\Delta q = q_i - q_{i+1}$. Comparing Equation (7) with Equation (8), the amount of thermal effort that can represent the temperature-induced internal force is identified as:

$$F_T = AE\alpha\Delta T \tag{9}$$

Considering the causality applied to the 1-junction elements of Fig. 2 and on the basis of the causality of the generated thermal effort as described in Eq. (9), the extra energy port that can represent the structural expansion phenomenon should be added to each 1-junction of the pure

elastic BG model (Fig. 2) to form a revised expansive BG model of the spool as depicted in Fig. 3.

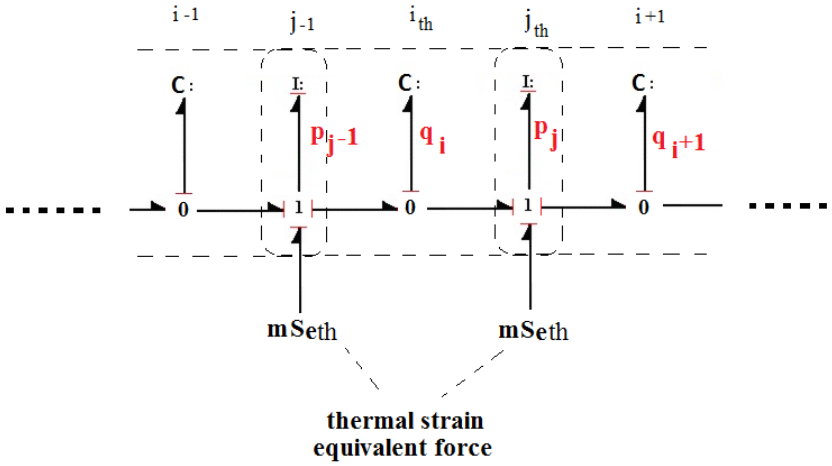

Fig. 3. Expansive beam Bond graph model

In Fig. 3, the added thermal strain equivalent force for the j_{th} junction is expressed as:

$$MS_{\text{eth}_j} = A_i E_i \alpha_i (T_i - T_{0_i}) - A_{i+1} E_{i+1} \alpha_{i+1} (T_{i+1} - T_{0_{i+1}}) \tag{10}$$

which will be added into Eq. (1) to form the new governing equation for the momentum of the j_{th} junction:

$$\dot{p}_j = \frac{q_i}{c_i} - \frac{q_{i+1}}{c_{i+1}} + MS_{\text{eth}_j} \tag{11}$$

Eqs. (11) and (2)-(3) form the new state equations for the expansive BG model of the spool. By injecting the equivalent modulated thermal effort source (10) into each junction, the momentum rate of each boundary will now not only be a function of the material parameters of the adjacent elements, but also a function of the temperature change. This additional link enables the resulting BG model to capture the dynamic behavior of the structural expansion accompanied by the kinematics of the chosen structure.

4. Consideration of material softening in elastic spool Bond graph model

It is well known that heating a structure under mechanical cyclic loading will result in changes in the system response in such a way that resembles the weakening of the system's stiffness, known as material softening. To consider this phenomenon inside the pure elastic beam structure given by Fig. 2, one can assume that the capacitance C of an element is modulated via the element's

temperature. It then seems that to represent the material softening phenomenon, the only alteration to Fig. 2 would be to replace the constant *C* with a modulated *C*, *MC*. However, this direct replacement without due diligence will in theory violate the energy conservation law that governs the dynamics within the domain. In essence, a modulated capacitor implies that there is an amount of energy that has been lost from or added to the domain. The energy difference between a constant capacitor and a modulated capacitor is indeed the quantity of a mysterious missing energy. Therefore, to implement a modulated *C* inside a structure, one must first identify the place where the missing energy has been consumed, and then investigate the consequence of overlooking this energy on the overall system dynamics. If the induced dynamic changes due to the missing energy could be observed in another domain or if the effects of these changes could be ignored within the domain of concern, the use of the modulated *C* would then become acceptable. These aspects are investigated in the following subsections, based on the fundamental physics behind the material stiffness and temperature induction.

5. Relevancy of material stiffness and thermal energy in elastic domain

Elastic module of most engineering materials is controlled by the atomic bond energy function [18]. For most materials, the amount of stretching experienced by a tensile specimen under a small fixed load is controlled in a relatively simple way by the tightness of the chemical bonds at the atomic level. This makes it possible to relate stiffness to the chemical architecture of the material.

The relation between atomic attractive and repulsive forces and energies in a material is shown in Fig. 4. The intersect of the total force and the characteristic length (r/σ) illustrates the unstressed atomic separation, r_0. This is also the point at which the potential energy U is minimum, as the summation of the total attractive and repulsive forces is equal to zero. To relate these curves to material stiffness for small deformations, the tangential line to the total force at the intersect represents the Hook's approximation of elastic force. This approximation provides a parabolic energy function, $U(r)$, about the minimum at r_0.

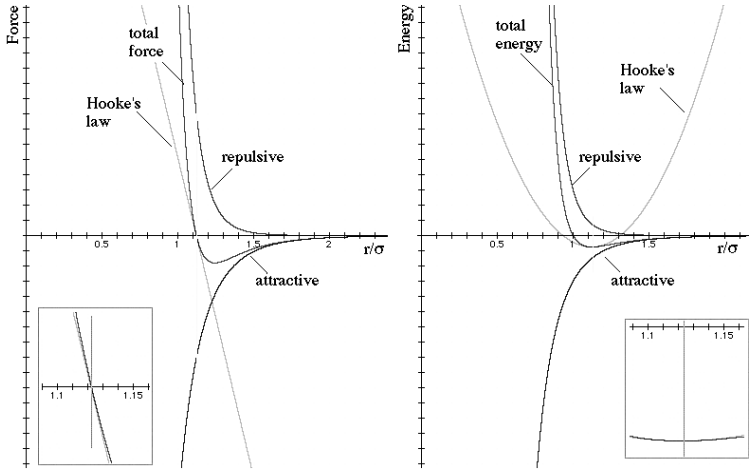

Fig. 4. Atomic total force and energy with respect to atomic distance [19]

Using the polynomial-curve assumption to analytically approximate the attractive and repulsive forces of Fig. 4 as realistic interatomic forces, the atomic potential function of the material can be represented as a superposition of the attractive and repulsive parts [19]:

$$U(r) = -\frac{a}{r^n} + \frac{b}{r^m} \tag{12}$$

where a, b, n and m are constants for an arbitrary material. Considering the derivative relation between potential and force, the resultant atomic force can be derived as:

$$F_r = n\frac{a}{r^{n+1}} - m\frac{b}{r^{m+1}} \tag{13}$$

The minimum in U occurs when $F_r = 0$ at r_0 where Equation (13) becomes:

$$r_0 = \sqrt[m-n]{\frac{mb}{na}} \tag{14}$$

To derive the material stiffness from the obtained energy function (12), assume a simple model of an arbitrary solid shown in Fig. 5 with the interatomic separation of r been represented by y in both perpendicular directions [18].

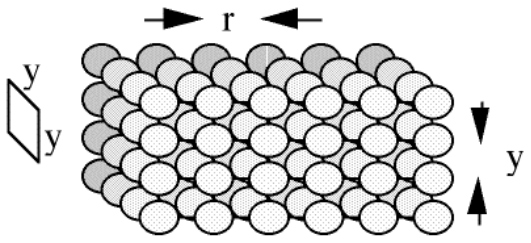

Fig. 5. An arbitrary material's atomic arrangement [18]

In classical solid mechanics, the stiffness (E) of a material is defined as the ratio of tensile stress to tensile strain. The tensile stress is the force per unit area, F/A, and the strain is the proportional increase in length parallel to the applied force, $\delta r/r$. Therefore, the definition of E gives:

$$E = \lim_{\delta r \to 0} \frac{\frac{\delta F}{A}}{\frac{\delta r}{r}} \cong \frac{dF}{dr}\frac{r}{A} \tag{15}$$

Taking the derivative of Equation (13) about the unstressed atomic separation (r_0) yields [18]:

$$E = \frac{(m-n)na}{{r_0}^{n+1}A} \tag{16}$$

Therefore, the Young's modulus with respect to the atomic forces can be presented as a function of the unstressed atomic separation, r_0, valid within the magnified range of Fig. 4. Equation (16) in principal indicates that under unstressed conditions, one can claim that the stiffness of a material is altered if and only if the unstressed atomic separation, r_0, is a function of temperature, $r_0(T)$.

To prove this claim, let's consider a more realistic potential function shown in Fig. 6 [18]. Clearly, the atomic potential function is not a symmetric curve. This asymmetry about the minimum in $U(r_0)$ is indeed the main reason for dilation. An unstressed system generally has sufficient thermal energy to reside at a level somewhat above the minimum in the bond energy function, and oscillates between the two positions labeled as A and B in Fig. 6, with an average position near r_0 [18]. If the internal energy is increased due to added heat, the system will then oscillate between the positions labeled as A' and B' with an average separation distance $\acute{r}_0$. Since the curve is anharmonic, the average separation distance is now greater than before. Therefore, the atomic separation distance is indeed seen as a function of temperature.

For a reasonable approximation, the relative thermal expansion about the initial unstressed atomic separation, Δr_0, is often related linearly to the temperature rise above the initial reference temperature, ΔT, and can be written as [20]:

$$\frac{\Delta r_0}{r_0} = \alpha_L \Delta T \tag{17}$$

where α_L is the coefficient of the linear thermal expansion. Correspondingly, the Young's modulus described in Equation (16) can be expressed as:

$$E = \frac{(m-n)na}{(r_0(1+\alpha_L \Delta T))^{n+1}A} \tag{18}$$

Equation (18) clearly indicates that the elastic modulus is a function of temperature change and, thus, must be modulated dynamically.

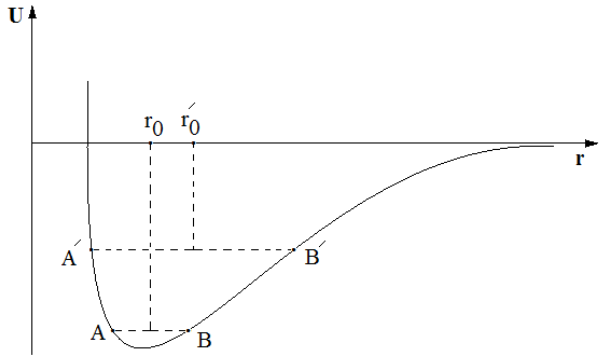

Fig. 6. Thermal expansion induced by asymmetry bond energy function [18]

6. Modulated elastic energy storage (MC) vs conservation of energy

As demonstrated in Equation (18), the elastic modulus of a system will decrease as temperature increases. Reducing the elastic modulus means that the considered elastic potential energy, U, of the system is reducing. This behavior can be found from the potential function depicted in Fig. 6. A higher thermal level for the system is seen to lead to a lower elastic energy level. This indicates that an isolated elastic energy field in the presence of heat exchange is not conservative, which simply means that there is a specific amount of energy interchange between the elastic domain and thermal domain. To keep the overall energy conserved, the thermal domain will now need to be incorporated into the modeling process via coupled capacity storage (i.e., multiport *C*). This will inevitably increase the complexity of the model drastically, and make the representation of the system in a single elastic domain impossible to achieve.

To avoid the undesirable modeling complexity and to derive a simple model of the system in the pure elastic domain that can reflect the temperature-dependent nature of the elastic modular, the concept of a modulated capacitor (*MC*) is suggested on condition that the energy conservation rule underpinning the BG technique be reserved.

To explore the possibility of replacing the constant *C* with *MC*, let's look into the considered elastic domain energy function, U, on the basis of atomic energy. Generally speaking, at the atomic

level, the internal energy of a material is composed of two parts: the atomic potential energy and the atomic kinetic energy. While elastic behavior of a material is mainly related to the atomic potential energy, heat power is solely contributed to the atomic kinetic energy. From this point of view, the implementation of the parabolic energy function in Fig. 4 based on the Hook's approximation, while providing a reasonable accuracy for the elasto-dynamic behavior of the elastic domain, would be seen to have excluded the atomic kinetic energy from the solution. The reason for excluding the atomic kinetic energy can be revealed by revisiting Fig. 6 where atomic energy variations around the temperature-dependent unstressed atomic separation parameter are observed. This amount of energy variations in the atomic kinetic domain is indeed the missing energy. The corresponding modulation of capacitance in the elastic domain is therefore seen to be the true reflection of this missing energy in the atomic kinetic domain. While the elasto-dynamics of the elastic domain represented by the Hook's approximation is clearly observable at a macroscopic level, the dynamics of the atomic kinetic domain represented by this missing energy is only detectable in a phonon scale [21] [22]. This fact proves that the dynamic changes caused by the "missing" atomic kinetic energy will have little effect on the elasto-dynamic of the system – the Hook's approximation thus holds. Consequently, it is justifiable to ignore the effect of the atomic kinetic energy in the scale of an elastic body. The missing energy once it is reflected to the elastic domain can then be seen as playing a negligible role in the overall dynamics of the system. Ignoring the missing energy in the elastic domain will then not shake the foundation of the energy conservation principle. This conclusion makes the implementation of *MC* in place of *C* permissible.

Utilizing Equation (18), a permissible modulated storage coefficient for the elastic domain can be derived as:

$$MC_i = \frac{L{r_0}^{n+1}(1+\alpha_L(T_i - T_0))^{n+1}}{(m-n)na} \tag{19}$$

Replacing *C* with *MC* (19) in the existing pure elastic BG model of Fig. 2 will adequately address the impact of material softening as part of the thermomechanical phenomena of the spool.

7. Thermomechanical-enhanced spool Bond graph modeling

Incorporating the proposed thermal effort discussed in Section 3, and the proposed modulated

capacitors discussed in Section 4 into the pure elastic beam model of Fig. 2, an elasto-expansive model of the spool that can reveal the behaviors of both structural dilation and material softening of the thermomechanical phenomena is generated. The resultant BG representation of the thermomechanical-enhanced model is shown in Fig. 7 where the thermal information of the system is added to both the capacitor via the signal port to the storage element and the inertia via the energy port to the momentum junction. These changes allow the thermomechanical phenomena of the spool to be fully represented in a single elastic domain.

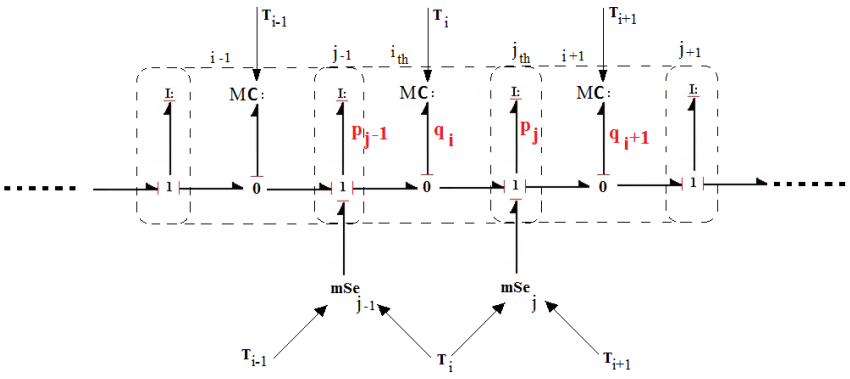

Fig. 7. Thermomechanical-enhanced beam Bond graph model

From Fig. 7, a new state equation for the momentum of the j_{th} junction is derived as:

$$\dot{p}_j = \frac{(m-n)na}{{r_0}^{n+1}}\left(\frac{q_i}{\left(1+\alpha_i(T_i-T_{0_i})\right)^{n+1}L_{0_i}} - \frac{q_{i+1}}{\left(1+\alpha_{i+1}(T_{i+1}-T_{0_{i+1}})\right)^{n+1}L_{0_{i+1}}} + \frac{\alpha_i(T_i-T_{0_i})}{\left(1+\alpha_i(T_i-T_{0_i})\right)^{n+1}} - \frac{\alpha_{i+1}(T_{i+1}-T_{0_{i+1}})}{\left(1+\alpha_{i+1}(T_{i+1}-T_{0_{i+1}})\right)^{n+1}}\right) \tag{20}$$

Eqs. (20) and (2)-(3) form the new set of governing equations sufficient for describing the thermomechanical phenomena of the spool. As revealed in Eq. (20), the momentum rate of each boundary of the configured element now depends on the temperature of the adjacent elements. The first two terms of Eq. (20) reflect the material softening dynamics of the spool, and the last two terms of Eq. (20) contain the structural dilation dynamics of the spool.

8. Simulation result and analysis

To evaluate the ability of the proposed thermomechanical-enhanced BG model to capture the spool's thermoelastic phenomena, a set of simulations including pure elastic vibration, heating,

and thermomechanical loading is performed on a simple undamped beam structure that mimics an arbitrary spool. The geometrical and material parameters of the beam are given in Table 1, and the 1D axial dynamics of the beam is to be investigated. To generate the discretized geometry, the chosen beam is reticulated into 20 uniform elements with the first and last elements being the end elements that receive external mechanical loading. It is assumed that the side surface of the beam is fully isolated and the beam is stress-free initially in the ambient room temperature. Sequentially, the validity of the proposed model in presenting pure elastic behavior of the beam is first checked in Fig. 8 and Fig. 9. The effectiveness of the suggested thermal effort in capturing the dynamics of structural expansion (thus nodal displacement) is then demonstrated in Fig. 11 and Fig. 12. Finally, the performance of the suggested modulated storage in revealing the behaviors of material softening is presented in Fig. 13.

Table 1. Beam geometrical and material parameters

Length	$\boldsymbol{l}$	$2.1e^{-1}m$
Cross section	A	$1e^{-4}m^2$
mass	m	$5.67e^{-2}kg$
Conductivity	λ	$2.73e^{2}\frac{J}{m.K}$
Density	ρ	$4e^{3}\frac{kg}{m^3}$
Molar mass	M	$2.698e^{-2}\frac{kg}{mol}$
Reference entropy @ 298K	s_0	$2.83e^{1}\frac{J}{mol.K}$
Specific heat	c_p	$8.97e^{2}\frac{J}{kg.K}$

To validate the proposed model in representing pure elastic behavior of the beam without thermal impacts, an axial mechanical cyclic load of amplitude 1N and frequency 1000 Hz is applied to the end elements of the beam. The resultant deformation of each element measured using its local axis with respect to time is presented in Fig. 8. It is seen that the external excitation induces a stress-wave propagation that results in rippled deformations of the elements that demonstrate the elastic behavior of the beam. In the absence of energy dissipation inside the system, farer elements to the ends are more flexible (thus much deformed) than the end elements. Fig. 9 shows the resultant force-deformation graph of each of the beam elements in its local axis.

The similarity between the obtained result and the Hook's stress-strain line for the elastic material verifies the integrity of the proposed model, and demonstrates that the proposed model is indeed behaving physically.

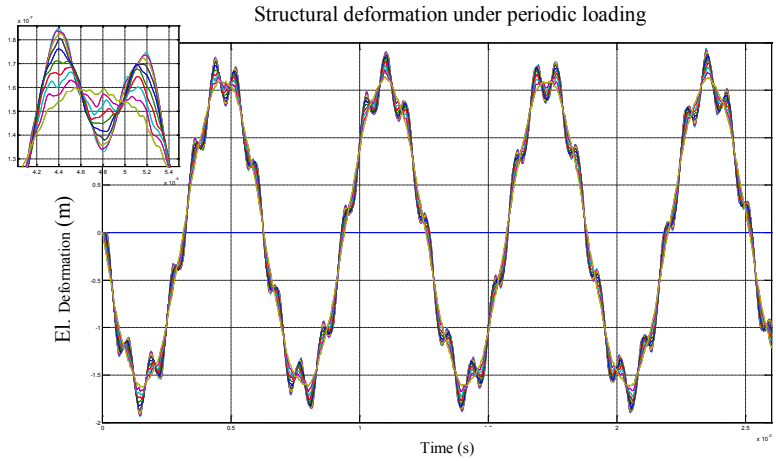

Fig. 8. Deformations of beam elements under axial mechanical cyclic loading

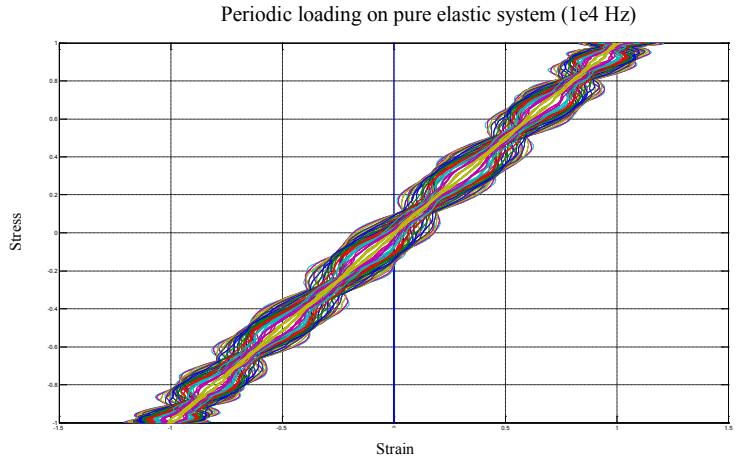

Fig. 9. Force-deformations of beam elements under axial mechanical cyclic loading

To evaluate the effectiveness of the suggested thermal effort in capturing the dynamics of elemental expansion, a temperature profile shown in Fig. 10 is selected to provide the temperature history of each element during the free-expansion process without mechanical loading. The chosen profile is the simulated result of a compatible 1D conduction model suggested in [23] [24]. The temperature input to each of the elements mimics a transient heating process of the isolated beam where the temperature of the both ends of the beam is raised up to 600K from ambient room temperature. Accordingly, the temperature of the side elements raises rapidly and a uniform temperature will be achieved by all elements eventually. During this process, as the temperature

profile to each element is different, the expansion pattern of each element is different as illustrated in Fig. 11. It is clearly shown that the expansion of the system is not homogenous alongside the beam. The elements closer to the hot spots of the beam experience more intense expansions than those of the far elements. This phenomenon results in imperceptible interactions between adjacent elements of the structure, which will cause different nodal behaviors for different elements during the expansion process. To physically illustrate this effect, consider the beam as the internal spool of a control valve in a cantilever configuration with its fixed left-end been connected to the pilot actuator and its free right-end indicating the location where the operational set-point of the system is defined. Fig. 12 shows the nodal global positions of the beam elements in this situation. It clearly shows that the nodal behavior of the free-end of the spool is drastically different than that of the fixed-end of the spool. The slow dynamics of the expansion can change the set-point of the valve, thus the operational level of the system, significantly without the interference of the valve's internal control system. In fact, in the presence of thermal loading, the nodal position of the spool (measured by the position of the free-end element) varies according to the local temperature of the system. Given that the nodal position of the spool is a deciding factor for the design of the valve's control strategies, if a strategy were designed using the pure elastic model of the system (Fig. 2) without including the thermal loading effect, the strategy would be bound to fail when used to regulate the thermoelastic behavior of the system.

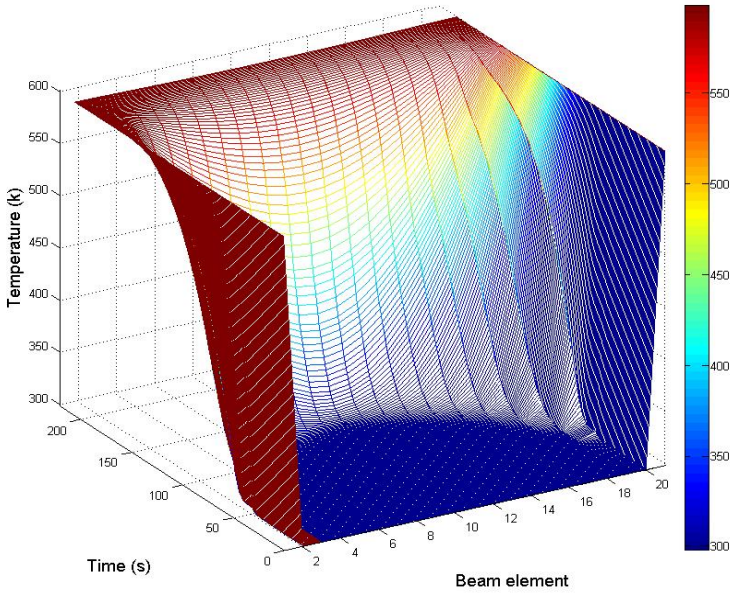

Fig. 10. Thermal input profile to beam elements

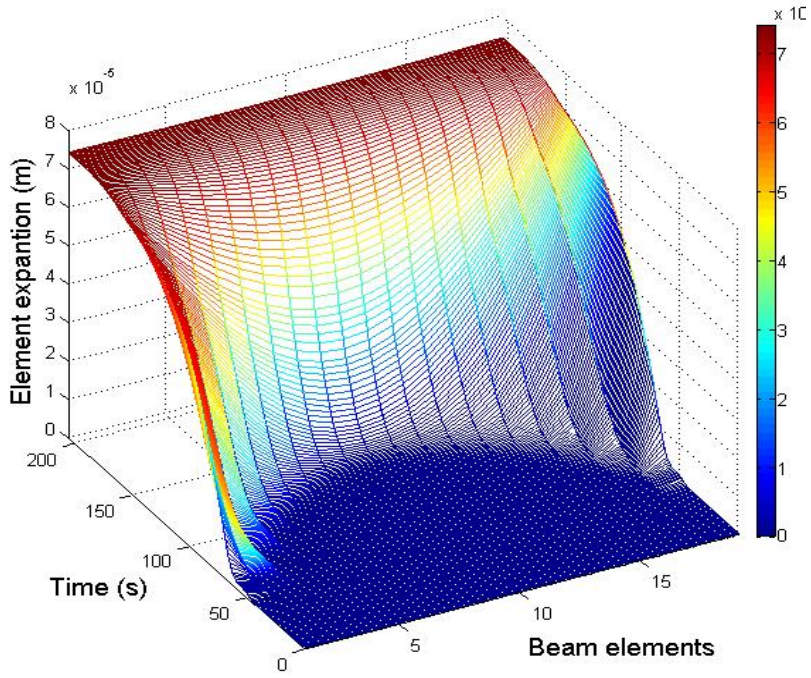

Fig. 11. Thermal expansions of beam elements

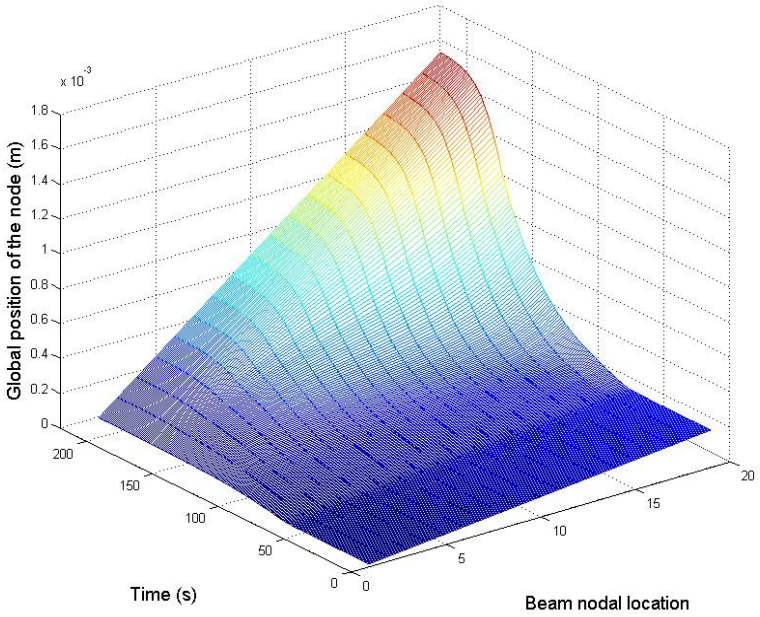

Fig. 12. Nodal global positions of beam elements

To investigate the capability of the suggested modulated storage in capturing the resultant

impacts of temperature-induced material softening, the behavior of the beam under cyclic mechanical loading is compared before and after the heating process. As the beam is modelled in 1D, the impacts due to material softening will be reflected by the change in the system response, which indicates the change in the beam's modes upon thermal loading. To this end, the following simulation sequence is arranged. Firstly, a high-frequency cyclic axial load (1N and 60000 Hz) is applied to the end elements of the beam to establish the behavior of the beam's modes before heating. Then, the temperature profile of Fig. 10 is applied to the beam while the mechanical loading is ceased to allow the structure to become fully expanded. Finally, the same mechanical loading is reapplied to the beam to demonstrate the change in the beam's modes due to material softening after heating. Fig. 13 shows the resultant oscillatory deformations of the center and end elements of the beam before (a) and after (b) heating. As can be seen, heating the system changes the range and frequency of the oscillation, which indicates the change in the system modes. The significant increase in amplitude and frequency does resemble the behavior of material softening due to heating. The suggested modulated storage in the proposed model is thus seen to be able to physically capture the effect of material softening within the system. The observed amplitude and frequency changes in the system response cannot be overlooked, as they potentially can propagate unwanted dynamics throughout the entire structure and place the whole system into an unstable situation. For instance, in the case of a liquid propulsion system, if the unwanted dynamics is propagated into the feed-system components, then cavitation and explosion would be the inevitable consequence.

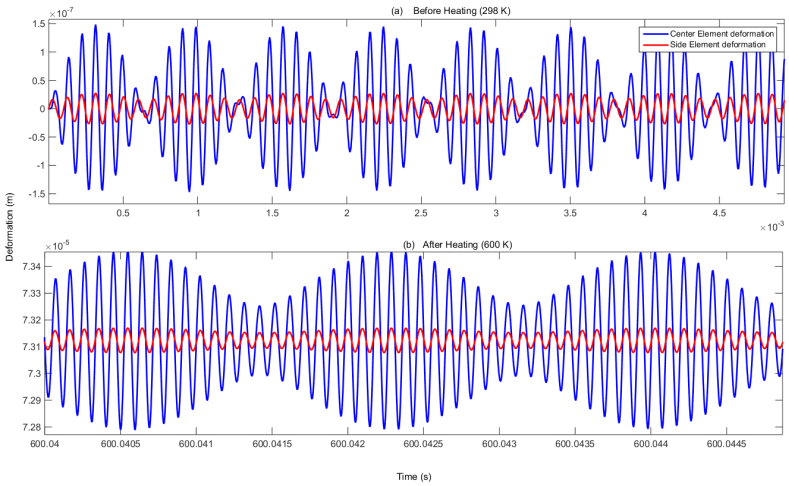

Fig. 13. Deformation of beam under axial cyclic loading and thermal loading

9. Conclusion

In this study, by means of the BG technique, an enhanced thermoelastic model is developed to address the thermomechanical phenomena present in typical control valves' internal moving components (spools). Using the concept of an equivalent thermal source, the structural expansion behavior of the system due to thermal loading is captured and its impact on altering the system set-point is demonstrated. By examining the elastic domain energy function at the atomic level, the concept of a modulated capacitor that complies with the energy conservation principle of the BG methodology is proposed. Using the modulated capacitor in the system's momentum equation, the material softening behavior of the system induced by heating is revealed and its effect on changing the system vibration modes is illustrated. The combined thermal-source and modulated-capacitor approach makes the modeling of the system's thermomechanical dynamics in a single elastic domain possible. The presented study explains the importance of unveiling the thermomechanical phenomena as a part of the dynamic examinations of the control devices under thermal loading.

The simulation results not only confirm the validity of the suggested thermomechanical-enhanced model of the system, but also demonstrate the potential benefit of the proposed approach in permitting the access of the system's physical details during the transient and allowing each physical behavior of the system to be examined individually. It is this latter point that offers a unique feature of the proposed approach in providing a useful tool for conceptual design, fault detection, reliability assessment, and structural optimization of other similar macro-scale control devices.

References

[1] H. Karimi, A. Nassirharand, A. Zanj, "Integration of modeling and simulation of warm pressurization and feed systems of liquid propulsion systems," *Acta Astronautica,* vol. 69, pp. 258-265, 2011.

[2] H. Karimi, A. Zanj, A. Najafi, "Optimization of GG Pressurization System Performance of LPE Pressure Vessels," in *16th. annual International conference on Mechanical Engineering-ISME*, Kerman, 2004.

[3] J. T. Odon, D. A. Kross, "Anallysis of general coupled thermoelasticity problems by the finite element method," Research Institute, Univ. of Alabama, Huntsville.

[4] J. Watton, " The design of a single-stage relief valve with directional damping," *Journal of*

Fluid Control Including Fluidics Quarterly, vol. 18, no. 2, p. 22–35, 1988.

[5] C. Chin, "Static and dynamic characteristics of a two stage pilot relief valve," *ASME Dynamic Systems Measurements and Controls,* vol. 113 , p. 280–28, 1991.

[6] D.C. Karnopp, R.C. Rosenburg, System Dynamics: A Unified Approach, Wiley Inter sciences, 1975.

[7] A. Mukherjee, R. Karmakar, Modeling And Simulation of Engineering System through Bondgraph, New Dehli: Narosa Publishing House, 2000.

[8] W. Borutzky, Bond Graph Methodology: Development and Analysis of Multidisciplinary Dynamic System Models, Springer, 2010.

[9] J. Amerongen, E. Coelingh , T. Vries , "Computer support for mechatronic control system design," *Robotics and Autonomous System,* vol. 30, 2000.

[10] J. J. Granda, The role of bond graph modeling and simulation in mechatronics systems, . An integrated software tool: CAMP-G, MATLAB-SIMULINK, Mechatronics, 2002.

[11] P. C. Breedveld, "Thermodynamic Bondgraphs: a new synthesis," *Int. J. Modeling and simulation,* vol. 1, pp. 57-61, 1981.

[12] A. Zanj, F. He, " Multi-Physical System Variable DOF Modeling: An Investigation on Hyro-Control Device Start Process,"in IEEE International Conference on Systems, man, and Cybernetics, Budapest Hungary, October, 2016.

[13] A. Zanj, H. Karimi, A. J. Gholi, M Shafiee, "Dynamic modeling of indirect hydro-control valve–Bondgraph approach," *Simulation Modeling Practice and Theory,* vol. 28, pp. 65-80, 2012.

[14] A. Zanj, H. H. Afshari, "Dynamic analysis of a complex pneumatic valve using pseudobond graph modeling technique," *Journal of Dynamic Systems, Measurement, and Control ,* vol. 135, no. 3, 2013.

[15] H. H. Afshari, A. Zanj, AB Novinzadeh, "Dynamic analysis of a nonlinear pressure regulator using bondgraph simulation technique," *Simulation Modeling Practice and Theory,* vol. 18, no. 2, pp. 240-252, 2010.

[16] A. Mukherjee, A. K. Samantaray, Bond Graph In Modeling, Simulation And Fault Identification, I. K. International Pvt Ltd, 2006.

[17] D. D. Reynolds, Engineering Principles in Acoustics, Boston: Allyn and Bacon Inc., 1981.

[18] D. Roylance, "Atomisic Basis of Elasticity," Department of Materials Science and Engineering, Massachusetts Institute of Technology, Cambridge, January 27, 2000.

[19] J. E. Lennard-Jones, "On the Determination of Molecular Fields," in *Proc. R. Soc. Lond.*, 1924.

[20] M. I. Ojovan, "Configurons: thermodynamic parameters and symmetry changes at glass transition," *Entropy ,* vol. 10, no. 3, p. 334–364, 2008.

[21] S. Volz, Microscale and Nanoscale Heat Transfer, Springer, 2010.

[22] V. P. Carey, G. Chen, C. Grigoropoulos, M. Kaviany, A. Majumdar, "A Review of Heat Transfer Physics," *Nanoscale and Microscale Thermophysical Engineering,* vol. 12, no. 1, p. 1–60, 2008.

[23] F. Cellier, Continuous System Modeling, New York, Verlag: Springer, 1991.

[24] A. Zanj, F. He, "Conduction Model Compatible for Multi-Physical Domain Dynamic Investigations: Bond Graph," in *18th International Conference on Engineering Systems Modeling, Simulation and Analysis*, Madrid, Spain, 2016.

DOMAIN-INDEPENDENT CONDUCTION DISCRETE MODEL COMPATIBLE FOR MULTI-PHYSICAL SYSTEM DYNAMIC INVESTIGATIONS

Amir Zanj, Fangpo He

Advanced Control Systems Research Group, School of Computer, Science, Engineering and Mathematics, Flinders University, Adelaide, Australia, e-mail: amir.zanj@flinders.edu.au

Abstract
In this paper, a novel domain-independent conduction model compatible for multi-physical system dynamic investigations is suggested. By means of a port-based approach, a classical nonlinear conduction model containing physical states is first represented. A compatible discrete configuration of the thermal domain in line with the elastic domain is then generated through the enhancement of the configuration of the conventional thermal element. The presented simulation results of a simple structure indicate that the proposed conductive model can reveal a wide range of dynamic behaviors of the thermal domain.

Keywords—Multi-physical system, conduction model, port-based modeling, dynamic interaction, physical modeling

1. INTRODUCTION

NORMALLY in multi-physical domain dynamic modeling, the thermal domain dynamics are typically replaced by fixed sources and resistors [1]. As long as the dissipated energy does not return to the system, this way of modeling can simplify the multi-physical system behavior without imposing major undesirable impacts on the system dynamics [2]. In reality, however, the dissipated energy does come back to the system in the form of thermal energy, and this returned energy may change the behavior of the system. For example, in extremely high-speed structures, the vibration-induced heating can cause unsolicited deformation, and the thermoelastic damping mechanism can result in changes in the system dynamics. These unpredicted dynamics would then make the control of the system difficult, e.g., in the case of controlling an aileron that is subjected to external aero-thermal loads [3]. To adequately investigate multi-physical system dynamics that have a strong connectivity with the thermal domain, it becomes necessary to include the thermal domain dynamics in the modeling of the system.

In a coupled multi-physical system, unlike some visible dynamics in other subdomains such as vibration in the mechanical subdomain, the dynamics of the thermal subdomain are not explicitly observable. A physical approach that can vividly reveal the nonlinear behavior of the thermal subdomain as well as its interactions with each of the other subdomains of the system is thus preferred. It is anticipated that by implementing such an approach, the interactive multi-physical

phenomena such as material softening and viscoelastic damping can be unveiled through the use of fundamental physics that govern the dynamics of the system. From this point of view, a port-based approach, known as the Bond graph (BG) approach that works on the basis of power continuity inside dynamic systems [4] [5] [6] [7] [8], is chosen for this study. The BG approach is principally capable of maintaining the integrity of the power transformation between different subdomains of a multi-physical system while extracting the system nonlinear governing equations from the interactive dynamics of the subdomains. The model thus generated is analytical in nature while potentially reflecting the true physical meaning of the system. This is a desirable feature of the BG approach over the other existing modeling approaches such as the FEM [9] [10] [11] techniques that are clearly unable to perform in the same context.

Although a physical-modeling approach is a vigorous way to capture the system's physical phenomena, lack of attention to the system geometry in forming the physical model's fundamental components (i.e., the energy components such as resistors, inertias, capacitors, and transformers that construct the dynamics of the system) can make it unusable for studies of multi-physical system dynamic behaviors in a discrete form. Given that in a discretized multi-physical system, different subdomains in principle share the same geometry properties, the transmitted information between the subdomains should thus have the same geometrical characteristics. However, due to the existing coupling between the subdomains, one subdomain's dynamic behavior may alter the existing properties (e.g., the length of the discretized segment) of the other related subdomains. In order to maintain the continuity of the power transmission between the different subdomains, the property changes of one subdomain must be reflected on the other related subdomains' properties that share the same geometry. If this requirement is overlooked, the generated model will be inaccurate in revealing the true physical interactions between different subdomains of the system. It is therefore essential to separate the energy components of different subdomains that are geometrically compatible to each other in order to effectively communicate the dynamic changes in properties among each of the associated subdomains. The consideration of geometrical compatibility between different physical subdomain elements is thus the key to success of the investigation of multi-physical phenomena using a physical approach.

This paper attempts to bridge the gap between a theoretically generated thermal model [1] and its practical realization in a multi-physical system setting using a discrete geometry that can reflect

the geometrical compatibility considerations. This attempt will relate the port-based discrete elements with the so-called finite-element approach to form a port-based finite-element method. By applying a novel concept of compatible elements to different subdomains, a multi-physical system can be effectively modelled using separate power distribution frames, each involving a subdomain that is physically connected with other subdomains. The interactions between these power frames will shape the total behavior of the multi-physical system. Accordingly, the dynamic impacts of the thermal subdomain onto the other subdomains (and vice versa) that constitute the thermal-included multi-physical phenomena will be physically unveiled.

To achieve this aim, a nonlinear 1-D conduction model suitable for thermo-elastic dynamic investigations is proposed in this paper. A domain-independent conductive discrete element with its thermal characteristics analogous to those of the mechanical elements is introduced using the concept of the port-based approach. The compatibility consideration of the proposed model will provide a guidance for the formation of the complex couplings between the thermal and elastic domains with less mathematical effort. The distinctive domain-independency feature of the conduction model will make it suitable for a wide range of multi-physical dynamic investigations, including studies involving aero-servo-thermo-elasticity.

The remainder of this paper is organized as follows. In Section II, after a brief explanation of the adjugate physical thermal variables, the calculation of the conventional thermal element is presented. In Section III, a BG representation of the conventional independent conduction model is derived, and its associated governing equations are extracted through the implementation of the port-based approach. In Section IV, a novel compatible thermal element is proposed, and the compatibility of its configuration with the new concept of a port-based finite-element thermo-elastic model is discussed together with the demonstration of the required modulated connections between a standard elastic element and a conductive thermal element. In Section V, to evaluate a capability of the proposed thermal element in discrete modeling, the thermal behavior of a 1-D conductive beam is simulated for different boundary conditions and the obtained results are discussed. Finally, the capability of the proposed domain-independent configured thermal element in modeling the dynamics of the heat conduction within an elastic body is concluded in Section VI.

2. DOMAIN-INDEPENDENT STATE VARIABLES OF THERMAL DOMAIN

In a physical modeling approach, the state variables of a multi-physical system are chosen on the basis of the physical system theory [12]. Accordingly, only the extensive variables of the system (such as entropy in the thermal subdomain) can be transferred between the elements of the different subdomains, resulting in changes in their associated potentials (such as temperature). From this point of view, the potentials of the system can be obtained from the constitutive equations that are functions of the extensive variables [13]. Implementing a physically-meaningful information transfer between different subdomains will result in a domain-independent modeling strategy. This strategy makes the thermal model connectable to the models of other subdomains effortlessly. The adjugate physical thermal variables that can form a domain-independent conduction model are explained as follows, based on the physical system theory.

According to the literature, in a well-insulated media, the 1-D heat propagation within the system can be described as [2]:

$$\frac{\partial T}{\partial t} = \sigma \frac{\partial^2 T}{\partial x^2} \tag{1}$$

Discretization of the right-hand side of Eq. (1) in space leads to:

$$\frac{\partial^2 T}{\partial x^2} \approx \frac{T(t, x_{i+1}) - 2T(t, x_i) + T(t, x_{i-1})}{\Delta x^2} \tag{2}$$

which in turn results in:

$$\frac{dT(t, x_i)}{dt} = \frac{\sigma}{\Delta x^2}\big(T(t, x_{i+1}) - 2T(t, x_i) + T(t, x_{i-1})\big) \quad (i \in 1, \dots, n) \tag{3}$$

where $T(t, x_i)$ denotes the i_{th} element's temperature at time t and location x_i , and σ is the diffusion time. Conventionally, to calculate the nodal temperature of the system, heat $\dot{Q}$ is used as energy flow between different discrete segments (thermal elements). Employing heat as the flow of the system will lead to the domain-dependency of the model. According to the physical system theory, to avoid the domain-dependency of the model, the flow of a subdomain is required to be the rate of the extensive state of the subdomain, and its corresponding effort (potential) is the constitutive equation of the subdomain dependent on state variables. Consequently, the power of a subdomain can be represented as a product of the flow and the effort of the subdomain. Given this requirement, heat can't be considered as the flow of the thermal subdomain as it is, in principal, the power of

the thermal subdomain including the potential.

It is known from the thermodynamic science that, for the thermal subdomain, entropy, s, is the justifiable extensive variable and temperature, T, is the resultant dependent variable. Therefore, according to the physical system theory, the rate of entropy must be chosen as the thermal flow and temperature must play the role of the effort of the thermal domain. The product of these two adjugate thermal variables, T and $\dot{s}$, forms the thermal power inside the system. In a reversible process, the entropy rate can be obtained as:

$$\dot{s} = \frac{\dot{Q}}{T} \tag{4}$$

It is clear that by implementing the entropy flow instead of the heat flow, the potential component of the conventional heat flow is removed. This gives the thermal model the ability to receive thermal power from different subdomains with different constitutive equations. The resultant thermal model will then be domain-independent.

3. BG MODEL OF THERMAL CONDUCTION

By employing the domain-independent conjugate thermal variable explained in Section II, a physical conduction model can be developed based on a port-based approach. The BG method is chosen as it is a powerful tool to adequately model a complex system with dynamic interactions between its multiple energy subdomains [4] [36]. In this method, a unique language is defined to represent quantities in different physical subdomains. By means of the energy conservation law, the BG method effectively describes the system dynamic behaviors in the form of energy dissipation, storage, and power flow.

Using the BG presentation, a 1-D conventional conduction model is described by a chain of dissipative, R, and capacitive, C, energy components [1], as shown in Fig. 1. In this model, it is assumed that the thermal energy can be stored in C components and dissipated while passing through R components. The model is then expressed by a series of resistive-capacitive energy components placed interlaced. Although this BG model is exceedingly beautiful, it is most certainly incorrect because there are no energy sinks in the model. As can be seen, the amount of energy dissipated by resistor R is going nowhere. A resistor may make sense in an electrical circuit

if the heating of the circuit is not of interest, but it is most certainly not meaningful when the system is itself in the thermal domain.

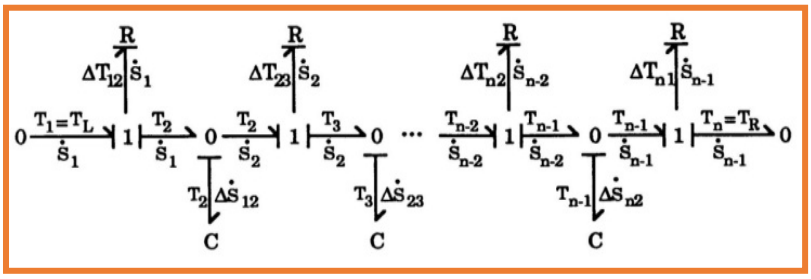

Fig. 1 Conventional BG heat conduction model [1]

Since resistors convert free energy irreversibly into heat, the problem can be easily rectified by replacing each resistor by a resistive source, an *RS*-component, shown in Fig. 2. The entropy generated by the *RS*-component can then be re-entered into the thermal subdomain. The causality of the thermal subdomain is always such, that the resistor is seen as a source of entropy, never as a source of temperature, since the sources of temperature are non-physical. The resultant BG model using *RS* instead of *R* is shown in Fig. 3. The temperature gradient leads to an additional entropy that is re-introduced at the nearest 0-junction. This arrangement provides a good approximation of the physical reality.

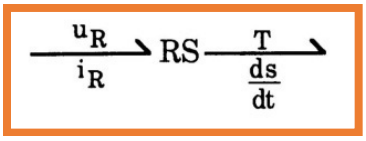

Fig. 2 BG RS-component [1]

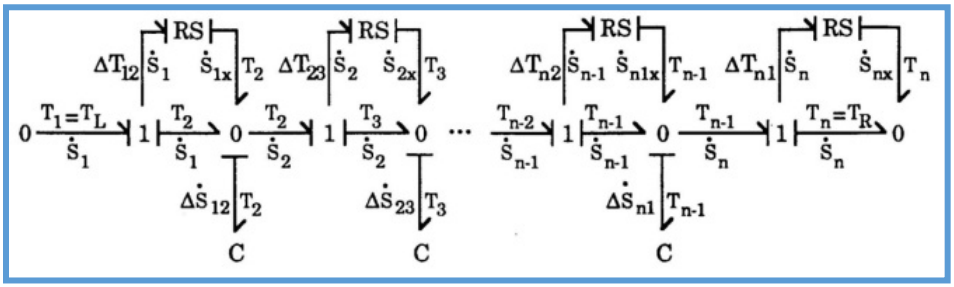

Fig. 3 Modified heat conduction BG [1]

On the basis of the resulting thermal BG integrative causality, the state equation of the i_{th} element of the thermal subdomain can be derived from its *C* energy storage component with respect to its state variable (thermal extensive state), $q_{th\,i}$, that denotes the amount of stored entropy, *s*, of the i_{th} capacitor. Considering the layout of R_j and C_i components shown in Fig. 3, one obtains:

$$\dot{q}_{th\,i} = \dot{s}_j - \dot{s}_{j+1} + \dot{S}_i^{gen} \tag{5}$$

where $\dot{s}_j$, $\dot{s}_{j+1}$ and $\dot{S}_i^{gen}$ are the amount of reversible inlet and outlet entropy flows, and the entropy generation rate (irreversible entropy flow), respectively. The internal thermal flow can be obtained as:

$$\dot{s}_{\,j} = \frac{1}{R_j}\left(C_{i-1}(q_{th\,i-1}) - C_i(q_{th\,i})\right) \tag{6}$$

where R_j is the resistant coefficient of the j_{th} RS-component and $C_i(q_{th\,i})$ is a capacitive function of the state of the i_{th} storage component representing the temperature (potential) of the element. Substituting Eq. (6) into Eq. (5) yields:

$$\dot{q}_{th\,i} = \frac{1}{R_j}\left(C_{i-1}(q_{th\,i-1}) - C_i(q_{th\,i})\right) - \frac{1}{R_{j+1}}\left(C_i(q_{th\,i}) - C_{i+1}(q_{th\,i+1})\right) + \dot{S}_i^{gen} \tag{7}$$

To identify R and C components of the BG model for the thermal subdomain, let's assume that the capacity of a long well-insulated rod to conduct heat is proportional to the temperature gradient. Using Eq. (4), one has:

$$\Delta T = \Theta.\dot{Q} = (\Theta.T).\dot{s} = R.\dot{s} \tag{8}$$

$$\Theta = \frac{l}{\lambda A} \tag{9}$$

where θ, λ, l and A are the thermal resistance, specific thermal conductance coefficient, length and cross-section area of the element, respectively. Considering Δx as the length of the j_{th} resistive energy component, the related resistance coefficient can be derived as:

$$R_j = \frac{\Delta x_j T_j}{\lambda_j A_j} \tag{10}$$

According to the Fourier heat conduction law, the capacity of a long well-insulated rod to store heat satisfies the capacitive law, thus:

$$\Delta\dot{s} = \frac{\gamma}{T}\frac{dT}{dt} = C\frac{dT}{dt} \tag{11}$$

$$\gamma = \rho V c \tag{12}$$

where c, ρ and V are the specific heat capacity, density, and volume of the element. Considering

l_i as the length of the i_{th} element, the related capacitance coefficient can be presented as:

$$C_i = \frac{c_i \rho_i A_i l_i}{T_i} \tag{13}$$

From Eqs. (10) and (13) it is clear that the thermal *R* and *C* components, contrary to their electrical and mechanical counterparts, are not constant parameters. This makes the thermal subdomain highly nonlinear. Also, it can be seen that the thermal resistance is proportional to temperature, whereas the thermal capacity is inversely proportional to temperature. Hence, the diffusion time constant $\sigma=RC$ is independent of temperature, and the generated state equation (7) according to the physical states is consistent with the heat conduction differential equation (3).

To calculate the effort, *T*, of the storage component presented as $C_i(q_{th\,i})$ in Eq. (6), integrate Eq. (11). The temperature of the element dependent on the local state can then be obtained as:

$$T_i = C_i(q_{th\,i}) = T_0 e^{\frac{1}{\rho V c}(q_{th\,i} - s_0)} \tag{14}$$

where T_0 and s_0 are, respectively, the reference temperature and entropy of the i_{th} element. Finally, to calculate $\dot{s}_{gen}$ for the solution of Eq. (7), consider the power transmission in Fig. 2 and the *RS* connections in the main BG body of Fig. 3. According to power continuity, the following relation can be derived for any *RS*-component of the model:

$$\dot{S}_i^{gen} T_i = \dot{s}_j\,(T_{i-1} - T_i) \tag{15}$$

Substituting Eqs. (6) and (14) into Eq. (15) yields:

$$\dot{S}_i^{gen} = \frac{1}{R_j} T_0 e^{\frac{1}{\rho V c}(q_{th\,i} - s_0)}\,(e^{\frac{1}{\rho V c}(q_{th\,i-1} - q_{th\,i})} - 1)^2 \tag{16}$$

The governing equation of heat conduction in the thermal subdomain is now closed. It is clear that the amount of entropy generated inside an element is a function of the state variable, $q_{th\,i}$, material characteristics, and geometrical parameters of the element.

By this stage, the extracted mathematical model is capable of capturing the dynamics of thermal conduction in a transient process. However, to enhance the capability of the model in use in multi-physical systems, the generated model will not be suitable unless the compatibility consideration of the model has been taken into account.

4. PORT-BASED HEAT CONDUCTION COMPATIBLE DISCRETE MODEL

For the generalized thermal model obtained in Section III, the multi-domain compatible characteristics of its energetic components will need to be generated in order for the model to become useful for a coupled multi-physical system. The compatible thermal model, once generated, will be able to be directly connected to other physical subdomains of the system that are identically reticulated.

To achieve this, unlike the conventional physical thermal element that can only obtain an optional property (such as capacity or resistivity) with respect to the geometrical location of the element within the model, each new thermal element is now required to have its own independent properties and internal energy components in such a way that the boundaries of the internal energy components symmetrically become congruous with the boundary of the element. This requirement, regardless of the geometrical position of the element, will provide a physical connection between the thermal internal energy components and the corresponding energy components of other physical subdomains where an identical discretization process has been applied. This physical connection will make the thermal model of the system effortlessly connectable to other physical (such as the elastic, electrical, or chemical) subdomain models, and thus directly suitable for multi-physical dynamic investigations.

A series configuration of the proposed domain-independent compatible thermal element is shown in Fig. 4. In this configuration, it is assumed that heat can be stored in the C part of the element, and can be dissipated while passing from one element to its adjacent element. On the basis of this assumption, for a 1-D element, it has been presumed that the center part of each element is the heat storage of the system where the memory characteristics belong to, and the two sides of each element are the parts in which the thermal energy is dissipated.

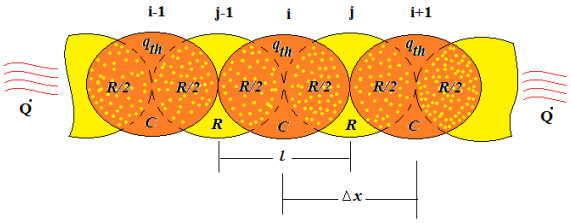

Fig. 4 1-D heat conduction schematic

The bi-dissipative consideration of the proposed thermal element makes it slightly different from

a conventional thermal element. According to the conventional representation (*RC*-chain), thermal energy can be stored in one side and dissipated from the other side of the element. This technique of discretization does not provide the power divergence information for each element, and thus the integration won't be achievable locally. This limitation makes the conventional models unsuitable for parallel computation.

To generate the proposed thermal element, it is assumed that each element of the system consists of both the dissipative and storage energy components. Unlike the conventional thermal element, the dissipation of the proposed thermal element is considered to be symmetrical with respect to the geometry of the element. To generate the symmetric dissipation of each element and, at the same time, maintain the continuity of the flux in a continuous geometry, the dual-shifted continuous reticulation of the energy components shown in Fig. 4 can be beneficial. Given that the boundary of each thermal element is bonded to move together with the adjacent elements, one can relate the dissipative behavior of each element to the dissipative mechanism of its adjoint boundaries known as the junction elements indexed by j. Considering the existing shifting between the storage component and the resistive components in the reticulated geometry, the dissipative characteristics of each junction elements can be produced by the dissipative parameters of the adjacent elements. This means that to generate the required flux crossing the boundary of each element, the local information can be employed. Therefore, dissipative parameters of each junction can be obtained with respect to the material and geometry properties of each element, which leads to the generation of a locally-integrative thermal element.

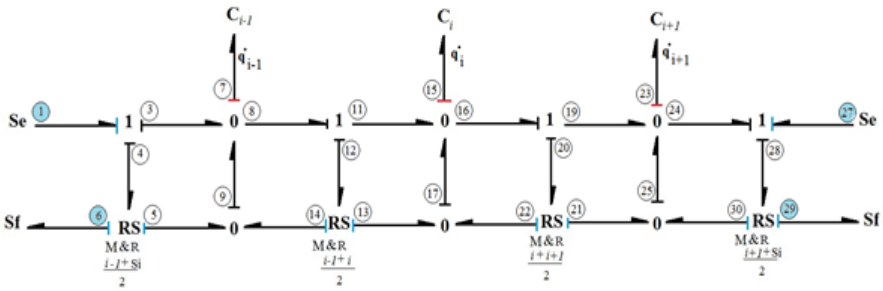

Fig. 5 1-D conduction BG model

The BG presentation of Fig. 4 is shown in Fig. 5. As can be seen, in the represented model, each element is considered as a C storage component together with the state variable, q_{th}, denoting the amount of stored entropy. In the proposed BG model, each C component is connected to its

adjacent elements via two intra-connection elements named earlier as junction elements. Assume that each element named after its junction element. As shown in Fig. 5, the characteristics of the junction elements are a weighted combination of its adjacent elements or the source and adjacent elements. Accordingly, one can assume that the generated entropy within each element can be obtained from a combination of the generated entropy of its adjacent junctions. Hence:

$$\dot{S}_i^{gen} = M_{jr}\dot{S}_j^{gen} + M_{j+1l}\dot{S}_{j+1}^{gen} \tag{17}$$

where $\dot{S}_i^{gen}$ is the amount of internal entropy generation denoting the irreversibility of the heat conduction process, and M_j is the switch working after each *RS*-component. This switch is responsible to conduct $\dot{S}_j^{gen}$ to the correct direction by comparing the neighborhood temperatures together as such:

$$\text{If } T_{i-1} < T_i \Rightarrow \begin{bmatrix} M_{jl} \\ M_{jr} \end{bmatrix} = \begin{bmatrix} 0 \\ 1 \end{bmatrix} \tag{18}$$

The net entropy generation for each element can be obtained as:

$$\dot{S}_i^{gen} = T_0 e^{\frac{1}{\rho V c}(q_{th\,i} - s_0)} \left(\frac{M_{jr}}{R_j} \left(e^{\frac{1}{\rho V c}(q_{th\,i-1} - q_{th\,i})} - 1\right)^2 + \frac{M_{j+1l}}{R_{j+1}} \left(e^{\frac{1}{\rho V c}(q_{th\,i} - q_{th\,i+1})} - 1\right)^2 \right) \tag{19}$$

To formulate the *RS*-components in the proposed configuration, one should first construct a weighted function. For simplicity, the mean functionality is selected for calculating the junction resistance:

$$R_j = \frac{R_{i-1} + R_i}{2} \tag{20}$$

Given the constitutive equation related to the *R* components in the classical thermodynamic is the Fourier equation, considering Eq. (10) for the j_{th} junction, the related resistivity can be obtained as:

$$R_j = \frac{T_0}{2} \left(\frac{l_{i-1} e^{\frac{1}{\rho V c}(q_{th\,i-1} - s_0)}}{\lambda_{i-1} A_{i-1}} + \frac{l_i e^{\frac{1}{\rho V c}(q_{th\,i} - s_0)}}{\lambda_i A_i} \right) \tag{21}$$

Considering the compatible entropy generation, $\dot{S}_i^{gen}$ and the resistivity of the system, R_j, the governing Eq. (7) for the port-based thermal element can be rewritten as:

$$\dot{q}_{th\,i} = \frac{\left(e^{\frac{1}{\rho_{i-1}A_{i-1}l_{i-1}c_{i-1}}(q_{th\,i-1}-s_0)} - e^{\frac{1}{\rho_i A_i l_i c_i}(q_{th\,i}-s_0)}\right)}{\left(\frac{1}{2}\left(\frac{l_{i-1}e^{\frac{1}{\rho_{i-1}A_{i-1}l_{i-1}c_{i-1}}(q_{th\,i-1}-s_0)}}{\lambda_{i-1}A_{i-1}} + \frac{l_i e^{\frac{1}{\rho_i A_i l_i c_i}(q_{th\,i}-s_0)}}{\lambda_i A_i}\right)\right)} - \frac{\left(e^{\frac{1}{\rho_i A_i l_i c_i}(q_{th\,i}-s_0)} - e^{\frac{1}{\rho_{i+1}A_{i+1}l_{i+1}c_{i+1}}(q_{th\,i+1}-s_0)}\right)}{\left(\frac{1}{2}\left(\frac{l_i e^{\frac{1}{\rho_i A_i l_i c_i}(q_{th\,i}-s_0)}}{\lambda_i A_i} + \frac{l_{i+1}e^{\frac{1}{\rho_{i+1}A_{i+1}l_{i+1}c_{i+1}}(q_{th\,i+1}-s_0)}}{\lambda_{i+1}A_{i+1}}\right)\right)} + e^{\frac{1}{\rho_i A_i l_i c_i}(q_{th\,i}-s_0)}$$
$$\left(\frac{M_{jr}\left(\frac{e^{\frac{1}{\rho_{i-1}A_{i-1}l_{i-1}c_{i-1}}(q_{th\,i-1}-s_0)}}{e^{\frac{1}{\rho_i A_i l_i c_i}(q_{th\,i}-s_0)}} - 1\right)^2}{\left(\frac{1}{2}\left(\frac{l_{i-1}e^{\frac{1}{\rho_{i-1}A_{i-1}l_{i-1}c_{i-1}}(q_{th\,i-1}-s_0)}}{\lambda_{i-1}A_{i-1}} + \frac{l_i e^{\frac{1}{\rho_i A_i l_i c_i}(q_{th\,i}-s_0)}}{\lambda_i A_i}\right)\right)} + \frac{M_{j+1l}\left(\frac{e^{\frac{1}{\rho_i A_i l_i c_i}(q_{th\,i}-s_0)}}{e^{\frac{1}{\rho_{i+1}A_{i+1}l_{i+1}c_{i+1}}(q_{th\,i+1}-s_0)}} - 1\right)^2}{\left(\frac{1}{2}\left(\frac{l_i e^{\frac{1}{\rho_i A_i l_i c_i}(q_{th\,i}-s_0)}}{\lambda_i A_i} + \frac{l_{i+1}e^{\frac{1}{\rho_{i+1}A_{i+1}l_{i+1}c_{i+1}}(q_{th\,i+1}-s_0)}}{\lambda_{i+1}A_{i+1}}\right)\right)}\right) \quad (22)$$

It is clear that the rate of change in entropy of each element, according to the direction of heat conduction, solely depends on the material and geometrical characteristics of a spatial element. This exclusivity of the proposed model makes the thermal element compatible with any other domains' elements with the same spatial references.

Accordingly, the generated model is suitable to be used in multi-physical domain dynamic investigations. For instance, in thermo-mechanical phenomena, it is known that mechanical loading can change the conductivity of the system. Considering Eq. (10), the resistance of each element is proportional to the length of its resistor's generalized length (Δx_i). Under mechanical loading, this parameter will vary during the thermal process, which can affect the conductivity of the system. By replacing the *RS*-components with a mechanically modulated resistivity, *MRS*, the impacts of mechanical deformation can be captured in the conductive behavior of the system. By means of a compatible 1-D BG representation of the elastic domain [15] with the proposed thermal model, the impact of elastic vibration on the conductivity of the system can be obtained from the connectivity of the system depicted in Fig. 6. It should be mentioned that the complete set of connections of thermal and elastic subdomain is not limited to what is shown in Fig. 6, however

the consideration of other connections is out of the interest of this paper.

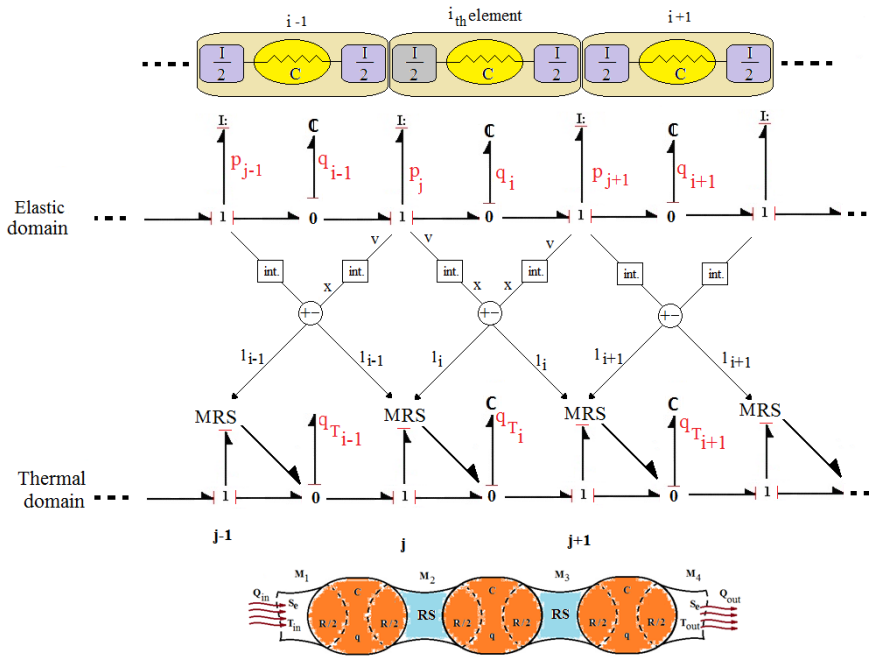

Fig. 6 Geometrical connectivity of thermal and elastic subdomains

5. 1-D CONDUCTION DYNAMIC SIMULATION

To evaluate the capability of the proposed thermal BG model in discrete modeling, the dynamic behavior of thermal conduction within a simple beam structure is analyzed. Two steps are taken: (i) To evaluate the ability of the proposed model to capture the heat conduction dynamics, a set of simulations including temperature pulse input and periodic thermal loading is performed for the chosen structure; (ii) To evaluate the compatibility of the proposed thermal elements with the other physical subdomains of the system, the elastic subdomain impact on heat conduction is investigated for the chosen structure. The geometrical and material parameters of the beam are given in Table 1, and the 1-D heat conduction dynamics of the beam are to be examined. To generate the discretized geometry, the chosen beam is reticulated into 20 uniform elements with the first and last elements being the boundary elements that can receive thermal input. It is assumed that the side surface of the beam is fully isolated and the beam is stress-free initially in the ambient room temperature. Sequentially, by employing the temperature input of Fig. 7, the validity of the generated model in presenting the thermal dynamics of the beam is first verified in Figs. 8 to 9. The capability of the model in capturing the dynamics of the thermal subdomain under periodic temperature loading of Fig. 10 is then presented in Figs. 11 and 12. Finally, to confirm the

compatibility of the generated thermal element with the elements of the elastic subdomain, the impact of thermal expansion on heat conduction is examined in Fig. 13 through coupling the thermal model with the elastic model presented in [15].

TABLE 1 :The Material and Geometrical Spool Properties

Length	l	$2.1e^{-1}m$
Cross section	A	$1e^{-4}m^2$
mass	m	$5.67e^{-2}kg$
Conductivity	λ	$2.73e^{2}\frac{J}{m.K}$
Density	ρ	$4e^{3}\frac{kg}{m^3}$
Molar mass	M	$2.698e^{-2}\frac{kg}{mol}$
Reference entropy @ 298K	s_0	$2.83e^{1}\frac{J}{mol.K}$
Specific heat	c_p	$8.97e^{2}\frac{J}{kg.K}$

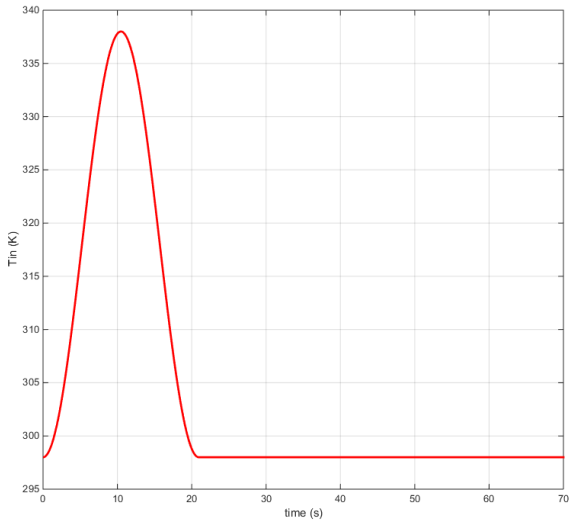

Fig. 7 Temperature input to the left side of the beam

To evaluate the capacity of the generated model in capturing the dynamics of the thermal subdomain, the pulse temperature input shown in Fig. 7 is considered as the boundary input to the left side of the beam. Fig. 8 shows the temperature profile of different elements of the beam during the simulation period. The relaxing dynamics of the conduction are evident in this behavior. The temperature of each element rises one after another, and decreases with a different pattern from the rising period. To explain this, one can consider that after the input pulse is vanished, the heat flow in the system is reversed such that the boundary elements start releasing heat to the environment and to the rest of the system.

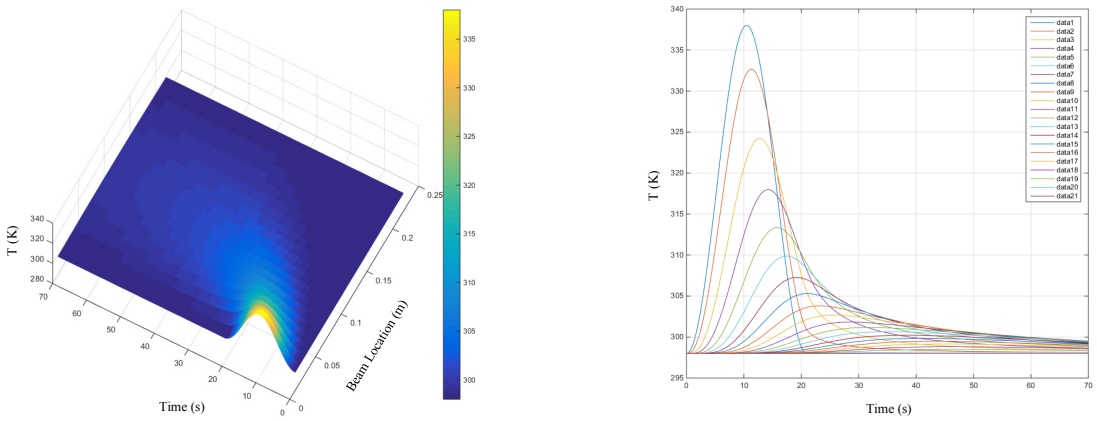

Fig. 8 Beam elements' thermal behavior

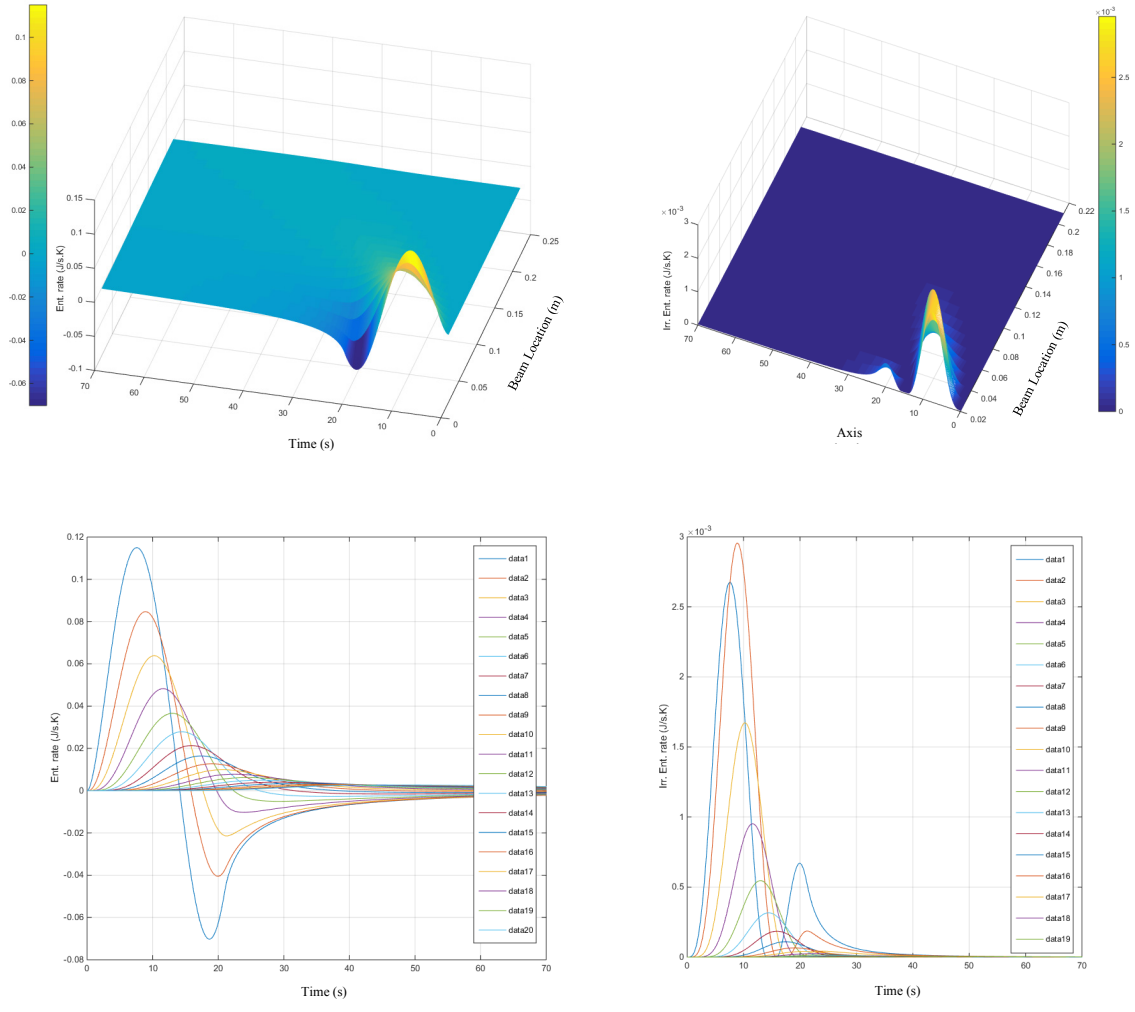

(a) (b)

Fig. 9 (a) Junction entropy flows, (b) Irreversible entropy generation rate

Fig. 9 (a), shows the entropy flow changes inside the system with respect to the considered input. The behavior of the entropy flow can vividly explain the resultant temperature profile of the system. As can be seen, neglecting the boundary element, the reversed entropy flow in the system is not as strong as its primary current. Therefore, the cooling process is to some extend slower than the heating process in this situation.

Fig. 9 (b) shows the amount of generated entropy rate during this process. The dissipated energy generated from the resistivity of the system can return to the system via this generated entropy rate which can alter the dependent variable, T, of the system. Accordingly, one can conclude that the resultant thermal dynamics of the system in principal can be presented as a result of both the irreversible entropy rate and the net reversible entropy rate shown respectively in Fig. 9 (a) and (b) for each element.

A close examination of Fig. 9 (b) shows that for the beam elements closer to the heat source, the profile of the irreversible entropy generation contains two peaks, whereas the input heat pulse was unique. One can explain that the first peak is a definite result of the external-pulse resultant temperature gradient and the second peak is induced by the internal dynamics of the thermal domain during the cooling period. This result clearly shows that there exist specific internal dynamics within the thermal domain which, accompanied by the introduced dynamics to the system via boundaries, can form the total behavior of the system.

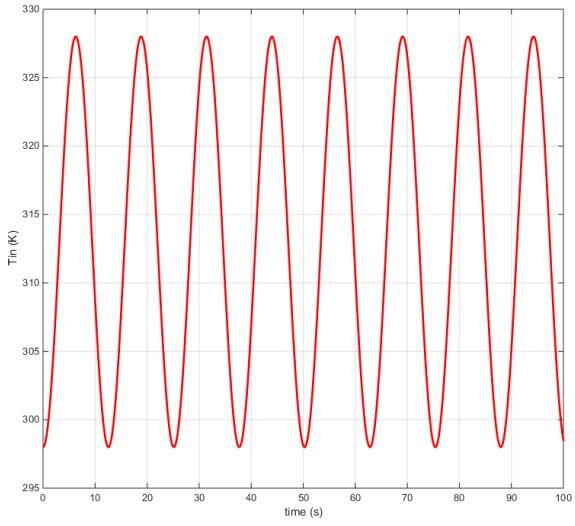

Fig. 10 Cyclic thermal input

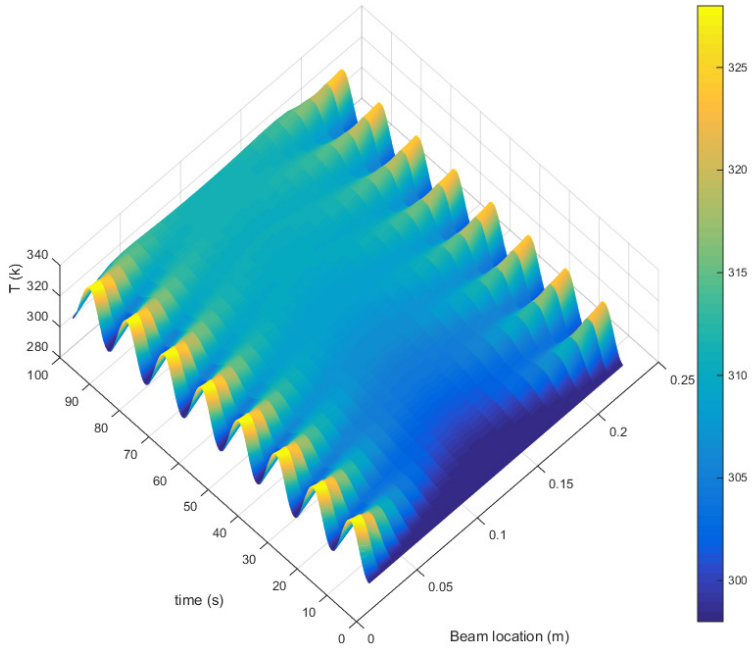

Fig. 11 Temperature contour alongside the beam during the periodic thermal input to both ends

To evaluate the capability of the proposed model in capturing the dynamics of the thermal subdomain under periodic loading, a sinusoidal thermal input shown in Fig. 10 is considered to be applied to both ends of the beam. Fig. 11 shows the resultant thermal behavior of the beam. As can be seen, the side elements of the beam is acting as a thermal filter for the central elements of the beam. This behavior highlights the slow dynamics of the thermal subdomain. As mentioned earlier, this dynamic behavior is the result of the thermal subdomain extensive variable exchange between elements. The reversible and irreversible entropy flows of the system are shown in Fig. 12 (a) and (b), respectively. It clearly shows the internal flow difference between the side elements and the central elements, which results in the formation of the observed temperature profile of the system.

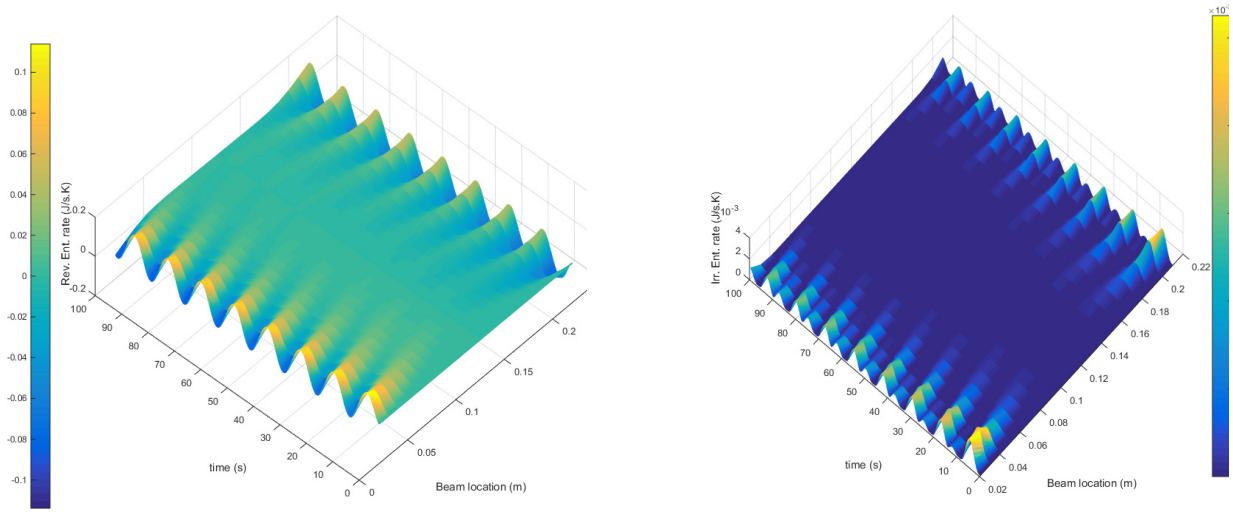

(a) (b)

Fig. 12 (a) Reversible entropy flow; (b) Irreversible entropy flow

To evaluate the capability of the proposed compatible thermal model in multi-physical systems dynamics investigation, the impact of the elastic deformation on the conductivity of the beam is selected to be examined. To achieve this, considering the geometrical connectivity of these two subdomains shown in Fig. 6, the impact of the dilation of the beam on the conductivity of the beam is to be discussed. To include the dilation, the compatible elastic BG model presented in [15] is employed. A temperature pulse shown as T_{in} in Fig. 13 (a) is considered as the input signal to the left boundary of the beam, and constant temperature T_{out} is considered as the right boundary condition of the beam. To distinctively clarify the dilation impacts of elastic subdomain on thermal subdomain dynamics, only the behaviors of every second segments along the beam is presented in Fig. 13. In Fig. 13 (a) the temperature profile of the beam is presented for an expansive beam. As can been seen, the thermal behavior of the beam follows the same pattern as the non-expansive elements shown earlier in Fig. 8. To highlight the existing dilative impacts on the conductivity of the system, the difference in the dynamic behaviors of the thermal subdomain between employing the expansive thermal element and employing the non-expansive thermal elements are presented in Fig.13 (b) to (d). In Fig. 13 (b), the negative difference indicates a slight lag in the temperature rise of the expanded elements. Given that temperature is an equilibrium-determinant variable that is dependent on the extensive variable of the element, this behavior indicates that the amount of the accumulated entropy of the element during the expansion process in the case of employing the expansive thermal elements are relatively lower than that of employing the non-expansive thermal

elements. The negative differences of the provided reversible and irreversible entropy flows, shown respectively in Fig. 13 (c) and Fig. 13 (d), can explain this shortage of the accumulated entropy. A rational reason to justify this change in entropy flow of the system can be obtained from Eqs. (6) and (19) which denote an inverse relativity of entropy flow with the expansive element's growing resistivity. Accordingly, since the expansion of the elements increases the resistivity of the corresponding junctions, and since the magnitude of the transferred entropy flow of the thermal subdomain is determined by the resistivity of the system, the process of expansion can cause a slight lag in the dynamics of the thermal subdomain as presented in Fig. 13 (b).

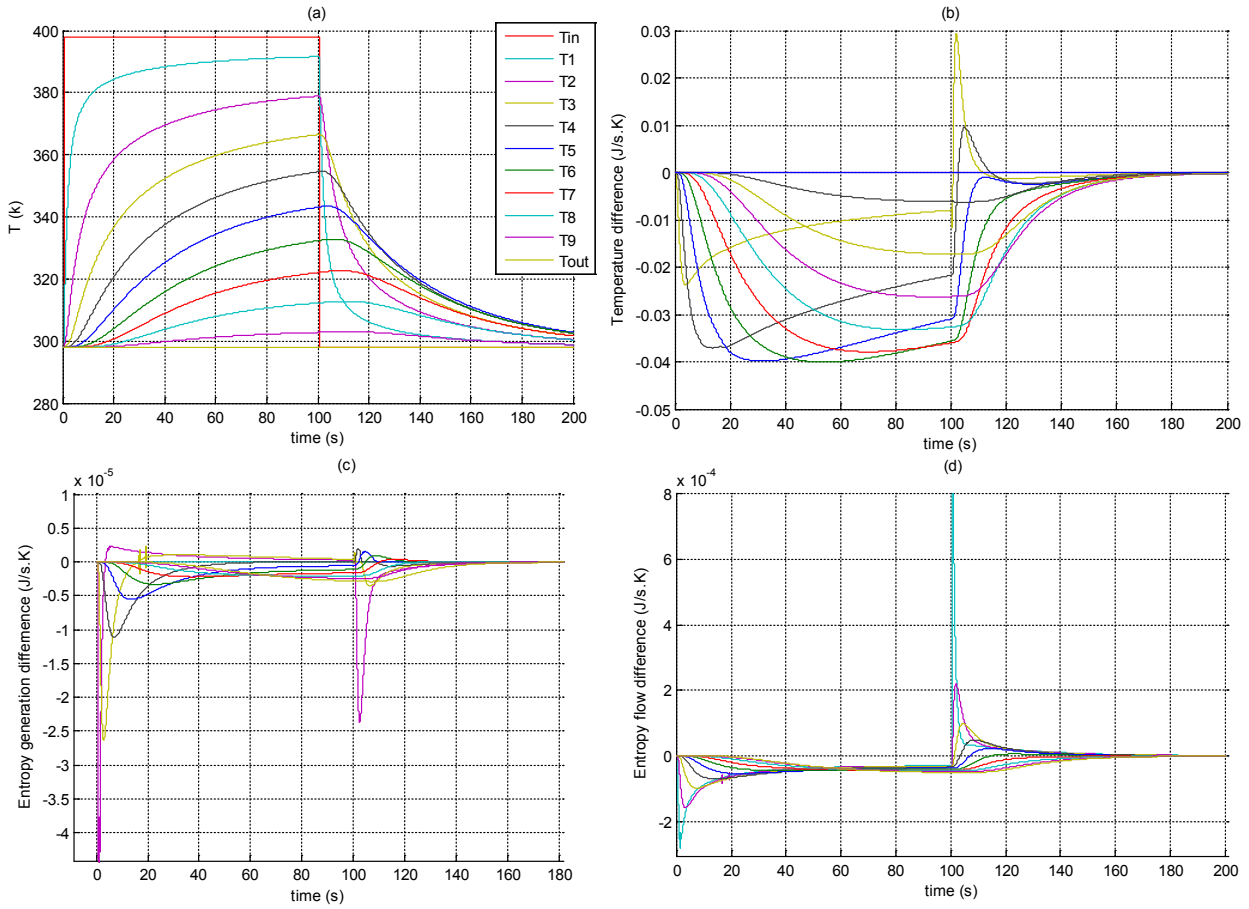

Fig. 13 Expansion impact on system conductivity: (a) Element temperature change due to pulse input at left side; (b) Difference in thermal behavior between fixed and expansive geometry situations; (c) Difference in entropy generation; (d) Difference in reversible entropy flow

The simulation results shown in this section indicate that although the selected connectivity between the thermal and elastic subdomains is weak, the dilation of the system due to the interaction of elastic and thermal subdomains does exist and can change the conductive

behavior of the system in a tractable level. In general industrial applications, this level of impacts may be negligible. However, in high-tech applications such as aerospace controlled structures or MEMS systems where critical and stringent temperature-control performances are required, this level of interactions must be considered. For instance, in the lithography printing systems of the ASML machines, the temperature needs to be controlled within the range of 1 mK in order to provide the printing ability in the order of Pico meter. In this case, designers will need to take the internal conduction dynamics of the system into account to be able to control the temperature of the device within the acceptable range.

6. CONCLUSION

In this paper to investigate the dynamics of heat conduction in multi-physical phenomena, a new configuration of energy component to form a domain-independent compatible thermal element is proposed. Using this configuration in a multi-physical domain setting, the impact of the thermal subdomain dynamics on the total dynamics of the system and vs can be examined. This method provides a useful tool for the management of the energy consumptions in multi-disciplinary systems where temperature control is an important issue. The discrete nature of the proposed thermal model is also ideally matched with parallel computation platforms that can reduce the required computation time significantly. This advantage can increase the likelihood of the proposed model in the development of control strategies.

The simulation results indicate the capability of the proposed model in capturing the dynamic behavior of the thermal subdomain in a discrete form. The obtained results also confirm the slow and relaxing behavior of the conduction in the system which is well-matched with the essential features of the thermal subdomain. The simulated thermoelastic results demonstrate that despite a weak connectivity between the elastic and thermal subdomains, the proposed model is able to capture the impact of multi-physical phenomena on the thermal subdomain and vice versa.

Reference

[1] F. Cellier, Continuous System Modeling, New York: Springer-Verlag, 1991.

[2] W. k. Nowacki, "Progress in Thermoelasticity," *European Mechanics Colloquium,* 1967.

[3] R. P. Starkey, D. D. Liu, P.C. Chen, A. Sengupta, K.T. Chang, "Integrated Aero-Servo-Thermo-Propulso-Elasticity (ASTPE) Methodology for Hypersonic Scramjet Vehicle Design/Analysis," in *48th AIAA Aerospace Sciences Meeting Including the New Horizons Forum and Aerospace Exposition*, Orlando, Florida, January, 2010.

[4] J. U. Thoma, Simulation by Bondgraph, springer, 1990.

[5] A. Mukherjee, R. Karmakar, Modeling And Simulation of Engineering System through Bondgraph, New Dehli: Narosa Publishing House, 2000.

[6] D.C. Karnopp, R.C. Rosenburg, System Dynamics: A Unified Approach, Wiley Inter sciences, 1975.

[7] H. Afshari, A. Zanj, "Dynamic Analysis of a Nonlinear Pressure Regulator Using Bond graph Simulation Technique," *Journal of Simulation Modeling Practice and Theory,* 2010.

[8] A. Zanj, H. Karimi, A.J. Gholi, M. Shafiee, "Dynamic Modeling of Indirect Hydro-Control Valve – Bond graph Approach," *Journal of Simulation, Modeling, Practice and Theory,* 2012.

[9] E. L. Wilson, Three-Dimensional Static and Dynamic Analysis of Structures, California: Conputers and Structures: Inc, Berkeley, 2002.

[10] H. F. Brinson, L. C. Brinson, Stress and Strain Analysis and Measurement," in Polymer Engineering Science and Viscoelasticity an Introduction, Springer, 2008, pp. 16-53.

[11] J. Peraire, P. O. Persson, "High-Order Discontinuous Galerkin Methods for CFD,In Adaptive High-Order Methods in Computational Fluid Dynamics," *World Scientific series in Advances in Computational Fluid Dynamics,* vol. 2, pp. 119-152, 2010.

[12] P. Breedveld, Physical System Theory In Therms of Bond graphs, Enschede: Univercity of Twente, 1984.

[13] W. Borutzky, Bond Graph Methodology: Development and Analysis of Multidisciplinary Dynamic System Models, Springer, 2010.

[14] A. Zanj, H. Afshari, "Dynamic Analysis of a Complex Pneumatic Valve Using Pseudobond Graph Modeling Technique," *Journal of Dynamic System, Measurement, and Control,* vol. 135, no. 2, 2013.

[15] A. Zanj, F. He, "A Thermomechnical Enhanced Elastic Model: Bond Graph Approach," in *23rd International Congress on Sound and Vibration*, Athens, Greece, July, 2016.

[16] A. Zanj, H. Afshari, "Dynamic Analysis of a Complex Pneumatic Valve Using Pseudobond Graph Modeling Technique," Journal of Daynamic System, Measurement, and Control, vol. 135, no. 3, 2013.

CHAPTER 4: THERMOELASTIC COUPLED MODEL FOR SOLID FIELD

Aim

The aim of this chapter is to reversibly couple the proposed thermal and elastic subdomains' models generated in Chapter 3.

Description

To achieve this aim, first, the generated distinctive power distribution of the existing subdomains is represented in the form of BG notation. Next, to provide a continuous power transmission between the thermal and elastic subdomains, a reversible coupling is designed and the corresponding multi-dimensional constitutive equations are derived that satisfy the Maxwell reciprocity. Finally, by employing the generated coupling, the thermal and elastic subdomains are connected dynamically. The outline of the presented activities is organized as follows:

Results

Implementing the energy-based strategies, a physical model that is capable of dynamically capturing the reversible thermal and elastic subdomains' interactions while preserving the fundamental physical natures of the thermoelastic phenomena, is generated. The generated model is domain-independent, and principally more suited to be connected to other physical domains than its conventional counterparts. The demonstrated capability of the generated model provides a unique benefit to the development of appropriate schemes for controlling structural vibrations under aerothermal loads.

Conclusion

Overall, a novel domain-independent nonlinear thermoelastic model suitable for multi-physical system dynamic investigations is achieved, with which the reversible dynamic coupling between the elastic and thermal subdomains is approachable without the use of the conventional weak connectivity assumption.

DOMAIN-INDEPENDENT REVERSIBLE THERMOELASTIC COUPLING: A BOND GRAPH APPROACH

Amir Zanj[1], Peter C. Breedveld[2], Fangpo He[3]

Abstract

In this paper a novel domain-independent nonlinear thermoelastic model suitable for multi-physical system dynamic investigations is proposed with which the coupling between the thermal and elastic subdomains can be obtained without the use of the conventional weak connectivity assumption. To achieve this, first, a distinctive power distribution of each subdomain is defined by means of the Bond graph notation, and the corresponding governing equation for each subdomain is extracted on the basis of the port-based approach. Next, to provide a continuous power transmission between the thermal and elastic subdomains, a reversible coupling is designed and the corresponding multi-dimensional constitutive equations are derived that satisfies the Maxwell reciprocity. Finally, by employing the generated coupling, the thermal and elastic subdomains are connected dynamically. Implementing the energy-based strategies, a physical model that is capable of dynamically capturing the reversible thermal and elastic subdomains' interactions, while preserving the fundamental physical natures of the thermoelastic phenomena, is generated. The generated model is domain-independent, and in principal more suited to be connected to other physical domains than its conventional counterparts. The demonstrated ability of the generated model provides a unique benefit to the development of appropriate schemes for controlling structural vibrations under aerothermal loads.

***Keywords*:** dynamic coupling, nonlinear modeling, thermoelastic phenomena, Bond graph modeling, multi-physical system modeling

1. Introduction

It is known that for a mechanical body, structural dilation and temperature variation coexist interactively – one behavior is both the cause and the consequence of the other behavior, and their

[1] PhD Candidate, Advanced Control System Research group, School of Computer Science, Engineering & Mathematics, Flinders University, Adelaide, Australia, email: amir.zanj@flinders.edu.au.
[2] Associate Professor, University of Twente, Robotics and mechatronics group, Enschede, Netherlands.
[3] Associate Professor, Advanced Control System Research group, School of Computer Science, Engineering & Mathematics, Flinders University, Adelaide, Australia.

coupled dynamics form the so-called thermoelastic phenomena [1] of the system. In general, unsolicited thermoelastic behaviors are classified into two categories: mechanical deformation due to dynamics of structural dilation, and material softening due to dynamics of temperature variation. While the former phenomenon can change the system's operating point, the latter phenomenon can alter the system's response modes. Neglecting these thermoelastic behaviors may have severe consequences. This is certainly true for a space craft's propulsion system where unpredicted structural deformation and material softening can lead to the loss of the system controllability, resulting in inevitable catastrophes [2]. Modeling and control of the thermoelastic behaviors thus become a critical part of the engineering system design.

To study the effect of thermoelastic phenomena on the overall dynamic behavior of a system, it is prudent to examine the mutual interactions between the thermal and elastic subdomains of the system and to characterize their individual effects on the system dynamics. A thermoelastic model that can reflect this nature of thermoelasticity becomes desirable. Since thermoelasitc behaviors are nonlinear and multi-physical, the model should not only be able to capture the coupled dynamics between the thermal and elastic subdomains, but also be compatible with the models of the other physical subdomains of the system. A domain-independent physical modeling approach, known as the Bond graph (BG) approach [3] [4] [5], is therefore preferred. It is anticipated that the model thus derived would give a clear physical meaning to the interactions between the thermal and elastic subdomains and, at the same time, provide a direct connecting platform to link with the models of the other subdomains of the system.

To obtain such a required model, the essential thermal and elastic coupling relations must be described mathematically first. An early attempt to couple the thermal and elastic subdomains was postulated by Duhamel [6], originator of the theory of thermal stresses, who initiated the dilatation term in the equation of thermal conductivity, but did not provide a thermodynamic justification of the resulting equation. This justification was then only partly attempted by Voigt [7] and Jefferies [8], until in 1956 when Biot [9] derived a full justification of the thermal conductivity equation on the basis of thermodynamics of irreversible processes [10]. It noted that although the coupling between thermal and elastic subdomains is weak, the qualitative differences are essential. Nowacki [1] focused on the foundations of thermodynamic theories, derived the differential equations of thermoelasticity, discussed their solution methods, and provided the general energy-based

variational theorems. The simplifications and assumptions (including weak connectivity) that were applied to the development of these works, however, resulted in high-order solutions that eventually lost the interactive nature of the underlying thermoelastic phenomena.

In the conventional methods, to drive the governing equations, Helmholtz free energy [1] is used instead of energy. This choice makes these modeling techniques domain-dependent and highly mathematical in nature, rather than domain-independent and physical. In these methods, the strain plays the role of the state of the elastic subdomain, and the temperature is chosen as the state of the thermal subdomain. In addition, the use of Helmholtz free energy suggests that temperature variations be assumed to play no role in the dynamic relations. From the physical system theory [11], strain is an energy state whereas temperature is an equilibrium-determining variable. Using these two variables as state variables of the respective subdomains will have obvious consequences. Firstly, the generated thermoelastic model will be incompatible with models of the other physical subdomains that utilize independent energy state variables, as the causality of the generated thermoelastic model will not be in line with the causalities of the other physical subdomains. Secondly, the energy conservation law that is universal for deriving and validating coupled dynamics of multi-physical domains will be disregarded in this case, as the generated thermoelastic model is not based on the principle of energy conservation. As a result, the accuracy of the classical models heavily relies on the accuracy of the measuring techniques and the order of the solutions. This has made these models unsuitable for insight dynamic investigations and control strategy developments.

The aim of this paper is therefore to generate a domain-independent nonlinear physical model of thermoelasticity suitable for multi-physical dynamic and control investigations. In contrast to the other strategies that focus on the accuracy of the result, the main goal here is to generate an effective coupled thermoelastic model that can provide clear relations between parameters and components associated with the thermoelastic behaviors of the system while, at the same time, keeping the physical insight of the phenomena alive. Using the port-based BG approach [12] [13] [14] [15], the generated model will avoid using some of the conventional assumptions, and offer a simple yet elegant representation of the system that can be implemented using less computational effort. Such a model is deemed to be more suitable for use in thermoelasticity analysis and control.

The remainder of this paper is organized as follows. In Section 2, a brief clarification of the

fundamental assumptions and relations of thermoelasticity is discussed. This is followed by the derivation of the mathematical model of a novel multiport thermoelastic reversible energy store using the BG approach in Section 3. In Section 4, the energetic meaning of the proposed ports is discussed, and the associated power continuous-interconnection structure that is essential for combining these design concepts together to form a comprehensive multi-physical model is defined. In Section 5, simulation results of the proposed domain-independent model for an arbitrary geometry are presented. The capabilities of the proposed model in capturing the physical thermoelastic behaviors and providing a useful tool for control strategy development are concluded in Section 6.

2. Conventional thermoelastic model and existing problem

For an un-deformed and unstressed homogeneous anisotropic elastic body, the conventional thermoelastic modeling procedure can be explained as follows. Define deformation $d(x,t)$ at position x and time t, and its associated temperature change $\theta(x,t) = T(x,t) - T_0$ where $T(x,t)$ is the instant absolute temperature, T_0 is the reference temperature, and $\theta(x,t)$ is related to mechanical stress $\sigma(x,t)$ and strain $\varepsilon(x,t)$. Traditionally, $\theta(x,t)$ is assumed to be small such that the impact of the elastic dynamics onto the thermal behavior can be neglected. Consequently, temperature $T(x,t)$ is selected as the state of the system.

To generate the conventional thermoelastic model, consider the thermodynamic relations of the irreversible processes [16]. The constitutive relations among the stress, strain, and temperature can be presented as:

$$\frac{d}{dt}\int \left(U + \frac{1}{2}\rho v_i . v_i\right) dV = \int B_i v_i \, dV + \int p_i v_i \, dA - \int q_i n_i \, dA \tag{1}$$

$$\int \frac{dS}{dt} dV = -\int \frac{q_i n_i}{T} dA + \int \Theta \, dV \tag{2}$$

where U is the internal energy, ρ is the density, S is the entropy, B_i are the components of the body forces, $p_i = \sigma_{ji}\, n_j$ are the components of the stress vector with σ_{ji} being the stress tensor and n_i being the components of the normal vector of the surface A, q_i are the components of the heat flux vector, $v_i = \frac{\partial X_i}{\partial t}$ are the velocity components, and the quantity Θ represents the generated entropy. For Eq. (1), the terms on the left-hand side represent the rate of increase of the internal and kinetic co-energies. The first term of the right-hand side is the rate of increase of the work of

the body forces, the second term is the rate of increase of the work of the surface tractions, and the last term is the energy acquired by the body by means of the thermal conductions. For Eq. (2), the left-hand side is the rate of increase of the entropy. The first term of the right-hand side represents the exchange of entropy with the surroundings, and the second term represents the rate of production of the entropy due to heat conduction.

In the conventional approach, the state equations are obtained by relating the components of the stress tensor, σ, with the components of the strain tensor, ε, as well as the components of the temperature, θ. To achieve this, using the equation of motion:

$$\sigma_{ji,j} + B_i = \rho\ddot{x} \tag{3}$$

and applying the divergence theorem:

$$\dot{U} = \sigma_{ji}\dot{\varepsilon}_{ji} - q_{i,i},\ \dot{S} = \Theta - \frac{q_{i,i}}{T} + \frac{q_i}{T^2}T_{.i} \tag{4}$$

under the slow conduction (weak connection) assumption, the Legendre transformation [17] of the energy equation shapes the Helmholtz free energy F as a function of strain ε_{ij} and temperature T which are chosen as the state variables of the energy storage of the thermoelastic field:

$$\dot{F} = \sigma_{ji}\dot{\varepsilon}_{ji} - \dot{T}S - T\left(\Theta + \frac{q_i}{T^2}T_{,i}\right) \tag{5}$$

Consider the standard form of time derivative of F as a function of the independent state variables:

$$\dot{F} = \frac{\partial F}{\partial \varepsilon_{ji}}\dot{\varepsilon}_{ji} + \frac{\partial F}{\partial T}\dot{T} \tag{6}$$

Conventionally, Θ, q_i, and σ_{ji} are assumed to be implicitly dependent on the time derivatives of ε_{ij} and T. The following equalities can then be derived by comparing Eq. (5) with Eq. (6):

$$\sigma_{ji} = \frac{\partial F}{\partial \varepsilon_{ji}},\ S = -\frac{\partial F}{\partial T},\ \Theta + \frac{q_i}{T^2}T_{,i} = 0 \tag{7}$$

The postulation of the thermodynamics of irreversible processes will be satisfied if $\Theta > 0$, i.e., $-q_i T_{,i}/T^2 > 0$. This condition can be satisfied by the Fourier law of heat conduction [9]. In principle, the first two relations of Eq. (7) imply the constitutive relations of the coupled thermoelastic field. To extract the functionality of the constitutive relations with respect to the considered state variables, $F(\varepsilon_{ij}, T)$ is expanded into an infinite series about the neighborhood of the natural state $F(0, T_0)$:

$$F(\varepsilon_{ij},T)=F(0,T_0)+\frac{\partial F(0,T_0)}{\partial \varepsilon_{ij}}\varepsilon_{ij}+\frac{\partial F(0,T_0)}{\partial T}(T-T_0)+\frac{1}{2}\left[\frac{\partial^2 F(0,T_0)}{\partial \varepsilon_{ij}\partial \varepsilon_{kl}}\varepsilon_{ij}\varepsilon_{kl}+2\frac{\partial^2 F(0,T_0)}{\partial \varepsilon_{ij}\partial T}\varepsilon_{ij}(T-T_0)+\frac{\partial^2 F(0,T_0)}{\partial T^2}(T-T_0)^2\right]+\cdots \tag{8}$$

To form the linear relations between stress, strain, and temperature change, only the linear and quadratic terms of the expanded form are taken into account. Considering $\varepsilon_{ij}=0$ when $T=T_0$, it can be assumed that $F(0,T_0)=0$. Therefore, for the natural state:

$$\frac{\partial F(0,T_0)}{\partial T}=-S(0,T_0)=0 \tag{9}$$

By taking the advantage of the first relation of Eq. (7), one has:

$$\sigma_{ij}(\varepsilon_{ij},T)=\left(\frac{\partial F}{\partial \varepsilon_{ij}}\right)_T=\frac{\partial F(0,T_0)}{\partial \varepsilon_{ij}}+\frac{\partial^2 F(0,T_0)}{\partial \varepsilon_{ij}\partial \varepsilon_{kl}}\varepsilon_{kl}+\frac{\partial^2 F(0,T_0)}{\partial \varepsilon_{ij}\partial T}\varepsilon_{ij}(T-T_0) \tag{10}$$

Assuming linear relations in small strains and infinitesimal temperature change, one obtains:

$$\frac{\partial^2 F(0,T_0)}{\partial \varepsilon_{ij}\partial \varepsilon_{kl}}=c_{ijkl},\quad \frac{\partial^2 F(0,T_0)}{\partial \varepsilon_{ij}\partial T}=-\beta_{ij},\quad \frac{\partial^2 F(0,T_0)}{\partial T^2}=n \tag{11}$$

Substituting the linear relations in Eq. (11) into Eqs. (8) and (10) yields:

$$F(\varepsilon_{ij},T)=\frac{1}{2}c_{ijkl}\varepsilon_{ij}\varepsilon_{kl}-\beta_{ij}\varepsilon_{ij}\,\theta+\frac{n}{2}\theta^2 \tag{12}$$

$$\sigma_{ij}=\frac{1}{2}(c_{ijkl}+c_{klij})\varepsilon_{kl}-\beta_{ij}\,\theta \tag{13}$$

$$\left(\frac{\partial \sigma_{ij}}{\partial \varepsilon_{ij}}\right)_T=c_{ijkl},\quad \left(\frac{\partial \sigma_{ij}}{\partial T}\right)_V=-\beta_{ij}, \tag{14}$$

In Eq. (13) the generalized Hooke's law known as the Duhamel-Neumann relation is recognizable, where the constants c_{ijkl} and β_{ij} play the role of material constants.

To extract the coupled thermoelastic model, the internal energy and entropy must be presented as functions of the chosen state variables. To ascertain this, revisiting the relations revealed in Eqs. (1)-(2), the differential form of energy and entropy equations can be derived as:

$$dU=\sigma_{ij}d\varepsilon_{ij}+TdS \tag{15}$$

$$dS=\left(\frac{\partial S}{\partial \varepsilon_{ij}}\right)_T d\varepsilon_{ij}+\left(\frac{\partial S}{\partial T}\right)_V dT \tag{16}$$

Substituting Eq. (16) into Eq. (15), the functionality of the energy and entropy equations with respect to the chosen state variables of the system can be found as:

$$dU=\left[T\left(\frac{\partial S}{\partial \varepsilon_{ij}}\right)_T+\sigma_{ij}\right]d\varepsilon_{ij}+T\left(\frac{\partial S}{\partial T}\right)_V dT \tag{17}$$

By satisfying the condition of total differential for energy equation, one has:

$$\frac{\partial}{\partial T}\left[T\left(\frac{\partial S}{\partial \varepsilon_{ij}}\right)_T + \sigma_{ij}\right] = \frac{\partial}{\partial \varepsilon_{ij}}\left[T\left(\frac{\partial S}{\partial T}\right)_V\right] \tag{18}$$

Hence:

$$\left(\frac{\partial S}{\partial \varepsilon_{ij}}\right)_T = -\left(\frac{\partial \sigma_{ij}}{\partial T}\right)_V \tag{19}$$

Consider the volumetric expansion term and utilize the thermodynamic relation:

$$\left(\frac{\partial S}{\partial \varepsilon_{ij}}\right)_T = \beta_{ij} \tag{20}$$

$$T\left(\frac{\partial S}{\partial T}\right)_V = \left(\frac{\partial U}{\partial T}\right)_V = c_v \tag{21}$$

where c_v is a specific heat term that is related to the unit volume at constant deformation. Applying Eqs. (20)-(21) to Eqs. (15)-(16), one can obtain the final form of the thermoelastic governing equations with respect to the selected state variables as:

$$dU = \sigma_{ij} d\varepsilon_{ij} + T\beta_{ij} d\varepsilon_{ij} + c_v dT \tag{22}$$

$$dS = \beta_{ij} d\varepsilon_{ij} + \frac{c_v}{T} dT \tag{23}$$

Substituting Eq. (10) into Eq. (23) and integrating Eqs. (22)-(23) with time with the assumption that for the natural state there exist *S* and *U* that equal to zero, the energy and entropy functions are obtained as follows:

$$U = \frac{1}{2} c_{ijkl} \varepsilon_{ij} \varepsilon_{kl} + T_0 \beta_{ij} \varepsilon_{ij} + c_v \theta \tag{24}$$

$$S = \beta_{ij} \varepsilon_{ij} + c_v log\left(1 + \frac{\theta}{T_0}\right) \tag{25}$$

Accordingly, the governing equations of the coupled thermoelastic system are closed. Eqs. (10) and (25) form the respective constitutive relations of the elastic and thermal subdomains. Eq. (24) forms the energy storage of the coupled system with respect to the chosen state variables (strain/deformation and temperature), where the first term represents the strain work, the second term represents the mutual interaction between deformation and temperature, and the last term represents the heat content in a unit volume.

Although the resultant model can solve a variety of thermoelastic problems, the implemented assumptions and the choice of the states for the coupled subdomains have introduced limitations to the model that significantly restrict its application areas, especially in multi-physical system dynamic investigations. As explained previously, since temperature is thermodynamically an equilibrium-determinant variable, not a true extensive variable, using it as the state variable of the

thermal subdomain together with heat flux as the correspondent flow will lead to domain-dependency of the resulting thermal dynamics. Consequently, the thermal subdomain cannot be presented as an independent physical subdomain containing its own power continuous energy frame. The power transformation between the different subdomains of a multi-physical system will not be achievable on the basis of the energy conservation which is a crucial principle for realizing the couplings between the subdomains. The generated thermal model will be unusable for thermoelastic systems that involve other physical subdomains such as aerothermodynamics or electrodynamics, as the dynamics of the thermal subdomain will be in principle dependent on the dynamics of the elastic subdomain.

3. Thermoelastic Bond graph model

In the following the problem related to the application of the conventional thermoelastic model in multi-physical system is addressed via retrieving the conservation principle in the procedure of modeling. To this aim, by means of the BG approach [3] [4] [5] a reversible thermoelastic coupled energy storage model is proposed, in which each subdomain of interest can remain independent and, thus, connectable to other physical subdomains.

In the BG notation, energy storage of a multi-physical system can be represented by a multiport capacitor that relates the information of each port to the corresponding physical subdomain [5] and forms the reversible interconnectivity of the different subdomains of the system. Using this notation in a thermoelastic coupled model, the energy storage element of the thermal and elastic subdomains can form an interconnected passage with which the thermal dynamic changes due to alteration in the elastic subdomain, and vice versa, can be captured in an energy conservative manner. A two-port capacity element, $\mathbb{C}$, as shown in Fig. 1 is therefore proposed for modeling the thermoelastic reversible coupling between the two subdomains:

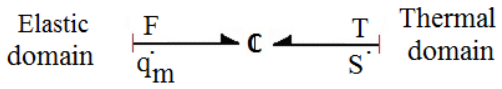

Fig.1 Two-port C model of the thermoelastic energy storage

In the proposed means of coupling, in order to make the model compatible with other physical subdomains, contrary to the conventional methods, entropy rate is considered as the time derivative

of the state for the thermal subdomain instead of heat. To define the constitutive equations of the potentials (F, T) for the suggested $\mathbb{C}$, since the integral causality is preferred, the true energy is considered as a function $U = U(q_m, S)$, where q_m and S are respectively the deformation and entropy of the system. Accordingly:

$$dU = \frac{\partial U}{\partial q_m} dq_m + \frac{\partial U}{\partial S} dS \tag{26}$$

By definition:

$$\left(\frac{\partial U}{\partial q_m}\right)_S = F \ , \left(\frac{\partial U}{\partial S}\right)_{q_m} = T \tag{27}$$

$$F = F(q_m, S) \quad , \quad T = T(q_m, S) \tag{28}$$

To define the conjugate (potentials) efforts for the $\mathbb{C}$ storage, let's start with the thermal subdomain where:

$$dT = \left(\frac{\partial T}{\partial q_m}\right)_S dq_m + \left(\frac{\partial T}{\partial S}\right)_{q_m} dS \tag{29}$$

According to the thermal energy at constant volume:

$$dU_{thermal} = C_v dT \tag{30}$$

$$\left(\frac{\partial T}{\partial S}\right)_{q_m} = \frac{T}{C_v} \tag{31}$$

where C_v is the specific heat in constant volume. To define the first term of Eq. (29), consider the Maxwell reciprocity and the Hook's law for 1D geometry:

$$\left(\frac{\partial T}{\partial q_m}\right)_S = \left(\frac{\partial F}{\partial S}\right)_{q_m} \tag{32}$$

$$F = AE\frac{q_m}{L} + \alpha AE(T - T_0) \tag{33}$$

$$\left(\frac{\partial T}{\partial q_m}\right)_S = \alpha AE \left(\frac{\partial T}{\partial S}\right)_{q_m} = \alpha AE \frac{T}{C_v} \tag{34}$$

where A, E, L, α, and T_0 are the element section area, material stiffness, element length, element axial heat expansion coefficient, and reference temperature, respectively. Substituting Eqs. (32)-(33) into Eq. (29) yields:

$$\frac{dT}{T} = \frac{\alpha AE}{C_v} dq_m + \frac{1}{C_v} dS \tag{35}$$

Considering an unstressed element and assuming constant specific heat, by integrating Eq. (35), the thermal effort can be presented as:

$$T = T_0 e^{\frac{\alpha AE}{C_v} q_m} e^{\frac{(S-S_0)}{C_v}} \tag{36}$$

Employing Eq. (36) to change the causality of Eq. (33) forms the elastic effort as:

$$F = AE\frac{q_m}{L} + \alpha AET_0(e^{\frac{\alpha AE}{C_v} q_m} e^{\frac{(S-S_0)}{C_v}} - 1) \tag{37}$$

Substituting the two constitutive Eqs. (36)-(37) into (26) forms energy function of the presented storage:

$$dU = \left(AE\frac{q_m}{L} + \alpha AET_0(e^{\frac{\alpha AE}{C_v} q_m} e^{\frac{(S-S_0)}{C_v}} - 1)\right)dq_m + \left(T_0 e^{\frac{\alpha AE}{C_v} q_m} e^{\frac{(S-S_0)}{C_v}}\right)dS \tag{38}$$

$$U = AE\frac{{q_m}^2}{2L} + C_v T_0 e^{\frac{\alpha AE}{C_v} q_m} e^{\frac{(S-S_0)}{C_v}} - \alpha AET_0 q_m \tag{39}$$

The resulting nonlinear multiport energy function of the thermoelastic domain, as shown in Eq. (39), contains a contribution relating to the displacement/strain and a contribution relating to the entropy, thus showing the combined effect of thermoelasticity. It is clear that the contributions of the thermal and elastic subdomains can now be individually expressed via the extensive parameters (displacement and entropy) of these two subdomains. This feature makes the proposed modeling technique domain-independent and physical. Knowing that the dynamic coupling between the thermal and elastic subdomains can be represented by the proposed $\mathbb{C}$ element, the next step is to install the proposed storage element in a thermoelastic junction structure.

4. Thermal and elastic subdomains' reversible coupling

In this section, by means of the proposed coupling, a novel thermoelastic model is generated with which the energy distribution frames of the involving physical subdomains are presented separately. To this aim, an arbitrary domain-independent elastic model will be connected to a compatible conductive model. The key connection joint used here will be the proposed $\mathbb{C}$ which describes the reversible, energy-conservative, nonlinear, and dynamic coupling between the thermal and elastic subdomains.

For simplicity a 1-D reticulated geometry shown in Fig. 2 is considered to describe the propagation of energy within the elastic subdomain [18]. In this elastic model, each element is composed of two storage components, generalized capacitor (spring), and generalized inertia (mass). In the configuration of each element, applying the acoustic assumption, the inertial component is considered to be placed at both boundaries, and the capacitor is assumed to be in the

center of the element. Avoiding additional complexity, only the axial elastic behavior of the element is considered here.

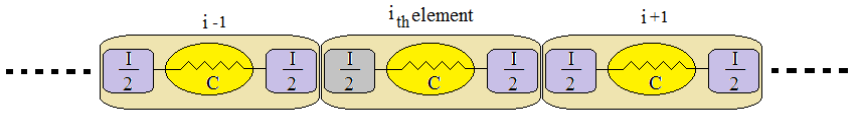

Fig.2 1-D geometry reticulation [18]

As this reticulated space is indeed a continuous system, the boundary of adjacent elements are bonded to move together. Thus, one can consider the above discretization as a junction-element chain in which the parameters of each junction is a weighted function of the related parameters of the adjacent elements. Fig. 3 shows the resultant BG model of the presented elastic subdomain. As can be seen, the internal energy can be stored at the boundaries in the form of kinetic energy and inside each element in the form of elastic energy. p_j and q_i are considered as the state variables of the *I*-type and *C*-type storage elements, respectively, where p_j denotes the momentum of each boundary and q_i indicates the relevant deformation of each element.

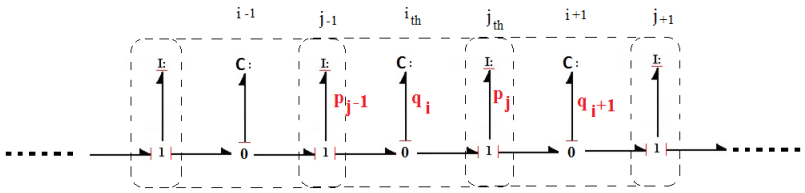

Fig.3 Bond graph of an elastic Beam

To identify the propagation of energy in the thermal subdomain, a 1-D domain-independent compatible conductive model introduced in [19] is chosen. In this model shown in Fig. 4, a thermoelastic friendly conductive element is represented using the Fourier heat conduction equation. As can be seen, each thermal element is consisted of a *C*-type storage with state variable, q_{Ti}, denoting the amount of stored entropy (S_i), and dissipative boundaries. In the proposed conductive model, each *C* storage is connected to the neighboring storages via resistive junction elements that inherit their resistive characteristics from the boundaries of the adjacent elements.

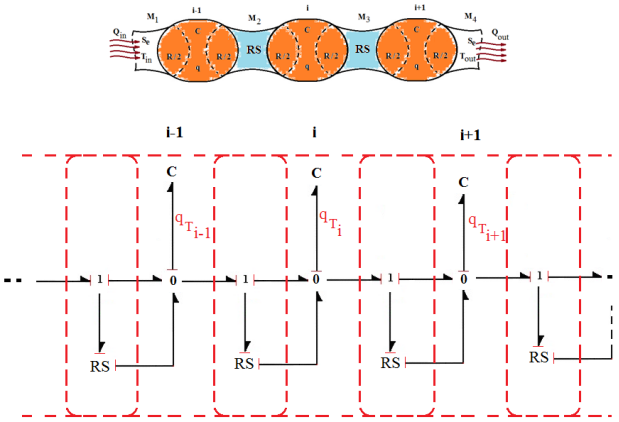

Fig.4 1-D conduction Bond graph model [19]

To finally generate the coupled presentation of the thermoelastic field, the single-port storage element of each subdomain (C) is replaced with the proposed two-port $\mathbb{C}$ storage element. Fig. 5 shows a BG representation of the reversibly coupled thermoelastic model. It shows that the interconnections of the two subdomains is through the storage of the system. Clearly, through this coupling, the products of effort and flow of the generated $\mathbb{C}$ ($F.\dot{q}_m$ and $T.\dot{S}$) form the continuous power interchanged between the thermal and elastic subdomains. Consequently, it is anticipated that, on the one hand, the thermal fluctuation of the system will affect the capacity of the elastic subdomain which will lead to mode-shape change and material softening and, on the other hand, the deformation of the structure in the elastic subdomain will lead to temperature change in the thermal subdomain.

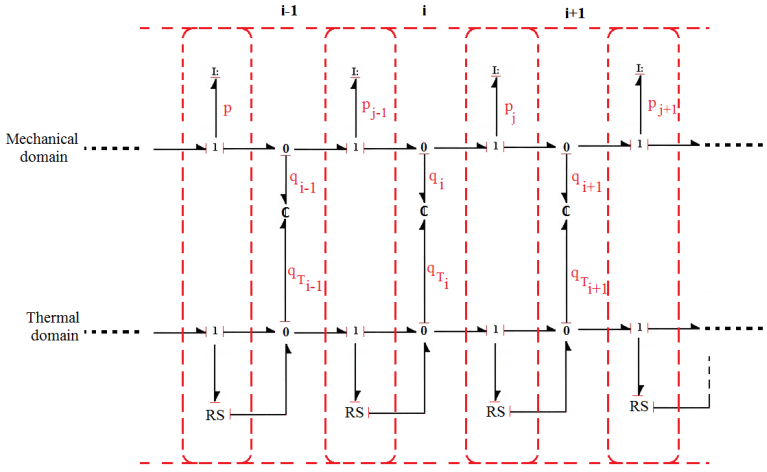

Fig.5 1-D thermoelastic Bond graph model

Considering the generated coupled thermoelastic BG model, the governing equations for a

single and port based thermoelestic element (the i_{th} element in a chain) can be extracted as below:

$$\dot{p}_j = A_i E_i \frac{q_{m_i}}{L_i} - A_{i+1} E_{i+1} \frac{q_{m_{i+1}}}{L_{i+1}} + \alpha_i A_i E_i T_{0_i} \left(e^{\frac{\alpha_i A_i E_i}{C_{v_i}} q_{m_i}} e^{\frac{(S_i - S_{0_i})}{C_{v_i}}} - 1 \right) - \alpha_{i+1} A_{i+1} E_{i+1} T_{0_{i+1}} \left(e^{\frac{\alpha_{i+1} A_i + 1 E_{i+1}}{C_{v_{i+1}}} q_{m_{i+1}}} e^{\frac{(S_{i+1} - S_{0_{i+1}})}{C_{v_{i+1}}}} - 1 \right) \tag{40}$$

$$\dot{q}_{m_i} = \frac{p_{j-1}}{I_{j-1}} - \frac{p_j}{I_j} \tag{41}$$

$$\dot{S}_{T_i} = \frac{1}{R_{j-1}} (T_{0_{i-1}} e^{\frac{\alpha_{i-1} A_{i-1} E_{i-1}}{C_{v_{i-1}}} q_{m_{i-1}}} e^{\frac{(S_{i-1} - S_{0_{i-1}})}{C_{v_{i-1}}}} - T_{0_i} e^{\frac{\alpha_i A_i E_i}{C_{v_i}} q_{m_i}} e^{\frac{(S_i - S_{0_i})}{C_{v_i}}}) - \frac{1}{R_j} (T_{0_i} e^{\frac{\alpha_i A_i E_i}{C_{v_i}} q_{m_i}} e^{\frac{(S_i - S_{0_i})}{C_{v_i}}} - T_{0_{i+1}} e^{\frac{\alpha_{i+1} A_i + 1 E_{i+1}}{C_{v_{i+1}}} q_{m_{i+1}}} e^{\frac{(S_{i+1} - S_{0_{i+1}})}{C_{v_{i+1}}}}) + \dot{S}_i^{gen} \tag{42}$$

$$\dot{S}_i^{gen} = \frac{T_{0_i} e^{\frac{\alpha_i A_i E_i}{C_{v_i}} q_{m_i}} e^{\frac{(S_i - S_{0_i})}{C_{v_i}}}}{R_{j-1}} \left(\frac{T_{0_{i-1}} e^{\frac{\alpha_{i-1} A_{i-1} E_{i-1}}{C_{v_{i-1}}} q_{m_{i-1}}} e^{\frac{(S_{i-1} - S_{0_{i-1}})}{C_{v_{i-1}}}}}{T_{0_i} e^{\frac{\alpha_i A_i E_i}{C_{v_i}} q_{m_i}} e^{\frac{(S_i - S_{0_i})}{C_{v_i}}}} - 1 \right)^2 \tag{43}$$

$$I_j = \frac{m_i}{2} + \frac{m_{i+1}}{2} \tag{44}$$

$$R_j = \frac{1}{2} \left(\frac{l_i T_{0_i} e^{\frac{\alpha_i A_i E_i}{C_{v_i}} q_{m_i}} e^{\frac{(S_i - S_{0_i})}{C_{v_i}}}}{k_i A_i} + \frac{l_{i+1} T_{0_{i+1}} e^{\frac{\alpha_{i+1} A_i + 1 E_{i+1}}{C_{v_{i+1}}} q_{m_{i+1}}} e^{\frac{(S_{i+1} - S_{0_{i+1}})}{C_{v_{i+1}}}}}{k_{i+1} A_{i+1}} \right) \tag{45}$$

where I_j is the boundary inertia and R_j is the thermal resistance parameter of each junction element. Eqs. (40)-(42) represent the rate of element's boundary momentum, deformation, and accumulated entropy, respectively, as nonlinear functions of the considered extensive states (q_m and S), geometrical parameters, and material parameters. It clearly shows that the thermal state appears in the elastic subdomain's momentum equation and the elastic state appears in the thermal subdomain's entropy equation. This in principal indicates the influences between the thermal and elastic subdomains. Eq. (43) demonstrates the amount of irreversibility occurring in the thermal subdomain. It is clear that this equation satisfies the second thermodynamic law as the amount of the generated entropy is always greater than zero. Further attentions to the generated state equations reveal that, although the elastic subdomain is considered to be non-dissipative (pure elastic), the irreversibility of the thermal subdomain can affect the elastic domain's behavior via the reversible connectivity of these two subdomains.

The above explanation demonstrates the distinctive novelty of the proposed method in utilizing the BG technique to expose physically-meaningful insights of internal dynamics of

multidisciplinary systems. It should be mentioned that to obtain a complete coupling between these two subdomains, the elastic dispersion of the system is also needed to be taken into account. However, since the main aim is to generate reversible thermoelastic coupling, further attention to inelasticity is not included here in this study.

5. Simulation analysis

To evaluate the ability of the proposed BG model to capture the thermoelastic phenomena, a set of simulation studies on a simple beam structure that is subjected to, respectively, low and high frequency elastic vibration, steady and cyclic heat transfer, and thermomechanical cyclic loadings, are performed. The geometrical and material parameters of the beam are given in Table 1, and the 1-D axial thermomechnical behavior of the beam is to be investigated. To generate the discretised geometry, the chosen beam is reticulated into 10 uniform elements with the first and last elements being the boundary elements that receive external mechanical and thermal loads. It is assumed that the side surface of the beam is fully isolated and the beam is stress-free initially in the ambient room temperature. Sequentially, the internal behaviors of the system are presented, respectively, in Figs. 6 to 10 with respect to low and high frequency external mechanical loads and in Figs. 11 to 13 with respect to steady and cyclic external thermal loads. The thermoelastic behaviors of the system with respect to simultaneous thermo-mechanical external loads are presented in Figs. 14 to 17.

Table 1. Geometrical and material parameters of the considered beam

Symbol	Description (unit)	Value	Symbol	Description (unit)	Value
$\boldsymbol{k}$	Conduction coefficient $(J/m.K)$	$2.73e^{2}$	m	Beam mass (Kg)	$5.67e^{-2}$
$\boldsymbol{E}$	Young modulus (N/m^{2})	$6.9e^{10}$	A	Cross section area (m^{2})	$1e^{-4}$
$\boldsymbol{C_v}$	Specific heat $(J/Kg.K)$	$8.97e^{2}$	l	Length (m)	$2.1e^{-1}$
$\boldsymbol{\alpha}$	Linear expansion $(1/K)$	$2.22e^{-5}$	M	Molar mass (kg/mol)	$2.698e^{-2}$
$\boldsymbol{S_0}$	Reference Entropy $(J/Kg.K)$	$2.83e^{1}$	n	Number of segments	10

5.1. Elastic effects on thermal domain

5.1.1. a. Low frequency vibration

To evaluate the impact of the elastic subdomain on the thermal subdomain, a sinusoidal external mechanical load shown in Fig. 6 (a) is applied axially to both ends of the free-beam structure. The resultant elastic deformation of the system is shown in Fig. 6 (b), which demonstrates the capability of the proposed model in capturing the elastic behavior of the system. Fig. 7 shows the corresponding behavior of the thermal subdomain, where Part (a) demonstrates the entropy change and Part (b) presents the resulting temperature profile. It is obvious that the temperature does not follow the same pattern as the entropy. While the entropy shows contraction that reduces its storage capacity, the temperature demonstrates rise as a result of the elastic contraction. This unexpected behavior can be explained by Parts (c) and (d) of Fig. 7 which illustrate, respectively, the element's entropy rate and entropy generation rate. It is clear in Part (c) that the contraction of the beam causes entropy to exit from all elements at the same time even with positive entropy generation (Part (d)). This means that a certain amount of entropy has found its way to leave the system leading the system to entropic interaction with the surrounding.

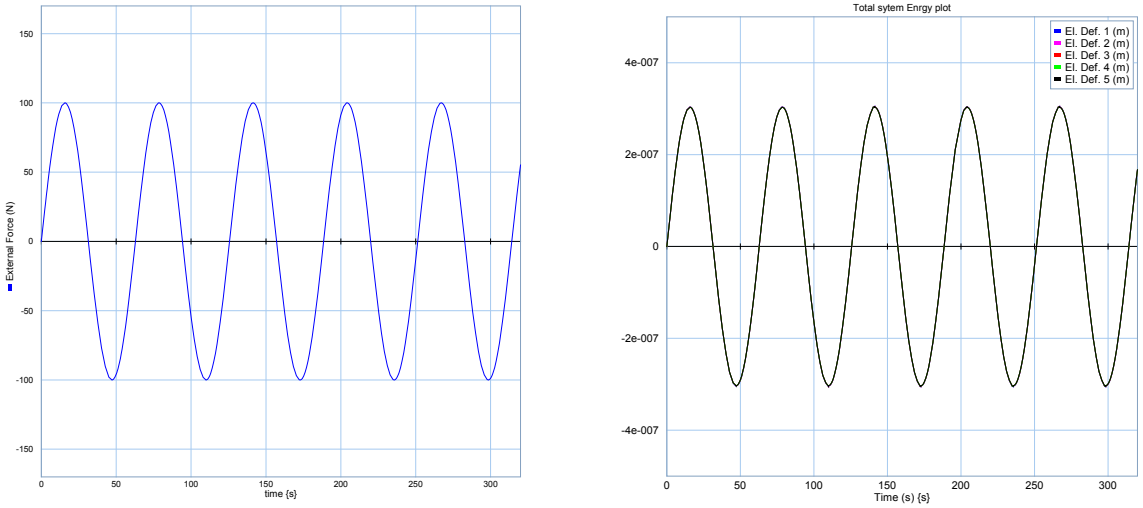

(a) (b)

Fig.6 Applied external force (a) and the resultant deformation (b)

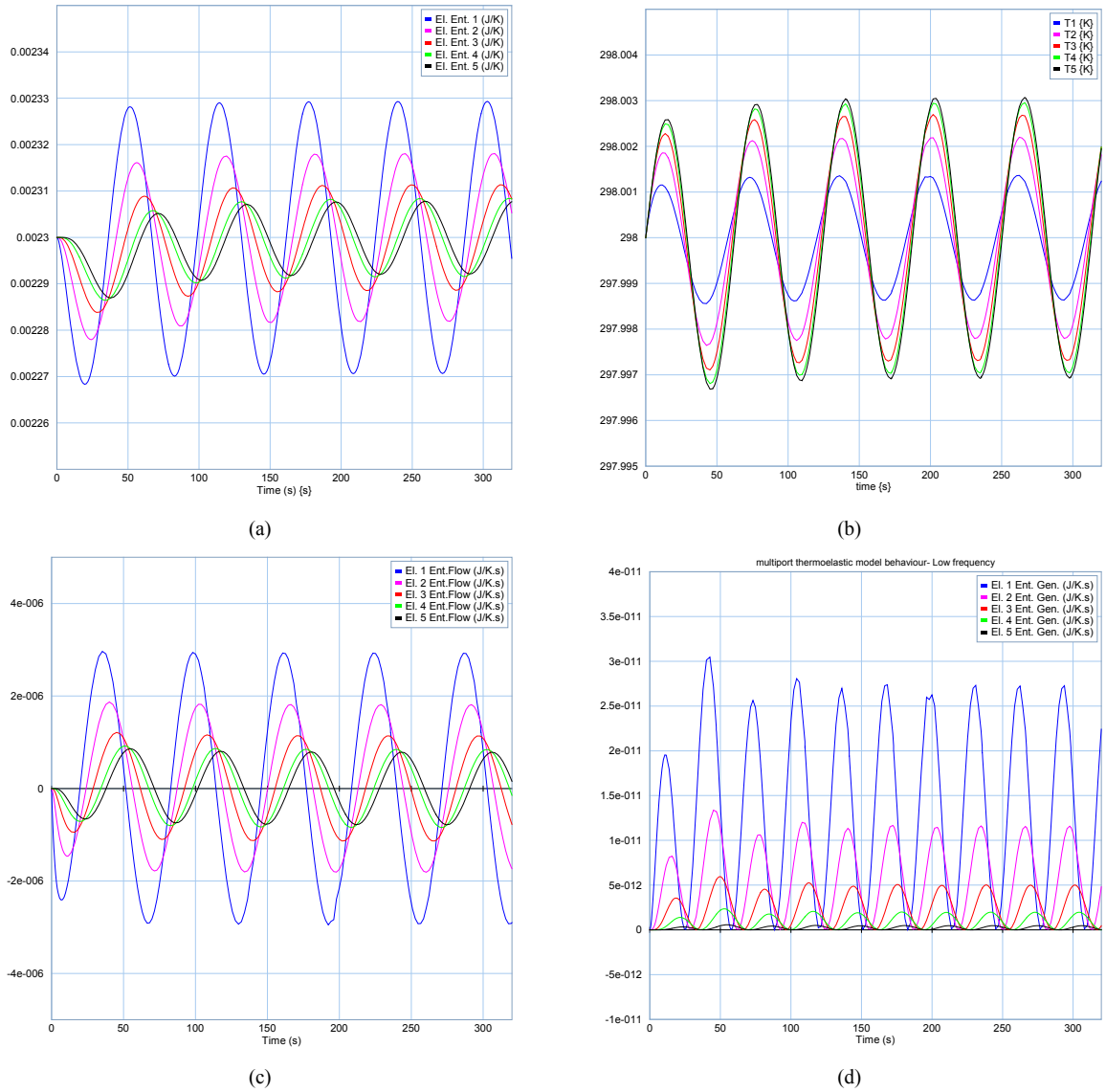

Fig.7 Deformation and entropy change of the system under cyclic loading

A comparison between the behaviors of the resultant elastic and thermal subdomains shown in Fig. 6 and Fig. 7 indicates the well-known fact that the thermal dynamics are relatively slower than the elastic dynamics. This fact has to be taken into account in developing control strategies for thermoelastic applications. The proposed model is seen to possess a unique ability to separately demonstrate the dynamics of these two subdomains.

5.1.2. b. High frequency vibration

To check the high-frequency interactions between the elastic and thermal subdomains, an external force shown in Fig. 8 (a) is considered to be applied axially to both ends of the free-beam

structure. With the high-frequency excitation, the elastic response of the un-damped structure, as presented in Fig. 8 (b), becomes more complicated. Increasing the frequency of the applied force is seen to introduce a shock wave propagation in the elastic subdomain, which produces superposed dynamics of the elastic subdomain. Thus, the energy transformation between the different subdomains will be subjected to a more complicated dynamic pattern.

Fig. 9 presents the thermal subdomain dynamic behavior with respect to the applied external force. A comparison between the elastic state variable, Fig. 8 (b), and the thermal state variable, Fig. 9 (a), reveals different energetic behaviors of these two subdomains. The highly-fluctuating oscillatory behavior of deformation in the elastic subdomain is in clear contrast to the calmly relaxing behavior of entropy in the thermal subdomain.

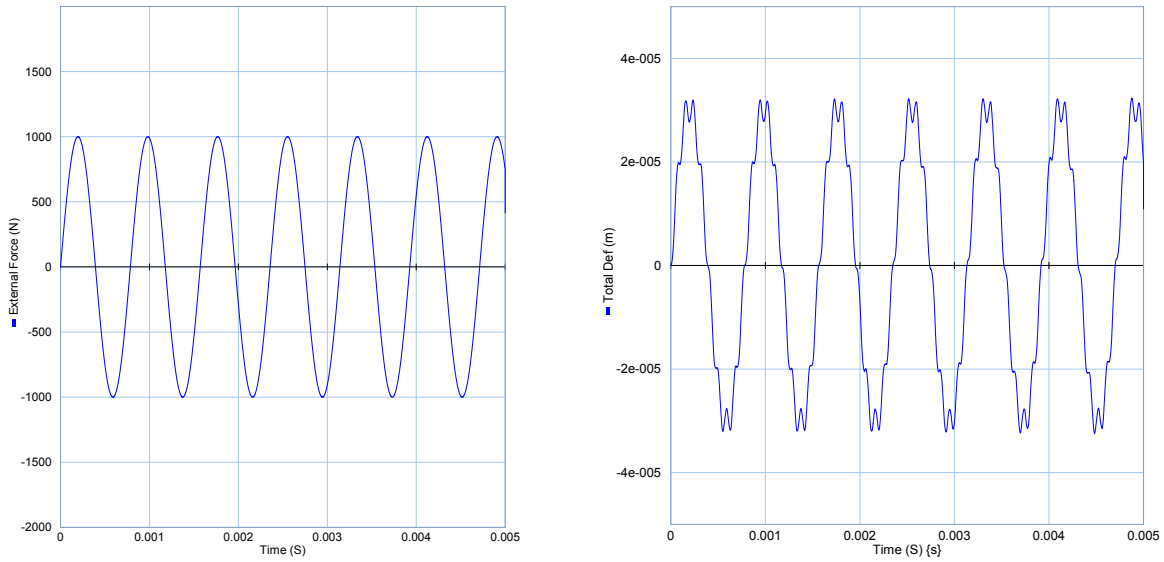

(a) (b)

Fig.8 High frequency vibration of the beam

It is noticed that, although entropy has a smooth behavior (Fig.9 (a)), temperature exhibits oscillations (Fig.9 (b)). This fact reflects the elastic shock-propagation impact on the thermal subdomain dynamics. It implies that to obtain a complete dynamic connection between the thermal and other involving subdomains in a multi-physical system, entropy should be used as a state of the system. Otherwise, a portion of system dynamics will be missed if one relies only on the capability of temperature measuring techniques.

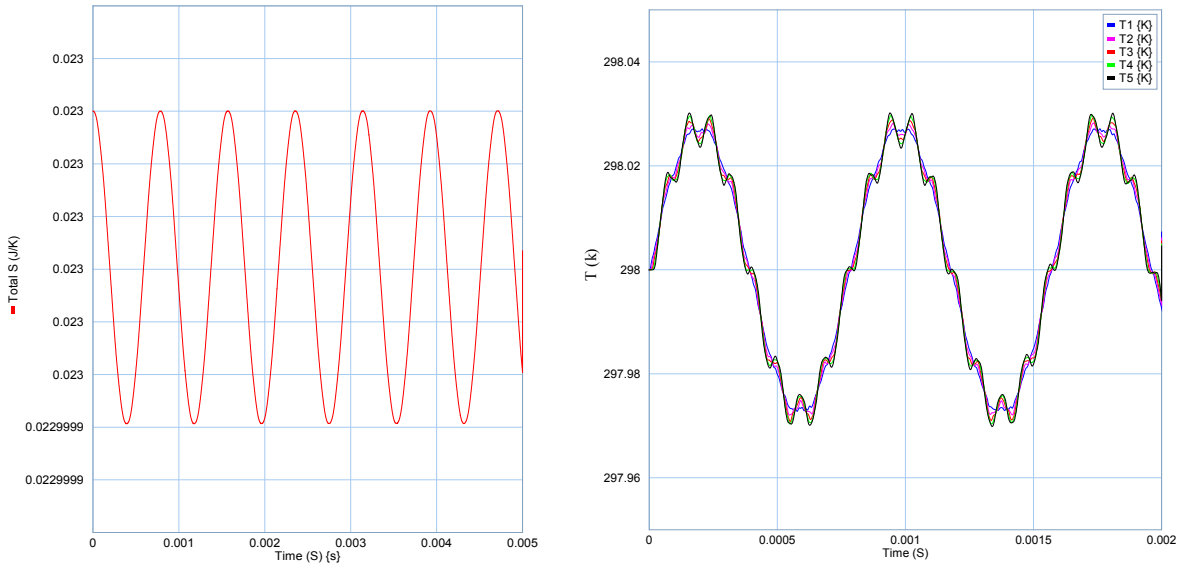

(a) (b)

Fig.9 Thermal domain dynamics in high frequency oscillations

Fig.10 shows the behavior of the system close to its natural frequency. Part (b) presents the total deformation profile under external force of Part (a), and Parts (c) and (d) demonstrates the corresponding entropy and temperature behaviors. As the elastic subdomain is considered to be non-dissipative, the deformation profile is in a repetitive pattern. However, there is a rising pattern in the entropy profile, as the nature of heat conduction within the system is irreversible. This behavior can be considered as the reason for thermoelastic damping phenomena in high-frequency oscillations. The generation of entropy leads to a gradual temperature rise in the thermal subdomain and a simultaneous structural expansion in the elastic subdomain. Since the resultant temperature rise is non-uniform across the structure owing to different elemental deformation, the resultant expansion of each element will vary from each other. Gradually, these dynamics will change the oscillatory behavior of each element in such a way that will disallow the elements to be unified to form a resonance mode.

One should realize that in a macroscopic level, the situation explained-above rarely happens, as for a real physical system there always exists a certain amount of dissipation in the elastic subdomain that would prevent this from happening. However, in a microscopic level (e.g., in a microelectronic device), the thermal consideration in high-frequency situations may become an important issue for critical control strategy (e.g. high precision control of lithography printing microstructures) development.

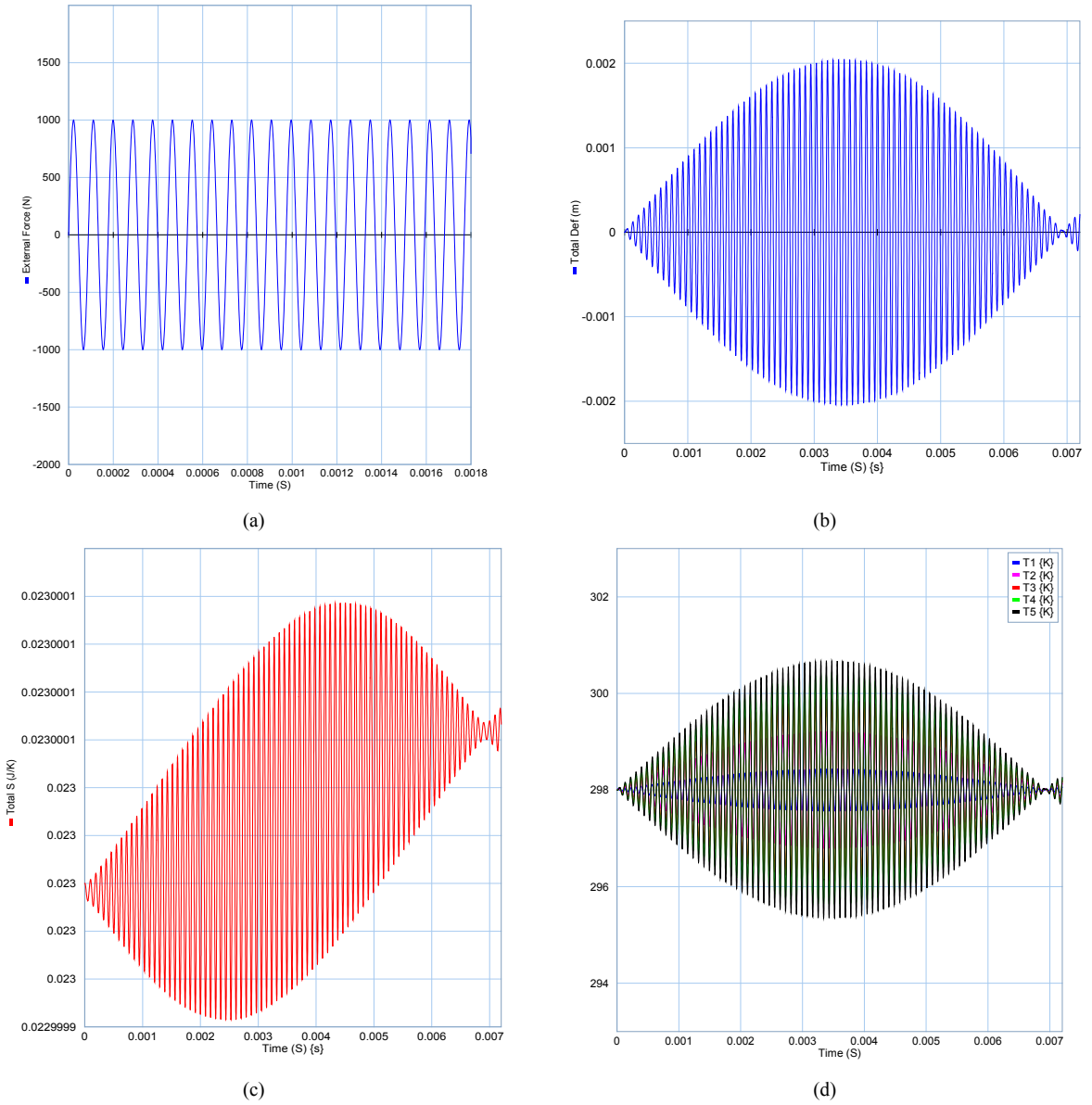

Fig.10 Dynamic behavior of the system close to natural frequency

5.2. Thermal effects on elastic domain

5.2.1. a. Free beam consideration

To discuss the impact of the thermal subdomain dynamics on the elastic subdomain dynamics, a force-free free-beam structure is considered where thermal power can transfer from its both ends. A step thermal input of 200 K is applied to both ends, and the resultant thermomechanical behavior is presented in Fig. 11. A gradual temperature rise in the system (shown in Part (a)) is seen to cause a gradual expansion of the system (shown in Part (b)). It should be mentioned that in the simulation

the contraction is considered to be positive, so the expansion is presented with negative quantity. The obtained simulation results reveal physical relaxing dynamics for both involving subdomains, which echoes the natural behavior of the system during the expansion process.

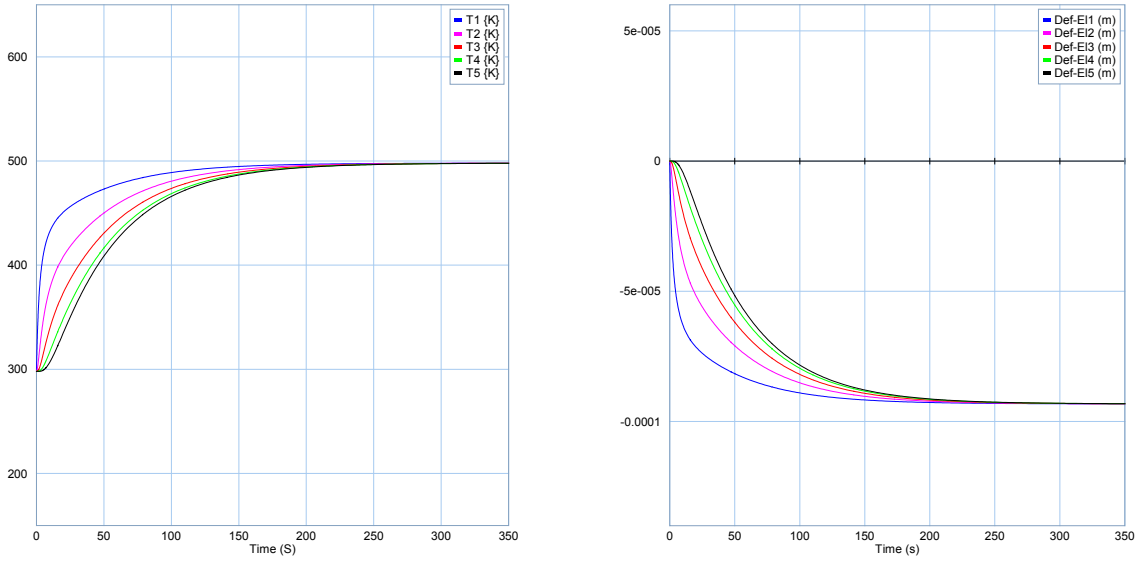

(a) (b)

Fig.11 Heat conduction inside a free beam

To investigate the impact of cyclic thermal loading on the structural dynamics, a low-frequency thermal input, as shown in Fig. 12 (a), is applied to the structure. The resultant temperature profile is presented in Fig. 12 (b). It is observed that the temperature fluctuations in the outer elements are higher than those in the center elements. Fig. 12 (c) shows that the resultant dilative behavior in the elastic subdomain follows the same pattern as the temperature behavior in the thermal subdomain. Fig. 12 (d) demonstrates the generated entropy within the system as a result of these fluctuations. The gradual growth in this graph can explain the gradual rise in the temperature profile.

From the temperature profile, it is clear that the deformation alongside the beam is dependent on the distance of the element from the heat source. This means that the dilation pattern of the system is not homogenous, which highlights the necessity for using different control strategies to stabilize high-speed structures under aero-thermo loads.

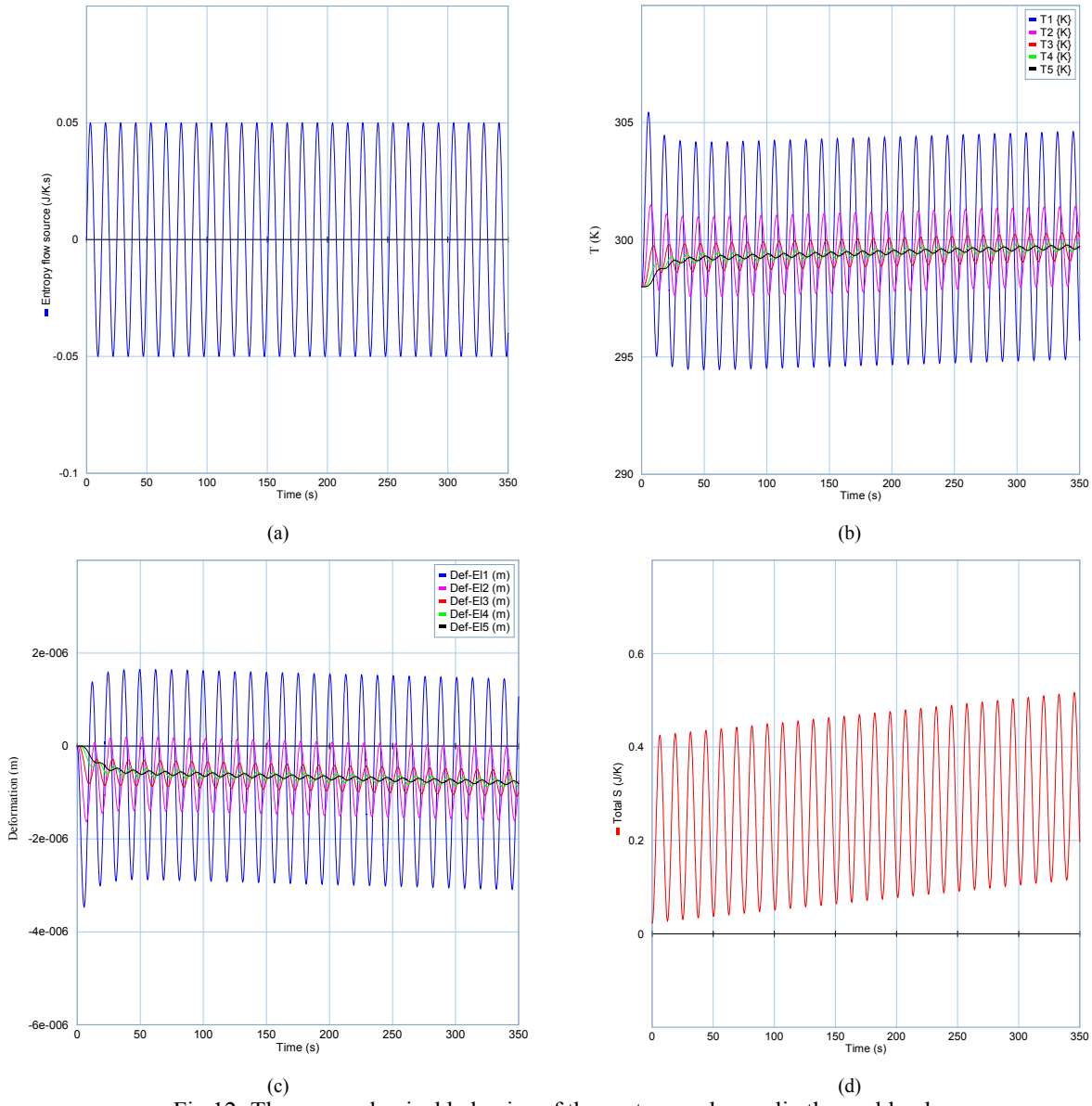

Fig.12 Thermomechanical behavior of the system under cyclic thermal load

5.2.2. b. Fixed-end beam consideration

To investigate the impact of thermal stress on structural dynamics, it is assumed that heat power can get into the beam from its fixed ends. Fig. 13 (a) shows the considered entropy flow source of the system. Fig. 13 (b) demonstrates the resultant thermal behavior which has almost the same nature as the free-beam thermal fluctuation shown in Fig. 7. In Fig. 13 (c) the resultant internal force for each element is presented. One can vividly see the growing rate of the thermal reaction force as a result of the thermal energy storage in the system. In Fig. 13 (d) the internal deformation (as an indicator of thermal strain) is presented. It is clear that the total deformation of the system

is equal to zero; however the elemental deformation varies depending on the distance of the element to the thermal source.

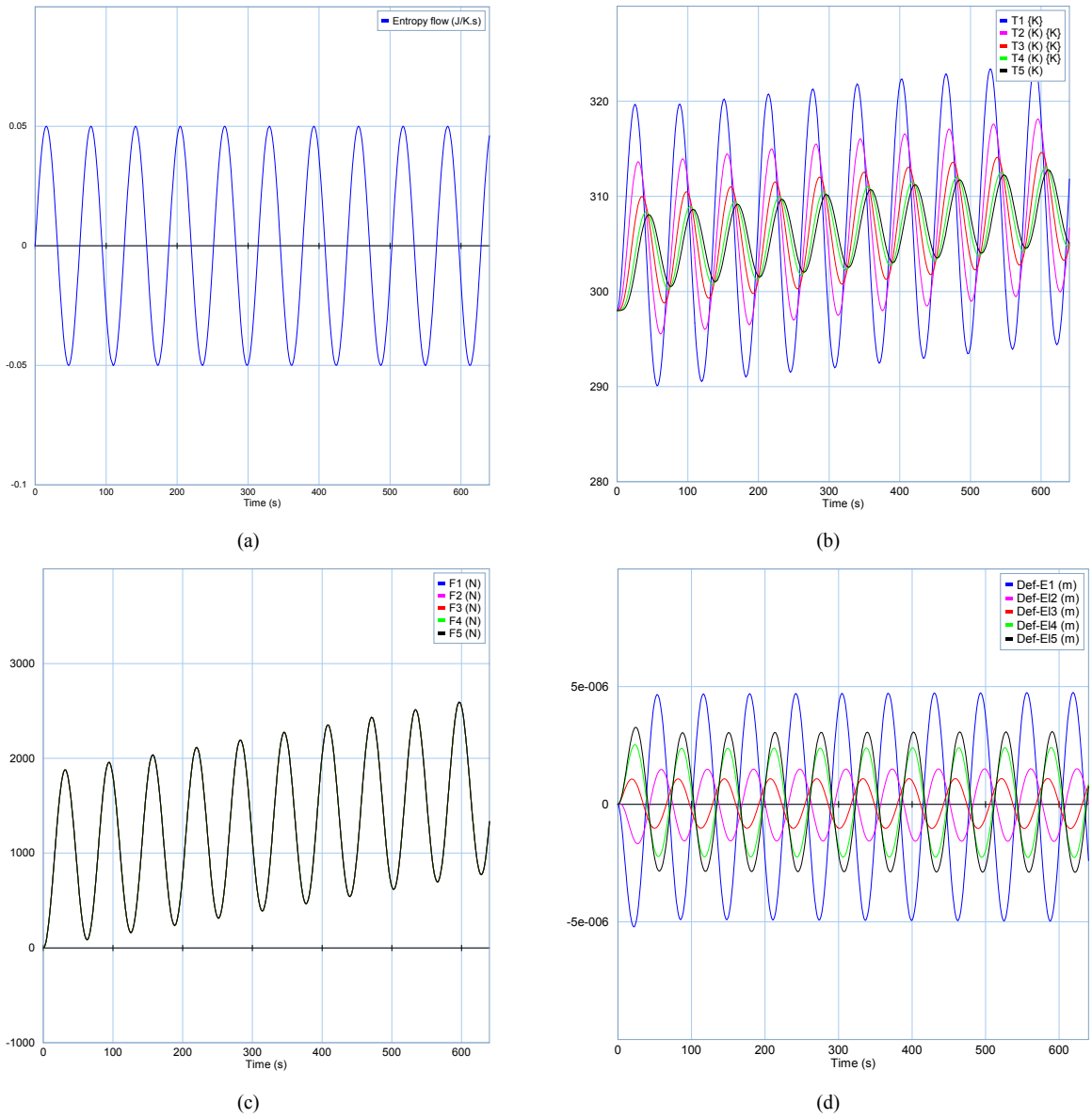

Fig.13 Fixed ends beam thermomechanical behavior

5.3. Free-beam under thermoelastic loading

To check the ability of the proposed model to track the internal dynamics under complex loading conditions, a mechanical load accompanied by a thermal load, shown respectively in Fig. 14 (a) and (b), are applied to both ends of the free-beam structure symmetrically. These loads are considered as flow sources into the system. In real conditions these loads are dynamically coupled together, thus, to obtain a more physical aero-thermo load, one would need to model the fluid flow

around the structure and then couple it dynamically with the proposed thermoelastic model to form a more reasonable aero or hydro-thermoelastic load.

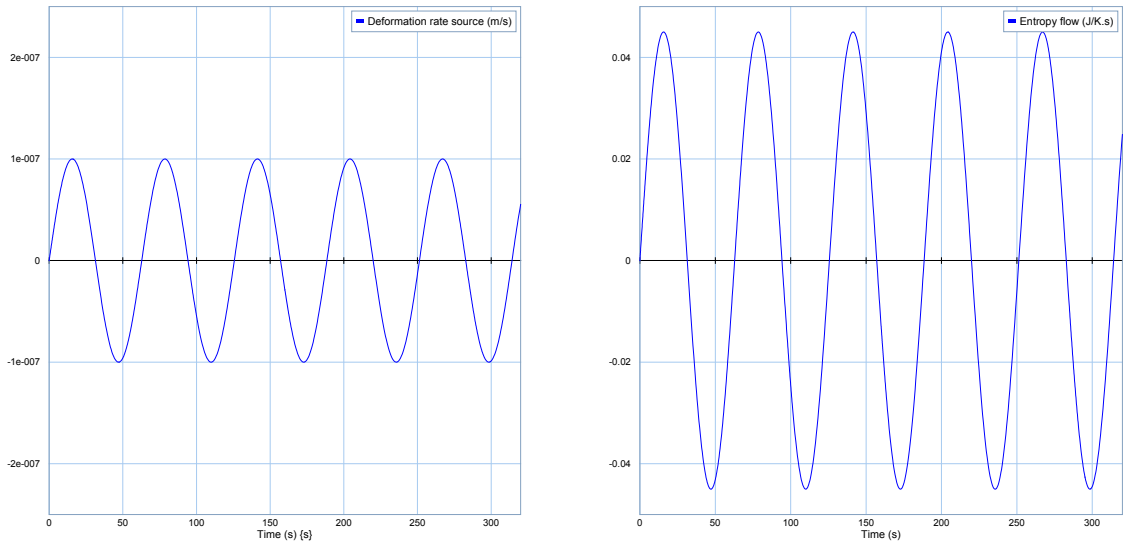

(a) (b)

Fig.14 Deformation rate source (a), Entropy flow source (b)

The resultant elements' deformation and temperature changes are depicted in Fig. 15 (a) and (b), respectively. One can see that the deformation behavior in this case is similar to the deformation behavior in the fixed-end-beam cyclic-thermal-loading case. This is because in the latter case, the reaction of the thermal stress on the structure at both fixed ends is in principal equivalent to applying a mechanical load on the structure, which makes the situation similar to the former case.

Fig. 15 demonstrates the energetic behavior of the beam under the considered mixed loading for a longer period of thermoelastic vibrations. Part (a) indicates the stored energy in the elastic subdomain, and Part (b) represents the corresponding energy change in the thermal subdomain. As can be seen, the styles of the energy consumptions of these two subdomains are totally different from each other. In the elastic subdomain, the potential of the domain (force) tends to have a non-dissipative and conservative behavior in each cycle, whereas in the thermal subdomain an accumulative-dissipative pattern of the potential (Temperature) can be observed. To explain the shifting pattern of the obtained results, one can consider that the added amount of energy to the system, as a result of the thermal subdomain irreversibility, can increase the temperature and

consequently the internal tension of the system. This unwanted energetic lift inside the system in a long term may result in unwelcoming deformations of the system.

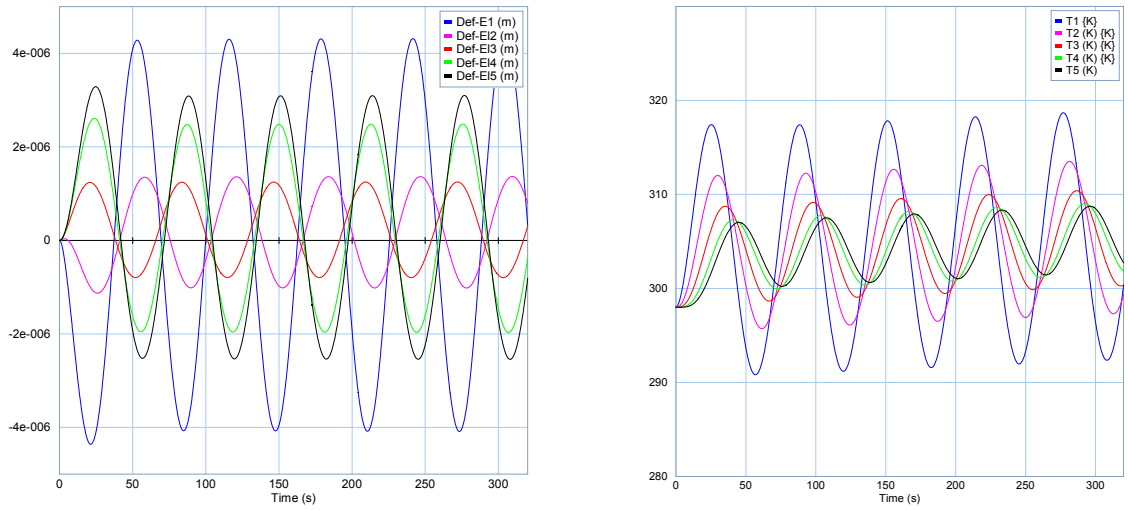

(a) (b)

Fig.15 Elemental deformation (a), Thermal behavior (b)

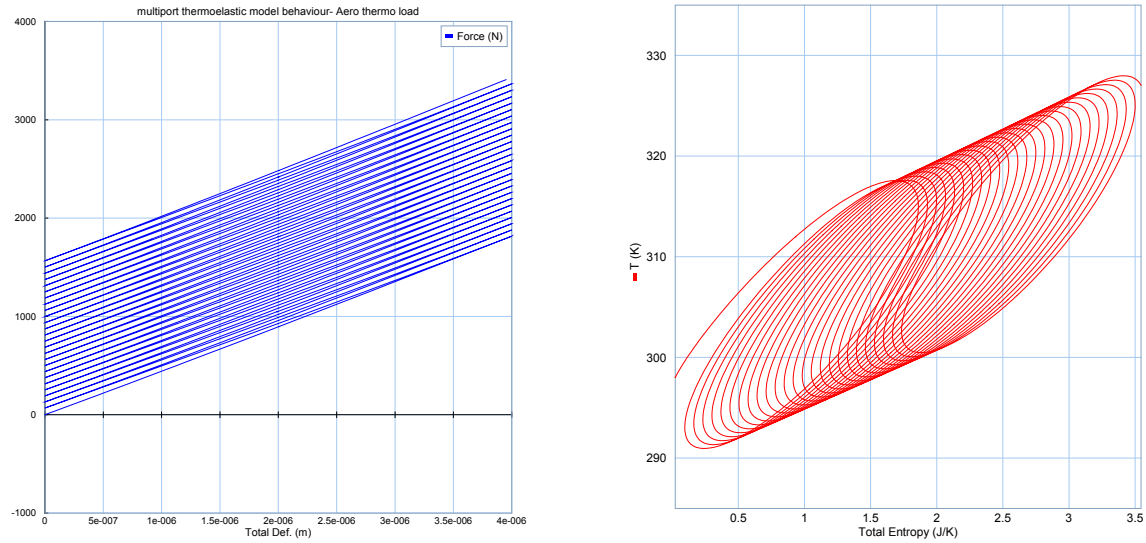

(a) (b)

Fig.16 Energetic behavior of the system under mixed loading

The fact revealed in Fig.16 indeed demonstrates the benefits of implementing conservation of energy in the proposed model. The clockwise rotation in the thermal subdomain and the counterclockwise rotation in the elastic subdomain show that the amount of energy transferred between these two subdomains is always oppositely equal to each other. This, thanks to the generated reversible energy storage, means that energy exiting from one subdomain is entered into

the other subdomain without loss. The different energetic patterns between the thermal and elastic subdomains, although indicate a weak coupling between the two subdomains, do show how this weak interaction can actually alter the performance of the system.

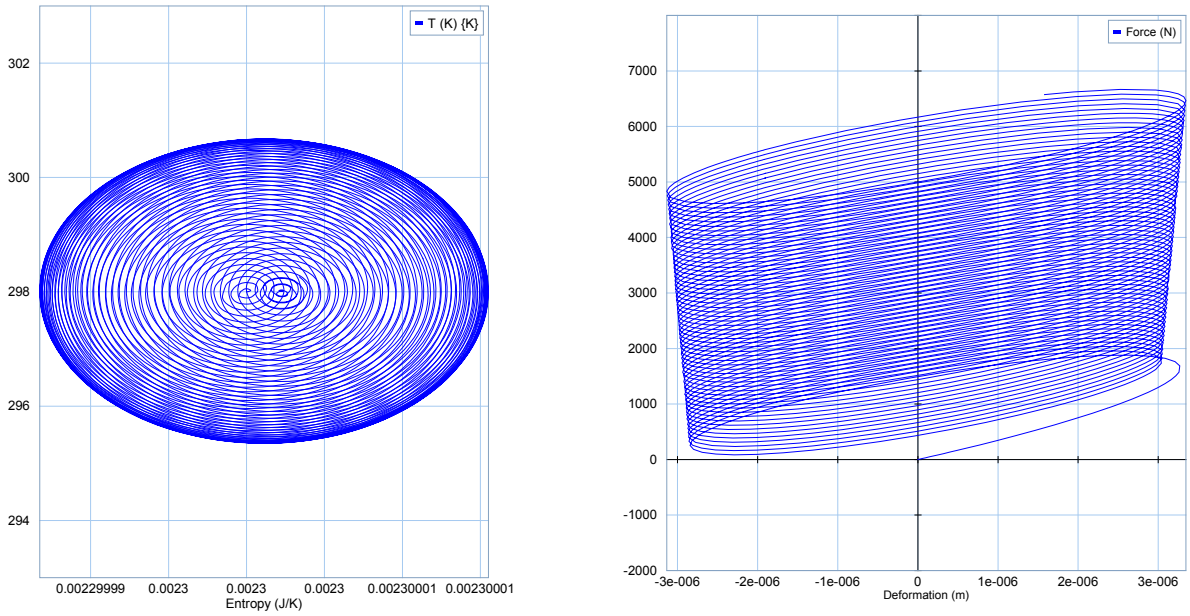

(a) (b)

Fig.17 Center element thermal behavior about natural frequency (a), fixed ends beam elastic behavior under thermal loading (b)

Having a clear understanding of the energetic behavior of a multi-physical system, especially in the form of a separate graph for each of the involving subdomains, can be a supportive tool for managing the energy consumption of the entire system. For example, knowing the local thermal behavior of the system about the natural frequency (such as Fig.17 (a)), in order to stabilize the system one can exclude a certain amount of entropy from the system via locally cooling the system. Alternatively, as in the case of a noise reduction application, knowing the local elastic behavior of the system (such as Fig.17 (b)), in order to suppress the undesired deformation one can compensate the impact of the stress growth inside the system via, for instant, implementing an effective active control mechanism.

6. Conclusion

In this study, by means of the BG method, a domain-independent, nonlinear, coupled thermoelastic model is generated for investigating the thermomechanical behavior of multi-physical systems. In this model, via the proposed energy conservative coupling, the reversible

dynamic interactions between the elastic and thermal subdomains are considered. The generated model is capable of not only describing the dynamic behavior of the system, but also providing a useful power frame within which the energy distribution of the system with respect to each of the involved subdomains is distinguishable.

The rational compatibility between the obtained results and the natural behavior of the system shows that the proposed model can unveil a high-degree of complexity of the system's internal dynamics under thermoelastic loading, which would otherwise be overlooked by other conventional models. In addition, the obtained separate energetic framework of the proposed model offers a considerable potential for the development of more control-oriented strategies that can address the individual dynamics of each of the participating subdomains, instead of the total dynamics of the multi-physical system.

References

[1] W. K. Nowacki, Progress in Thermoelasticity, Warszawa: European Mechanics Colloquium, 1967.

[2] H. karimi, A. Nassirharand, A. Zanj, "Integration of modeling and simulation of warm pressurization and feed systems of liquid propulsion systems," *Acta Astronautica J.,* vol. 69, no. (5-6), p. 258–265, 2011.

[3] J. Amerongen, E. Coelingh , T. Vries , "Computer support for mechatronic control system design," *Robotics and Autonomous System,* vol. 30, 2000.

[4] J. J. Granda, The role of bond graph modeling and simulation in mechatronics systems, . An integrated software tool: CAMP-G, MATLAB-SIMULINK, Mechatronics, 2002.

[5] P. Breedveld, Physical System Theory In Therms of Bond graphs, Enschede: Univercity of Twente , 1984.

[6] J. M. O. Duhamel, "Second memoire sur lesphenomenes thermome'eaniques," *J. de l'Ecole Polytechn.,* vol. 15, pp. 1-15, 1837.

[7] W. Voigt, Lehrbuck der Kristallphysik, Teubner, 1910.

[8] H. Jeffreys, "The thermodynamics of an elastic solid," in *Proc. Camb. Phil. Soc., 26*, 1930.

[9] M. A. Biot, "Thermoelasticity and irreversible thermodynamics," *J. Appl. Phys.,* vol. 27, 1956.

[10] S. R. D. Groot, Thermodynamics of irreversible processes, Amsterdam,, 1952.

[11] P. C. Breedveld, Physical System Theory In Therms of Bond graphs, Enschede: Univercity of Twente, 1984.

[12] J. Thoma, Simulation by Bond graph, Verlag, Gemany: Springer, 1990.

[13] A. Mukherjee, R. Karmakar , Modeling and Simulation of Engineering Systems through Bon dgraph, New Delhi, India: Narosa Publishing House, 2000.

[14] H. Afshari, A. Zanj, "Dynamic Analysis of a Nonlinear Pressure Regulator Using Bondgraph Simulation Technique," *Journal of Simulation Modeling Practice and Theory,* 2010.

[15] A. Zanj, H. Karimi, A.J. Gholi, M. Shafiee, "Dynamic Modeling of Indirect Hydro-Control Valve - Bondgraph Approach," *Journal of Simulation, Modeling, Practice and Theory,* 2012.

[16] B. A. Boley, J. H. Weiner, Theory of thermal stresses, New York: John Wiley, 1960.

[17] R. Courant, D. Hilbert, Methods of Mathematical Physics, Verlag: Willey-VCH, 2004.

[18] A. Zanj, F. He, "A Thermomechnical Enhanced Elastic Model: Bond Graph Approach," in *23rd International Congress on Sound andVibration*, Athen, Greece, July, 2016.

[19] A. Zanj, F. He, "Conduction Model Compatible for Multi-Physical Domain Dynamic Investigations: Bond Graph Approach," in *18th International Conference on Engineering Systems Modeling, Simulation and Analysis*, Madrid, Spain, March, 2016.

CHAPTER 5: THERMOVISCOELASTIC COUPLED MODEL FOR SOLID FIELD

Aim

The aim of this chapter is to generate an energy-based thermovisvoelastic model for the solid filed from the coupled model presented in Chapter 4.

Description

To achieve this aim, the irreversible coupling between the present subdomains of the solid field is generated and added to the reversibly coupled thermoelastic model. To do so, first, energy-based domain independent models of the existing dissipative mechanisms of the solid field are generated, which highlights the physical meaning of all aspects of the anelastic behavior of the system. Then, by installing the generated dissipative mechanisms in the form of resistive components into the already-coupled thermoelastic model, the irreversible energetic interactions between the elastic and thermal subdomains are included into the model to form an energy-based thermoviscoelastic model. The aforementioned achievements are released in two papers:

In the first paper, a physical combined viscoelastic model is proposed to generate the viscoelastic model suitable for multi-physical domain dynamic investigations. To this end, energy-based viscoelastic models are first generated for the existing conventional viscoelastic models, and their embedded dispersive mechanisms are interpreted physically by means of the BG method. Next, by including the interpreted dissipative mechanisms into the relative subdomains of the elastic domain, an energy-based combined viscoelastic model is proposed. The content of this paper is organized as follows:

In the second paper, the reversibly coupled subdomains of the solid field, generated in Chapter 4, are irreversibly coupled via installing the physical dispersive mechanisms presented in the first paper. Also, the impacts of geometrical and material changes on the system dynamics are added to the model via the compatibility consideration of the energetic components of different subdomains. The content of this paper is organized as follows:

Results

The proposed model provides a connectable energetic structure of the solid field with which the general dynamics of the system are obtained from the constructive dynamics of each of the subdomains. This special capability of the model leads to an automatic capturing of the thermo-mechanical phenomena inside the system. The obtained simulation results for a simple beam structure demonstrate the impacts of the internal dynamics on the observable behavior of the system, and prove the capability of the model in covering a wide range of thermo-mechanical behaviors including material softening, vibrational heating, dilation, relaxation, conduction, and damping of the solid field.

Conclusion

Overall, a novel thermoviscoelastic model is generated in which the general thermo-mechanical behavior of the system is generated from the interactive dynamics of its existing subdomains including the irreversibility induced by the true physical nature of the system.

ENERGY-BASED VISCOELASTIC MODEL: A PHYSICAL APPROACH FOR MATERIAL ANELASTIC BEHAVIOR

Amir Zanj[1], Fangpo He[2], Peter C. Breedveld[3]

Understanding the true nature of viscoelastic behaviors in multi-physical systems has always been a challenging issue in the system dynamic investigations, as each existing physical subdomain of the system may follow a different attenuation pattern during the dynamic process. In this study, to generate a viscoelastic model suitable for multi-physical domain dynamic investigations, a physical combined viscoelastic model is proposed. To this aim, by means of the Bond graph approach, an energy-based conventional viscoelastic model is first generated, and its embedded dispersive mechanisms are interpreted physically. By including the interpreted dissipative mechanisms into the relative subdomains of an elastic domain, an energy-based combined viscoelastic model is then proposed. The obtained simulation results indicate that the proposed viscoelastic model is able to capture a variety of viscoelastic behaviors in the system with respect to the true physical nature of the system.

Keyword: Bond graph modeling, Multi-physical systems, Energy-based modeling, Domain-independent modeling, Dispersive Mechanism

1. Introduction

To a high degree, elasticity is a suitable characteristic for modeling wave propagation through materials. No real materials, however, are perfectly elastic, but rather anelastic. In real medium, wave energy is gradually converted into heat. Attenuation of propagated waves in some cases, such as in viscoelastic materials, is quite significant and could be a source of erroneous results in forward modeling, inversion, and imaging if neglected [1]. Thus, analyzing the mechanics of viscoelastic materials has been proven to be extremely challenging.

Many classical viscoelastic models of materials have been put forward, such as the Maxwell, the Voigt, and the Standard Linear Solid (SLS) models [2] [3]. In addition, various fractional viscoelastic models of materials have been presented and their constitutive relations discussed in [4] [5] [6] [7] [8]. In these models, existing viscoelastic dynamics are presented using mechanical

[1] PhD Candidate, Advanced Control Systems Research Group, School of Computer Science, Engineering and Mathematics, Flinders University, Adelaide, Australia, e-mail: amir.zanj@flinders.edu.au
[2] Associate Professor, Advanced Control Systems Research Group, School of Computer Science, Engineering and Mathematics, Flinders University, Adelaide, Australia, e-mail: fangpo.he@flinders.edu.au
[3] Associate Professor, Robotics and mechatronics group, University of Twente, Enschede, The Netherlands

analogous components (such as springs and dashpots) and curve fitting techniques. The resultant models merely mimic the observable behaviors of the systems, but do not include the compound physical connections between the parameters (e.g. material and geometrical parameters) of the systems. They do not, therefore, adequately expose the physical concepts of viscoelasticity underpinning the dynamics of the systems.

The problem associated with the conventional modeling techniques can generally be traced back to the use of the dispersive mechanisms (e.g. retardation and relaxation mechanism) [9] [10] [11] that only pays attentions to the regeneration of the attenuated dynamics of the systems and ignores the true casual interactions between the energetic components (e.g. capacity, inertia, and resistivity) of the systems. This negligence leads to the separation of the models from their intended internal energetic behaviors of the systems, and results in a limited applicability of these models. Given that the viscoelastic behavior of a system is a true reflection of the system's kinetic, potential, and thermal subdomains' energetic interactions, the conventional models are deemed to be unsuitable for multi-physical system dynamic investigations.

The non-physical nature of the conventional models also limits the valid ranges of these models as frequently reported in the literature. Being disconnected from the physics of the systems, the generated models rely on combined parameters (such as relaxation time) to produce the dispersive behaviors of the systems. This makes the models incapable of distinguishing the dynamics of the same shape but different nature, thus unable to reveal specific physical behaviors of the systems on the level of their ongoing phenomena. Although attempts have been made to broaden the valid ranges of these models by employing more dispersive mechanisms that are activated in difference frequencies (e.g., the Maxwell–Wiechert model [12]), the added combined parameters are still unable to include the missing physics in the models that allow the tracking of the physical phenomena within the systems.

Given the deficiencies associated with the conventional models, it becomes obvious that a physical viscoelastic model will be desirable if the ability to capture and track the continuing viscoelastic behavior of a system is of concern. The required model should employ typical parameters that can carry distinctive physical meanings of the system, and should provide ongoing dynamics that can reveal clear energetic interactions between involving physical components of the system. The level of physical details contained in such a model will decide the range of

suitabilities for the model's application.

To generate such a physical viscoelastic model suitable for multi-physical system dynamic investigations, the Bond graph (BG) modeling technique [13] [14] [15] [16] [17] [18] [19] is suggested in this paper. Working on the basis of physical system theory, the BG technique provides a continuous power exchange frame between the existing physical subdomains of a multi-physical system, and produces the behavior of the system on the basis of power conservative interactions between the existing energetic components of the system. The model thus generated is analytical in nature while potentially reflecting the true physical meaning of the system. This physical model then provides a meaningful insight of the ongoing dynamics in viscoelastic phenomena.

The embedded physical lucidity of the proposed viscoelastic model can also provide a physical explanation to the limitations of the conventional models and, thus, lead to the development of a more physical approach that can extend the valid range of the generated model. In addition, using the BG approach, the domain-independency of the proposed approach can provide a low-cost dynamic coupling capability between the generated model and the models of other subdomains. This capability is particularly beneficial for multi-physical domain dispersive dynamic investigations. It also provides a desirable basis for the design of applicable control strategies to identify and suppress the undesired behavior of the system.

To develop the proposed viscoelastic model, the remainder of this paper is organized as follows. In Section II, the fundamentals of viscoelasticity in the mechanical domain and the problem relating to the implementation of the conventional methods are explained. An energy-based conventional viscoelastic model is then generated in Section III using the BG terminology, and the physical interpretation of the viscoelastic phenomena occurring inside the model is explained. By employing the obtained physical dispersive mechanisms, an inclusive viscoelastic model incorporating all aspects of energy dissipation of the system is proposed. In Section IV, the simulation results of the proposed energy-based combined viscoelastic model together with its conventional counterparts in BG representations are analyzed, and their corresponding capabilities in capturing the viscoelastic behavior of the system are demonstrated. The entangled viscoelastic behavior of material is then concluded in Section V where the use of the proposed viscoelastic model is justified and the reason for the limited applicability of the conventional models is revealed.

2. Fundamental issues of conventional viscoelasticity

From the literature, the fundamentals of viscoelasticity are mainly interpreted on the basis of the observed behavior of a system, not on the basis of the energetic interaction within a system. The theory of viscoelasticity [10] and its associated issues can be highlighted as follows.

The basic hypothesis in conventional viscoelastic theory focuses on the fact that a current value of the stress tensor depends on the history of the strain tensor [11] [20]. Considering the linear functional and continuous strain history, the Riesz' representation theorem [21] allows the function to be rewritten as a convolution integral:

$$\sigma(t) = G(0)\varepsilon(t) + \int_0^t G(t-\tau)\,\dot{\varepsilon}(\tau)d\tau \tag{1}$$

where $\sigma(t)$ and $\varepsilon(t)$ denote the stress and strain of the system, respectively; $\dot{\varepsilon}(\tau)$ is the time derivative of the strain; G is the stress relaxation function and is the viscoelastic analogue to the Lame constant, μ, in linear elasticity. To define G, which is the key point to evaluate the viscoelastic behavior of the system, disregarding the physical nature of this function, it is assumed that the Laplace transform of stress relaxation function, $\hat{G}$, can be approximately represented by a rational function as:

$$s\hat{G}(s) = \frac{Q(s)}{P(s)} \tag{2}$$

$$P(D) = \sum_{k=0}^{N} p_k D^k \tag{3}$$

$$Q(D) = \sum_{k=0}^{N} q_k D^k \tag{4}$$

where p_k and q_k are polynomials, D is the differential operator d/dt, and N is an arbitrary integer. Accordingly, the differential operator form of the stress-strain relation in Eq. (1) can be represented as:

$$P(D)\sigma(t) = Q(D)\varepsilon(t) \tag{5}$$

By taking the Laplace transform of Eq. (5), one has:

$$P(s)\hat{\sigma}(s) - \frac{1}{s}\sum_{k=1}^{N} p_k \sum_{r=1}^{k} s^r \sigma^{(k-r)}(0) = Q(s)\hat{\varepsilon}(s) - \frac{1}{s}\sum_{k=1}^{N} q_k \sum_{r=1}^{k} s^r \varepsilon^{(k-r)}(0) \quad (6)$$

Assuming that the order of Q is less than or equal to the order of $P + 1$ and that $sP(s)/Q(s)$ has no multiple roots, one can express G as a constant plus a sum of $N + 1$ (or less) inverse first-order polynomials:

$$G(s) = K + \sum_{k=0}^{N} \frac{a_k}{b_k + s} \quad (7)$$

By taking the inverse Laplace transform of Eq. (7), the general solution for G in the time domain is obtained as:

$$G(t) = K + \sum_{k=0}^{N} C_k e^{-\frac{t}{\tau_k}} \quad (8)$$

The obtained G can reveal the viscoelastic behavior of the system by fitting the obtained parameters K, C_k, and τ_k about an operational point.

It is clear that in the theory of viscoelasticity the attempt is to generate a fading functional between the stress and strain of the system, whereas the actual viscoelastic behavior of the system is a result of the interactive dynamics of the system energetic components. Since these internal interactions are not observable, they are not tractable in an experimental attempt. Accordingly, the majority of the conventional viscoelastic models using this theory such as the Maxwell, the Voigt, and the SLS models [22] can only show the relaxing behavior of the system without paying attention to the physical reasons behind the phenomena. Although a conventional model can be a useful tool for investigating the relaxing behavior of the system, literature shows a low capability of such a model in covering the whole range of relaxation dynamics of a system [22], especially in the case of a multi-physical system where the role of the internal interactions becomes more significant.

In a conventional viscoelastic model, although the molecular motion of the system can be visualized by allocating the analogous mechanical elements, spring and dashpot [5], in the form of the Maxwell and Voigt arms shown in Fig. 1, the introduced combined parameters of the model (such as the relaxation time τ) can be the source of an erroneous justification of the viscoelastic behavior when the parameters of the model are modulated. To explain this, consider the SLS model

shown in Fig. 2 in a variable temperature system. The constitutive equation is simplified as:

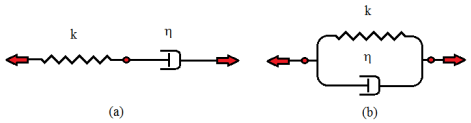

Fig.1 Viscoelastic model: Maxwell arm (a), Voigt arm (b)

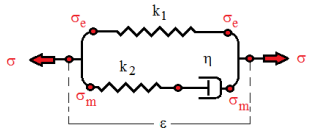

Fig.2 Standard linear solid (SLS) viscoelastic model

$$\frac{\sigma(t)}{\varepsilon_0} = k_1 + k_2 e^{-\frac{t}{\tau}} \tag{9}$$

$$\tau = \frac{\eta}{k_2} \tag{10}$$

where for the analogous mechanical component of the model k_1, k_2, and η present the elasticity of the system, the elasticity of the Maxwell arm, and the viscosity coefficient of the dashpot, respectively. Eq. (10) indicates the relaxation time of the model as a combined parameter expressed by the ratio of the viscosity and elasticity of the considered dispersive mechanism (Maxwell arm). To include the thermal impact in the model, generally the relaxation time is required to be modulated. Considering the relation between the relaxation time and the elasticity of the system, this modulation may reflect as a change in the elasticity of the system which is indeed the parameter forming the capacity of the system. From physical system theory, it is known that any changes in the capacity of a system will undoubtedly separate the system from its history, as the energy level of the system is changed. Therefore, modulation of the introduced parameters of the model will lead to disconnecting the model from its physical background. The combination of k_i and η_i in the form of one significant parameter is thus seen to limit the valid range of the conventional viscoelastic model.

3. Energy-based viscoelastic model: a physical approach

To find the relation between a viscoelastic model and the energetic behavior of its corresponding system, the energetic interaction of the dispersive mechanism is required to be defined with respect to the involving subdomains of the system. To achieve this, in this paper it is

proposed that a dispersive model for each involving subdomain is first generated, and the generated models are then combined in a power continuous form. By doing so, it is anticipated that the resultant model of the system will automatically capture the various physical phenomena occurring inside the system, including the viscoelastic phenomena.

To generate the physical dispersive model for each involving subdomain, one needs to identify the dissipation nature of different subdomains. To do this, a physical explanation of the existing entropic behavior of the conventional viscoelastic models is identified by means of the BG approach. The comparison between the physical interpretation of the existing dispersive mechanisms (relaxation and/or retardation) of the conventional viscoelastic models and that of the energy dissipative components of each subdomain can lead to the identification of the assortment of the dispersive mechanisms that can form an energy-based viscoelastic model.

In the following, the procedure explained above will be conducted to generate the proposed energy-based viscoelastic model for a 1D reticulated structure.

3.1. Domain-independent pure elastic models

To define the energetic interaction between the involving subdomains of an elastic system, Rayleigh beam's discrete geometry, suggested in [23], is employed. Fig. 3 shows a 1D distributed space on the basis of the acoustic assumption. According to this assumption, the elastic energy of the reticulated space can be stored in the center of each element and the movements of the boundaries are inertial. As this reticulated space is indeed a continuous system, the adjacent boundary of each two consecutive elements are bonded to move together. Therefore, one can consider the above discretization as a junction-element chain, in which each element represents the potential subdomain and each junction represents the kinetic subdomain with its parameters being a weighted function of the related parameters of the adjacent elements.

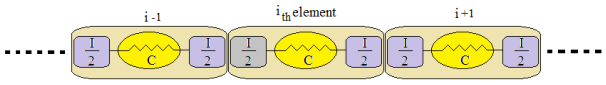

Fig.3 1-D Rayleigh distributed geometry

The BG representation of Fig. 3 is shown in Fig. 4. The considered state variables for the i_{th} element and j_{th} junction are q_i and p_j which denote the deformation of each element and the momentum of each boundary, respectively. According to the conservation of energy, the state

equations of each junction-element are derived as:

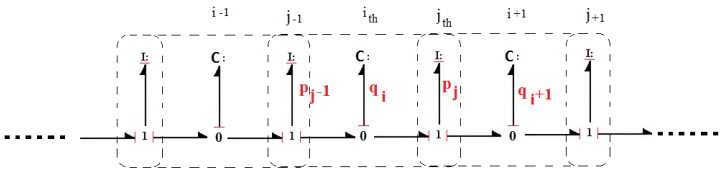

Fig.4 1-D decomposed elastic model

$$\dot{p}_j = \frac{q_i}{C_i} - \frac{q_{i+1}}{C_{i+1}} \tag{11}$$

$$\dot{q}_i = \frac{p_{j-1}}{I_{j-1}} - \frac{p_j}{I_j} \tag{12}$$

$$I_j = \frac{m_i}{2} + \frac{m_{i+1}}{2} \tag{13}$$

where I_j is a function of the adjacent elements' mass representing the boundary inertance, and C_i is a function of the geometrical and material parameters of the i_{th} element representing the capacitance of the element. The presented model via the geometry and material related parameters is able to model the dynamics of a pure elastic system with respect to the dynamics of the kinetic and potential subdomains. To add the viscoelastic considerations to the model according to the BG approach, the energy is required to be dissipated while transferring between the subdomains of the system. To this aim, in the following the conventional viscoelastic models, namely the Maxwell, the Voigt, and the SLS models, will be interpreted physically to define the required resistive components for the presented elastic model.

3.2. Domain-independent Maxwell viscoelastic model

Consider the series arrangement of the mechanical element in the Maxwell model shown in Fig. 1 (a). The relaxation mechanism embedded in this model can be interpreted as a dissipative component for the potential subdomain and placed in series with the capacity of each segment. The equivalent BG representation of the Maxwell model is presented in Fig. 5 where a resistor is placed inside each element and in series with the storage element. This means that the internal energy of each medium can be saved or dissipated, resulting in a long term stress release (creep) in the system.

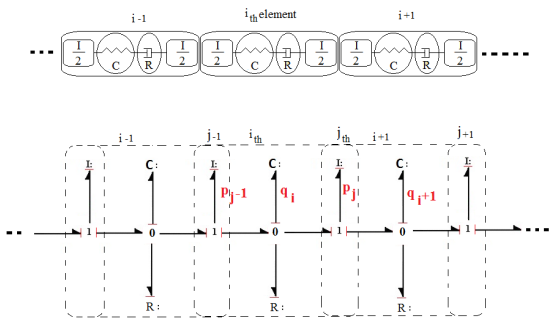

Fig.5 Maxwell model Bond graph representation of viscoelasticity

For the BG model presented in Fig. 5, the governing equations of the Maxwell model can be obtained as:

$$\dot{p}_j = \frac{q_i}{C_i} - \frac{q_{i+1}}{C_{i+1}} \tag{14}$$

$$\dot{q}_i = \frac{p_{j-1}}{I_{j-1}} - \frac{p_j}{I_j} - \frac{q_i}{R_i C_i} \tag{15}$$

By integrating Eq. (15) and comparing the result with the constitutive equation in Eq. (9), the BG representation of the Maxwell relaxation time is equivalent to:

$$\tau_i = R_i C_i \tag{16}$$

From the Hook's relation for 1D reticulation, the storage coefficient is also presented as [23]:

$$C_i = \frac{L_{0_i}}{A_i E_i} \tag{17}$$

where L_{0_i}, A_i, and E_i are the initial length, contact surface, and Young modulus of each segment (geometry element), respectively. The Maxwell relaxation time can then be expressed as a function of the geometrical and material parameters of each segment:

$$\tau_i = R_i \frac{L_{0_i}}{A_i E_i} \tag{18}$$

3.3. Domain independent Kelvin-Voigt model

The Voigt model is well-known for systems under cyclic loading. As shown in Fig. 1 (b), the entropic dashpot of the Voigt model is placed in parallel with the main elasticity of the system. This model is known to capture the retardation behavior of the system. A BG representation of the Voigt model is given in Fig. 6 where the energy entered into each medium is distributed between

a resistor and a storage component with the same flow rate but different effort. This means that the system using the Voigt model can always conserve the internal potential energy without relaxing it.

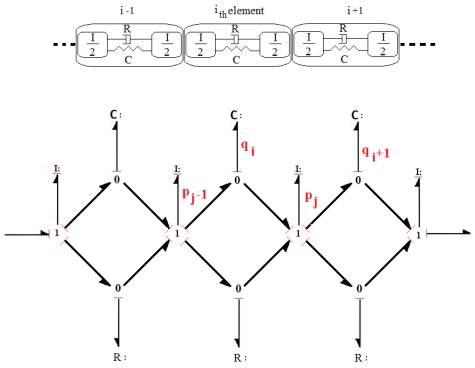

Fig.6 Voigt model Bond graph representation of viscoelasticity

To extract the state equations of the Voigt model, by slightly changing the presented BG model to eliminate the existing loop, the BG presented in Fig. 7 is suggested. Accordingly, the state equations for the i_{th} segment and j_{th} junction are derived as:

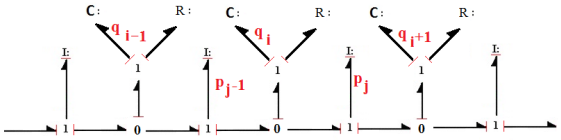

Fig.7 Loop-less Kelvin-Voigt model Bond graph representation of viscoelasticity

$$\dot{p}_j = \frac{q_i}{C_i} + R_i\left(\frac{p_{j-1}}{I_{j-1}} - \frac{p_j}{I_j}\right) - \frac{q_{i+1}}{C_{i+1}} - R_{i+1}\left(\frac{p_j}{I_j} - \frac{p_{j+1}}{I_{j+1}}\right) \tag{19}$$

$$\dot{q}_i = \frac{p_{j-1}}{I_{j-1}} - \frac{p_j}{I_j} \tag{20}$$

Comparing the Maxwell and Voigt BG models, one can notice that unlike the Maxwell model where the elastic energy of the system is dispersed, in the Voigt model the momentum energy of the system is dissipated as indicated by the causality of the resistive component. To explain this, consider the state equations of these two models. While the relaxation behavior in the Maxwell model occurs in the potential subdomain, the retardation behavior in the Voigt model occurs in the kinetic subdomain. This shows that these two viscoelastic models in fact describe two different phenomena occurring in different subdomains. Based on this finding, one can conclude that a combination of the Maxwell and Voigt methodologies is required to cover all the dissipation

aspects of a real system.

3.4. Domain independent SLS model

The SLS model attempts to include the dissipation impacts on both potential and kinetic subdomains; however, the obtained combination has a missing part. A Maxwell-like SLS BG model is presented in Fig. 8 where a Maxwell arm is placed inside the system parallel to the main elasticity of the element. This allows the system to have a certain amount of relaxation and retardation.

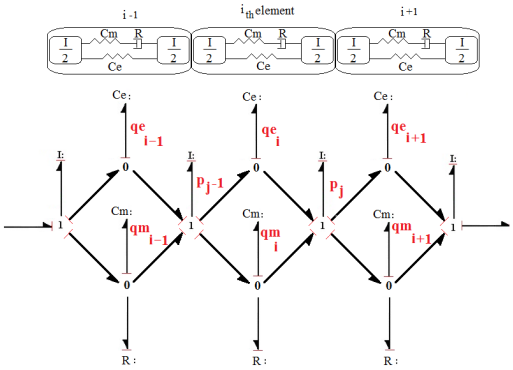

Fig.8 SLS model Bond graph representation of viscoelasticity

As shown in Fig. 8, an internal state is added to each segment. This added state temporarily stores elastic energy inside the segment, thus allowing the energy to relax to form creepy-like dynamics. Define the added state, q_m, as the displacement of the Maxwell arm, and change the elastic state to q_e to represent the elastic displacement. The governing equations for this model can then be derived as:

$$\dot{p}_j = \frac{q_{e_i}}{C_{e_i}} + \frac{q_{m_i}}{C_{m_i}} - \frac{q_{e_{i+1}}}{C_{e_{i+1}}} - \frac{q_{m_{i+1}}}{C_{i+1}} \tag{21}$$

$$\dot{q_{e_i}} = \frac{p_{j-1}}{I_{j-1}} - \frac{p_j}{I_j} \tag{22}$$

$$\dot{q_{m_i}} = \frac{p_{j-1}}{I_{j-1}} - \frac{p_j}{I_j} - \frac{q_i}{R_i C_{m_i}} \tag{23}$$

As can be seen, dissipative terms appear partially in the potential subdomain state equations (Eqs. (22) and (23)), however no direct viscoelastic impact is found in the kinetic subdomain state equation (Eq. (21)). Although indirect viscoelastic impacts are shown in the kinetic subdomain via temporary forces generated in the system (the last two terms of Eq. (21)), there is no sign of

dispersion in the kinetic subdomain. This finding reveals that there is a missing part in the SLS model that will limit its performance in cyclic loading. It also explains the reason why there is not much success in expanding the valid ranges of the SLS-like viscoelastic models even with the use of more complex means such as the Weichert model shown in Fig. 9 [12].

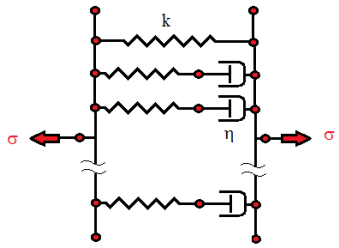

Fig.9 Weichert viscoelastic model

3.5. Domain independent combined linear solid (CLS) model

As has been seen, the BG technique can physically clarify the fundamental differences between relaxation and retardation mechanisms of the system using constructive components to form the viscoelastic behavior. Accordingly, to generate a complete model including all required dispersive mechanisms, a combination of the Maxwell and Voigt models is therefore proposed in which the direct dissipation can occur in both subdomains. The proposed model is named as the Combined Linear Solid (CLS) model whose BG configuration is shown in Fig. 10 where the simplest form of combining the Maxwell arms in parallel with the Voigt legs is presented.

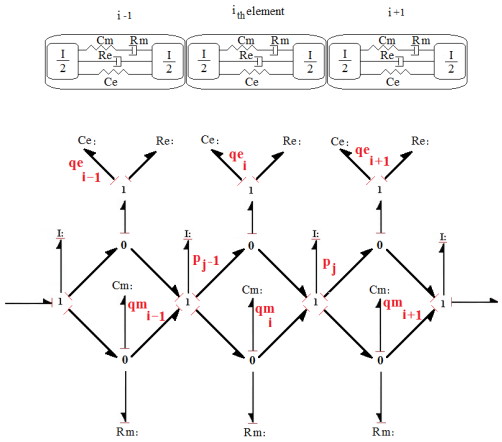

Fig.10 CLS model Bond graph representation of viscoelasticity

Consider the index of m and e denoting, respectively, the Maxwell and elastic parameters. The state equations for the proposed model can be derived as:

$$\dot{p}_j = \frac{q_{e_i}}{C_{e_i}} + \frac{q_{m_i}}{C_{m_i}} - \frac{q_{e_{i+1}}}{C_{e_{i+1}}} - \frac{q_{m_{i+1}}}{C_{m_{i+1}}} + R_{e_i}\left(\frac{p_{j-1}}{I_{j-1}} - \frac{p_j}{I_j}\right) - R_{e_{i+1}}\left(\frac{p_j}{I_j} - \frac{p_{j+1}}{I_{j+1}}\right) \tag{24}$$

$$\dot{q_{e_i}} = \frac{p_{j-1}}{I_{j-1}} - \frac{p_j}{I_j} \tag{25}$$

$$\dot{q_{m_i}} = \frac{p_{j-1}}{I_{j-1}} - \frac{p_j}{I_j} - \frac{q_{m_i}}{R_{m_i}C_{m_i}} \tag{26}$$

It is clear that, similar to the SLS model, the CLS configuration is also a 3-DOF system. The last two terms of Eq. (24) indicate the direct dispersive impact on the kinetic subdomain, which include the retardation dynamics of the model. The last term in Eq. (26) indicates the energy dissipation in the potential subdomain, which can be counted as the root of the long-term response of the system including creep and relaxation dynamics. Unlike the SLS model, in the CLS model the energy transformation in both subdomains is dispersive as demonstrated in Eqs. (24) and (26). Generating bidirectional attenuated dynamic interactions between the subdomains makes the CLS model capable of capturing the viscoelastic behavior of the system under high-frequency cyclic loading where the SLS model fails to perform.

The physical interpretation of the existing dispersive mechanisms associated with the conventional methods has revealed that the dissipation of the system and the resultant viscoelastic behavior are the direct result of two phenomena occurring simultaneously inside different physical subdomains. These two phenomena are by nature different from each other. The difference between the orders of R_m and R_e can explain this claim. By implementing Eqns. (17) and (13) in Eqns. (24) and (26), for a uniformly discretized homogeneous material, one can present the flowing relaxation time for both the kinetic and potential subdomains:

$$\tau_k = \frac{R_e}{I} \tag{27}$$

$$\tau_p = R_m C_m \tag{28}$$

It is clear that to obtain a logical relaxation time, in the kinetic subdomain the resistant coefficient is required to be in the order of the allocated mass of the segment, whereas in the potential subdomain the resistant coefficient is required to be defined in the order of the Young modulus of the segment. This fact highlights that the observed viscoelastic behavior of the system is indeed constructed by separate dynamic behaviors and, thus, separate parameters in different scales are required to regulate the model. The negligence of this fact in the conventional

viscoelastic modeling techniques has resulted in divisions of models into two different categories: models suitable for long-term response and models proper for cyclic loading. The consideration of separate relaxation time and retardation time as shown in the proposed CLS model, however, can result in generating an integrated viscoelastic model proper for all aspects of viscoelastic phenomena, thus a much wider valid range of the CLS model.

3.6. Temperature dependency of viscoelasticity

Traditionally, to include the temperature dependency in the conventional models, relaxation time is modulated via temperature input. In Section II, it has been claimed that the consideration of relaxation time as a ratio of viscosity coefficient to Young modulus can limit the valid range of the conventional models, and also, be the reasons for some erroneous outcomes especially at the presence of temperature fluctuations. To investigate this claim, in the following the physical interpretation of relaxation time modulation is highlighted via the energy-based modeling strategy.

To include the thermal subdomain influence on the elastic subdomain, consider the energy-based thermal model presented in [24] together with the CLS model, as shown in Fig. 11. The dissipated energy is seen to enter into the thermal subdomain, and change the temperature of the system via the *RS* energy links. Considering the energetic meaning of relaxation time, the modulation of this parameter can be presented as modulating its constructive components via the thermal information (signal lines shown as dash lines in Fig. 11) of the system. Modulation of resistance is permitted as resistance is proportional to the instantaneous information (effort and flow) [14] of the system. However, modulation of capacitance will undoubtedly violate the conservation of energy within the system, as capacitance is in an integrative relation with the instantaneous information of the system [13] and, thus, contains the memory of the model. One can see how modulation of relaxation time can result in disconnecting the model from the physical causality of the system leading to a limited range of validity. It should be mentioned that instead of modulation, to maintain the capacity conservation, the one-dimensional capacity would be required to be replaced by a multi-dimensional thermoelastic capacitor [25]. This possibility is beyond the interest of this study.

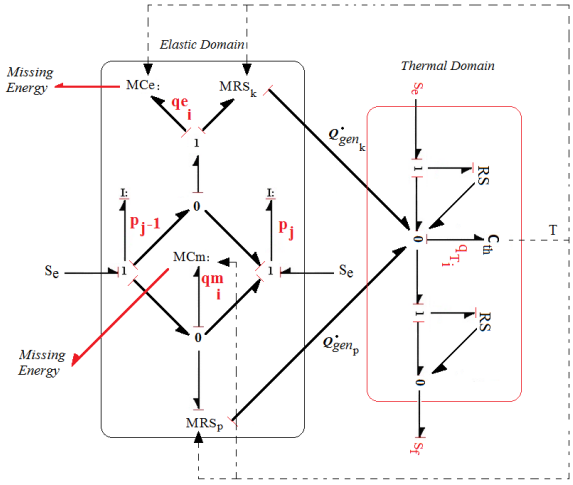

Fig.11 Possible thermal interaction of viscoelastic model

Considering the coupled model shown in Fig. 11, the amount of the dissipated energy can be obtained as:

$$\dot{Q}_{gen_{tot}} = \dot{Q}_{gen_k} + \dot{Q}_{gen_p} \tag{29}$$

$$\dot{Q}_{gen_k} = RS_k {f_k}^2 \tag{30}$$

$$\dot{Q}_{gen_p} = RS_p {e_p}^2 \tag{31}$$

$$f_k = \frac{p_{j-1}}{I_{j-1}} - \frac{p_j}{I_j} \tag{32}$$

$$e_p = \frac{q_{m_i}}{C_{m_i}} \tag{33}$$

where RS_k and RS_p can be defined with respect to the geometry and material properties. Therefore, the total heat generated as a result of viscoelastic phenomena for each element can be calculated as:

$$\dot{Q}_{gen_{tot_i}} = RS_{k_i}\left(\frac{p_{j-1}}{I_{j-1}} - \frac{p_j}{I_j}\right)^2 + RS_{p_i}\left(\frac{q_{m_i}}{C_{m_i}}\right)^2 \tag{34}$$

This dissipated energy is another criterion reflecting the nature of the dispersive mechanism employed by the viscoelastic model. This criterion will be used in Section IV as a comparative tool to highlight the fundamental differences between the proposed and the conventional dispersive mechanisms.

4. Simulation and result analysis

To compare the difference and capability of the proposed CLS model with the conventional models in capturing the viscoelastic phenomena, the axial behavior of a simple 1D discrete structure under cyclic loading is simulated. To generate the discretized geometry, the chosen structure is reticulated into 10 uniform elements with the first and last elements being the boundary elements that receive external mechanical loads. It is assumed that all side surfaces of the structure are fully isolated and the system is stress-free initially in the ambient room temperature. Sequentially, in Subsections IV.A and IV.B, the obtained results of the Maxwell and Voigt BG models shown in Figs. 12 to 15 are compared for cyclic tension of a soft tissue the properties of which are listed in Table 1. In Subsections IV.C and IV.D, the obtained results of the SLS and CLS BG models shown in Figs. 16 to 18 are compared for high and low frequency cyclic loading of a metallic alloy the properties of which are listed in Table 2.

Table 1. Material and geometrical cartilage properties

Length	l	$2.1e^{-1}m$
Cross section	A	$1e^{-4}m^2$
mass	m	$5.67e^{-2}kg$
Conductivity	λ	$2.73e^{2}\frac{J}{m.K}$
Density	ρ	$4e^{3}\frac{kg}{m^3}$
Stiffness	E	$2.698e^{-2}\frac{kg}{mol}$
Viscosity	s_0	$2.83e^{1}\frac{J}{mol.K}$
Specific heat	c_p	$8.97e^{2}\frac{J}{kg.K}$

Table 2. Material and geometrical beam properties

Length	l	$2.1e^{-1}m$
Cross section	A	$1e^{-4}m^2$
mass	m	$5.67e^{-2}kg$
Conductivity	λ	$2.73e^{2}\frac{J}{m.K}$
Density	ρ	$4e^{3}\frac{kg}{m^3}$
Molar mass	M	$2.698e^{-2}\frac{kg}{mol}$
Reference entropy @ 298K	s_0	$2.83e^{1}\frac{J}{mol.K}$
Specific heat	c_p	$8.97e^{2}\frac{J}{kg.K}$

4.1. Maxwell model

The results obtained from the Maxwell BG model of the system for the applied external force given in Fig. 12 (a) are presented in this Subsection. The obtained deformation of each segment and the energetic behavior of the system are shown in Fig. 12 (b) and Fig. 12 (c), respectively. They indicate the relaxation behavior of the system as expected of the Maxwell model. For instance, the ratcheting of the system is clearly visible in Fig. 12 (c) which is one of the most wanted behaviors in viscos materials [26]. The dissipated energy profile is shown in Fig. 12 (d). It can be concluded that the magnitude of the energy loss in the Maxwell dispersive model is considerable.

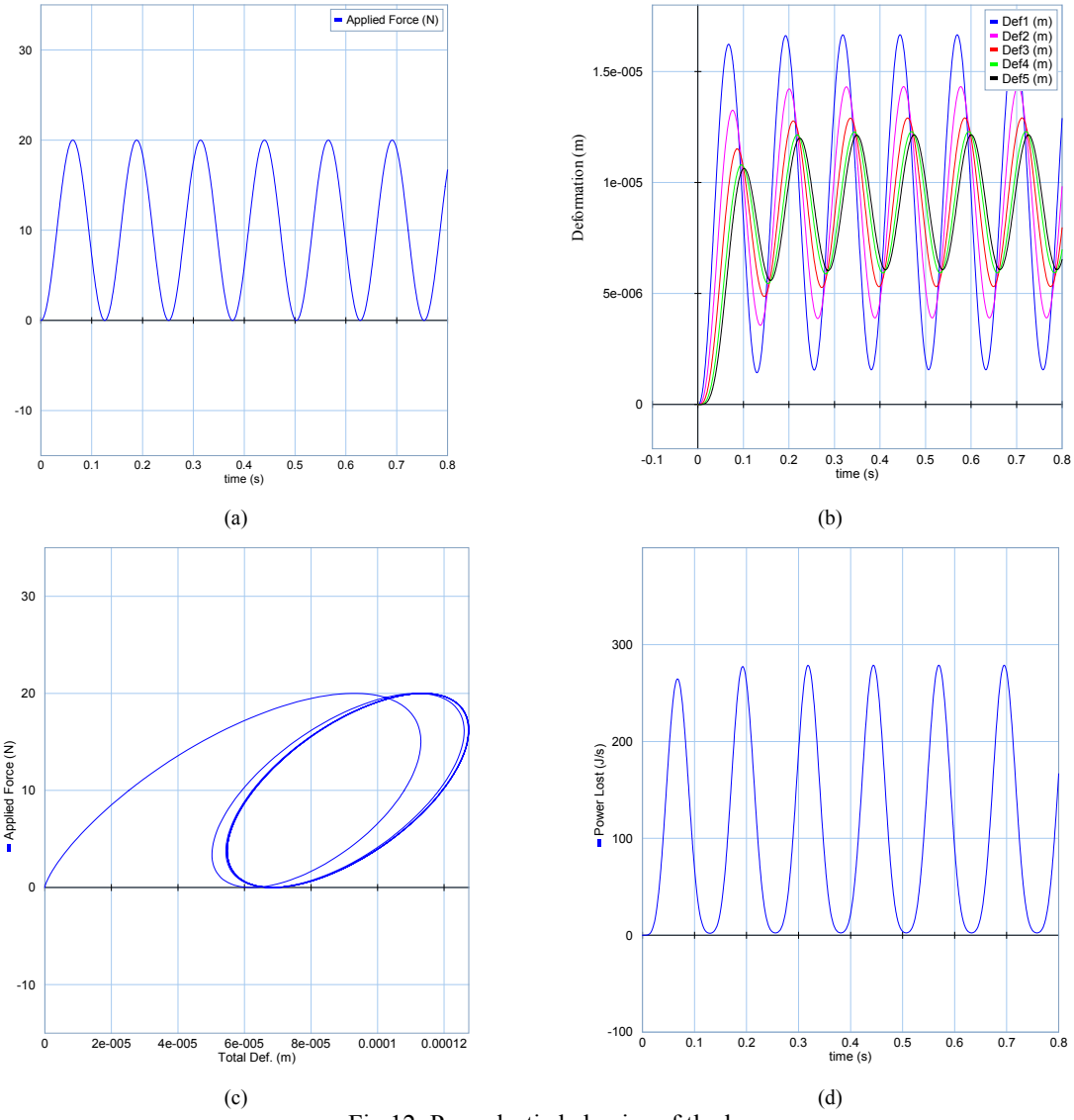

Fig.12 Pure elastic behavior of the beam

To physically identify the depressive mechanism of the Maxwell model and to relate the considered dissipative coefficient with the material parameters, the resistance of the model is increased to the extent equal to the capacitance of the system. The obtained result for the same external force is depicted in Fig. 13. Surprisingly, the deformation graph shown in Fig. 13 (b) demonstrates the elastic-like behavior of the system. In Fig. 13 (c) the energetic behavior of the system reminds the Hook's force-deformation graph for elastic models. In Fig. 13 (d) the resultant dissipated energy of the system indicates that despite the increase in resistivity of the system, the amount of dissipated energy as compared to Fig.12 (d) remains almost negligible. Collectively, one can conclude that in the Maxwell model increasing the resistivity leads to decreasing the viscoelasticity of the system.

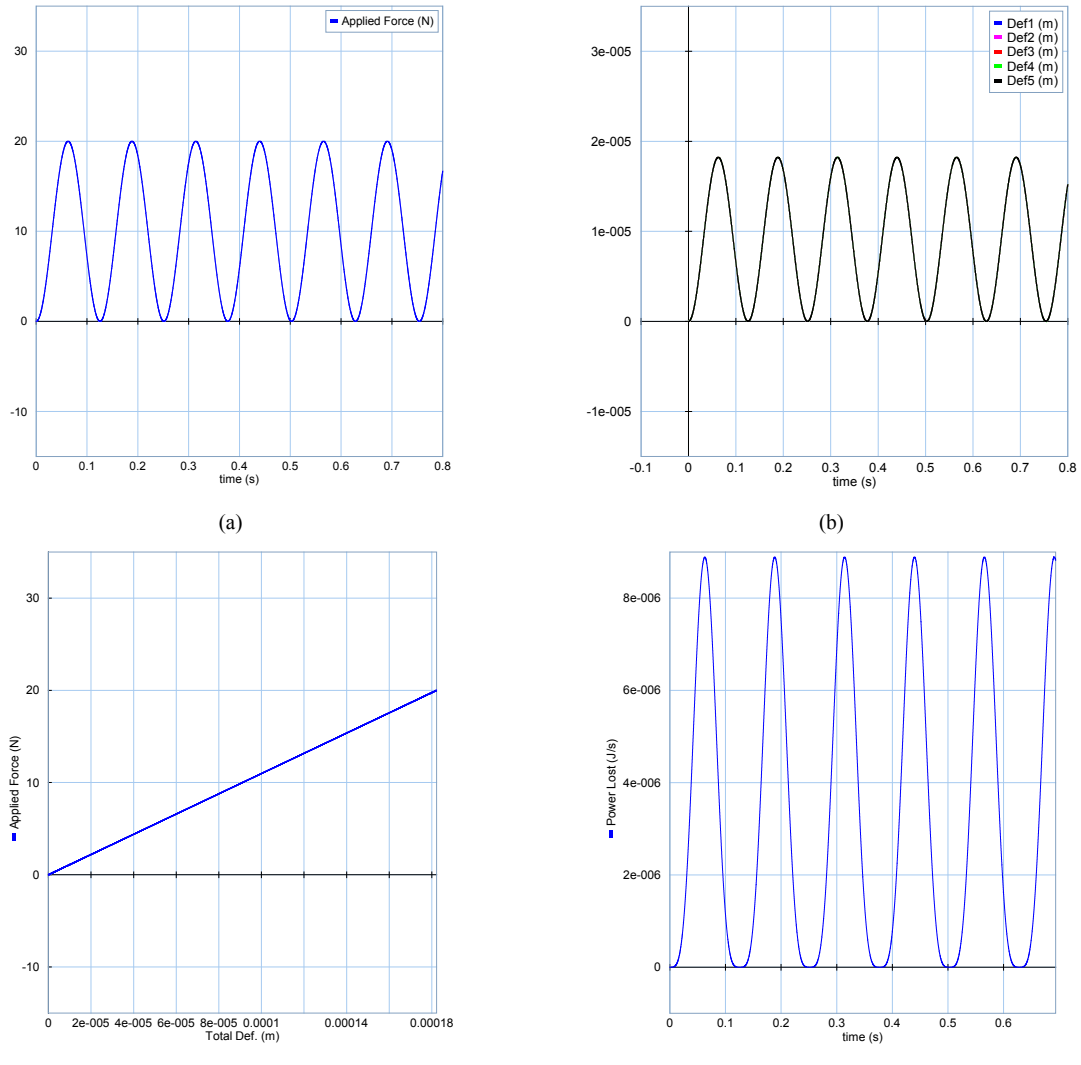

Fig.13 Cartilage viscoelastic behavior under Maxwell model

To explain this conclusion, consider the Maxwell energetic component structure shown in Fig. 5. The strain rate (the considered flow traveling between the kinetic and potential subdomains) is seen to be free to select between the storage or resistance components of the system. Hence, similar to electric circuits, when the resistivity on the way is high and when there is a possibility to select between the resistor and capacitor of the system, naturally the energy entering into the segment will be stored in the capacitor instead of being dissipated. Thus, more pure elastic behavior is achievable with higher resistivity in the Maxwell model. The Maxwell resistor in principal can be an indicator of the material parameter relating to the hardness of the system.

4.2. Voigt model

To compare the Voigt model with the Maxwell model described above, in this Subsection a similar energetic behavior of the system via the Voigt model is generated using the same loading situation and through changing the resistive parameter. Fig. 14 shows the viscoelastic behavior of the system obtained from the Voigt model. The energetic behavior shown in Fig. 14 (c) is similar to that presented in Fig.13 (c), but the internal dynamics presented in Fig. 14 (b) are different from those presented in Fig.13 (b). It seems that the external dynamics of the Voigt model cannot find the way to enter into the system, whereas the deformation variation of different segments of the Maxwell model can vividly indicate the stimulated dynamics of the system. To explain this, examine the amount of the Voigt resistance (R_e). To generate the Maxwell-like behavior via the Voigt model, a higher amount of resistivity, almost the same size as that of the elasticity of the system, is needed. According to the BG representation of the Voigt configuration (Fig. 6), the strain rate (flow of the system) is not permitted to be divided between the resistor and capacitor of a segment; rather, it must be bonded together and go through both of the components simultaneously. By doing so, the higher amount of resistivity will oppose the strain rate to flow into the segment, causing the system to behave like a rigid body. By resisting the strain rate to flow into the system, although the resistivity is high, the amount of dissipated energy in the Voigt model, as shown in Fig. 14 (d), is considerably low as compared to that of the Maxwell model shown in Fig. 13 (d).

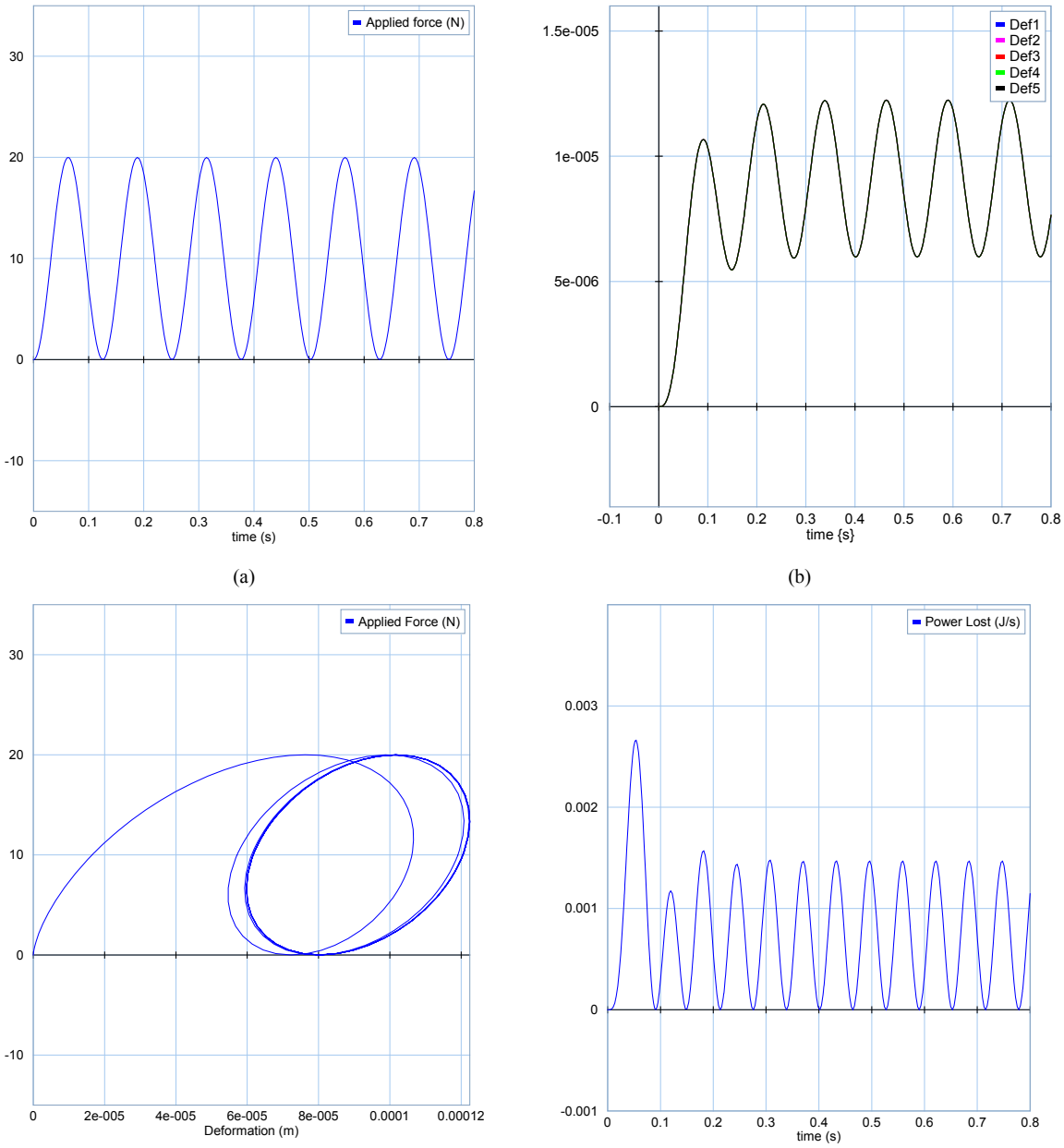

Fig.14 Cartilage viscoelastic behavior under Voigt model

From what explained above, one can clearly ascertain that although the observable behaviors of the system in these two models are well-matched, their essences reflect two completely different physical dynamics of the system. These fundamental differences become more evident in high-frequency loading cases, especially when the models are in strain-rate control. Fig. 15 compares the force deformation behaviors of the Maxwell (Fig. 15 (a)) and Voigt (Fig. 15 (b)) models for an Aluminum alloy of Table 2 in higher frequency ($\omega = 1e^4$ rad/s). In this case, the Maxwell model

is evidently seen to be unable to demonstrate the retardation behavior.

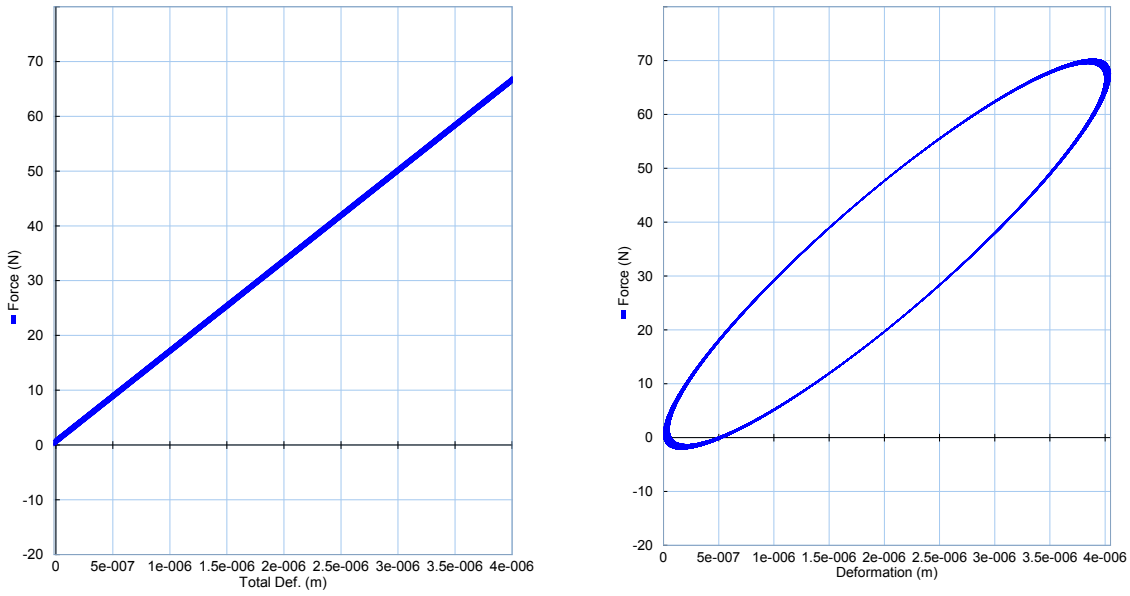

(a) (b)

Fig.15 Maxwell (a) vs Voigt (b) under high-frequency loading

The comparison between the Maxwell and Voigt models indicates that these two models present two different aspects of the viscoelastic phenomena. Thus, both the Maxwell and Voigt dissipative mechanisms become necessary to be included if all aspects of the viscoelastic behavior of a system are of concern. This fact can be considered as an introduction to generate a combined model such as the SLS; however, a right combination still requires a right physical insight of the system.

4.3. SLS model

To evaluate the performance of the SLS model, a high-frequency force-control load ($\omega = 7e^6$ rad/s) is considered to be applied to both ends of the chosen 1-D structure of Table 2. Fig. 16 demonstrates the deformation behavior of each segment. Surprisingly, despite of employing a combined method, the Maxwell-like SLS model is still unable to capture any damping behavior of the system. The deformation shown in Fig. 16 (a) demonstrates that the applied dynamics have introduced shocking waves into the structure. Having energy dissipative components inside the system, one would anticipate a damped response from the system. However, the force deformation behavior depicted in Fig. 16 (b) indicates that, despite the existence of internal energy dissipation, the damping behavior has not appeared in the system. This is clearly shown in Fig. 16 (c). To

explain this, one can relate it to the missing part of the SLS modeling approach. As explained in Subsection IV.C, in this model there is no direct dissipation in the kinetic subdomain of the system, thus making the model unable to perform desirably under high-frequency situations when the role of the kinetic subdomain becomes dominant.

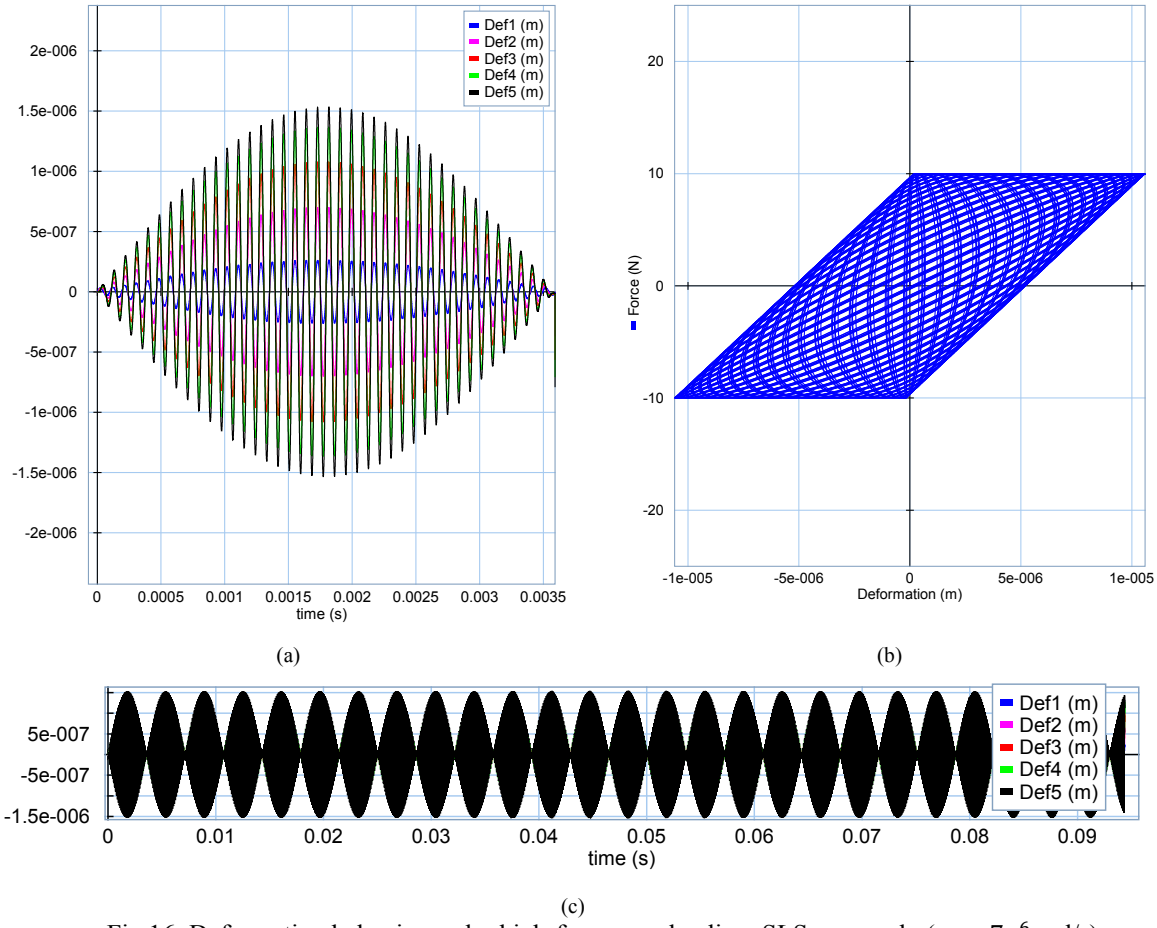

Fig.16 Deformation behavior under high-frequency loading, SLS approach, ($\omega = 7e^6$ rad/s)

4.4. CLS model

To examine the proposed CLS model, consider the same condition as applied to the SLS model. The obtained force deformation of the CLS model is shown in Fig. 17 (a) where, in contrast to Fig.16 (b), the damping behavior of the system is clearly demonstrated. As can be seen, after a finite number of oscillations the dissipative mechanism embedded in the kinetic subdomain of the proposed CLS model drags the system out of the initial resonant mode, and stabilizes the system into a new oscillatory condition.

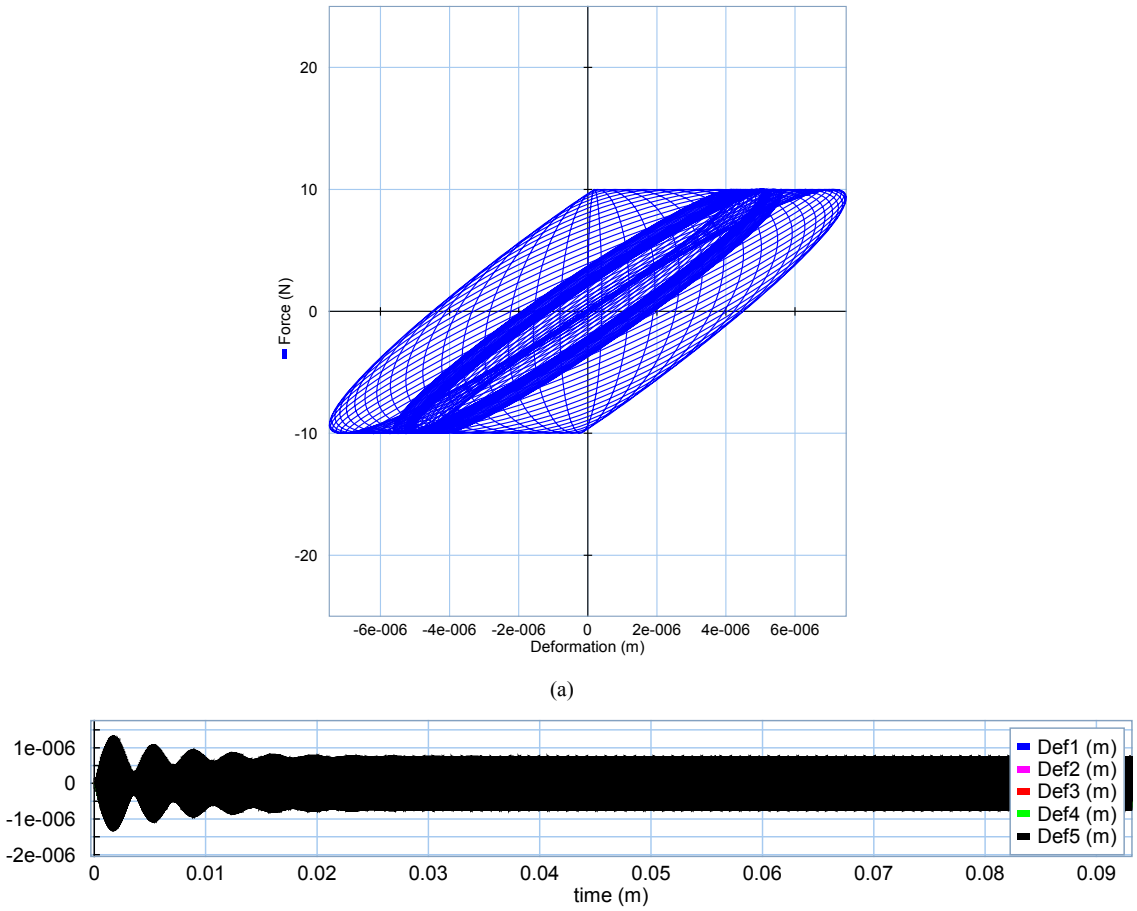

Fig.17 CLS model behavior under high-frequency loading ($\omega = 7e^6$ rad/s)

Fig.17 (b) demonstrates the response of the system with respect to time. It is clear that some internal frequencies have totally vanished from the oscillation. To clarify the mechanism for this cancellation, closely examine the internal dynamics of the system at a lower frequency that is far enough from the natural frequency so that no resonance of the internal dynamics of the system could occur. A comparison between the obtained result from the SLS model shown in Fig.18 (a) and that from the CLS model shown Fig.18 (b) clarifies the significant role of the added dissipation mechanism to the kinetic subdomain of the proposed CLS model. One can see that in the CLS model within each cycle of the oscillation the internally generated noise of the system is being dissipated, whereas in the SLS model no dissipation can be captured.

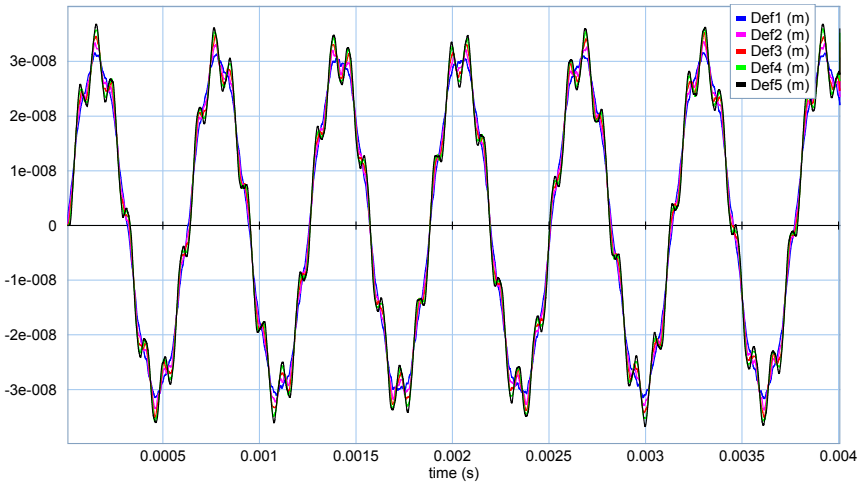

(a)

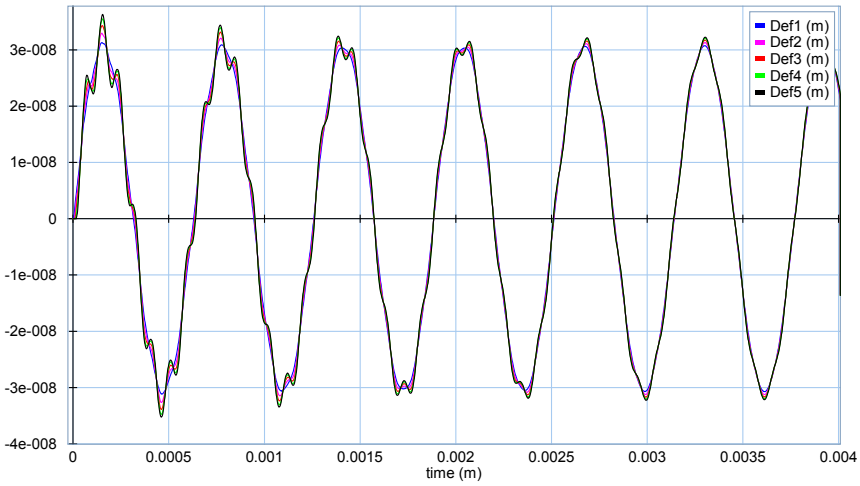

(b)

Fig.18 Comparison between SLS (a) and CLS (b) under high-frequency loading ($\omega = 1e^4$ rad/s)

5. Conclusion

In this paper by mean of the BG approach an energy-based combined viscoelastic model, namely the CLS model, is proposed based on the fusion of the conventional dispersive mechanisms. The comparison between the conventionally generated models and their BG representations indicates that the observable viscoelastic behavior of the system is in fact a direct result of two different dispersive mechanisms which act in two different subdomains of the system. Although both dispersive mechanisms result in energy dissipation, their impacts on the dynamics of the system are fundamentally different in different situations. Therefore, to describe the attenuation pattern of wave propagations in the system, both relaxation and retardation parameters are necessary for the whole range of frequencies. Furthermore, it is discovered that by employing

the so-called relaxation time variable in the conventional viscoelastic models, the resistive and capacitive parameters of the system are combined in the system governing equations, which will limit the application of these models to a narrow range of fitted spectrum and single-domain dynamic investigations while viscoelasticity solely is a multi-physical domain phenomena including thermal subdomain.

By relating the viscoelastic behavior of a mechanical domain to the dissipation of its subdomains, a four-parameter CLS model is developed. The comparison between the obtained results indicates that although the mathematical interpretations of both the proposed model and the conventional SLS model are the same, there exists a significant difference between the performances of these two models. This highlights that in the CLS model the dynamic level in which the viscoelastic behavior of the system is formed is lower than that in the SLS model. Thus, more detailed interactions between the various subdomains of the system can be revealed in the CLS model in contrast to its conventional counterparts. With the use of the energy-based modeling technique, generating a model, such as the CLS, at the level of subdomains is entirely feasible. This feature has allowed the proposed CLS model to sufficiently reveal the impacts of the subdomain interactions and specialized dissipation mechanisms on forming the comprehensive viscoelastic behavior of the system.

References

[1] H.P. Liu, D. L. Anderson, H. Kanamori, "Velocity dispersion due to anelasticity," *Geophys. J. Roy. Astr. Soc.,* pp. 41-58, 1967.

[2] J. Ferry, Viscoelastic Properties of Polymers, N.Y.: J. Wiley, 1970.

[3] R. Lakes, Viscoelastic Solid, N.Y.: CRC Press, 1999.

[4] C. Friedrich, "Relaxation and retardation function of the Maxwell model with fractional derivatives," *Rheol. Acta,* vol. 30, 1991.

[5] H. Schiessel, R. Metzler, A. Blumen, T.F. Nonnenmacher, "Generalized viscoelastic models: Their fractional equations with solutions," *J. Phys. A: Math. Gen.,* vol. 25, 1995.

[6] T. Pritz, "Five-parameter fractional derivative model for polymetric damping materials," *J.*

Sound Vibration , vol. 265, pp. 935-952, 2003.

[7] R. Metzler, T.F. Nonnenmacher, "Fractional relaxation processes and fractional rheological models for description of a class of viscoelastic materials," *Int. J. Plast.,* vol. 19, 2003.

[8] J.G. Liu, M.Y. Xu, "Higher-order fractional constitutive equations of viscoelastic materials involving three different parameters and their relaxation and creep functions," *Mech. Time-Depend. Mater,* vol. 10, 2006.

[9] P.C. Powell, A.J. Ingen Housz, Engineering with Polymers, Cheltingham: Stanley Thornes Publishers, 1998.

[10] D. Hudgin, Polymer Viscoelasticity: Stress and Strain in Practice, N.Y.: Marcel Dekker, 2000.

[11] L. Kari, "On the wave guide modeling of dynamic stiffness of cylindrical vibration isolations," *Journal of Sound and Vibration,* vol. 244, no. 2, pp. 211-257, 2001.

[12] S.J. Zhu, X.T. Weng, G. Chen, "Modeling of the stiffness of elastic body," *Journal of Sound and Vibration,* vol. 262, p. 1–9, 2003.

[13] J. Thoma, Simulation by Bondgraph, Verlag, Germany: Springer , 1990.

[14] A. Mukherjee, R. Karmakar, Modeling and Simulation of Engineering Systems through Bond graph, New Delhi, India: Narosa Publishing House, 2000.

[15] D.C. Karnopp, R.C. Rosenburg, System Dynamics: A Unified Approach, Wiley Inter sciences, 1975.

[16] H. Afshari, A. Zanj, "Dynamic Analysis of a Nonlinear Pressure Regulator Using Bondgraph Simulation Technique," *Journal of Simulation Modeling Practice and Theory,* 2010.

[17] A. zanj, H. Afshari, "Dynamic Analysis of a Complex Pneumatic Valve Using Pseudo-Bond Graph Modeling Technique," *Journal of Dynamic Systems, Measurement, and Control,* vol. 135, no. 3, 2013.

[18] A. Zanj, H. Karimi, A.J. Gholi, M. Shafiee, "Dynamic Modeling of Indirect Hydro-Control Valve - Bondgraph Approach," *Journal of Simulation, Modeling, Practice and Theory,* vol. 28, pp. 65-80, 2012.

[19] A. Zanj, F. He, "Multi-Physical System Variable DOF Modeling: An Investigation on Hyro-Control Device Start Process,"in IEEE International Conference on Systems, man, and

Cybernetics, Budapest Hungary, October, 2016.

[20] R. M. Christensen, Theory of viscoelasticity - An introduction, Academic Press, Inc, 1982.

[21] F. Riesz, "Sur les opérations fonctionnelles linéaires," *C. R. Acad. Sci. Paris,* vol. 149, p. 974–977, 1909.

[22] D. Roylance, "Engineering Viscoelasticity," Massachusetts Institute of Technology, Cambridge, MA 02139, October, 2001.

[23] A. Zanj, F. He, "A Thermomechnical Enhanced Elastic Model: Bond Graph Approach," in *in 23rd International Congress on Sound andVibration*, Athen, Greece, July, 2016.

[24] A. Zanj, F. He, "Conduction Model Compatible for Multi-Physical Domain Dynamic Investigations: Bond Graph Approach," *World Academy of Science, Engineering and Technology, International Journal of Mechanical, Aerospace, Industrial, Mechatronic and Manufacturing Engineering,* vol. 10, no. 3, pp. 524-535, 2016.

[25] A. Zanj, F. He, "Domain-Independent Thermoelastic Coupling Suitable for Aero-thermoelastic Modeling," in *23rd International Congress on Sound & Vibration*, Athens, Greece, July, 2016.

[26] H. Hübel, "Basic conditions for material and structural ratcheting," *Nuclear Engineering and Design,* vol. 162, no. 1, pp. 55-65, March 1996.

DOMAIN-INDEPENDENT THERMOVISCOELASTIC MODEL: A BOND GRAPH APPROACH

Amir Zanj[1], Fangpo He[2], Peter C. Breedveld[3]

Abstract-

Controlling the thermo-mechanical behavior of a multi-physical system has always been a challenging issue, as the general behavior of the system in this case is a result of complex energetic transactions between the system's existing physical subdomains. In this study, a novel thermoviscoelastic model is proposed in which the thermo-mechanical behavior of the system is generated from the interactive dynamics of its involving subdomains. To this aim, by means of the Bond graph approach, the dynamic behavior of each subdomain is first generated separately with respect to the interactions of its own energetic components. The dynamics of all involving subdomains are then coupled via generating reversible and irreversible interactions between the counterpart energetic components of different subdomains. The impacts of geometrical and material changes on the system dynamics are finally added to the model via the compatibility consideration of the energetic components of different subdomains. The proposed model provides an energetic structure with which the general dynamics of the system are obtained from the constructive dynamics of each of the subdomains. This special capability of the model leads to an automatic capturing of the thermo-mechanical phenomena inside the system. The obtained simulation results for a simple beam structure demonstrate the impacts of the internal dynamics on the observable behavior of the system, and prove the capability of the model in covering a wide range of thermo-mechanical behavior including material softening, vibrational heating, dilation, relaxation, conduction, and damping.

Keywords: multi-physical system, thermoviscoelastic modeling, material softening, discrete modeling, irreversible thermodynamic, coupled dynamics.

1. Introduction

Normally, to control the structural deformation of a high-speed vehicle, one must consider the aero or hydro-elasticity of the system. In extreme conditions, the thermal impacts that can change both the geometrical and material parameters of the system (e.g., expansion, material stiffness, and damping) must be taken into account. Given that the system control strategies will largely depend

[1] PhD Candidate, Advanced Control Systems Research Group, School of Computer Science, Engineering and Mathematics, Flinders University, Adelaide, Australia, e-mail: amir.zanj@flinders.edu.au
[2] Associate Professor, Advanced Control Systems Research Group, School of Computer Science, Engineering and Mathematics, Flinders University, Adelaide, Australia, e-mail: fangpo.he@flinders.edu.au
[3] Associate Professor, Robotics and mechatronics group, University of Twente, Enschede, The Netherlands

on these parameters, the thermal impacts are seen to significantly affect the performance as well as the reliability of the system [1].

In general, the thermal impacts on a system can be induced by two different scenarios: directly from the heat entered into the structure due to the solid and fluid interface interactions known as the aero or hydro-thermo loading [2], and indirectly from the heat generated inside the structure as a result of the internal structural damping mechanisms known as the dissipated energy [3]. The aero-thermo heat load is then added to the heat internally generated. This thermal energy transactions inside the system can interact with other existing energy streams (e.g. the potential or kinetic energy streams) of the system reversibly and irreversibly, resulting in unpredicted changes of the general behavior of the system. The discipline dealing with these phenomena called thermoviscoelasticity [4]

According to the approaches used for constructing mathematical models of thermoviscoelastic bodies, the conventional methodologies describing thermoviscoelasticity can be divided into two main categories [5]. The first and the most general method is based on the theory of fading memory [6]. According to this theory, stresses depend not only on the values of strains and temperature at the given time instant, but also on their values at the previous time instants. In addition, material remembers the recent past better than the remote past [7]. In this method, the obtained constitutive equations of the linear thermoviscoelasticity are derived on the basis of the convolution relation between stress and strain in media. Accordingly, the fixed stand to derive the generalize equations of the thermoviscoelaticity is just based on the observable behavior of the system which does not reveal the interactive nature of the thermoviscoelastic phenomena. The implementation of this method purely relies on mathematical constrains and measuring techniques, neglecting the physical nature of the phenomena.

The second method for dealing with thermoviscoelasticity is based on the use of standard rheological models [8] [9] that introduce a set of parameters, known as relaxation times, to explain the dissipative behaviors of the systems. Although physical elements are employed in rheological models to generate and describe the dissipative behaviors, the use of the generated relaxation times as the main outcome of the method does not satisfy the energetic behaviors of the systems especially at the presence of high-temperature fluctuations [10].

A variety of problems relating to thermoviscoelasticity has been solved by employing the

existing methods explained above. However, there are problems, such as the dependency of the acoustic wave attenuation factor to a signal frequency, remain unsolved. The solutions to these problems may become approachable via considering the physical nature of the thermoviscoelastic phenomena. It is known that thermoviscoelasticity in principal reveals a multi-physical phenomenon in which the overall behavior of a system is a result of several existing dynamics between the engaging physical subdomains. Accordingly, to comprehensively describe such an interactive behavior of the system, a multi-physical approach would be required to unveil the interactions between the subdomains dynamically. This required approach would be in clear contrast to the existing methods that merely rely on the external behavior of the system and are unable to describe the internal interactions of the system. While the existing methods could only be useful for single-domain problems, the required approach would have the capacity to deal with multiple-physical problems by exposing the interactive passage between the different subdomains and, thus, revealing the truth behind any specific behavior of the system [11].

In this study to generate a physical understanding of thermoviscoelastic phenomena, by means of a port-based approach known as the Bond graph (BG) approach [12] [13], a physical presentation of thermoviscoelasticity on the basis of physical system theory [14] is introduced and a new model of thermoviscoelasticity is proposed. The proposed model will decompose the thermoviscoelastic domain into a set of corresponding primary physical subdomains to realize the attempt of discovering possible internal interactions between the involving subdomains. The model will produce separate energy cycles for different subdomains, thus offering the opportunity to identify the possible reversible and irreversible interactive connections between the subdomains. The generalized equations of the model would be expected to carry more physical insights of the system, thus providing a justifiable basis upon which more complex dynamics of the system could be identified using the existing causality of the physical phenomena. The energetic picture of the system provided in the model would generate a dynamic map of power distributions within the system that can be used to better manage and control the complex dynamic behavior of the system under coupled thermomechanical loading.

To generate the required multi-physical nonlinear thermoviscoelastic constitutive model, the reminder of this paper is organized as follows. In Section II, the classical fundamental of linear thermoviscoelasticity is briefly explained, and the drawback of implementing the conventional

methods is pointed out. In Section III, using the BG approach, a novel thermoviscoelastic model is proposed. To generate the proposed model, the BG representations of the elastic and thermal domains are first developed in Subsections III-I and III-II for a simple beam structure. By means of the reversible and irreversible couplings introduced in Subsections III-III and III-V, these domains are then connected together to form a physical thermoviscoelastic domain in Subsection III-VI. In Section IV, for the chosen structure, the capability of the proposed model in capturing thermoviscoelasticity is discussed. The suitability of the proposed approach in physically describing the complex dynamic behavior of the system and assisting with specialized energy management is then concluded in Section V.

2. The classical fundamental of thermoviscoelasticity and its problems

To examine the capability and limitation of conventional thermoviscoelastic models, the fundamental theory relating to the conventional thermoviscoelasticity is briefly reviewed and the related problems regarding the implication of these approaches in multi-physical system applications are highlighted.

As mentioned earlier the general approaches concerning thermoviscoelasticity can be divided into two main categories: memory fading and rheological approaches. To generate the constitutive equations of thermoviscoelasticity for both categories, almost identical strategies are employed. Fundamentally, from a classical point of view, for any material under consideration the stress tensor at each point, σ_{ij}, can be split into two parts [15]:

$$\sigma_{ij} = \sigma_{ij_r} + \sigma_{ij_{ir}} \tag{1}$$

where σ_r and σ_{ir} respectively represent the reversible and irreversible portions of the stress tensor with the following constitutive equations:

$$\sigma_r = \frac{\partial H(\varepsilon, \theta)}{\partial \varepsilon} \tag{2}$$

$$\sigma_{ir} = \frac{\partial D(\dot{\varepsilon})}{\partial \dot{\varepsilon}} \tag{3}$$

Here H stands for the Helmholtz free energy as a function of strain ε and temperature $\theta = (T - T_0)$ with T and T_0 being the instantaneous and reference temperature, respectively; D is the dissipation potential of the material given as a function of strain rate $\dot{\varepsilon}$:

$$H(\varepsilon,\theta)=\frac{1}{2}a_{ijkh}(\varepsilon_{kh}-\alpha_{kh}\theta)\big(\varepsilon_{ij}-\alpha_{ij}\theta\big)-\frac{1}{2}\big(\beta+a_{ijkh}\alpha_{ij}\alpha_{kh}\big)\theta^2 \tag{4}$$

$$D(\dot{\varepsilon})=\frac{1}{2}b_{ijkh}\dot{\varepsilon}_{kh}\dot{\varepsilon}_{ij} \tag{5}$$

where a, b, α, and β respectively denote the elasticity tensor, the viscosity tensor, the thermal expansion tensor, and the coupled thermoelastic tensor. Considering the symmetry of the mentioned tensors for homogenous materials, the reversible and the irreversible stress of the system can be presented as:

$$\sigma_{ij_r}=\frac{1}{2}a_{ijkh}(\varepsilon_{kh}-\alpha_{kh}\theta) \tag{6}$$

$$\sigma_{ij_{ir}}=b_{ijkh}\dot{\varepsilon}_{kh} \tag{7}$$

To generate the constitutive Eqs. (6) and (7), the Helmholtz free energy function is used. Given that in principal the Helmholtz energy function is a Legendre transformation of internal energy of the system with respect to entropy, implementing this functionality simply means the dynamic interactions between the thermal and elastic domains are neglected. This leads to a domain-dependency of the temperature calculation of the system. Consequently, modeling of dynamic coupling between external thermal load (aero-thermo load) and internal thermal load (dissipated thermal energy) to form the general thermal load on the structure becomes out of reach. Although this may not be an issue for single-field studies (e.g., in thermoelastic phenomena where different dynamic levels between the thermal and elastic domains are expected), it becomes a significant issue in fluid-solid-interface (FSI) problems (e.g., in aerothermoelastic phenomena where multiple interactions of structure with surrounding fluid play a key role in forming the external loads). Thus, to satisfy the modeling requirement, the dynamic consideration of internal thermal domain becomes indispensable.

Other problems may arise by employing the classical methods, such as the non-physical nature of material models frequently used to relate material properties (*a* and *b*) with constitutive equations. For example, in the rheological approach, using the Kelvin-Voigt solid model, the constitutive equation is [8]:

$$\sigma=2G\varepsilon+2G\tau_k\dot{\varepsilon}+E\left[\left(K-\frac{2}{3}G\right)\varepsilon-\frac{2}{3}G\tau_k\dot{\varepsilon}-\alpha K\theta\right] \tag{8}$$

whereas using the Maxwell Solid model, the constitute equation is [8]:

$$\dot{\sigma} + \frac{1}{\tau_m}\sigma = 2G\dot{\varepsilon} + E\left[\left(K - \frac{2}{3}G\right)\dot{\varepsilon} + \frac{K}{\tau_m}\varepsilon - \alpha K\left(\dot{\theta} + \frac{1}{\tau_m}\theta\right)\right] \tag{9}$$

Here K denotes the bulk modulus, G is the shear modulus, τ_k is the strain relaxation time, and τ_m is the stress relaxation time. Although the resultant constitutive equations are different in appearance, in nature both use the same dissipative mechanism called relaxation time (τ) which in the fading memory approach will be replaced with relaxation function and convolution integral [7]:

$$\sigma = \int_0^t \varphi_1(t-\tau)\frac{\partial\varepsilon(\tau)}{\partial\tau}d\tau + E\left[\int_0^t \varphi_2(t-\tau)\frac{\partial\varepsilon(\tau)}{\partial\tau}d\tau - \int_0^t \varphi_3(t-\tau)\frac{\partial\theta(\tau)}{\partial\tau}d\tau\right] \tag{10}$$

where φ_i are the relaxation functions that must satisfy the second law of thermodynamics.

The problem with the implemented dissipative mechanism is that, in the majority of the conventional thermoviscoelastic models, either by means of the relaxation time parameters or by means of the relaxation functions, the anelastic behavior of a body is produced solely from its observable behavior. However, the thermoviscoelastic behavior of a body is a multi-physical domain phenomenon which is a direct result of the interactions among all involving physical subdomains. The inter-domain interactions, as a constructive feature that forms the multi-physical phenomenon, are not obtainable from the observable behavior of the body [11]. Regenerating the behavior of the system without considering its true formation procedure, although can reflect the behavior under especial conditions, will not be able to adequately predict the behavior of the body when the operational condition changes as it occurs in FSI problems.

In addition, the conventional models are unable to predict the response of multi-disciplinary systems, especially when the subdomain interactions cause changes in the parameters of the system. For instance, in the elastic domain the relaxation time (τ) could be a beneficial parameter to explain the strain rate dependency of stress in the system; however; at the presence of the thermal domain the temperature dependency of its two components (stiffness and viscosity) can violate the conservation of energy. The stiffness of the system is the parameter forming the memory of the elastic domain and any changes in this parameter disregarding its impact on other involving domains' memories will undoubtedly separate the system from its history and, thus, violate the conservation low. This will then limit the ability of the model to be coupled with other physical domains.

Considering the above explanations, to truly capture the multi-physical phenomena in a multiple domain setting, one needs to model the interactions of the domains in a physical and conservative way. If a model can satisfy the general physics, such as energy conservation and continuity, of the system, it will be able to automatically capture the phenomena occurring inside the system. The conventional models as demonstrated above clearly fail to present such a desirable performance.

3. Decomposed domain-independent thermoviscoelastic model

To physically explain the thermomechanical behavior of a system, a decomposed domain-independent multi-physical model is proposed. The proposed model provides a meaningful understanding of the ongoing phenomena of the system via decomposing the existing complex behavior of the system into its primary physical (elastic and thermal) domain dynamics. To generate such a thermoviscoelastic model, a domain-independent dispersive model of each domain is first developed using the BG approach that can separately describe the energetic interactions within each of the domains. The possible reversible and irreversible energetic couplings between the domains are then installed inside the model to form an integrated decomposed model. Finally, the interactive modulations including deformation-modulated conductivity and temperature-modulated mechanical resistivity are added to the model. The obtained thermoviscoelastic model will provide a clear dynamic map of the system's energy propagation with which the energy consumption of each domain can be dealt with separately with respect to the dynamic interactions of domain's energetic components (inertance, resistance, and capacitance). This added capability of the model will in turn provide the dynamic coupling capability between a domain of one field and its corresponding domain of another field (e.g., the thermal domain of the solid field and the thermal domain of the fluid field in a FSI problem). This clear physical understanding of the system can then be used to manage and control undesired features of the thermoviscoelastic phenomena. It should be mentioned that, to demonstrate the concept and to avoid unnecessary complexity in deriving the generalized thermoviscoelastic equations of the proposed model, a 1D beam structure is considered in this study.

3.1. Dissipative elastic domain BG model

To generate a distributed dispersive elastic model, the Rayleigh discrete geometry of a beam

structure suggested in [16] is employed. On the basis of the acoustic assumption used in the Rayleigh reticulation, the mass of each element is considered to be at the boundaries of the element, and the elasticity of the element is assumed to be in the center of the element. This means that the elastic energy of the reticulated space will be stored in the center of each element, whereas the kinetic energy of the elastic domain will be saved at the boundaries of each element [16]. Fig. 1 shows the discrete Rayleigh beam structure of a finite number of elements. Since this reticulated space is indeed a continuous system, the adjacent boundaries of each two consecutive elements are bonded to move together. Therefore, one can consider the above discretization as a junction-element chain in which each element represents the potential subdomain of the elastic domain and each junction represents the kinetic subdomain of the elastic domain.

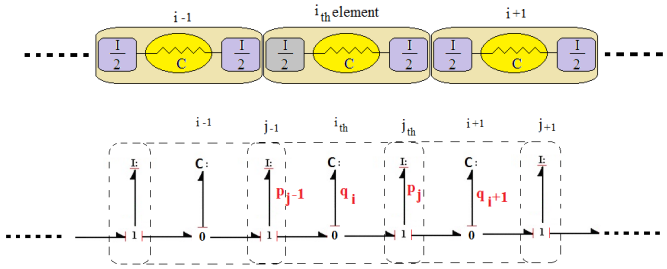

Fig.1 1D Rayleigh distributed geometry and its corresponding BG representation

For the BG representation shown in Fig. 1, the considered state variables for the i_{th} element and j_{th} junction are q_i and p_j which denote the deformation and the momentum, respectively. According to the conservation of energy, the state equations of each junction-element are derived as:

$$\dot{p}_i = \frac{q_{j-1}}{C_{j-1}} - \frac{q_j}{C_j} \tag{11}$$

$$\dot{q}_i = \frac{p_{j-1}}{I_{j-1}} - \frac{p_j}{I_j} \tag{12}$$

$$I_j = \frac{m_i}{2} + \frac{m_{i+1}}{2} \tag{13}$$

$$C_i = \frac{L_{0_i}}{A_i E_i} \tag{14}$$

where I_j is the boundary inertance defined as a function of the adjacent elements' masses, and C_i represents the capacitance of the element as a function of its geometrical and material parameters. Parameters L_{0_i}, A_i, and E_i stand for the initial length, contact surface, and Young modulus of the

element, respectively. It should be mentioned that in the boundary elements of the structure, considering the type of the boundary (Neumann or Dirichlet) and the location (left or right in 1D structure) of the boundary, the corresponding terms in Eqs. (11) or (12) will be replaced by the terms relevant to the external sources (e.g., force or velocity).

Using the geometrical and material parameters of the system, the presented model is able to generate the dynamics of the system in a pure elastic nature. To add the dispersive considerations to the model, according to the BG approach, there is a need to add an adequate number of resistive elements to certain points of the presented elastic BG model [10]. For this, in the following, energy-based presentations of the so-called conventional viscoelastic models, namely the Maxwell and Voigt models, will be added to the suggested model.

3.1.1. Maxwell BG model

From the literature, the Maxwell model is known as a spring-dashpot mechanism in series [17]. Considering the arrangement of the energetic component in the suggested elastic model of Fig. 1, the BG model shown in Fig. 2 can be the representative of the Maxwell anelastic model [10]. In this model, a resistor is placed inside each element in series with the storage component. This means that the internal energy of each element can be saved and dissipated. The series configuration of the energetic components (resistor and capacitor) in the Maxwell model allows the system to be relaxed during a long term loading.

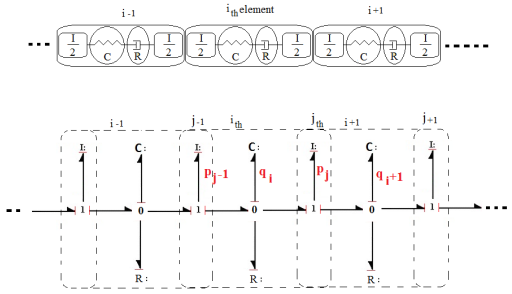

Fig.2 Maxwell model BG representation

With respect to the BG model presented in Fig. 2, Eq. (12) is changed to:

$$\dot{q}_i = \frac{p_{j-1}}{I_{j-1}} - \frac{p_j}{I_j} - \frac{q_i}{\tau_i} \tag{15}$$

$$\tau_i = R_i C_i \tag{16}$$

where R_i indicates the resistance of the system, and can be obtained from the viscosity of the material. Eqs. (11) and (15) form the state equations of the potential and kinetic subdomains of the considered anelastic domain, respectively. The physical representation of the equations highlights the fact that in the Maxwell model the energy of the system is dissipated just in the potential subdomain. This means that inside the kinetic subdomain of the system the energy consumption is still reversible. This explains why under highly dynamic situation the Maxwell model fails to present a proper energy loss for the system.

3.1.2. Kelvin-Voigt BG model

Another anelastic model frequently used for modeling materials is the Kelvin-Voigt model in which the resistive components are considered in parallel with the capacitive components of the system [10]. Unlike the Maxwell model, this model is well known for the system investigation under cyclic loading [17].

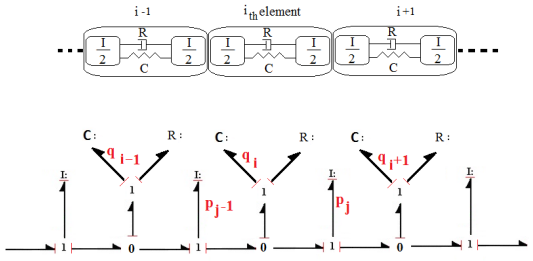

Fig.3 Loop-less Kelvin-Voigt BG model [10]

The BG representation of the Kelvin-Voigt model is shown in Fig. 3. Accordingly, the energy entered into each medium is distributed between a resistor and a storage component with the same flow rate but different effort. This means that the system working under the Voigt model can always hold the elastic energy without relaxing it, and the sensitivity of the system is mainly on the loading rate applied to the system. According to the presented BG, the governing equations for the kinetic and potential subdomains on the basis of the Kelvin-Voigt model are defined as:

$$\dot{p}_j = \frac{q_i}{C_i} + R_i\left(\frac{p_{j-1}}{I_{j-1}} - \frac{p_j}{I_j}\right) - \frac{q_{i+1}}{C_{i+1}} - R_{i+1}\left(\frac{p_j}{I_j} - \frac{p_{j+1}}{I_{j+1}}\right) \tag{17}$$

$$\dot{q}_i = \frac{p_{j-1}}{I_{j-1}} - \frac{p_j}{I_j} \tag{18}$$

From the obtained governing equations, it is attainable that in the Kelvin-Voigt model the

energy is dissipated just in kinetic subdomain, and the potential subdomain stays reversible. Also, by comparing Fig. 2 and Fig. 3 one can notice that in the Voigt model, in contrast to the Maxwell model, the causality of the resistive elements is flow-based. This shows that these two viscoelastic models, in fact, describe two different phenomena in two different subdomains. Therefore, as a result of this physical consideration of anelastic models, an advanced model combining both the Maxwell and Voigt terminologies together is needed to consider all sorts of dispersions inside the system. Since the advancement of anelastic material models is beyond the interest of this paper, in the following, to generate the physical thermoviscoelastic model, the BG representation of the Maxwell model is selected to present the dispersive elastic domain.

3.2. Thermal domain BG model

A conduction model for the discrete geometry of the previous section will be generated using the geometrical reticulation and BG representation of a 1D conductive system shown in Fig. 4. As can be seen, the energy propagation in the thermal domain can be described by a chain of dissipative, R, and capacitive, C, energy components which are placed interlaced [18]. In this model, it is assumed that the thermal energy is stored in C component, and is dissipated while passing through R component. Given that the thermal sink is directly connected to the thermal source in the thermal domain [19], one can say that in the thermal domain each resistive component (R) acts as a two-port non-return transmitter (shown as RS in Fig. 4) with which the dissipated energy can re-enter to the thermal domain. The causality of the return side is always such that the resistor is seen as a source of the entropy rate, never as a source of the temperature because the sources of temperature are non-physical [16].

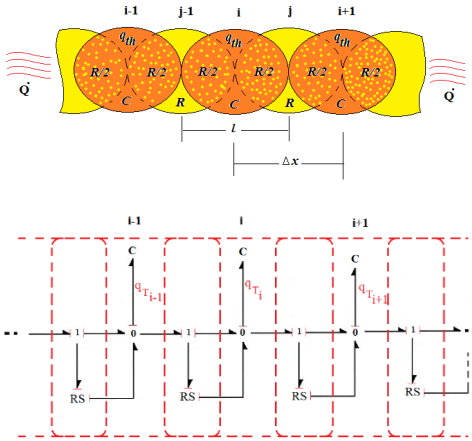

Fig.4 One dimensional heat conduction schematic

Based on the obtained thermal BG integrative causality, the state equation of the thermal domain is derived by defining all the entropy flow to the storage component of the system:

$$\dot{q}_{th_i} = \dot{s}_{j-1} - \dot{s}_j + \dot{S}_i^{gen} \tag{19}$$

where q_{th_i} denote the amount of stored entropy, s, of the i_{th} element; $\dot{s}_{j-1}$, $\dot{s}_j$, and $\dot{S}_i^{gen}$ are the amounts of reversible inlet and outlet entropy flows and the entropy generation rate, respectively. Considering the resistive constitutive equation of the thermal domain, the internal flow crossing the j_{th} boundary of the segment can be derived as:

$$\dot{s}_j = \frac{1}{R_j}(\psi_i(q_{th_i}) - \psi_{i+1}(q_{th_{i+1}})) \tag{20}$$

where R_j is the resistant coefficient of the j_{th} RS component, and $\psi_i(q_{th_i})$ is the i_{th} constitutive equation of the thermal domain. Substituting Eq. (20) into Eq. (19), the state equation of the thermal domain can be expressed as:

$$\dot{q}_{th_i} = \frac{1}{R_{j-1}}(\psi_{i-1}(q_{th\,i-1}) - \psi_i(q_{th\,i})) - \frac{1}{R_j}(\psi_i(q_{th\,i}) - \psi_{i+1}(q_{th\,i+1})) + \dot{S}_i^{gen} \tag{21}$$

Assuming that the capacity of a long well-insulated rod in conducting heat is proportional to the temperature gradient [18], the resistive parameter R is then described by:

$$\Delta T = \Phi.\dot{Q} = (\Phi.T).\dot{s} = R.\dot{s} \tag{22}$$

where Φ is the thermal resistance and, by considering the Fourier law for 1D structure, can be derived as:

$$R_j = \frac{\Delta x_j T_j}{k_j A_j} \tag{23}$$

in which k and A are specific thermal conductance coefficient and cross-section area of the j_{th} junction, respectively, and Δx is the generalized length of the j_{th} resistive energy component.

Considering the capacity component of the segment, the constitutive equation of the thermal domain, ψ, can be defined as the relation between the equilibrium-determinant variable of the thermal domain, T, and the extensive variable of the thermal domain, q_{th}:

$$T = \psi(q_{th}) \tag{24}$$

Given the capacitive law in constant volume, one has:

$$Q = \rho V c \frac{dT}{dt} \tag{25}$$

where c, ρ, and V are respectively the specific heat, density, and volume of the segment. Considering the relation between the conjugate variables of the thermal domain, one writes:

$$Q = T\dot{q}_{th} \tag{26}$$

By substituting Eq. (25) and the time derivative of Eq. (24) into Eq. (26), for the i_{th} element the following relation is obtained:

$$\frac{d\psi_i}{dq_{th_i}} = \frac{\psi_i}{c_i \rho_i A_i l_i} \tag{27}$$

where l_i is the length of the i_{th} storage component. By integrating Eq. (27) with respect to the reference condition, the constitutive relation of the thermal domain is defined as:

$$T_i = \psi_i(q_{th_i}) = T_0 e^{\frac{1}{\rho_i V_i c_i}(q_{th_i} - s_0)} \tag{28}$$

where T_0 and s_0 are respectively the reference temperature and entropy for the i_{th} segment.

To define the generated entropy rate, $\dot{S}_i^{gen}$, in Eq. (21), consider the continuous power transmission of the two-port *RS*-component and the resistive constitutive equation for each junction:

$$\dot{S}_i^{gen} T_i = \dot{s}_{j-1}\,(T_{i-1} - T_i) \tag{29}$$

$$\dot{s}_j\, R_j = (T_i - T_{i+1}) \tag{30}$$

Substituting Eqs. (28) and (30) into Eq. (29), the generated entropy rate of each segment is derived as:

$$\dot{S}_i^{gen} = \frac{1}{R_{j-1}} T_0 e^{\frac{1}{\rho_i V_i c_i}(q_{th_i} - s_0)}\,(e^{\frac{1}{\rho_i V_i c_i}(q_{th_i} - q_{th_{i-1}})} - 1)^2 \tag{31}$$

Accordingly, the governing equation of the thermal domain is closed.

Since the generated thermal and elastic models are to be coupled to form the integrated thermoviscoelastic model, the geometrically compatibility conditions of their counterpart energy components must be satisfied. Each thermal segment is then required to have its own independent properties and internal energy components (R, C) in such a way that the boundaries of the internal energy components symmetrically become congruous with the boundary of the segment. Also,

each parameter of the thermal junctions, indexed by j, is required to be obtainable from the corresponding parameters of the adjacent elements via the same weighting function as that used in the elastic domain. Accordingly, similar to the elastic model, the memory characteristics of the thermal domain that carry the material and geometrical information are at the center part of each segment, whereas the resistivity characteristics of the thermal domain are at the two sides of each segment. To form the resistive component in the suggested configuration, assume the mean functionality:

$$R_j = \frac{R_i + R_{i+1}}{2} \tag{32}$$

From Eqs. (23) and (28), one has:

$$R_j = \frac{T_0}{2}\left(\frac{l_i e^{\frac{1}{\rho V c}(q_{th_i} - s_0)}}{k_i A_i} + \frac{l_{i+1} e^{\frac{1}{\rho_{i+1} V_{i+1} c_{i+1}}(q_{th_{i+1}} - s_0)}}{k_{i+1} A_{i+1}}\right) \tag{33}$$

It is clear that by substituting Eqs. (28), (31), and (33) into Eq. (21), the rate of the change in the entropy of each element will be dependent on the material and geometrical characteristics of a spatial element. This exclusivity of the suggested model makes the thermal element compatible with any other domains' elements that have the same spatial references, and leads to the appropriateness of the thermal model in multi-physical domain dynamic investigations.

3.3. Thermoelastic reversible energetic coupling

The generated dispersive elastic and thermal models provide two separate energy lines that can illustrate the power transactions in each of the domains individually. At this stage, the reversible dynamic connection of the two domains is added to the model, which clarifies the continuous non-entropic power transformation between the thermal and elastic domains. The memories of these two domains (saved in their capacity components) are required to be reversibly coupled. To achieve this, the storage components of both domains are replaced with the two-port storage [20] shown in Fig. 5. This multiport storage, named as the reversible thermoelastic coupling, contains the information from both the thermal and elastic domains that can form the new coupled constitutive equation for the coupled domains. By installing this energy component to the model, the thermal dynamic changes are expected to be captured via alteration in the elastic domain, and vice versa, in an energy conservative manner. It should be mentioned that, to replace the existing storage of the domains with the reversible thermoelastic coupling, the compatibility of the storage

components of the thermal and elastic domains is mandatory and satisfied while developing the thermal model.

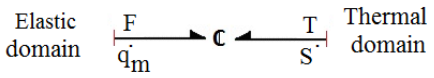

Fig.5 Two-port C model of the thermoelastic energy storage [20]

The replacement of the storage components mathematically means the change of the constitutive relation of each domain with two dimensional constitutive equations that are reciprocal together. To extract the new constitutive equations of each domain, assume that the total energy stored inside the two-port capacitor is a function of the extensive states of both the thermal and elastic domains as:

$$U = U(q_m, S) \tag{34}$$

where q_m represents the deformation and S is the entropy of each segment. Considering the energy as a first-order homogenous function, the energy change in the field can be expressed as:

$$dU = \frac{\partial U}{\partial q_m} dq_m + \frac{\partial U}{\partial S} dS \tag{35}$$

where by definition the constitutive equations of the elastic and thermal domains are:

$$F(q_m, S) = \left(\frac{\partial U}{\partial q_m}\right)_S , T(q_m, S) = \left(\frac{\partial U}{\partial S}\right)_{q_m} \tag{36}$$

in which F and T are defined earlier as the efforts (potentials) of the elastic and thermal ports, respectively. The deferential form of the constitutive equation for both domains with respect to the new variables can be presented as:

$$dT = \left(\frac{\partial T}{\partial q_m}\right)_S dq_m + \left(\frac{\partial T}{\partial S}\right)_{q_m} dS \tag{37}$$

$$dF = \left(\frac{\partial F}{\partial q_m}\right)_S dq_m + \left(\frac{\partial F}{\partial S}\right)_{q_m} dS \tag{38}$$

To start with the thermal domain constitutive relation, for the second term of the right hand side of Eq. (37), given the thermal energy Q at constant volume,

$$\partial Q = T\partial s = C_v dT \tag{39}$$

and considering the constant specific heat C_v, one can conclude:

$$\left(\frac{\partial T}{\partial S}\right)_{q_m} = \frac{T}{C_v} \tag{40}$$

To define the first term of Eq. (37), by taking the advantage of the reciprocity of the two constitutive equations and the Hook's law for 1D geometry, one has:

$$\left(\frac{\partial T}{\partial q_m}\right)_S = \left(\frac{\partial F}{\partial S}\right)_{q_m} \tag{41}$$

$$F = AE\frac{q_m}{L} + \alpha AE(T - T_0) \tag{42}$$

Taking the partial derivative of Eq. (42) with respect to entropy and comparing it with Eq. (41) yield:

$$\left(\frac{\partial T}{\partial q_m}\right)_S = \alpha AE\left(\frac{\partial T}{\partial S}\right)_{q_m} = \alpha AE\frac{T}{C_v} \tag{43}$$

Substituting Eqs. (40) and (43) into Eq. (37) produces:

$$\frac{dT}{T} = \frac{\alpha AE}{C_v}dq_m + \frac{1}{C_v}dS \tag{44}$$

Considering the relaxed initial condition at ambient room temperature, the new constitutive equation of the thermal domain is extracted by intergrading Eq. (44):

$$T = T_0 e^{\frac{\alpha AE}{C_v}q_m} e^{\frac{(S-S_0)}{C_v}} \tag{45}$$

The constitutive equation of the elastic domain can be obtained by using Eq. (45) to change the causality of Eq. (42), resulting in:

$$F = AE\frac{q_m}{L} + \alpha AET_0(e^{\frac{\alpha AE}{C_v}q_m} e^{\frac{(S-S_0)}{C_v}} - 1) \tag{46}$$

By substituting the two constitutive relations Eqs. (45) and (46) into Eq. (35) and integrating, the potential function of the two-port storage field is obtained as:

$$U = AE\frac{{q_m}^2}{2L} + C_v T_0 e^{\frac{\alpha AE}{C_v}q_m} e^{\frac{(S-S_0)}{C_v}} - \alpha AET_0 q_m \tag{47}$$

The obtained nonlinear multiport energy function of the thermoelastic domain contains a contribution relating to displacement/strain and a contribution relating to the entropy, thus showing the combined effect of thermoelasticity.

Fig. 6 shows the updated BG representation of the reversibly coupled thermoelastic model. As can be seen, the interconnections of the two domains is through the storage of the system. This leads to a dynamic capture of the elastic deformation effect on the thermal domain, parallel with

the thermal load impact on the elastic domain, with less linearization and more physical insight.

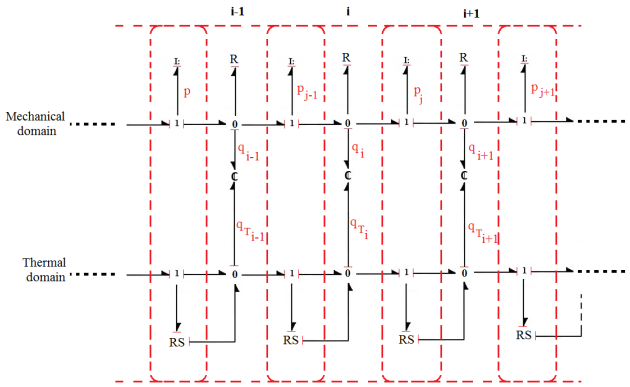

Fig.6 Reversibly coupled thermoviscoelastic BG representation

Considering the BG representation of the coupled domain, the governing equations for a single port-based thermoelestic element (the i_{th} element in a chain) are extracted as follows where, to avoid the confusion between the parameters of the coupled domain, the indexes *m* and *th* are used to indicate the elastic and thermal parameters, respectively:

$$\dot{p}_{m_j} = A_i E_i \frac{q_{m_i}}{L_i} - A_{i+1} E_{i+1} \frac{q_{m_{i+1}}}{L_{i+1}} + \alpha_i A_i E_i T_{0_i} \left(e^{\frac{\alpha_i A_i E_i}{C_{vi}} q_{m_i}} e^{\frac{(q_{th_i} - S_{0_i})}{C_{vi}}} - 1 \right) - \alpha_{i+1} A_{i+1} E_{i+1} T_{0_{i+1}} \left(e^{\frac{\alpha_{i+1} A_i + 1 E_{i+1}}{C_{vi+1}} q_{m_{i+1}}} e^{\frac{(q_{th_{i+1}} - S_{0_{i+1}})}{C_{vi+1}}} - 1 \right) \tag{48}$$

$$\dot{q}_{m_i} = \frac{p_{m_{j-1}}}{I_{m_{j-1}}} - \frac{p_{m_j}}{I_{m_j}} - \frac{A_i E_i q_{m_i}}{R_{m_i} L_i} \tag{49}$$

$$\dot{q}_{th_i} = \frac{1}{R_{th_{j-1}}} (T_{0_{i-1}} e^{\frac{\alpha_{i-1} A_{i-1} E_{i-1}}{C_{vi-1}} q_{m_{i-1}}} e^{\frac{(q_{th_{i-1}} - S_{0_{i-1}})}{C_{vi-1}}} - T_{0_i} e^{\frac{\alpha_i A_i E_i}{C_{vi}} q_{m_i}} e^{\frac{(q_{th_i} - S_{0_i})}{C_{vi}}}) - \frac{1}{R_{th_j}} (T_{0_i} e^{\frac{\alpha_i A_i E_i}{C_{vi}} q_{m_i}} e^{\frac{(q_{th_i} - S_{0_i})}{C_{vi}}} - T_{0_{i+1}} e^{\frac{\alpha_{i+1} A_i + 1 E_{i+1}}{C_{vi+1}} q_{m_{i+1}}} e^{\frac{(q_{th_{i+1}} - S_{0_{i+1}})}{C_{vi+1}}}) + \dot{S}_{th_i}^{gen} \tag{50}$$

$$\dot{S}_{th_i}^{gen} = \frac{T_{0_i} e^{\frac{\alpha_i A_i E_i}{C_{vi}} q_{m_i}} e^{\frac{(q_{th_i} - S_{0_i})}{C_{vi}}}}{R_{th_{j-1}}} \left(\frac{T_{0_{i-1}} e^{\frac{\alpha_{i-1} A_{i-1} E_{i-1}}{C_{vi-1}} q_{m_{i-1}}} e^{\frac{(q_{th_{i-1}} - S_{0_{i-1}})}{C_{vi-1}}}}{T_{0_i} e^{\frac{\alpha_i A_i E_i}{C_{vi}} q_{m_i}} e^{\frac{(q_{th_i} - S_{0_i})}{C_{vi}}}} - 1 \right)^2 \tag{51}$$

$$I_{m_j} = \frac{m_i}{2} + \frac{m_{i+1}}{2} \tag{52}$$

$$R_{th_j} = \frac{1}{2} \left(\frac{L_i T_{0_i} e^{\frac{\alpha_i A_i E_i}{C_{vi}} q_{m_i}} e^{\frac{(q_{th_i} - S_{0_i})}{C_{vi}}}}{k_i A_i} + \frac{L_{i+1} T_{0_{i+1}} e^{\frac{\alpha_{i+1} A_i + 1 E_{i+1}}{C_{vi+1}} q_{m_{i+1}}} e^{\frac{(q_{th_{i+1}} - S_{0_{i+1}})}{C_{vi+1}}}}{k_{i+1} A_{i+1}} \right) \tag{53}$$

Eqs. (48), (49), and (50) form the updated state equations of the coupled thermal and elastic domains that represent the rates of the element's boundary momentum, deformation, and accumulated entropy, respectively, as nonlinear functions of the considered extensive states (q_m and q_{th}), geometrical parameters, and material parameters. Eq. (51) demonstrates the amount of irreversibility occurring in the thermal domain. It is clear that this equation satisfies the second thermodynamic law, as the amount of the generated entropy is always greater than zero.

3.4. Thermoelastic irreversible energetic coupling or thermoviscoelastic coupling

As mentioned earlier, in the thermal domain, the thermal sink is connected to the thermal source. Since the dissipation in other domains turns to heat, a more complete statement is that the thermal domain is in principal the sink of other physical domains in terms of energy dissipation. Thus, the dissipated energy from the elastic domain has to be transferred to the thermal domain. Given that this transformation of energy is irreversible, a non-return two-port energy transducer introduced in [10] as a resistive-source component (*RS*) is now required to be installed inside the system to irreversibly connect the elastic domain to the thermal domain.

This new connection is presented in Fig. 7 where the dissipated energy in the elastic side of the system is seen to return to the system in the thermal side. This returned energy can then change the dynamics of the thermal domain which is coupled with the elastic domain. Hence, the whole dynamics of the system will be altered as a result of this interaction.

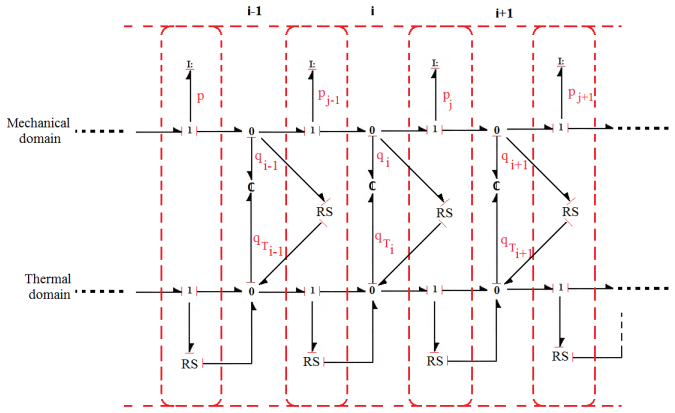

Fig.7 Coupled thermoviscoelastic model

To include the impact of this irreversible transaction on the thermal domain, it is required to calculate the amount of the entropy rate generated as a result of this transaction, and then add this

amount to the thermal state equation. To do this, assume that the transferred energy stays conservative while transferring between the domains. According to the allocated conjugate variables of each port shown in Fig. 8, the power transaction can be presented as:

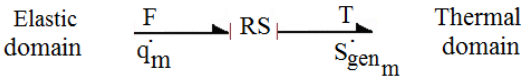

Fig.8 Mechanical *RS*-element conjugate variables

$$\dot{q}_m F = \dot{S}_{gen_m} T \tag{54}$$

For the i_{th} element, considering the constitutive equation of the resistive component with respect to its causality, the introduced entropy rate to the elastic domain can be calculated as:

$$\dot{S}_{gen_{m_i}} = \frac{{F_{R_i}}^2}{R_{m_i} T_i} \tag{55}$$

where F_R denotes the resistive effort and can be calculated as:

$$F_{R_i} = \frac{A_i E_i}{L_i} q_{m_i} \tag{56}$$

Substituting Eqs. (45) and (56) into Eq. (55), the generated entropy is derived as:

$$\dot{S}_{gen_{m_i}} = \frac{\left(\frac{A_i E_i}{L_i} q_{m_i}\right)^2}{R_{m_i} T_{0_i} e^{\frac{\alpha_i A_i E_i}{C_{v_i}} q_{m_i}} e^{\frac{(q_{th_i} - S_{0_i})}{C_{v_i}}}} \tag{57}$$

As can be seen, the mechanical generated entropy equation is always greater than zero, which satisfies the second thermodynamic low. Adding Eq. (57) to the right hand side of Eq. (50), the new state equation for the thermal domain is defined as:

$$\begin{aligned}
\dot{q}_{th_i} = {} & \frac{1}{R_{th_{j-1}}} \left(T_{0_{i-1}} e^{\frac{\alpha_{i-1} A_{i-1} E_{i-1}}{C_{v_{i-1}}} q_{m_{i-1}}} e^{\frac{(q_{th_{i-1}} - S_{0_{i-1}})}{C_{v_{i-1}}}} - T_{0_i} e^{\frac{\alpha_i A_i E_i}{C_{v_i}} q_{m_i}} e^{\frac{(q_{th_i} - S_{0_i})}{C_{v_i}}} \right) \\
& - \frac{1}{R_{th_j}} \left(T_{0_i} e^{\frac{\alpha_i A_i E_i}{C_{v_i}} q_{m_i}} e^{\frac{(q_{th_i} - S_{0_i})}{C_{v_i}}} - T_{0_{i+1}} e^{\frac{\alpha_{i+1} A_i + 1 E_{i+1}}{C_{v_{i+1}}} q_{m_{i+1}}} e^{\frac{(q_{th_{i+1}} - S_{0_{i+1}})}{C_{v_{i+1}}}} \right) \\
& + \frac{T_{0_i} e^{\frac{\alpha_i A_i E_i}{C_{v_i}} q_{m_i}} e^{\frac{(q_{th_i} - S_{0_i})}{C_{v_i}}}}{R_{th_{j-1}}} \left(\frac{T_{0_{i-1}} e^{\frac{\alpha_{i-1} A_{i-1} E_{i-1}}{C_{v_{i-1}}} q_{m_{i-1}}} e^{\frac{(q_{th_{i-1}} - S_{0_{i-1}})}{C_{v_{i-1}}}}}{T_{0_i} e^{\frac{\alpha_i A_i E_i}{C_{v_i}} q_{m_i}} e^{\frac{(q_{th_i} - S_{0_i})}{C_{v_i}}}} - 1 \right)^2 \\
& + \frac{\left(\frac{A_i E_i}{L_i} q_{m_i}\right)^2}{R_{m_i} T_{0_i} e^{\frac{\alpha_i A_i E_i}{C_{v_i}} q_{m_i}} e^{\frac{(q_{th_i} - S_{0_i})}{C_{v_i}}}}
\end{aligned} \tag{58}$$

It can be seen that the mechanical resistive parameter now interferes with the entropy rate of the system according to an irreversible process. By this stage, Eqs. (48), (49), and (58) collectively form the state equations of the reversibly and irreversibly coupled thermoviscoelastic system.

3.5. Thermoelastic interactive modulations

In addition to the energetic connections between the thermal and elastic domains presented via energy ports, there exists information transformation between the non-memory components (resistors) of the system with which modulation of these parameters are possible. In the port-based approach, as long as a parameter of the system does not form the capacity of the system directly or indirectly, the modulation of resistive parameters are permitted. On the basis of this statement, there exist two more possible connections between the mechanical and thermal resistive parameters of the system. The modulation of these two parameters will lead to the deformation-modulated conductivity and temperature-modulated viscoelasticity of the model, which physically extends the capability of the model to a wider range of thermo-mechanical loading. In the following, these modulations will be added to the model.

3.5.1. Deformation-modulated conductivity

From experiment, it is known that mechanical loading can change the conductivity of a system. Considering Eqs. (23) and (33), the resistance of each element is proportional to the length of the element (L). This parameter of the system will vary under mechanical load, leading to the change of the conductivity of the system. To add this interaction to the model, the length of the element should be considered as a variable instead of a constant. As shown in Fig. 9, by replacing the thermal *RS*-component with a deformation-modulated resistivity, *MRS*, the desired connection is generated between the two domains. As can be seen, from the integration of the boundary velocity, the location of each boundary is obtained to generate the instantaneous length of each element. It should be mentioned that the main reason for using boundary velocity to generate each segment's instantaneous length, instead of directly using the deformation of the element, is that in the Maxwell or any other solid models that allow the system to be relaxed, deformation is independent from the variation of length, since there exists an irreversible deformation inside the system.

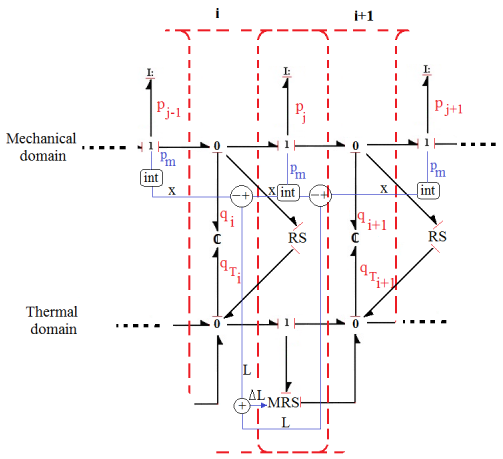

Fig.9 Geometrical connectivity of thermal and elastic domain

Considering the above explanations, the deformation-modulated thermal resistance can be obtained as:

$$ML_i = x_{0_j} + \int \frac{p_{m_j}}{I_{m_j}} dt - x_{0_{j-1}} - \int \frac{p_{m_{j-1}}}{I_{m_{j-1}}} dt \tag{59}$$

where x_0 is the initial location of each boundary (node) in the global axis. By replacing the elemental length with the Modulated length in Eq. (53), the deformation-modulated conductive resistance can be obtained as:

$$MR_{th_j} = \frac{1}{2}\left(\frac{ML_i T_{0_i} e^{\frac{\alpha_i A_i E_i}{C_{vi}} q_{m_i}} e^{\frac{\left(q_{th_i} - S_{0_i}\right)}{C_{vi}}}}{k_i A_i} + \frac{ML_{i+1} T_{0_{i+1}} e^{\frac{\alpha_{i+1} A_{i+1} E_{i+1}}{C_{vi+1}} q_{m_{i+1}}} e^{\frac{\left(q_{th_{i+1}} - S_{0_{i+1}}\right)}{C_{vi+1}}}}{k_{i+1} A_{i+1}}\right) \tag{60}$$

3.5.2. Thermal-modulated mechanical resistivity

It is frequently observed that heating most material changes the viscoelastic behavior of the system by changing its viscosity-related parameters. Considering the Maxwell model used to generate the material model in this study, the parameter to be modulated is the resistive parameter R_m. Accordingly, as shown in Fig. 10, the mechanical *RS*-components are replaced with the *MRS*-components in the model, and the corresponding signal ports are added to the model.

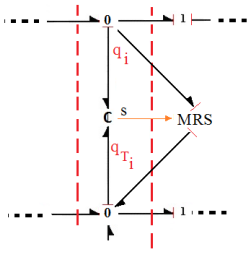

Fig.10 Temperature dependency of mechanical resistors

The modulated elastic resistance can then be presented as:

$$MR_{m_i} = R_{m_{0_i}} - B_i T_{0_i}\left(e^{\frac{\alpha_i A_i E_i}{C_{v_i}} q_{m_i}} e^{\frac{(q_{th_i} - S_{0_i})}{C_{v_i}}} - 1\right) \tag{61}$$

where R_{m_0} is the related viscosity parameter at the room temperature and B_i is the correlative parameter. Accordingly, Eqs. (49) and (58) are changed to:

$$\dot{q}_{m_i} = \frac{p_{m_{j-1}}}{I_{m_{j-1}}} - \frac{p_{m_j}}{I_{m_j}} - \frac{A_i E_i q_{m_i}}{MR_{m_i} L_i} \tag{62}$$

$$\begin{aligned}\dot{q}_{th_i} = {} & \frac{1}{MR_{th_{j-1}}}\left(T_{0_{i-1}} e^{\frac{\alpha_{i-1} A_{i-1} E_{i-1}}{C_{v_{i-1}}} q_{m_{i-1}}} e^{\frac{(q_{th_{i-1}} - S_{0_{i-1}})}{C_{v_{i-1}}}} - T_{0_i} e^{\frac{\alpha_i A_i E_i}{C_{v_i}} q_{m_i}} e^{\frac{(q_{th_i} - S_{0_i})}{C_{v_i}}}\right) \\ & - \frac{1}{MR_{th_j}}\left(T_{0_i} e^{\frac{\alpha_i A_i E_i}{C_{v_i}} q_{m_i}} e^{\frac{(q_{th_i} - S_{0_i})}{C_{v_i}}} - T_{0_{i+1}} e^{\frac{\alpha_{i+1} A_i + 1 E_{i+1}}{C_{v_{i+1}}} q_{m_{i+1}}} e^{\frac{(q_{th_{i+1}} - S_{0_{i+1}})}{C_{v_{i+1}}}}\right) \\ & + \frac{T_{0_i} e^{\frac{\alpha_i A_i E_i}{C_{v_i}} q_{m_i}} e^{\frac{(q_{th_i} - S_{0_i})}{C_{v_i}}}}{MR_{th_{j-1}}}\left(\frac{T_{0_{i-1}} e^{\frac{\alpha_{i-1} A_{i-1} E_{i-1}}{C_{v_{i-1}}} q_{m_{i-1}}} e^{\frac{(q_{th_{i-1}} - S_{0_{i-1}})}{C_{v_{i-1}}}}}{T_{0_i} e^{\frac{\alpha_i A_i E_i}{C_{v_i}} q_{m_i}} e^{\frac{(q_{th_i} - S_{0_i})}{C_{v_i}}}} - 1\right)^2 \\ & + \frac{\left(\frac{A_i E_i}{L_i} q_{m_i}\right)^2}{MR_{m_i} T_{0_i} e^{\frac{\alpha_i A_i E_i}{C_{v_i}} q_{m_i}} e^{\frac{(q_{th_i} - S_{0_i})}{C_{v_i}}}}\end{aligned} \tag{63}$$

It should be mentioned that since the aim of this study is to generate the physical framework for possible connections between different physical domains, a simple linear functionality between the mechanical resistance and temperature is assumed. Using more complicated relativity is out of the scope of this study.

3.6. Proposed thermoviscoelastic model

Incorporating the proposed reversible and irreversible interactions with the presented modulations, a domain-independent thermoviscoelastic model that can reveal the interactive behaviors of the system is proposed. The collective BG representation of the proposed coupled

model is shown in Fig. 11 where a unique framework that reveals the physical insight of the power distribution of the system is provided.

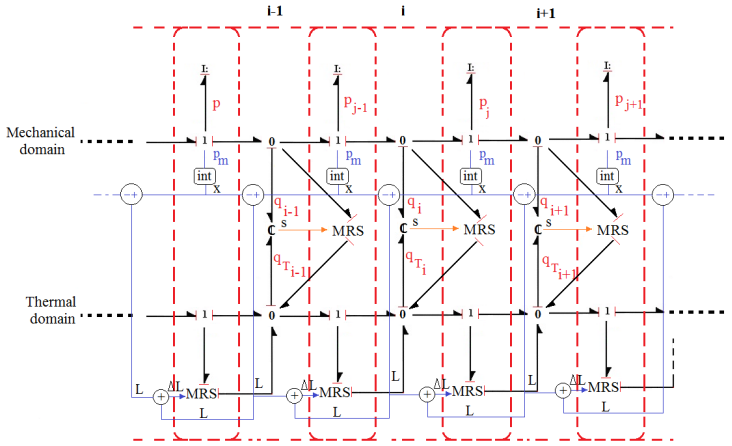

Fig.11 Thermoviscoelastic BG model

$$\dot{p}_{m_j} = A_i E_i \frac{q_{m_i}}{L_i} - A_{i+1} E_{i+1} \frac{q_{m_{i+1}}}{L_{i+1}} + \alpha_i A_i E_i T_{0_i} \left(e^{\frac{\alpha_i A_i E_i}{C_{vi}} q_{m_i}} e^{\frac{(q_{th_i} - S_{0_i})}{C_{vi}}} - 1 \right) - \alpha_{i+1} A_{i+1} E_{i+1} T_{0_{i+1}} \left(e^{\frac{\alpha_{i+1} A_{i+1} E_{i+1}}{C_{vi+1}} q_{m_{i+1}}} e^{\frac{(q_{th_{i+1}} - S_{0_{i+1}})}{C_{vi+1}}} - 1 \right) \tag{64}$$

$$\dot{q}_{m_i} = \frac{p_{m_{j-1}}}{I_{m_{j-1}}} - \frac{p_{m_j}}{I_{m_j}} - \frac{A_i E_i q_{m_i}}{MR_{m_i} L_i} \tag{65}$$

$$\dot{q}_{th_i} = \frac{1}{MR_{th_{j-1}}} \left(T_{0_{i-1}} e^{\frac{\alpha_{i-1} A_{i-1} E_{i-1}}{C_{vi-1}} q_{m_{i-1}}} e^{\frac{(q_{th_{i-1}} - S_{0_{i-1}})}{C_{vi-1}}} - T_{0_i} e^{\frac{\alpha_i A_i E_i}{C_{vi}} q_{m_i}} e^{\frac{(q_{th_i} - S_{0_i})}{C_{vi}}} \right) - \frac{1}{MR_{th_j}} \left(T_{0_i} e^{\frac{\alpha_i A_i E_i}{C_{vi}} q_{m_i}} e^{\frac{(q_{th_i} - S_{0_i})}{C_{vi}}} - T_{0_{i+1}} e^{\frac{\alpha_{i+1} A_{i+1} E_{i+1}}{C_{vi+1}} q_{m_{i+1}}} e^{\frac{(q_{th_{i+1}} - S_{0_{i+1}})}{C_{vi+1}}} \right) + \frac{T_{0_i} e^{\frac{\alpha_i A_i E_i}{C_{vi}} q_{m_i}} e^{\frac{(q_{th_i} - S_{0_i})}{C_{vi}}}}{MR_{th_{j-1}}} \left(\frac{T_{0_{i-1}} e^{\frac{\alpha_{i-1} A_{i-1} E_{i-1}}{C_{vi-1}} q_{m_{i-1}}} e^{\frac{(q_{th_{i-1}} - S_{0_{i-1}})}{C_{vi-1}}}}{T_{0_i} e^{\frac{\alpha_i A_i E_i}{C_{vi}} q_{m_i}} e^{\frac{(q_{th_i} - S_{0_i})}{C_{vi}}}} - 1 \right)^2 + \frac{\left(\frac{A_i E_i}{L_i} q_{m_i} \right)^2}{MR_{m_i} T_{0_i} e^{\frac{\alpha_i A_i E_i}{C_{vi}} q_{m_i}} e^{\frac{(q_{th_i} - S_{0_i})}{C_{vi}}}} \tag{66}$$

Eqs. (64)-(66) form the final set of governing equations sufficient for describing the ongoing thermoviscoelastic phenomena of the system on the basis of energy conservation of the system. As revealed in Eq. (64), the momentum rate of each boundary of the segment now reversibly (via q_{th}) depends on the temperature of the adjacent elements. Also, according to Eq. (65), the deformation rate of each element is now irreversibly (via MR_m) dependent on the element

temperature. Similar to the elastic domain, Eq. (66) reveals that the entropy rate of the system is now reversibly (via q_m) and irreversibly (via MR_m and MR_{th}) related to the deformation of the system. The coupled nature of the system is seen to be fully exposed physically.

4. Simulation result

To highlight the capability of the proposed thermoviscoelastic model in capturing the details of the thermomechanical phenomena inside a system, several loading conditions for the presented beam structure in Fig. 12 is considered. Although simple, the chosen structure can mimic many engineering systems in practice.

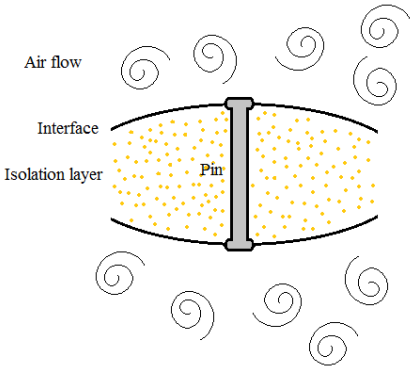

Fig.12 A simplified schematic of a connecting link in supersonic structures subjected to aero-thermo load

To define the system under investigation, a fully-isolated beam is considered with the top and bottom ends being the boundary of the system where the axial aero-thermo load can be applied. To define the initial condition, a stress-free beam resting at the room temperature is considered. Avoiding complexity, the beam structure is reticulated into 10 uniform elements with the characteristics listed in Table 1, and the axial thermoelastic behavior is to be investigated.

Table 1. Geometrical and material parameters of the considered beam

Symbol	Description (unit)	Value	Symbol	Description (unit)	Value
$\boldsymbol{k}$	Conduction coefficient $(J/m.K)$	$2.73e^{2}$	m	Beam mass (Kg)	$5.67e^{-2}$
$\boldsymbol{E}$	Young modulus (N/m^2)	$6.9e^{10}$	A	Cross section area (m^2)	$1e^{-4}$
$\boldsymbol{C_v}$	Specific heat $(J/Kg.K)$	$8.97e^{2}$	l	Length (m)	$2.1e^{-1}$
$\boldsymbol{\alpha}$	Linear expansion $(1/K)$	$2.22e^{-5}$	M	Molar mass (kg/mol)	$2.698e^{-2}$
$\boldsymbol{S_0}$	Reference Entropy $(J/Kg.K)$	$2.83e^{1}$	n	Number of segments	10

Sequentially, the impact of a mechanical cyclic load on the thermal behavior and the impact of a thermal load on the mechanical behavior of the system are presented in Figs. 13-15 where the reversible dynamic interaction of the system between the thermal and elastic domains is demonstrated. In Fig. 16 the irreversible energy transaction between the two domains is presented highlighting the role of the *RS*- components. To reveal the modulation impact on the energetic transaction of the system, the behavior of the system is finally presented in Figs.17-18.

4.1. Reversible energetic transactions

To investigate the role of the embedded domain-independent reversible coupling in the energetic transaction between the thermal and elastic domains, the deformation source presented in Fig. 13 (a) is chosen to be applied to both boundary elements of the elastic domain symmetrically, while the thermal domain is considered fully isolated. The resultant mechanical behavior of the beam is presented in Fig. 13 (b). The stress relaxation of the system and the hysteresis loss presented in this graph demonstrate a good agreement with the natural mechanical behavior of an anelastic system. Fig. 13 (c) and (d) present the corresponding thermal behavior of the system. As can be seen, similar fluctuations can be tractable in the thermal domain, which reflects the role of the considered multiple storage in the model. The initial fluctuations in Fig. 13 (c) shows the reflection of the relaxation behavior of the system in the thermal domain. This behavior can be explained with respect to the considered dispersive solid body of the model. In the chosen Maxwell body used in the model, dissipation is accompanied with releasing the state variable of the potential subdomain (q_m). Considering the logarithmic term associated with q_m in the constitutive equation of the thermal domain of the coupled field, the obtained fluctuation of the thermal domain's potential (effort) is anticipated. The energetic behavior in Fig. 13 (d) indicates that the dynamic fluctuation in the thermal domain is non-entropic and reversible. Considering the fully-isolated beam, this fluctuation will not generate heat inside the system. Thus, the considered coupling is reversible.

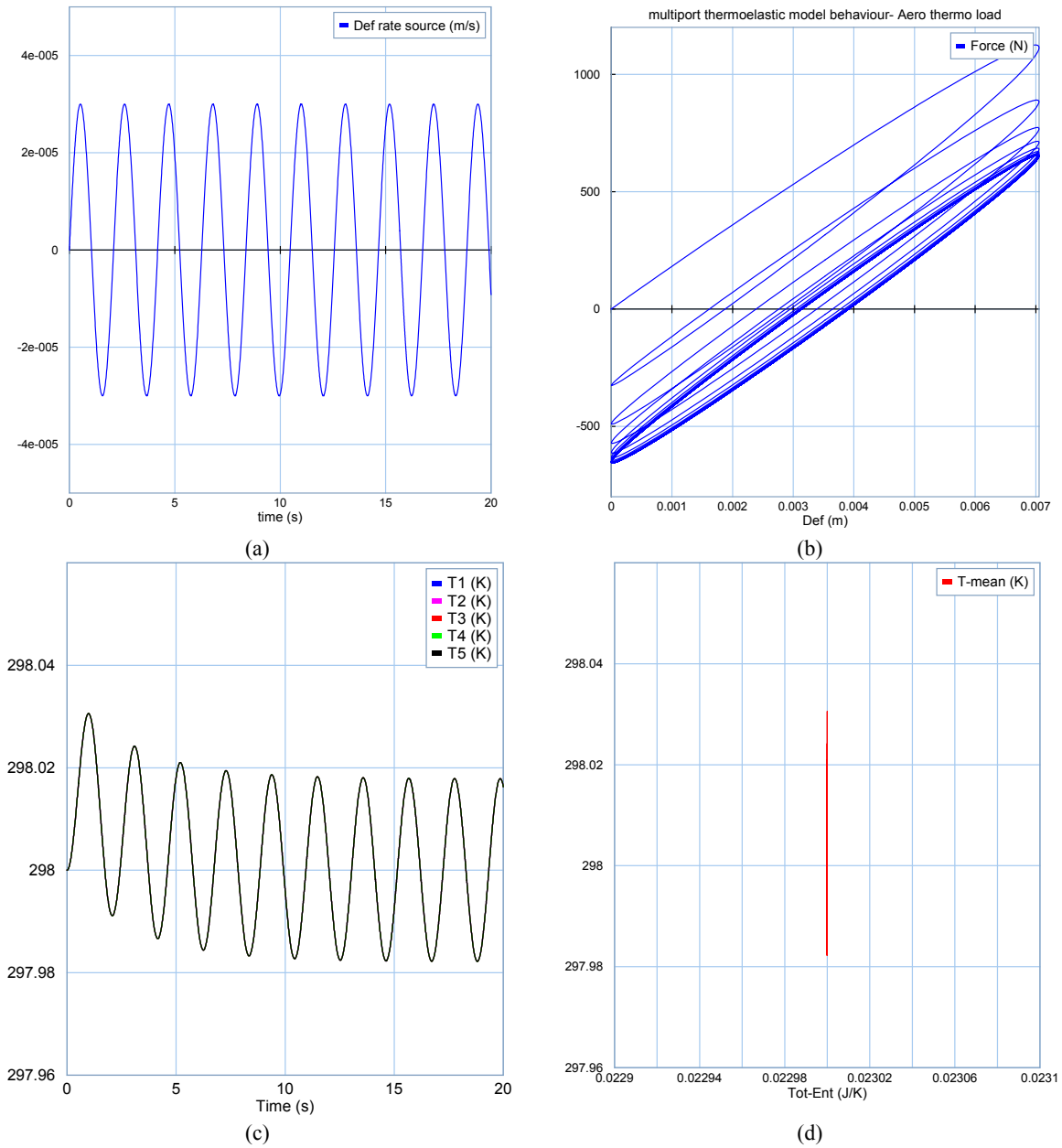

Fig.13 Mechanical vibration impacts on thermal domain dynamics

The thermoelastic loading is simulated for the chosen system to investigate the impact of the thermal domain dynamics on the elastic domain. To this aim, mimicking the heating process of a fixed-end beam, the entropy flow source shown in Fig. 14 (a) is considered for the thermal domain together with a zero deformation rate for the elastic domain. The considered thermal source, in principal, mimics a cyclic heating process of the system, and is applied to the top and bottom ends of the beam symmetrically while the side surfaces of the beam remain isolated. As a result, the temperature of each segment rises one by one as shown in Fig. 14 (b). As can be seen, for the

closer segments to the boundary, more thermal fluctuations are observed, which highlights the slow dynamics of the thermal domain. Fig. 14 (c) and (d) present the energetic behavior of the thermal domain, which indicates the accumulation of entropy that heats the system during this process as naturally anticipated.

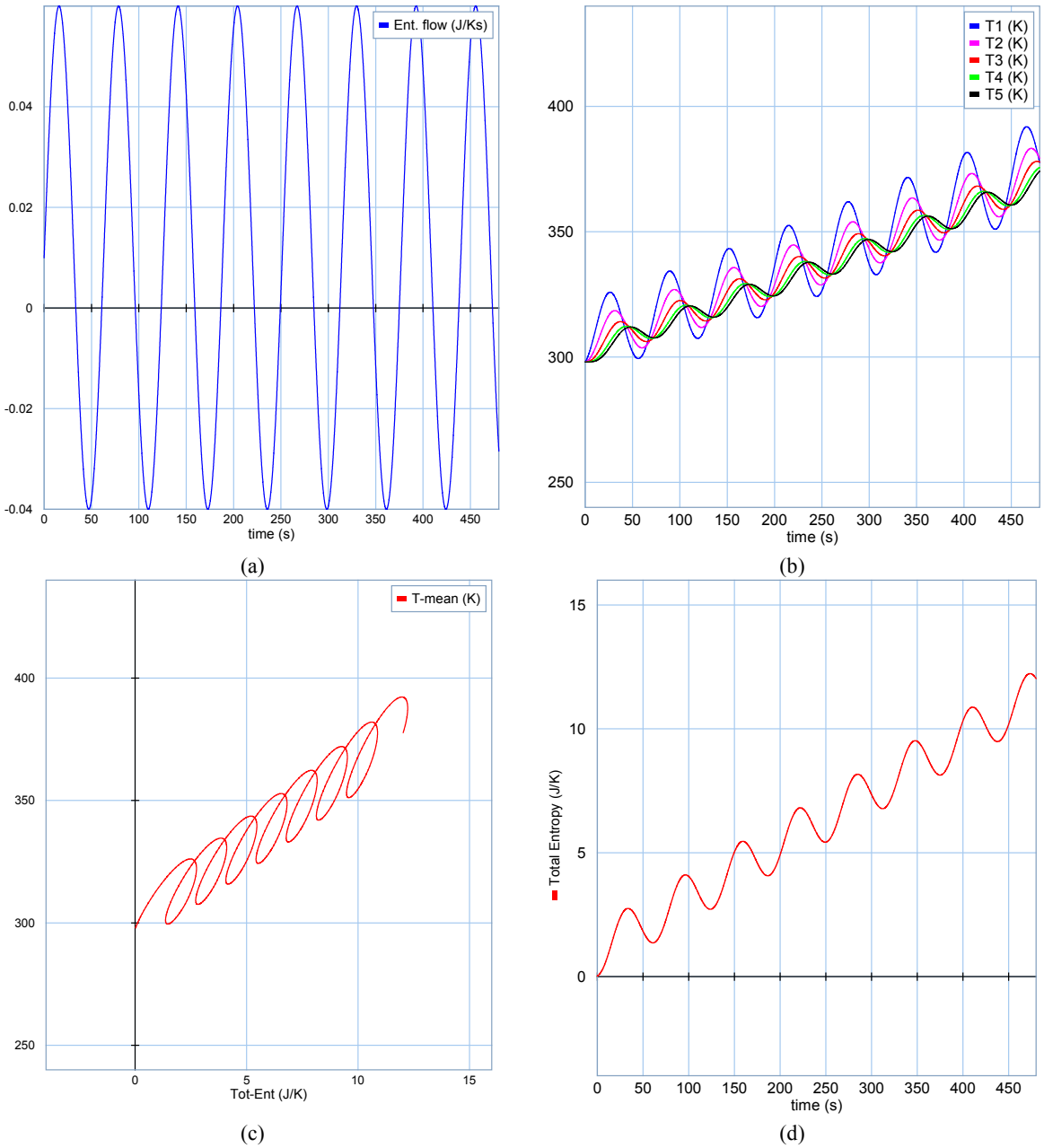

Fig.14 Thermal domain response to cyclic heating

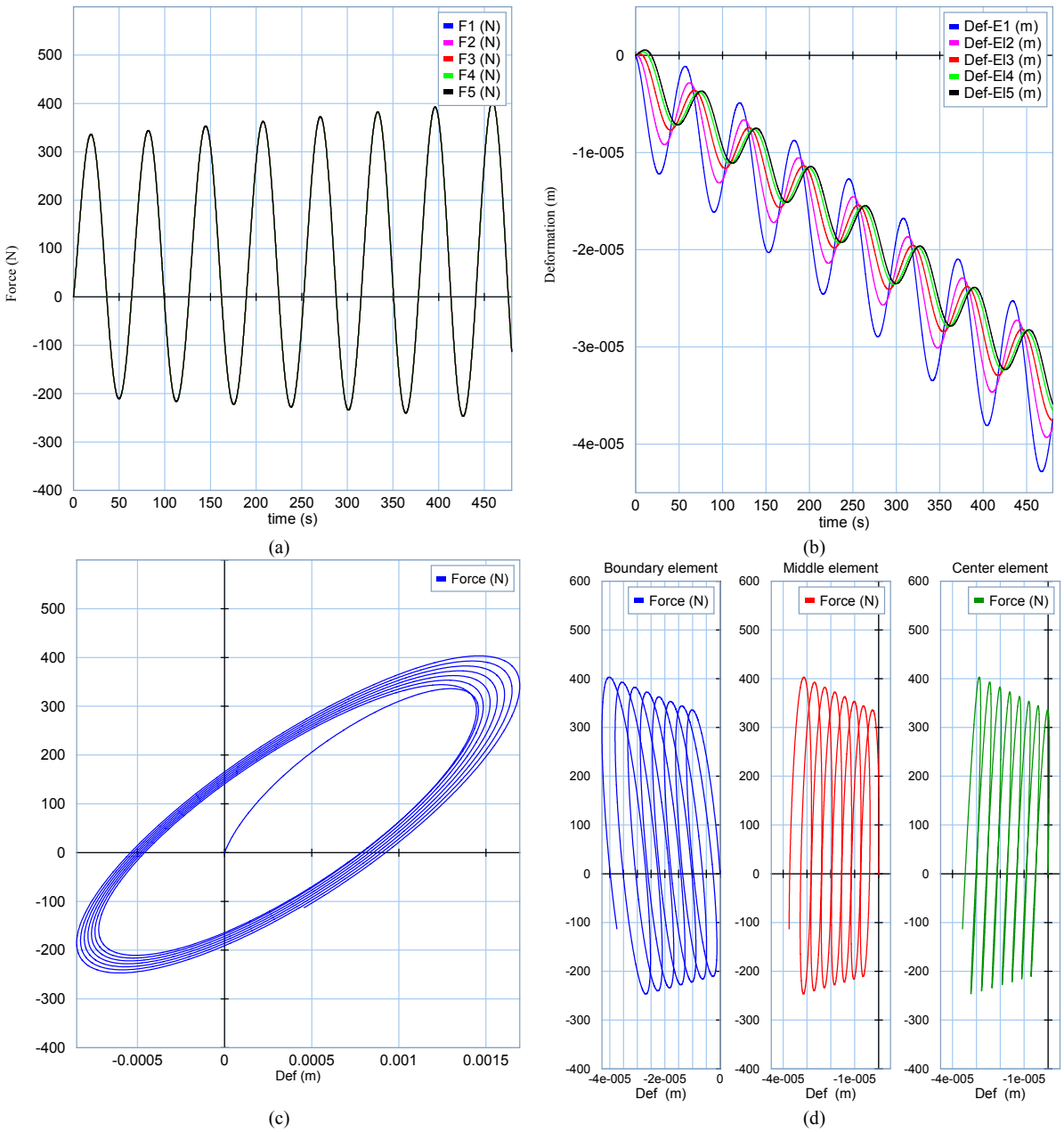

Fig.15 Thermal domain impacts on elastic domain behavior

In Fig. 15, the corresponding dynamic behavior of the elastic domain is presented. Fig. 15 (a) shows the internal force fluctuation of each segment. As the beam is considered fixed from both ends, heating the system will lead to generating internal thermal reaction force between the elements. In an isolated system, this internal force follows the similar patter as the temperature behavior. As can be seen, the internal force has a slight rising pattern as the time goes by. The reason for this behavior is found from the natural expansion of the system. Accordingly, if the mechanical boundary of the system were free to move, the expansion shown in Fig. 15 (b) would

be delivered by the system. However, in a fixed boundary situation, the deformation does not occur inside the system as a result of rising the generated thermal reaction force introduced to the system by the boundaries. The parameters shown in Fig. 15 (b) in principal are the extensive state of the elastic domain with which the potential energy (elastic energy shown in Fig. 15 (c)) can be saved inside the system in the form of tension or contraction. Considering the contraction as positive quantity in Fig. 15 (b), at the early period of the haeting process, the graph clearly indicates that the central elements of the beam are under contraction while the other elements have already under tension.

In Fig. 15 (c), the total energetic behavior of the elastic domain is presented. The expanding pattern of the graph clearly shows the process of rising the potential energy level of the system during the expansion process. Considering the behavior presented in Fig. 15 (b), one can anticipate that the total energetic behavior of the elastic domain is in fact the combination of several energetic behaviors of different segments as shown in Fig. 15 (d). Having the capability of decomposing the observable behavior of the system into its constructive elements can be a desirable tool in managing the energy of the system. For instance, in the case of controlled structures (e.g., deformation controlled), this capability can help to define more intelligent and energy efficient control strategies for the system.

In general, as claimed in this study, the core behavior of the system is developed on the basis of the reversible energetic interactions of the storage components of different subdomains of the system.

4.2. Irreversible energetic transactions

To add the irreversibility impact on the general behavior of the system, the irreversible energy transaction between the two domains is investigated. To this aim, the boundary condition assigned to the system is a cyclic mechanical deformation rate with a magnitude of 30 μm and frequency of 0.5 Hz for the elastic domain, and a zero entropy rate for the thermal domain. The considered boundary condition mimics the vibration in a fully-isolated beam. Fig. 16 (a) presents the energy dissipation pattern of the elastic domain. At the early period of the simulation time, the difference between the dissipated power during the contraction and tension of the system is observed. As can be seen, for this period, the total resultant dissipated power contracting the system is more than

that expanding it; however, by continuing the process these two amounts become equal. This phenomenon, in fact, can be interpreted as the reflection of the stress relaxation of the system on the basis of the considered dispersive mechanism. It is known from experiment that the obtained data after certain oscillation of the structure under cyclic lodging are valid to present the behavior of the system, and the calculation of the initial time has always been an issue. Thanks to the BG energetic presentation of the system with which a physical base is introduced to this problem that may be helpful for calculating this initial time. Accordingly, the initial time for data gathering can be considered as the moment after the period taken for the dissipated energies in tension and contraction becoming equal.

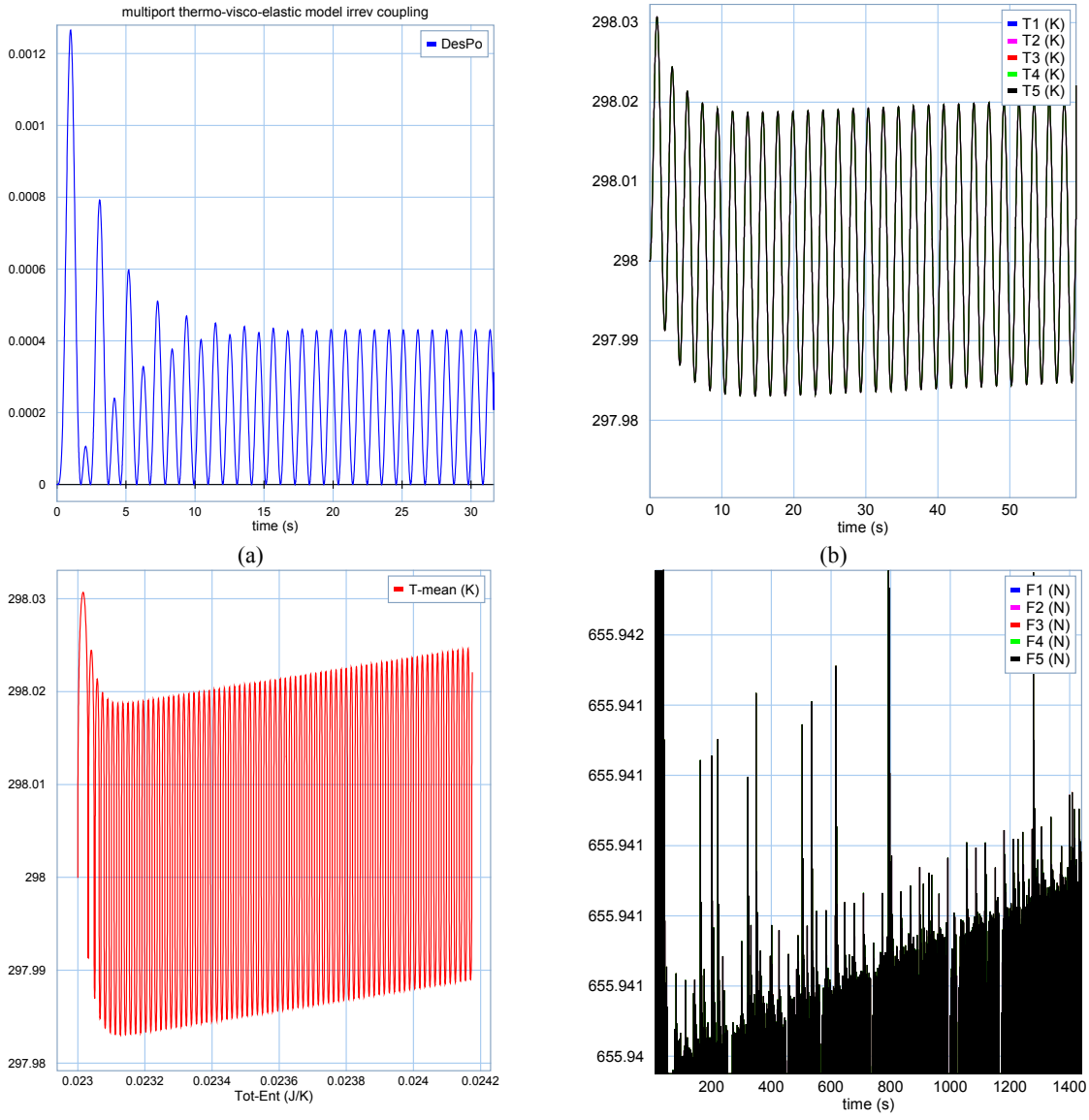

Fig.16 Irreversible energetic interaction in thermo-mechanical phenomena

As mentioned earlier, the general sink for the dissipated energies of other domains is the thermal domain. Considering the isolated system under investigation, the dissipated power shown in Fig. 16 (a) will be transferred to the thermal domain, leading to the rise in temperature of the system as shown in Fig. 16 (b) and (c). The comparison between the temperature fluctuation shown in Fig.13 (c) and the reversible coupling thermal behavior of Fig.13 (d) reveals the role of the irreversible transferred power in increasing the entropy of an isolated system. Increasing the entropy level and, thus, the temperature of the system in a long run will result in generating a thermal reaction force (thermal stress) inside the system as shown in Fig.13 (d). Neglecting this phenomenon may cause some unpredicted behavior of the system. The obtained results indicate the capability of the proposed model in presenting the dynamics of the system at a level in which such intangible dynamics of the system are attainable. This feature of the proposed model makes it suitable for micro-scale multi-physical system dynamic investigations (e.g., the thermo-mechanical phenomenon investigation in MEMS devices).

4.3. Modulation impacts on energetic transaction

To demonstrate the effects of embedded modulations of the proposed model on dynamic behaviors of the chosen beam, the impact of expansion on conductivity is first examined via modulating the geometrical characteristics of the thermal domain. The impact of heating on elastic behaviors of the system is then studied via modulating the material parameters of the chosen beam.

4.3.1. Deformation-modulated thermal domain

Considering the geometrical connectivity of the thermal and elastic domains shown in Fig. 9, the impact of dilation on conductivity is to be discussed. To generate the required deformation, a pulse temperature source shown as T_{in} in Fig. 17 (a) is considered as the top-boundary input to the beam, and a constant temperature source T_{out} is considered as the bottom-boundary input to the beam. For the elastic domain, free-beam condition is created via zero force-source inputs to both boundaries.

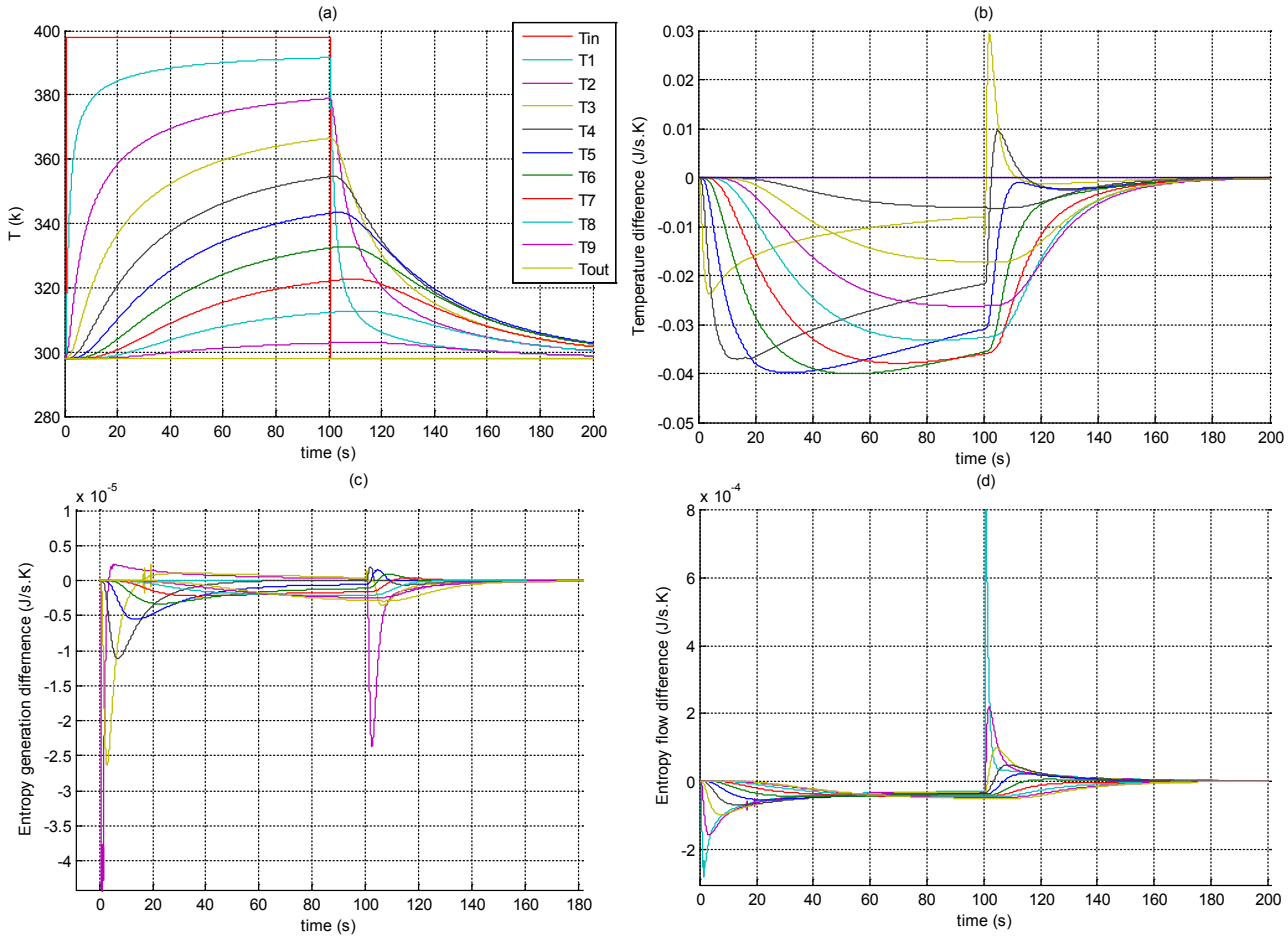

Fig.17 Expansion impact on system conductivity: (a) Element temperature change due to pulse input at left side; (b) Difference in thermal behavior between fixed and expansive geometry situations; (c) Difference in entropy generation; (d) Difference in reversible entropy flow

In Fig. 17 (a) the thermal behavior of the expansive beam is presented. As can be seen, the temperatures of different elements of the beam rise sequentially until the thermal source vanishes whereupon the temperature of the system gradually decreases to the room temperature. To highlight the existing dilative impacts on the conductivity of the system during this process, the difference in dynamic behaviors of the thermal domain between applying the deformation-modulated thermal resistivity and employing the constant thermal resistors are presented in Fig. 17 (b) to (d). In Fig. 17 (b), the negative difference indicates a slight lag in the temperature rise of the expanded elements. Given that the temperature is an equilibrium-determinant variable dependent on the extensive variable of the element, this behavior indicates that the amount of the accumulated entropy of the element during the expansion process in the case of employing the expansive thermal elements is relatively lower than that of employing the non-expansive thermal elements. The negative differences of the provided reversible and irreversible entropy flows,

shown respectively in Fig. 17 (c) and Fig. 17 (d), can explain this shortage of the accumulated entropy. A rational reason for justifying this change in entropy flow of the system can be obtained from Eqs. (20) and (33) which denote an inverse relativity of entropy flow with the expansive element's growing resistivity. Since the expansion of the elements increases the resistivity of the corresponding junctions, and also the resistivity of the system determines the magnitude of the transferred entropy flow of the thermal domain, the process of expansion can cause a slight lag in the dynamics of the thermal domain as presented in Fig. 17 (b).

The above simulation results indicate that, although the selected connectivity between the thermal and elastic domains is weak, the dilation of the system can change the conductive behavior of the system in a tractable level. In general industrial applications, this level of impacts may be negligible. However, in high-tech applications, such as in aerospace controlled structures or MEMS systems where critical and stringent temperature-control performances are required, this level of interactions must be considered.

4.3.2. Temperature-modulated elastic domain

To investigate the temperature dependency of the viscosity of the selected material on the general dynamics of the system, the behavior of the chosen beam will be compared before and after heating. To this aim, a similar vibrational source as that shown in Fig. 13 (a) is applied to the both ends of the beam symmetrically. In addition, the viscosity parameter of the system is reduced to magnify the viscoelastic behavior of the system. To generate the heating process, an entropy rate pulse with a magnitude of $0.09\ (J/sK)$ is applied to the system after 30 s for a period of 40 s. For the rest of the simulation, the system is considered isolated from the surrounding. Fig. 18 (a) shows the thermal behavior of the system during this process. As can be seen, the temperature of the system remains constant for 30 s, and then gradually rises till 70 s. By vanishing the thermal source from the system, the side elements release their thermal energy into the center elements. This causes the side and center elements to follow different temperature patterns until the whole system becomes isothermal again. In Fig. 18 (b) the internal force inside the system is presented. Applying heat to the system leads to a sequentially sharp rise and then a smooth drop in the internal force of the system till the end of the heating process. By vanishing the heat source, after a slight rise in the internal force, the system is stabilized at a lower internal force level. To explain this complex behavior, consider the internal force level of the system before heating as the initial level,

and divide the observed force behavior into four stages: first rise, first drop, second rise, and final. The reason for the first rise in the system is similar to what has been explained for the behavior of the system presented in Fig. 15 (c) and (d). In this case, the slow dynamics of the thermal domain (as compared with the elastic domain) leads to a propagation of the thermal reaction force alongside the system before propagating the material characteristic changes. Hence, the added heat to the system is reflected as the addition of the thermal reaction force to the internal force of the system at the beginning. However, by penetrating the thermal dynamics into the central elements, the stored energy of the system is relaxed via reducing the viscosity of each segment with respect to its current temperature. This can justify the behavior of the system during the first drop. The reason for the second rise can be found in the dynamic behavior of the thermal domain after vanishing the heat source. As shown in Fig. 18 (a), after the 70^{th} s to reach to the second equilibrium, the elements closer to the boundaries lose temperature, while the central elements become hotter. Considering the amount of temperature fluctuation for each element during this period, it can be obtained that the viscosity of the boundary elements recovers more than that of the central elements. This increases the elasticity of the system and allows the system to be stabilized at the final force level. The resultant dissipated power of the system during this process is presented in Fig. 18 (c) where less energy dissipation is seen for a heated system as the level of the internal force is lower. For a controlled structure, this means that a heated system is more energy efficient than a cold system, thus requiring less energy to maintain the performance of the system.

Fig. 18 (d) presents the general dynamic behavior of the system during the above-described process. The clockwise rotation of the Maxwell hysteresis ellipsoid is vividly demonstrated in this behavior. In the literature, this thermoelastic phenomenon is known as temperature-induced material softening. Occurring this phenomenon inside the structure leads to the change of the system dynamic response upon which control strategies for the system can be designed. Unlike the conventional methods in which the system observable behavior is regenerated via fitted parameters, the thermoelastic phenomenon captured here in this study is a result of the energetic interactions of the involving subdomains. It is evident that using the physical approach proposed in this paper, any changes in the complex dynamics of a system will become tractable on the basis of the energy transformation between the energetic components of the system. This distinctive feature of the proposed model allows the validity of the model to be extended to a much wider

range within which the physical insight of thermo-mechanical phenomena of the system can be revealed by the model.

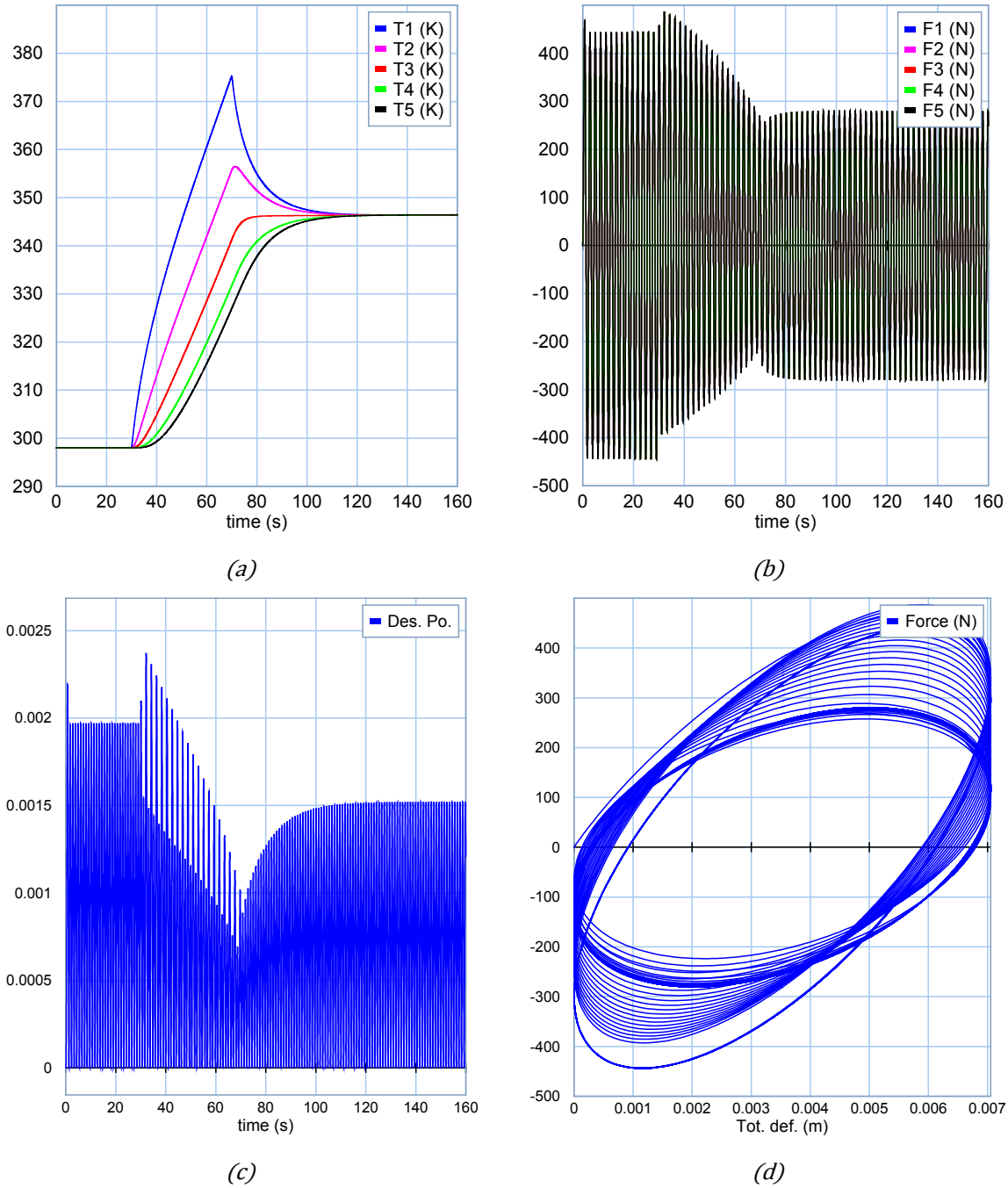

(a) *(b)* *(c)* *(d)*

Fig.18 Temperature dependency of thermo-mechanical behavior-viscosity modulation

5. Conclusion

In this paper, a domain-independent thermoviscoelastic model is developed using the BG

approach. By employing the proposed model, the complex thermo-mechanical behavior of a system can be obtained on the basis of the energetic interactions of the involving physical subdomains. To derive this model, the reversible and irreversible dynamic interactions between the elastic and thermal domains are generated together with the use of inter-domain modulations.

To clarify the impact of the internal energetic interactions on the general behavior of the system, different thermo-mechanical loading conditions are simulated for a chosen discrete structure. The obtained results in general demonstrate a good agreement with the natural behaviors of the system. Several thermo-mechanical phenomena including dilation, thermal stress, relaxation, vibrational heating, and material softening are successfully captured during the simulation. The effect of the deformation of the system on the conductivity of the system is evidently tracked. On the basis of the attained physical insight of the system, it is clear that the changes in the viscosity of the system can be the main cause for the dynamic response changes of the system under temperature fluctuations.

The physically generated thermo-mechanical behavior clarifies that the general behavior of a system is in principal a combined result of different dynamics produced by different elements of the system that can vary dynamically with regard to the location of the external source applied to the system. Constructing the general dynamics of the system from its constructive dynamics with respect to the geometry of the system makes the proposed model suitable for controlled-structure dynamic examinations. The domain-independency of the model will also provide a desirable foundation upon which more complex multi-physical system dynamic investigations can be conducted. The physical nature of the proposed model allows it to become a suitable candidate for use in modeling different-scale dynamic systems including MEM

References

[1] H. karimi, A. Nassirharand, A. Zanj, "Integration of modeling and simulation of warm pressurization and feed systems of liquid propulsion systems," *Acta Astronautica J.,* vol. 69, no. (5-6), p. 258–265, 2011.

[2] J. McNamara, P. Friedmann, "Aeroelastic and Aerothermoelastic Analysisof Hypersonic

Vehicles:Current Status and Future Trends," in *48th AIAA/ASME/ASCE/AHS/ASC Structures, Structural Dynamics, and Materials Conference*, Honolulu, Hawaii, 2013.

[3] E. A. Ivanova, "Derivation of theory of thermoviscoelasticity by means of two-component medium," *Acta Mechanica,* vol. 215, no. 1, pp. 261-286, 2010.

[4] A. D. Freed, A. I. Leonov, "A thermodynamic theory of solid viscoelasticity," NASA Technical Documents, 2002.

[5] E. A. Ivanova, "On one Model of Generalized Continuum and its," in *Mechanics of Generalized Continua*, Berlin Heidelberg, Springer-Verlag, 2011, pp. 151-174.

[6] C. Truesdell, "A first course in rational continuum mechanics," *Pure and Applied mathematics,* vol. 1, pp. 359-364, 1977.

[7] R. M. Christensen, Theory of voscoelasticity, Dover Publications, 2003.

[8] A. M. Freudental, H. Geiringer , The mathematical theories of the inelastic continuum, Berlin, Göttingen, Heidelberg: Springer-Verlag, 1958.

[9] G. E. Mase, Theory and problems of continuum mechanics, McGray-Hill Book Company, 1970.

[10] A. Zanj, F. He, P. C. Breedveld, "Domain Independent Viscoelastic Model: A Bond Graph Approach," *Sound and vibration,* 2016. (Under Revision).

[11] A. Zanj, F. He, "Multi-Physical Domain Variable DOF Modeling: Bond Graph Approach," *Mechatronics, IEEE/ASME Transactions on,* p. (Under review), 2016.

[12] R. R. D.C. Karnopp, System Dynamics: A Unified Approach, Wiley Inter sciences, 1975.

[13] D.C. Karnopp, D.L. Margolis, R.C. Rosenburg, System Dynamics–Modeling and Simulation of Mechatronic Systems, John Wiley & Sons, 2000.

[14] P. Breedveld, Physical System Theory In Therms of Bond graphs, Enschede: Univercity of Twente, 1984.

[15] G. A. Francfort, P. M. Suquet, "Homogenization and mechanical dissipation in thermoviscoelasticity," *Archive for Rational Mechanics and Analysis,* vol. 96, no. 3, pp. 265-293, 1986.

[16] A. Zanj, F. He, "A Thermomechnical Enhanced Elastic Model: Bond Graph Approach," in *23rd International Congress on Sound and Vibration*, Athen, Greece, JUly, 2016.

[17] D. Roylance, "Engineering Viscoelasticity," Massachusetts Institute of Technology, Cambridge, MA 02139, October, 2001.

[18] F. Cellier, Continuous System Modeling, New York: Springer-Verlag, 1991.

[19] A. Zanj, F. He, "Conduction Model Compatible for Multi-Physical Domain Dynamic Investigations: Bond Graph Approach," *World Academy of Science, Engineering and Technology, International Journal of Mechanical, Aerospace, Industrial, Mechatronic and Manufacturing Engineering,* vol. 10, no. 3, pp. 524-535, 2016.

[20] A. Zanj, P. C. Breedveld, F. He, "Domain-independent Thermoelastic Modeling: a Bond Graph Approach," p. (To be published), 216.

[21] Amalendu Mukherjee, Arun Kumar Samantaray, Bond Graph In Modeling, Simulation And Fault Identification, I. K. International Pvt Ltd, 2006.

[22] J. U. Thoma, Simulation by Bondgraph, springer, 1990.

[23] J. Amerongen, E. Coelingh , T. Vries , "Computer support for mechatronic control system design," *Robotics and Autonomous System,* vol. 30, 2000.

[24] J. J. Granda, The role of bond graph modeling and simulation in mechatronics systems, . An integrated software tool: CAMP-G, MATLAB-SIMULINK, Mechatronics, 2002.

[25] A. Zanj, F. He, "A Thermomechnical Enhanced Elastic Model: Bond Graph Approach," in *23rd International Congress on Sound and Vibration*, Athens, Greece, July, 2016.

CHAPTER 6: ENERGY-BASED MODELING OF THE FLUID FIELD

Aim

The aim of this chapter is to develop an energy-based model of the fluid field compatible with that of the solid field using the BG methodology.

Description

To achieve this aim, first, a new decomposition of the fluid field is developed with respect to the conservation equations. Next, by defining a set of multi-dimensional energetic components, possible reversible and irreversible connections between the subdomains of the fluid field are clarified, with which distinctive energy transformation between the subdomains as well as energy transportation within the fluid field become identifiable. Finally, an energetic network of the fluid field compatible with that of the solid field is achieved, which demonstrates the power transactions within the fluid field in a conservative manner. The content of this chapter is organized as follows:

Results

The generated fluid-field model is capable of presenting the complex behavior of the system attached to the system energetic memory. This capability can result in generating the behavior of the system from its physical constructive elements, thus providing a physical insight into the ongoing phenomena of the system. The presented results for the considered examples confirm this capability of the proposed model.

Conclusion

An energy-based compressible conductive model of the fluid field with identical decomposition to the solid field is generated, in which the general dynamics of the fluid field are presented in the form of a set of distinguishable and meaningful relations between the reversible and irreversible interactions of the energy components of the existing subdomains of the fluid field.

ENERGY-BASED COMPRESSIBLE CONVECTIVE MODEL PROPER FOR AEROTHERMOELASTIC DYNAMIC INVESTIGATION: A BOND GRAPH APPROACH ON FSI PROBLEMS

A. Zanj[1]*, F. He[2], P. C. Breedveld[3]

Abstract

In this study, attempt is made to relate the dynamics of a compressible convective fluid to the energetic interactions between the existing physical subdomains of the field. Accordingly, the general dynamics of the system are presented in the form of a set of distinguishable and meaningful relations between the reversible and irreversible interactions of the energy components of the subdomains. To this aim, the energetic decomposition of the fluid field is first developed from conservation equations. By defining multi-dimensional energetic components, possible reversible and irreversible connections between the subdomains are then clarified with which distinctive energy transformation between the subdomains and energy transportation within the fluid field become identifiable. Finally, the general energetic network of the system is achieved, which demonstrates the power transactions within the system in a conservative manner. The model thus generated is capable of presenting the complex behavior of the system attached to the system energetic memory. This capability can result in generating the behavior of the system from its physical constructive elements, thus providing a physical insight into the ongoing phenomena of the system. The presented results for the considered examples confirm this capability of the proposed model.

Keyword: Energy-based modeling, Compressible flow, Multiple-field dynamic modeling, Heat and mass transfer, Irreversible thermodynamic, Aerothermodynamics.

1. Introduction

One of the key issues in modeling fluid dynamic systems with viscous, compressible, and thermal effects is the competent modeling of the transformation of mechanical to thermal energy and its irreversibility [1]. Considering the fluid field as a multi-physical system containing thermal, kinetic, and potential subdomains, the right understanding of the internal energetic transactions is

[1] Research assistant in Advanced Control System Research group, School of Computer Science, Engineering & Mathematics, Flinders University, Adelaide, Australia, email: amir.zanj@flinders.edu.au
[2] Associate Professor in School of science and engineering, Flinders University, Adelaide, Australia
[3] Associate Professor in robotics and mechatronics group, University of Twente, Enschede, Netherlands

based on the right coupling between the reversible and irreversible dynamics of the involving physical subdomains.

The Navier-Stokes (NS) equations are commonly known as a presentation of conservation equations for the fluid field with the soundest physical basis. Although the combination of mass, momentum, and energy conservation provides a comprehensive representation of the ongoing dynamics of the fluid field, it lacks the provision of individual energetic interactions (i.e., power network) of the system with respect to the physical subdomains present in the model. Although the generated model can represent the combined energetic behavior of the fluid field, it is unable to separate the energetic impacts of each physical subdomain on the general behavior of the fluid field. The latter aspect becomes an essential capability of the model in cases where external physical fields interact with the fluid field, such as in fluid-solid-interaction (FSI) problems where multi-physical subdomains in multiple fields are typically involved. In these complicated cases, a well-posed data transformation between the involving fields can only be obtained if the continuity of the power transformations is satisfied. In order to fulfil the power-continuity requirement, it becomes desirable to present a decomposed interactive power network that can provide separate power transformations between the counterpart physical subdomains of the involving fields. The NS solutions obviously fail in this aspect.

Many attempts for constructing energetically-correct network models for fluid-system dynamics have been reported, with a majority of them being in pseudo Bond graph (BG) terms [2] [3] [4]. Using thermodynamic concepts, these methods provide the energetic network of the system by developing power continuous transformations between the introduced energetic components of the present physical subdomains. Generating the governing equation of the system with respect to the conservative interactions of the implemented components provides a clear map with which the mathematical well-posedness regarding the conservation principles of the generated models can be automatically satisfied. In these models, the reversible energy transformations between the subdomains occur in multi-dimensional capacitors (energy storage components), and the irreversible energy transportations within a field occur in multi-dimensional resistors (energy dissipative components). Although the generated storage components provide a clear view of mechanical to thermal energy transformations, the generally-considered convective variable, enthalpy, can limit the application of these models especially in multiple-field cases such as a FSI

problem where the resistive components are mainly considered as the connective components between the elements of the two fields.

Indeed, enthalpy that has been considered as the state variable of the convective flow in these models is not a physical state variable, rather a combined thermodynamic variable that includes the information relating to different states of the existing physical subdomains. Because of this, although the energy storage in the system is decomposed with respect to the existing physical subdomains, the energy transportation within the field remains combined. Knowing that the decomposition of power transportation is a key requirement for energetically-connecting different subdomains of different fields, the use of a combined transportation variable (enthalpy) undoubtedly limits the application areas of the ensuing models to single-field investigations. Furthermore, as revealed in [5], the use of enthalpy as the transportation variable can lead to the blindness of the models in capturing some ongoing phenomena such as throttling that occurs frequently on an oscillatory interface. It then becomes evident that the existing energy-based decomposed models in the current form are not suitable for multiple-field dynamic investigations.

In the current study, an enhanced convection model with decomposed energy transportation is proposed to generate a proper convective model suitable for FSI problems. In this model, the decomposed power trans*port*ation as well as the decomposed power trans*form*ation can provide a distinctive power distribution of the system with possible power connection gates to other physical subdomains of different fields. To this aim, we propose separate convection of entropy and volume in place of mere enthalpy convection. As a result, even in an isothermal situation the pressure can generate the flow of matter that convects entropy. Furthermore, the added possibility of volume convection at an interface where motion of the attached boundary can occur, will lead to the translation of the Lagrangian coordinate frame's motion into changes expressed in the Eulerian coordinate frame (proposed as the VIDA technique in [6]). Collectively, these added capabilities of the model will make it suitable for multiple-field dynamic investigations.

In order to achieve what has been proposed above, the remainder of this paper is organized as follows. In Section II, the procedure of energetic decomposition of the NS equations is briefly explained, and the multi-dimensional energy components of compressible convective fluid flow are introduced. In Section III, by considering the characteristics of air as an ideal gas, the governing equation of a 1D compressible convective flow for variable geometry is extracted. Section IV

highlights the capability of the generated model in demonstrating the energetic interactions of the system using an example that simulates the convective flow in a 1D flexible duct. The capability of the model in presenting the power-continuous transaction between the elements and components of the fluid filed is then concluded in Section V.

2. Power decomposition of convective field

In this section, using the general power structure of the system obtained from the conservation equations, the energetic components of a convective fluid field are first defined, followed by the definitions of the reversible and irreversible connections between these components. This will lead to the formation of a general energetic network of the system that presents a junction structure of the fluid field with which discretization of simultaneous time and geometry is achievable.

Consider the conservation equations of a single-phase-single-component fluid [7]:

$$\frac{\partial \rho}{\partial t} = -\nabla.(\rho v) \tag{1}$$

$$\rho\frac{\partial v}{\partial t} = -\rho\nabla(\frac{1}{2}v.v) + \rho v \times (\nabla \times v) - \nabla P + \rho G + \nabla.\tau \tag{2}$$

$$\rho\frac{\partial u_V}{\partial t} = -\nabla(u_V v) - \nabla q - P\nabla.v + \nabla v:\tau + \rho\psi \tag{3}$$

where ρ, v, P, G, τ, u_v, q, and ψ are respectively the density, velocity, pressure, body force per unit mass, viscos stress tensor, internal potential energy per unit volume, heat flux, and heat source. A continuous power structure of the system from the existing conservations (mass, momentum, and internal energy) can be defined via the following procedure. Given the intensive form of the total energy as the sum of the internal energy, u_V, and kinetic co-energy per unit volume, k_V,

$$e_V(\rho, v, S_V) = u_V(\rho, S_V) + \frac{1}{2}\rho v^2 \tag{4}$$

the general power balance of the system with respect to the considered intensive states (ρ, v, and S_V denoting density, velocity, and entropy per unit volume, respectively) can be presented as:

$$\frac{de_V}{dt} = \left(\frac{\partial e_V}{\partial \rho}\right)_{v,S_V}\frac{d\rho}{dt} + \left(\frac{\partial e_V}{\partial v}\right)_{\rho,S_V}\frac{dv}{dt} + \left(\frac{\partial e_V}{\partial S_V}\right)_{\rho,v}\frac{dS_V}{dt} \tag{5}$$

Eq. (5) in principal forms the general frame of the power structure within the system. The terms appearing in the right-hand side of Eq. (5) correspond to the power balance equation of the present

physical subdomains (in the form of the product of the conjugate variables of each subdomain). The partial derivatives appearing in each term of the right-hand side of Eq. (5) correspond to the potentials (efforts), and the time derivatives of the independent variables are the flows of the corresponding subdomains.

Using the conservation equations and the following potentials (attainable from Eq. (4)):

$$\mu_V = \left(\frac{\partial e_V}{\partial \rho}\right)_{v,S_V} = \left(\frac{\partial u_V}{\partial \rho}\right)_{S_V} + \frac{1}{2}v^2 = g + k = \frac{1}{\rho}(u_V + P - TS_V) + \frac{1}{2}v^2 \tag{6}$$

$$p_V = \left(\frac{\partial e_V}{\partial v}\right)_{\rho,S_V} = \rho v \tag{7}$$

$$T = \left(\frac{\partial e_V}{\partial S_V}\right)_{\rho,v} = \left(\frac{\partial u_V}{\partial S_V}\right)_{\rho} \tag{8}$$

where μ_V, p_V, and T are the mass potential per unit volume, momentum per unit volume, and temperature, and g and k are the Gibbs free energy and kinetic co-energy per unit mass, the power balance equation of the mass subdomain can be simply obtained from multiplying μ_V by Eq.(1):

$$\underbrace{\mu_V \frac{\partial \rho}{\partial t}}_{power} = \underbrace{-\nabla.(\rho \mu_V v)}_{divergence\ term} + \underbrace{\rho v \nabla g + \rho v \nabla k}_{coupling\ terms} \tag{9}$$

The kinetic subdomain power balance equation can be derived by considering the following relations:

$$\big(v \times (\nabla \times v)\big).v = 0 \tag{10}$$

$$(\nabla.\tau).v = \nabla.(\tau.v) - \nabla v : \tau \tag{11}$$

and making a scalar product of velocity and Eq. (2):

$$\underbrace{p_V \frac{\partial v}{\partial t}}_{power} = \underbrace{\rho v.\nabla k}_{coupling\ term} + \underbrace{\nabla.(\tau.v)}_{divergence\ term} - \underbrace{v.\nabla P}_{coupling\ term} + \underbrace{\rho G v}_{source\ term} + \underbrace{\nabla v : \tau}_{coupling\ term} \tag{12}$$

Finally, the thermal subdomain power balance equation can be obtained via substituting Eqs. (6), (8), and (9), into Eq. (3):

$$\underbrace{T \frac{\partial S_V}{\partial t}}_{power} = \underbrace{-\nabla.(q + TS_V v)}_{divergence\ term} \underbrace{- \rho v.\nabla k - v.\nabla P - \nabla v : \tau}_{coupling\ terms} + \underbrace{\rho \psi}_{source\ term} \tag{13}$$

As can be seen, in the power balance equations (Eqs. (9), (12), and (13)) of the fluid field, three types of terms can be distinguishably identified in the power transportation process: the divergence

terms, the source terms, and the coupling terms, which makes it possible to present the balance equation of each subdomain in a systematic form as:

$$\Phi_i f_i = \sum_{\Omega=1}^{m} \psi_{i,\Omega} + \sum_{\Gamma=1}^{o} \nabla_{i,\Gamma} + \sum_{j=1, j\neq i}^{n} C_{i,j} \tag{14}$$

where $\psi_{i,\Omega}$, $\nabla_{i,\Gamma}$, and $C_{i,j} = -C_{j,i}$ are respectively the body source power that constitutes the different power sources external to the system, the divergence power that takes into account the power introduced to the element through the spatial boundary Γ_{th}, and the coupling power that represents the internal power transformation.

To clarify the existing relations between the various subdomains, the energetically decomposed power structure obtained above is graphically presented for a unit volume in Fig. 1. It is clear that the distinctive feature of the presented power frame is a general energetic network of the system which reveals the inertial, viscous, compressible, and thermal energetic interactions as well as the power dissipation of the generated irreversibility. This capability will help the formation of a correct understanding of the given system.

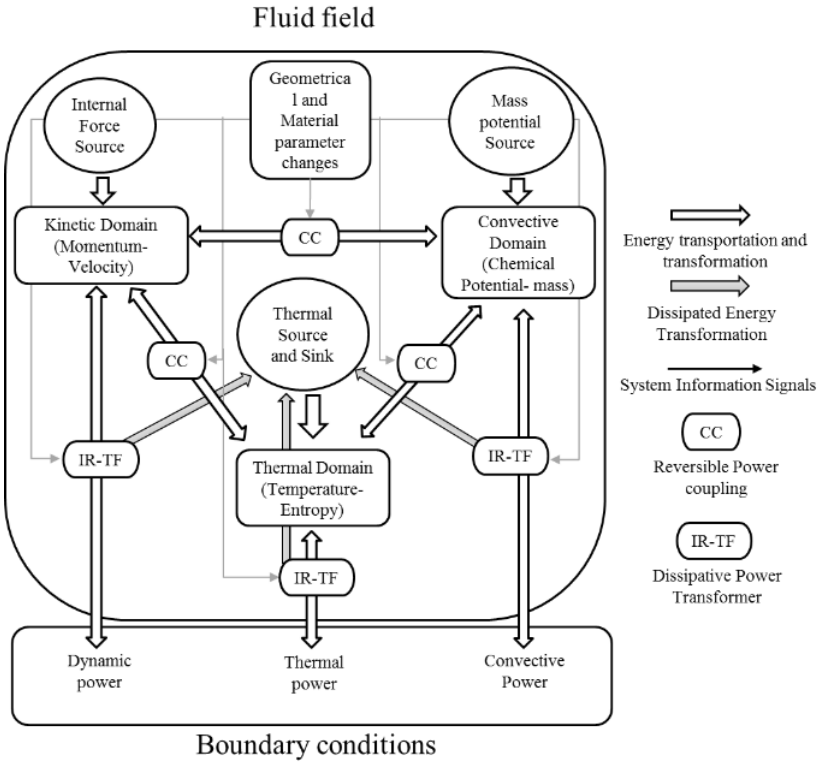

Fig. 1 Graphic Presentation of energetical power decomposition of a unit volume

To generate a mathematically well-posed convective junction structure model from the generated physical insight of the system, the energetic components and their possible interconnections are defined with respect to the existing physical causality of the system. Consider the generalized form of Eq. (5) for *n* number of state variables,

$$\frac{dE}{dt} = \sum_{i=1}^{n} \Phi_i f_i \tag{15}$$

the total power of the system is generated as the sum of the reciprocal potentials $\Phi_i(x_1, \dots, x_n) = \frac{\partial E}{\partial x_i}$ times the time-derivative $f_i = \dot{x}_i$ of the state variables, x_i, where each potential function represents the constitutive equation of each subdomain, and the time-derivative of each state variable forms the collective flow of each unit of the subdomain.

As the energy remains conserved in each unit, the considered potential functions of the system form an *n*-dimensional storage component (capacitor) for the convective field, where the interred power to the unit is saved. The continuous reversible power transformations between the subdomains occur via these energy components. These potentials can be generated with respect to the geometrical P_g and material P_m parameters of the system as a function of the chosen state variables satisfying the Maxwell reciprocity. By means of the energy storage components, the instantaneous magnitude of the state variable is generated via time integration of the collective flow of each subdomain. In doing so, energy storage of the system carries the memory information of the field, with which time marching is achieved for the model. Furthermore, by means of the generated information from the storage components, the potential gradients required to generate the separate flows of the subdomains are provided for the model.

Given that the energy can be irreversibly dissipated while transferring between the capacitors, the resistive components, **R**, of the system can be defined via relating the divergence terms of the adjacent spatial boundaries. This connection can be obtained with respect to the dissipative mechanism of each domain, R_i, and as a function of the instantaneous material and geometrical parameters of the adjacent units. Since these components contain the information relating to the proportionality of the potentials and flows of the system, the geometry marching of the model is attainable via these components.

Finally, to generate the well-posed network structure, connect the energetic components of the model for each of the subdomains. This is done via defining the collective flows from the instantaneous information of the system. Thanks to the well-organized power structure of the system, the collective flows can be systematically obtained via dividing each of the balance equations by the corresponding potentials. The generalized flow equations which in principal are the state of the system can then be energetically decomposed as follows:

$$f_i = \sum_{\Omega=1}^{m} \frac{\psi_{i,\Omega}}{\Phi_i} + \sum_{\Gamma=1}^{o} \frac{\nabla_{i,\Gamma}}{\Phi_i} + \sum_{j=1,j\neq i}^{n} \frac{C_{i,j}}{\Phi_i} \tag{16}$$

By defining the power terms appearing in Eq. (16) with respect to the current information provided by energetic components, the set of governing equations for the convective field will be closed.

The body source power terms can be directly defined from the considered source information. The divergence power term is defined as a function of the potential gradient $\nabla\Phi_i$ provided by capacitor and the dissipative mechanisms, R_i, of the resistors of each subdomain:

$$\nabla_{i,\Gamma} = \mathbb{f}_i(\nabla\Phi_{i_\Gamma}, R_{i_\Gamma}) \tag{17}$$

where Γ_j denote the j_{th} spatial boundary of the considered unit. Given that the coupling terms in the state equations appear as a result of the dependency of the convective state variables [8], the coupling power terms and the divergence power term obtain a proportional relation. As so, considering the power conservation, the coupling power terms for each subdomain can be presented as:

$$C_{i,j} = MTF_{i,j,}\nabla_i \tag{18}$$

where $MTF_{i,j}$ is defined as weighted functions of the state ratio of the connected subdomains (i and j). Accordingly, by defining all the existing terms in Eq. (16), the required collective flow of each subdomain is obtained by means of the existing information of the system. However, to define the collective flow of the thermal subdomain, there exists yet another parameter to be defined: the entropy generation rate of each subdomain.

Given that the transferred energy is dissipated irreversibly while transferring, and knowing that the sink for all forms of dissipated energy is the thermal subdomain, there exists an irreversible power transformation from other subdomains to the thermal subdomain. Accordingly, by

considering a conserved non-return power transformation and the dissipative mechanism of each subdomain, the following irreversible power transformation, ∇^{irr}, is added to the thermal subdomain's divergence power term:

$$\nabla^{irr} = \sum_{i=1}^{n} \sum_{\Gamma=1}^{o} \frac{\nabla \Phi_{\Gamma_i}{}^2}{R_{\Gamma_i}} \tag{19}$$

Accordingly, with the consideration of irreversibility, the collective flow of the thermal subdomain can be presented as:

$$f_s = \sum_{\Omega=1}^{m} \frac{q_\Omega}{T} + \frac{\nabla^{irr}}{T} + \sum_{\Gamma=1}^{o} \frac{\nabla_{s,\Gamma}}{T} + \sum_{j=1, j\neq s}^{n} \frac{c_{s,j}}{T} \tag{20}$$

By generating the handshaking connections between the divergence power terms of each of the subdomains of the neighboring units regarding the corresponding adjacent boundaries, the junction structure of the fluid field shown in Fig. 2 is obtained with which the simultaneous time and geometry discretization is achievable for the system.

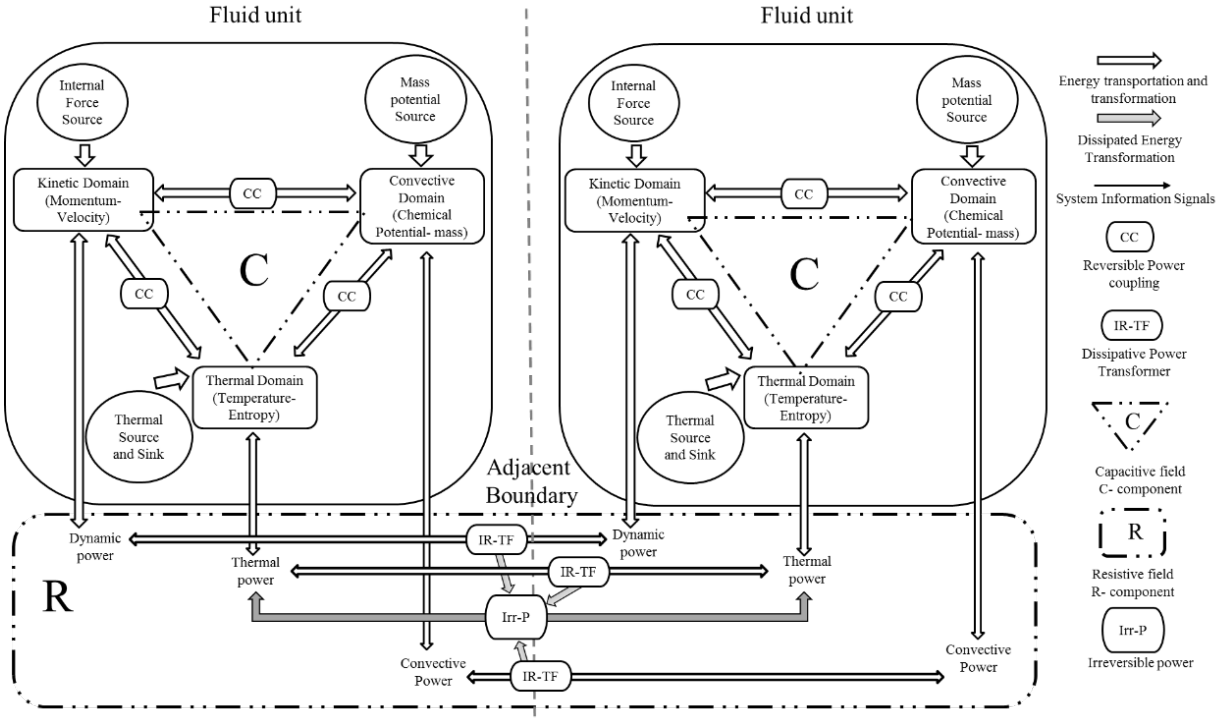

Fig. 2 Convection field decomposed junction structure

As can be seen, in the presented energetic junction structure of the system, the capacitors are located within each unit, while the resistors play the role of the connectors of the energy units that

provide the possibility of handshaking connections between the counterpart subdomains.

The anti-symmetry of the appeared coupling terms in the balance equations reveals that if the total form of energy convection is considered for the system, as in the NS method, then although the general transportation of the energy can be obtained, the internal interactions of the existing subdomains stay unvalued, as via summation of the balance equations to form the total energy balance the coupling terms will be canceled out from the equations. This added capability could be a beneficial advantage in multi-disciplinary system dynamic investigations such as in FSI problems where a clear understanding of different forms of power transmissions between the fields is demanded especially when the impacts of the thermal subdomain becomes significant.

3. Energy-based 1D convective model

In this section, to demonstrate the capability of the proposed method in developing a well-posed model, the governing equations of a 1D compressible convection field are extracted for ideal gas. To this aim, sequentially, the convective field is decomposed with respect to the general physical states, the arrangement of the energetic component is defined for the 1D convective field, the decomposed power structure of the system is presented using the BG notation, the correctness of the generated BG model is checked via causality allocation, the state equations corresponding to the generated BG model is extracted, and finally the potential functions together with the resistive and coupling coefficients are defined.

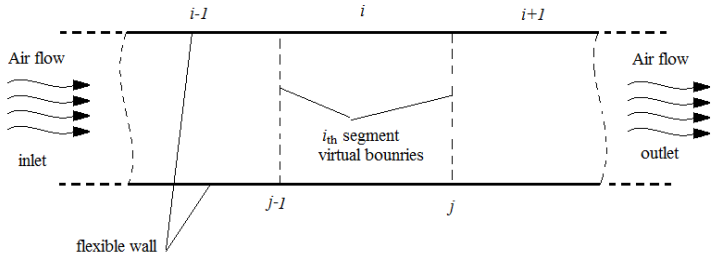

Fig. 3 1D air duct

3.1. Decomposition of the field

Consider the 1D discretized duct with flexible walls shown in Fig. 3 in which compressible air can transfer alongside the duct. Since the attempt in this study is to generate a suitable model for multiple-field dynamic investigations, the domain-independency of the model is of interest [9]. Therefore, the general physical states: mass m, momentum p, entropy S, and volume V are selected

with their corresponding potentials being mass potential μ, velocity v, temperature T, and pressure P. Considering the selected conjugate variables, the fluid field is physically decomposed to mass, kinetic, potential (acoustic), and thermal subdomains.

3.2. Defining the energetic components of the field

Considering the junction structure obtained in Section II, each segment can be considered as the energy storage component (capacitor), and each connecting junction becomes the location for the resistive components of which the parameters are a function of both the material and geometrical parameters of the adjacent segments. Accordingly, the junction structure shown in Fig. 4 can be presented for the physically decomposed system containing four separate energy lines.

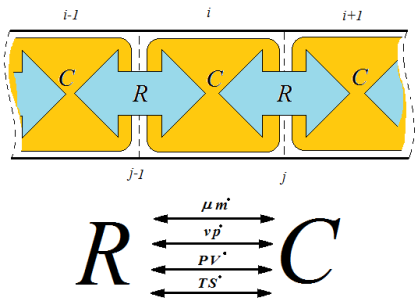

Fig. 4 Decomposed 1D fluid field

3.3. Generating the power structure of the system

As mentioned in Section II, since the reversible connections among the subdomains occur in the capacitors and the irreversible non-return interactions occur in the resistors, the general frame for the power structure of the system can be elegantly depicted in the BG notation as shown in Fig. 5. As can be seen, the total power of the system is decomposed into four separate power lines, each indicating the energy flow of the corresponding subdomain. All the present subdomains are reversibly connected via *C*-components, and the collective flow for each subdomain can be obtained from the corresponding *0*-junctions containing the divergence and coupling power terms provided by *1*-junctions (the boundaries of the segment) and the flow source terms S_{f_i}. The irreversible connections of the subdomains are depicted by *RS*-components that act as non-return power transformers to the thermal subdomain. The coupling transformers (MTF_{i-j} and MGY_{i-j}) of the energy transportation in *1*-junctions provide the required convective information of each

subdomain with respect to the natural dependency of the considered physical states of the system.

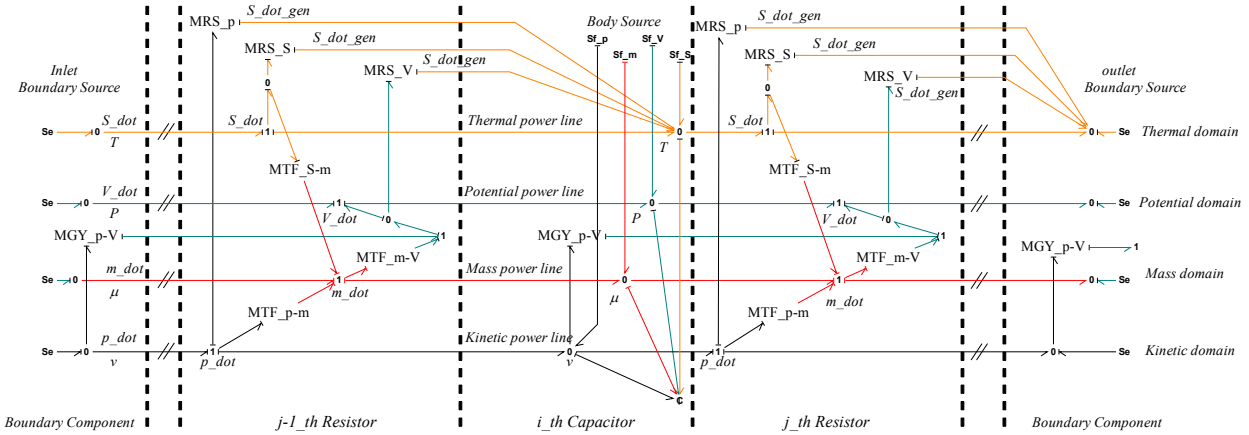

Fig. 5 BG presentation of the general power structure of the fluid field

The arrangement of the causality lines, provided by the global conservation laws, confirms the correctness of the proposed power structure. Thus, the well-posedness of the generated state equations from the obtained model is granted.

3.4. Extracting the state equations

Given that the collective flow of each subdomain is the state equation of the subdomain, a set of state equations corresponding to the generated power structure shown in Fig. 5 for the i_{th} segment can be presented as:

$$\dot{m}_i = \dot{m}_{j-1} - \dot{m}_j + S_{f_{m_i}} \tag{21}$$

$$\dot{p}_i = \dot{p}_{j-1} - \dot{p}_j + S_{f_{p_i}} \tag{22}$$

$$- M_{GY_{p-V}{}_i}\left(\frac{1}{M_{TF_{m-V}{}_j}}\left(\mu_i - \mu_{i+1} + M_{TF_{S-m}{}_j}(T_i - T_{i+1})\right.\right.$$

$$\left.\left. + M_{TF_{p-m}{}_j}\left(v_i - v_{i+1} - R_{p_j}\frac{M_{TF_{p-m}{}_j}}{M_{TF_{m-V}{}_j}}\frac{1}{M_{GY_{p-V}{}_i}}v_i\right)\right) - (P_i - P_{i+1})\right)$$

$$\dot{S}_i = \dot{S}_{j-1} - \dot{S}_j + S_{f_{S_i}} + \dot{S}_{irr}^{gen}{}_i \tag{23}$$

$$\dot{V}_i = \dot{V}_{j-1} - \dot{V}_j + S_{f_{V_i}} \tag{24}$$

where $\dot{x}_j$ $(x = m, p, V, S)$ corresponds to the introduced flow to the segment from the j_{th} spatial boundary, and $\dot{S}_{irr}^{gen}{}_i$ denotes the collective generated entropy rate of the segment, named the

irreversible flow. Knowing that the coupling power and the divergence power transport to the segment via a unique flow, the flows cross the j_{th} boundary of the i_{th} segment can be defined as:

$$\dot{m}_j = \frac{1}{M_{TF_{m-V_j}}} \frac{1}{M_{GY_{p-V_i}}} v_i \tag{25}$$

$$\dot{p}_j = M_{TF_{p-m_j}} \frac{1}{M_{TF_{m-V_j}}} \frac{1}{M_{GY_{p-V_i}}} v_i \tag{26}$$

$$\dot{S}_j = \frac{T_i - T_{i+1}}{R_{S_j}} + M_{TF_{S-m_j}} \frac{1}{M_{TF_{m-V_j}}} \frac{1}{M_{GY_{p-V_i}}} v_i \tag{27}$$

$$\dot{V}_j = \frac{1}{M_{GY_{p-V_i}}} v_i - \frac{P_i - P_{i+1}}{R_{V_j}} \tag{28}$$

knowing the dissipated power is transferred to the thermal subdomain via generated entropy rate of each subdomain, by considering the resistive components of each subdomain as ideal non-return transducers, the irreversible flow to the thermal subdomain can be calculated as:

$$\dot{S}_{irr}^{gen}{}_i = \dot{S}_p^{gen}{}_i + \dot{S}_V^{gen}{}_i + \dot{S}_S^{gen}{}_i \tag{29}$$

where:

$$\dot{S}_p^{gen}{}_i = \frac{1}{T_i} \frac{(v_{i-1} - v_i)^2}{R_{p_{j-1}}} \tag{30}$$

$$\dot{S}_V^{gen}{}_i = \frac{1}{T_i} \frac{(P_{i-1} - P_i)^2}{R_{V_{j-1}}} \tag{31}$$

$$\dot{S}_S^{gen}{}_i = \frac{1}{T_i} \frac{(T_{i-1} - T_i)^2}{R_{S_{j-1}}} \tag{32}$$

The external body sources' flows (S_{f_i}) appearing in the state equations are defined with respect to the considered situation of the system. For simplicity, a non-gravitational, non-reactive, and non-radiative flow is considered here, as so, the body flow sources appearing in the state equations vanish.

The state equations of the system are considered to be closed, if the potentials, coupling factors, and dissipative coefficients can be presented as functions of the state variables ($x = m, p, V, S$), material parameters (P_m), and geometrical parameters (P_g) of the segment.

3.5. Defining the subdomains' potentials (n-dimensional constitutive equation)

To derive the potential functionalities, by rewriting Eq. (15) as a collective form of the internal energy (U) plus the kinetic energy (K), i.e., $E(m,p,V,S) = U(m,V,S) + K(m,p)$, the following relations can be presented for the potentials:

$$\left(\frac{\partial E}{\partial m}\right)_{p,V,S} = \left(\frac{\partial U}{\partial m}\right)_{V,S} + \left(\frac{\partial K}{\partial m}\right)_{p} = g(m,V,S) + k(m,p) = \mu(m,p,V,S) \tag{33}$$

$$\left(\frac{\partial E}{\partial p}\right)_{m,V,S} = \left(\frac{\partial K}{\partial p}\right)_{m} = v(m,p,) \tag{34}$$

$$\left(\frac{\partial E}{\partial V}\right)_{m,p,S} = \left(\frac{\partial U}{\partial V}\right)_{m,S} = P(m,V,S) \tag{35}$$

$$\left(\frac{\partial E}{\partial S}\right)_{m,p,V} = \left(\frac{\partial U}{\partial S}\right)_{m,V} T(m,V,S) \tag{36}$$

To start with the thermal subdomain, by considering Eq. (36), the differential form of the constitutive equation of the thermal subdomain can be presented as:

$$dT = \left(\frac{\partial T}{\partial m}\right)_{V,S} dm + \left(\frac{\partial T}{\partial V}\right)_{m,S} dV + \left(\frac{\partial T}{\partial S}\right)_{m,V} dS \tag{37}$$

Considering the energy law at constant volume and the thermal subdomain's adjugate variables (T, S), the last term of Eq. (37) can be obtained as:

$$\left(\frac{\partial T}{\partial S}\right)_{m,V} = \frac{T}{mc_v} \tag{38}$$

where c_v is the specific heat in constant volume and considered to be constant. By taking the advantage of the thermodynamics' first law for an ideal gas, the second term of Eq. (37) can be defined as:

$$\left(\frac{\partial T}{\partial V}\right)_{m,S} = -\frac{RT}{Vc_v} \tag{39}$$

Finally, the first term of Eq. (37) with respect to the Gibbs equation for an ideal gas is presented as:

$$\left(\frac{\partial T}{\partial m}\right)_{V,S} = \frac{T}{c_v}\left(\frac{R}{m} - \frac{S}{m^2}\right) \tag{40}$$

By subletting Eqs. (38)-(40) into Eq. (37) and by integrating the obtained complete differential

equation, the constitutive equation of the thermal subdomain is obtained as:

$$T = T_0 \left(\frac{V_0 m}{m_0 V}\right)^{\frac{R}{c_v}} e^{\frac{\left(\frac{S}{m} - \frac{S_0}{m_0}\right)}{c_v}} \tag{41}$$

where T_0, m_0, V_0, and S_0 are the reference temperature, mass, volume, and entropy, respectively.

Similar to the thermal subdomain, the differential form of the potential subdomain (P, V) constitutive equation can be written as:

$$dP = \left(\frac{\partial P}{\partial m}\right)_{V,S} dm + \left(\frac{\partial P}{\partial V}\right)_{m,S} dV + \left(\frac{\partial P}{\partial S}\right)_{m,V} dS \tag{42}$$

Given that in a conservative field reciprocal relations do exist between the partial differential terms of the constitutive equations, the last term of Eq. (42) can be obtained as:

$$\left(\frac{\partial P}{\partial S}\right)_{m,V} = \left(\frac{\partial T}{\partial V}\right)_{m,S} = -\frac{RT}{V c_v} \tag{43}$$

Considering the partial derivative of the ideal gas equation with respect to volume:

$$\left(\frac{\partial P}{\partial V}\right)_{m,S} = \frac{mR}{V}\left(\frac{\partial T}{\partial V}\right)_{m,S} - \frac{mRT}{V^2} \tag{44}$$

and substituting Eq. (39) into Eq. (44), the second term of Eq. (42) can be defined as:

$$\left(\frac{\partial P}{\partial V}\right)_{m,S} = \frac{P(R + c_v)}{V c_v} \tag{45}$$

Finally, by substituting Eq. (40) into the partial derivative of the ideal gas equation with respect to mass, the first term of Eq. (42) is obtained as:

$$\left(\frac{\partial P}{\partial m}\right)_{V,S} = P \frac{1}{m} \left(\frac{S}{c_v m} - \frac{R}{c_v} - 1\right) \tag{46}$$

By substituting Eqs. (43), (45), and (46) into (42) and by integrating the resultant equation, the constitutive equation of potential subdomain is obtained as:

$$P = P_0 \left(\frac{V_0 m}{m_0 V}\right)^{\frac{R - c_v}{c_v}} e^{\frac{\left(\frac{S}{m} - \frac{S_0}{m_0}\right)}{c_v}} \tag{47}$$

Considering the kinetic energy equation $K = \frac{p^2}{2m}$ and Eq. (34), the potential of the kinetic subdomain can be defined as:

$$v = \frac{p}{m} \tag{48}$$

The last potential to be defined is the potential of the mass subdomain. Knowing that the mass potential is the summation of the Gibbs free energy and the kinetic energy per unit mass, i.e., $\mu = g + k$, and considering the Gibbs-Duhem relation, $mdg = VdP - SdT$, the deferential form of the Gibbs free energy is presented as:

$$\begin{aligned} dg = &\left(\frac{V}{m}\left(\frac{\partial P}{\partial m}\right)_{V,S} - \frac{S}{m}\left(\frac{\partial T}{\partial m}\right)_{V,S}\right) dm + \left(\frac{V}{m}\left(\frac{\partial P}{\partial V}\right)_{m,S} - \frac{S}{m}\left(\frac{\partial T}{\partial V}\right)_{m,S}\right) dV \\ &+ \left(\frac{V}{m}\left(\frac{\partial P}{\partial S}\right)_{m,V} - \frac{S}{m}\left(\frac{\partial T}{\partial S}\right)_{m,V}\right) dS \end{aligned} \tag{49}$$

From an extensive but straightforward analysis, with respect to the obtained partial derivatives, g is defined as:

$$g = \frac{g_0}{\left(R - \frac{S_0}{m_0}\right)}\left(\left(c_v - \frac{S}{m}\right)\left(\frac{V_0 m}{m_0 V}\right)^{\frac{R}{c_v}} e^{\frac{\left(\frac{S}{m} - \frac{S_0}{m_0}\right)}{c_v}} + c_v\right) \tag{50}$$

Considering the kinetic energy equation, k simply is defined as:

$$k = \left(\frac{\partial K}{\partial m}\right)_p = -\frac{p^2}{2m^2} \tag{51}$$

By adding Eq. (50) with Eq. (51), the final form of the mass potential is then obtained as:

$$\mu = \frac{g_0}{\left(R - \frac{S_0}{m_0}\right)}\left(\left(c_v - \frac{S}{m}\right)\left(\frac{V_0 m}{m_0 V}\right)^{\frac{R}{c_v}} e^{\frac{\left(\frac{S}{m} - \frac{S_0}{m_0}\right)}{c_v}} + c_v\right) - \frac{p^2}{2m^2} \tag{52}$$

Collectively, Eqs. (41), (47), (48), and (52) form the constitutive equations of the system with which the reversible interactions among the subdomains occur in each segment.

3.6. Defining the transportation coupling factors

To define the transportation coupling factors including transformation and gyration coupling factors, imagine an exchange of matter between two adjacent storages convect internal energy, and accordingly the intrinsic property of matter (densities). The flow of matter can be regarded as a continuous addition in the direction of the flow of infinitesimal simple systems, which have to be additive in the thermodynamical sense. The internal energy and the properties of these infinitesimal systems can only be described intensively by specific properties [10]. Since the Gibbs-Duhem equation relates the potential gradient of the existing subdomain for the adjacent

boundary of the neighboring segments (storages), the transformation coupling factors can be defined as the ratio of the reversible transportation flow of the subdomain to the flow of matter, which in principal is the intensive form of the state variable of each subdomain:

$$M_{TF_{m-V}} = \frac{V}{m} \tag{53}$$

$$M_{TF_{p-m}} = \frac{p}{m} \tag{54}$$

$$M_{TF_{S-m}} = \frac{S}{m} \tag{55}$$

The anisotropy induced by the momentum of the flow of matter results in non-reciprocity of the power transportation. The embedded gyration coupling between the kinetic and mass subdomains reflects this non-reciprocity of the system. Considering the power continuity of the gyration coupling, and taking into account the BG presentation of the convective field in Fig. 5, the gyration coupling factor is obtained from the ratio of the kinetic effort (potential) to the potential subdomain's flow, where for the chosen system:

$$M_{GY_{p-m}} = \frac{1}{A} \tag{56}$$

where A is the surface of the adjacent boundary of the neighboring segments.

3.7. Defining the dissipative mechanisms

The final step to close the state equations is to define the dissipative mechanisms of the field, R_s, R_p, R_V. To start with R_s, considering the Fourier conduction equation, the dissipative mechanism with respect to the chosen system can be presented as:

$$R_s = \frac{\Delta x T}{k_T A} \tag{57}$$

where Δx and k_T are the generalized length of the resistive component and the conduction coefficient of the gas, respectively.

Given that the dissipation of energy in the potential subdomain occurs as a result of geometrical changes (expansion or contraction) in the direction of the power flow, by considering a quadratic relation between the pressure difference and volumetric flow, $\Delta P = \rho \dot{V}^2 / 2A_d^2$, R_V can be defined as:

$$R_V = sign(\dot{V})\frac{m|\dot{V}|}{2A_d^2 V} \tag{58}$$

where A_d is the actual cross section area and can be defined with respect to the geometry of the spatial boundary and the local pressure loss coefficient, ξ , as $A_d = \xi A$.

To define the dissipative mechanism in the kinetic subdomain, given that the internal shear force can dissipate the kinetic power of the system, by comparing stokes hypothesis with the appearing terms of the momentum balance equation (Eq. (12)), the following relation can be defined for the kinetic subdomain dissipative mechanism:

$$R_p \propto \frac{\Delta x}{\mu_p} = \frac{3}{2\mu_p A} \tag{59}$$

where μ_p is the viscosity of the gas.

Accordingly, all the required coefficients appearing in the state equations of the system have now been defined on the basis of the chosen system's material and geometrical parameters, as well as the states of the system.

In the proposed model, the decomposed power trans*port*ation as well as the decomposed power trans*form*ation provide a distinctive power network of the system in which the possible power connection gates to external physical domains belonging to different fields are highlighted. This added capability to the model makes it suitable for multiple-field dynamic investigations, especially for FSI problems.

4. Simulation and analysis

In this section, to highlight the capability of the generated model in demonstrating the interactive dynamics of the convective field, two separate scenarios are chosen to be investigated via simulating the transient behavior of a compressible flow in a 1D flexible duct. Firstly, to examine the appropriateness of the generated model in discrete-system dynamic investigations, a discharge process is selected with the chosen duct as the connecting pipe between two different pressure chambers (1 and 2) as shown in Fig. 6 (a). In this scenario, the accumulated mass in Chamber 1 is discharged into the system, demonstrating the mechanics of mass and heat transfer within the system. Secondly, to demonstrate the energetic interactions between different physical subdomains and the suitability of the proposed model for use in multiple-field system studies, the

propagation of a volumetric perturbation resulted from fluid-solid interactions is investigated for an externally-excited system shown in Fig. 6 (b).

For simplicity, it is considered that the chosen duct is uniformly discretized into 6 segments, and the axial dynamics for the lumped presentation of the system with the material and geometrical parameters listed in Table 1 is to be investigated. Unstressed room condition is considered as the initial condition of the system, and the system is fully isolated from its surroundings.

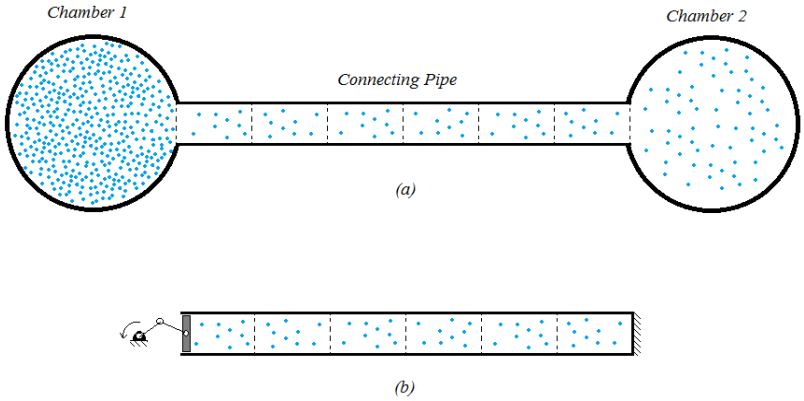

Fig. 6 a) Connecting pipe, b) Wave generator

Table 1. Geometrical and material properties of the convective duct

$\boldsymbol{l}$	Length	$\boldsymbol{2.1e^{-1}}$ $(\boldsymbol{m})$
$\boldsymbol{A}$	Cross section area	$1e^{-4}$ (m^2)
$\boldsymbol{n}$	Number of segments	6
$\boldsymbol{P_0}$	Initial pressure	101315 (pa)
$\boldsymbol{T_0}$	Initial temperature	298 (k)
$\boldsymbol{R}$	Individual gas constant	286.9 $(J/kg/K)$
$\boldsymbol{c_P}$	Specific heat capacity @ P_{cte}	1005 $(J/kg/K)$
$\boldsymbol{c_V}$	Specific heat capacity @ V_{cte}	718 $(J/kg/K)$
$\boldsymbol{k}$	Air conduction coefficient	$2.57e^{-2}$ $(J/m/K/s)$
$\boldsymbol{\mu_p}$	Air viscosity	$5.81e^{-5}$ $(kg/m/s)$

For the first scenario, to check the appropriateness of the developed model in capturing the general dynamics of the system, a transient convective flow is generated within the system by connecting the mass, momentum, volume, and entropy flow sources to the corresponding energy lines of the left boundary of the first segment and the right boundary of the last segment. Since in a compressible flow the different energetic flows of the system are interrelated, the external capacitor components, named as Chamber 1 and Chamber 2 in Fig. 6 (a), are considered to generate the meaningful boundary flows for the system. Initially, Chamber 2 is in equilibrium with the duct, while Chamber 1 is resting above the atmospheric pressure and temperature ($P_{0_{ch1}} =$

125810 pa & $T_{0_{ch1}} = 440\ K,\ V_{ch1\&2} = 10\ V_{segment}$). The corresponding boundary flows of the pipe is then provided by simulating the closed system including the two chambers and the connecting pipe. Accordingly, by running the simulation, the contracted gas in Chamber 1 is anticipated to be expanded in the closed system generating a flow of matter alongside the duct.

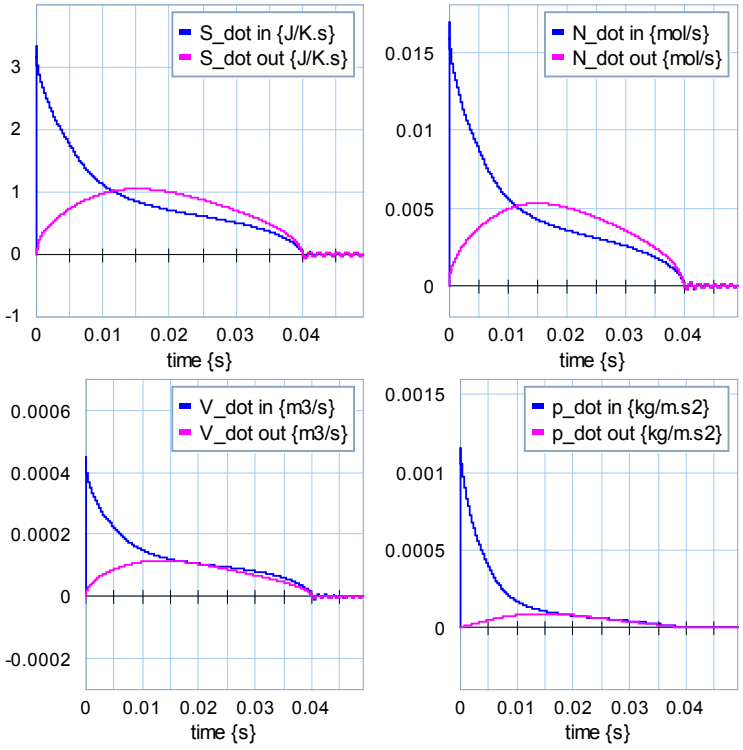

Fig. 7 Boundary flows of the system Fig. 6 (a)

Fig. 7 shows the energetic boundary flows of the pipe. Parts (a), (b), (c), and (d) correspondingly demonstrate the entropic, molar, volumetric, and momentum reversible boundary flows of the system, with which the reversible energy transportations occur to and from the system. The blue lines, demonstrating the inlet flows, show the flows of the considered extensive states to the system with their respective initial high-rate values leading to the final zero-rate value at the end of the simulation time. The pink lines show the outlet flows of the extensive states from the system with their initial and final values equal to zero. This behavior, as it has been anticipated, clearly demonstrates the process of discharging Chamber 1 into the connecting pipe and Chamber 2.

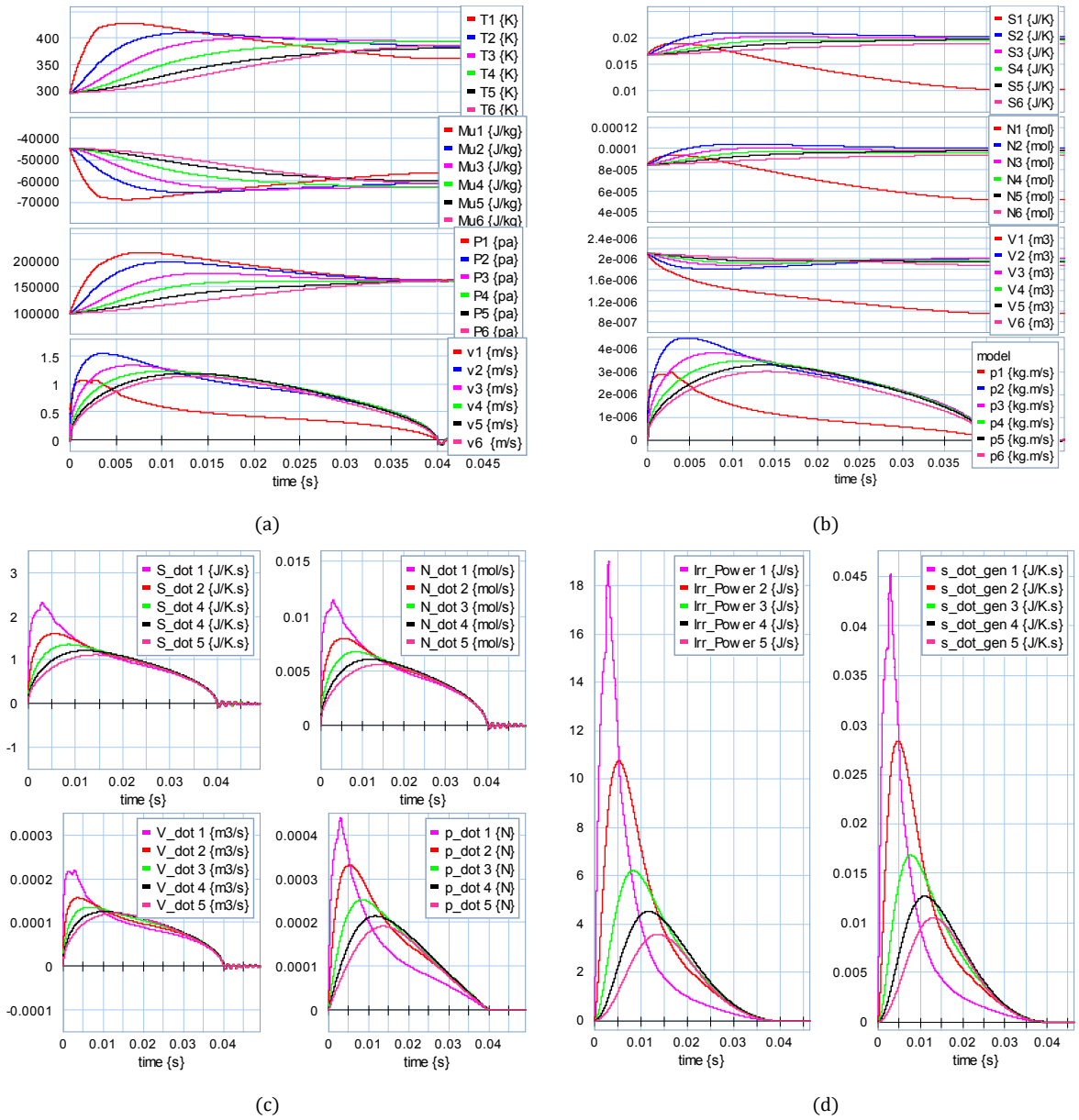

Fig. 8 Connection pipe internal dynamic behavior

The corresponding internal dynamics of the connecting pipe are presented in Fig. 8. Part (a) presents the potentials corresponding to the different physical subdomains of the system. As can be seen, by releasing the gas into the pipe, the pressure and temperature of different segments initially increase sequentially, and then settle in a higher equilibrium level by the end of the process. Similarly, the internal velocity of each segment increases initially, and by the time that the system becomes stabilized in the new equilibrium, the velocity tends to zero again. Part (b) presents the amount of accumulated extensive states of each segment. As can be seen, in the new

equilibrium condition, all the segments, except for the first segment, contain more states than the initial condition, demonstrating the distribution of matter from Chamber 1 to the rest of the system. The strange behavior of the first segment can be explained via the consideration of its neighboring chamber. However, since the aim here is to demonstrate the capability of the generated model in showing the ongoing dynamics in a discrete model, the explanation of the above phenomena is omitted for brevity. Collectively, from Parts (a) and (b) of Fig. 8, the reversible power transformation between the subdomains can be achieved within each segment.

In Part (c) of Fig. 8, a different flow of the system is presented where the reversible power transportation occurs between the counterpart subdomains of the neighboring segments. As can be seen, all the obtained flows follow the similar patterns as the inlet and outlet flows. Part (d) of Fig. 8 presents the irreversible mechanical power transformation from the kinetic subdomain to the thermal subdomain. This transformation occurs via the generated entropy rate shown in the right graph of Fig. 8 (d). This amount of entropy is added to the system as a result of the kinetic power transportation between the neighboring segments. A closer comparison between the reversible and irreversible flows of the system, especially at the later part of the simulation where there exists an oscillatory fluctuation in the system, reveals the consistency of the generated model with the second thermodynamic law, as the irreversible flows are positive definite even though the reversible flows obtain negative values.

Despite the coarse discretization of the system as well as a simple considered functionality to generate the required parameters of the proposed model, collectively the results presented in Figs. 7 and 8 demonstrate an adequate agreement between the simulated results and the general convective behaviors of such systems. This consistency indicates the aptness of the proposed model in revealing the reversible and irreversible internal dynamics of discrete systems.

In the second scenario, to demonstrate the capability of the proposed model in unveiling the physical interactions between the physical subdomains, the propagation of an external excitation inside the closed system shown in Fig. 6 (b) is examined. As the system is considered to remain closed during the simulation, no flow of matter is expected to enter into or be removed from the system. Consequently, the internal dynamics of the system can be considered as a mere result of the reversible and irreversible interactions among the subdomains. Accordingly, to keep the system closed, zero boundary flows are considered for thermal, mass, and kinetic subdomains, and to

generate an external excitation to the system, a sinusoidal pulse with an amplitude of 0.5 $\frac{m^3}{s}$, and frequency of 1082.25 Hz is considered as the volumetric flow for the left boundary of the system. It is expected that the generated disturbance propagates alongside the system.

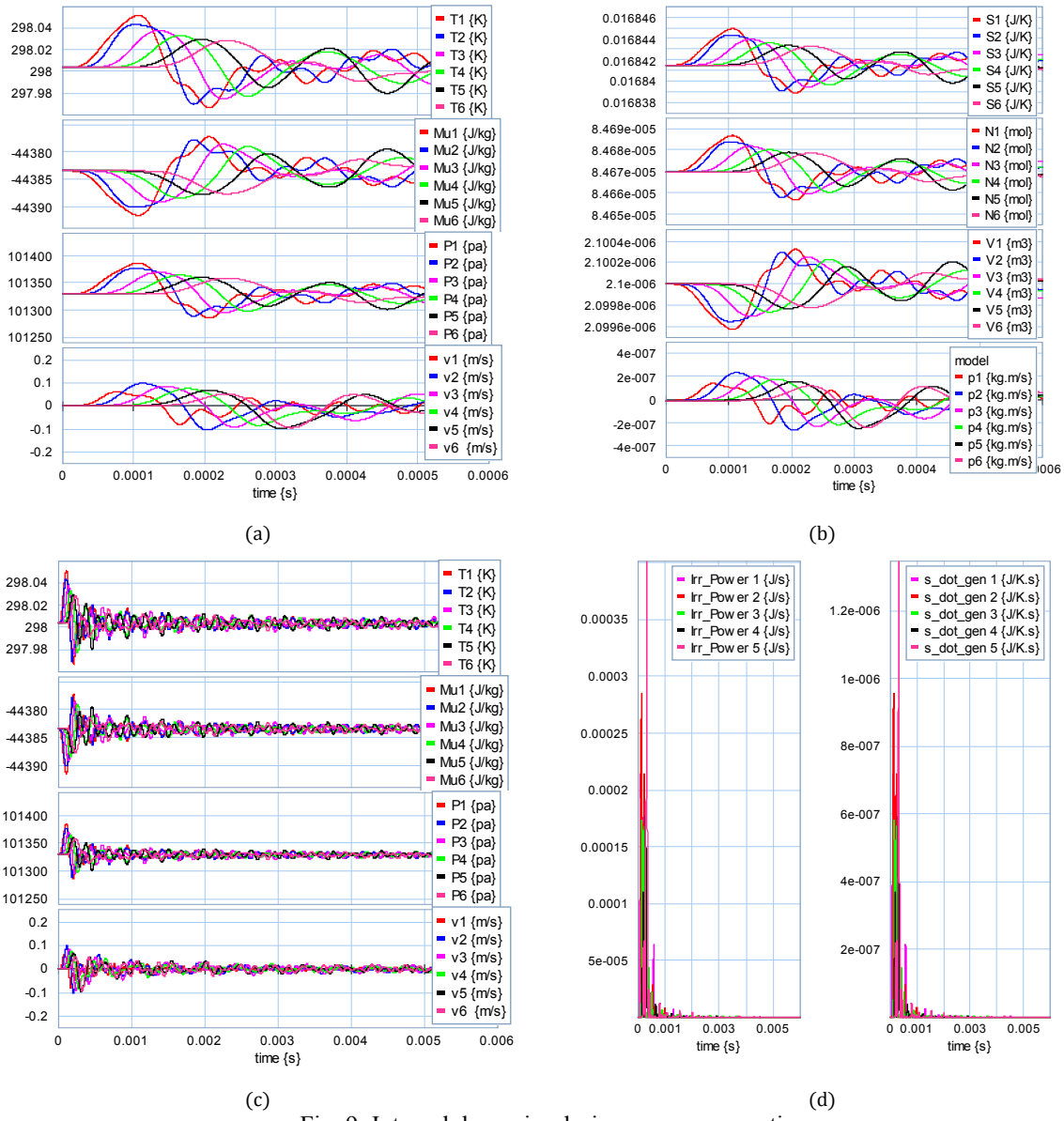

Fig. 9 Internal dynamics during wave propagation

The dynamic behavior of the system in responding to the considered excitation is presented in Fig. 9. Parts (a) and (b) demonstrate the dynamic behaviors of the potentials and the states of the subdomains at the early period of the simulation. As has been expected, the movement of the generated wave is clearly observable in the system. Part (c) shows the system results for the whole simulation time. As can be seen, the obtained results indicate the stability of the model, as the

system returns to its initial equilibrium condition. In Part (d), the irreversibility of the system is presented. Although the magnitude of the obtained irreversible power transactions between the kinetic and thermal subdomains is considerably low, stabilization of the system is a direct result of these existing irreversible transactions. One can see that, no matter how negligible the value of the intrinsic irreversibility of the system is, it can physically stabilize the model and make the use of mathematically-generated stabilizers pointless in the model. The capability of including the intrinsic dissipation of the system with respect to its physical subdomains' interactions can be counted as another state-of-the-art of the proposed decomposition methodology as compared to other conventional decomposition techniques.

In general, the result presented in Fig. 9 demonstrates that the proposed model is capable of capturing complex nonlinear behaviors of the system in spite of its simplicity, which highlights the significance of the added physical insights shown in the proposed model. Accordingly, since there exists a physical causality within the model, physical outcomes from the model are expected, with which a variety of behaviors of the system can be captured without intentionally regenerating them via added mathematical constraints. For instance, from Fig. 10 (a I-III), one can simply realize that although the dynamic behavior of the system is changing due to an increased frequency of the inlet perturbation, the disturbance in the system is traveling with a constant speed. This behavior is captured in the system as a result of the physical relations between the extensive states and the potentials of the system, not through mathematically-embedded constrains. Another example is the capture of noise compensation phenomena when an opposite similar input is applied to the other boundary of the system as shown in Fig. 10 (b I-II). It is clear that releasing an opposite noise to the system from the left end has led to the decrease of the fluctuation magnitude of the system; however, since there exists a natural lag in the system, the complete cancelation does not occur. This captured behavior highlights the sound physics behind such phenomena in the system. Obtaining the behavior of the system connected to the physical essence of the phenomena, via connecting the system to its natural memory, would lead to broadening the valid range of such models and reducing the costs of simulation.

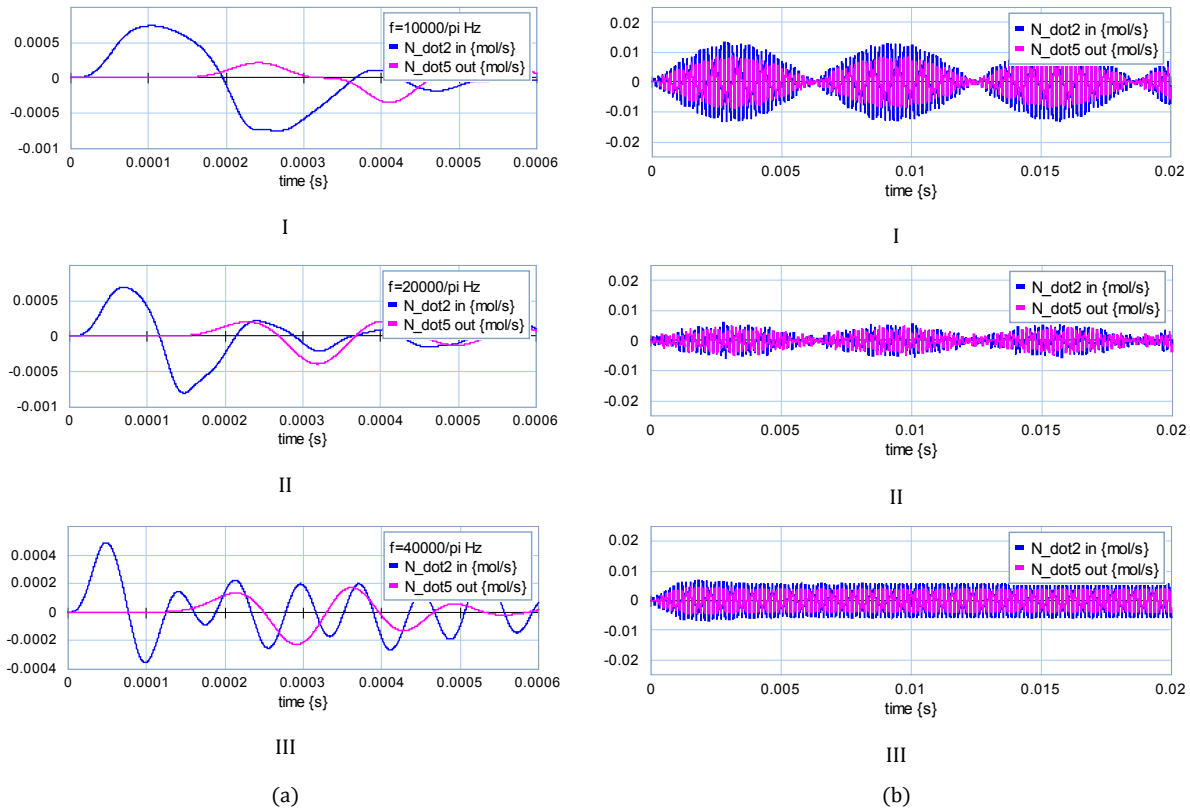

Fig. 10 Sensitivity analysis of the behavior of the system

The physical decomposition of the system further leads to the domain-independency of the model, which makes the connection of physical subdomains possible regardless of the disciplines where the subdomains may belong to. This capability can broaden the application of the generated model in multi-disciplinary system dynamic investigations. For instance, Fig. 10 (b III) shows the impacts of external heat transfer on the general behavior of the system whose initial behavior is presented in Fig. 10 (b I). It is clear that the transferred heat into the system has totally changed the behavior of the system. Now, imagine the source of the transferred heat into the system as a hot interface. The coupled dynamics of heat transfer between the surface and the system can be obtained simply by connecting the thermal energy lines of the fluid and solid fields, if the model of the solid field has been generated using a similar terminology. In addition, one can see in an interactive multi-physical problem such as a supersonic FSI problem where the power transaction between the fields is a combined aero-thermo dynamic load, the physically-decomposed power transactions provided by the energetic decomposition of the two fields can be a great help to discover the unsolved problems relating to aerothermoelasticity.

5. Conclusion

In this study, a domain-independent energy-based nonlinear model is developed for compressible convective flow. By means of the proposed decomposition of the fluid field into thermal, mass, potential, and kinetic subdomains, the general complex dynamics of the system are developed on the basis of the conservative reversible and irreversible energetic interactions of the present physical subdomains. The dynamics of the system obtained in this way are directly connected to the physical memory of the system, and thus, provide the possibility of capturing the ongoing phenomena of the system including the energetic transactions between the mechanical and thermal subdomains.

The domain-independency of the generated model can be counted as a desirable feature for dynamic investigations of multi-disciplinary systems, as the complex power transactions between the disciplines can be decomposed with respect to the present similar physical subdomains of different fields. Furthermore, the developed energetic network of the system provides a useful tool for control strategy development and energy management of the system.

The obtained relations discussed in this study can also be used to define proper relations for corresponding CFD modeling studies. The generated BG model of one segment can serve to generate the partial differential equations via a limited operation on the geometry of the segment to provide a full freedom of choice for numerical-solution techniques. The authors hope that other modelers will find inspiration to use this approach in their own research.

References

[1] J. L. Balino, A.E. Larreteguy, E. F. Gandolfo Raso, "A general bond graph approach for computation fluid dynamics," *Simulation Modeling Practic and Theory,* vol. 14, pp. 884-908, 2006.

[2] D. C. Karnopp, "Bond graph modeling philosophy for thermofluid systems," *ASME Trans., Journal of Daynamic System Measurment and Cntrol,* vol. 100, no. 1, pp. 70-75, 1978.

[3] D. C. Karnopp, "States variables and pseudo Bond geaph for compressible thermofluid systems," *ASME Trans., Journal of Dynamic System Measurment and Control,* vol. 101, no.

3, pp. 201-204, 1979.

[4] D. L. Magolis, "Modeling of two-stroke internal combustion engine dynamics using Bond graph technique," *ASME Trans.,,* pp. 2263-2275, 1976.

[5] P. C. Breedveld, N. Hogan, "Energetically Proper Modeling of A Simple Trottling Process," in *IMACS l. MathMod, Technical University*, Vienna, Austria, Vol. 1, pp- 37- 40, 1994.

[6] A. Zanj, P. C. Breedveld, F. He, "Variable Interface Dynamic Adaptation (VIDA) technique: A Novel Approach to adjust Lagrangian Frame and Eulerian Frame at Flattering Interface," in *AIAA Modeling and Simulation Technologies Conference*, Grapevine, Texas, January, 2017.

[7] G. Hetsroni, Handbook of Multiphase Systems, Hemisphere Publishing Corporation, 1982, ISBN 0-07-028460-1.

[8] J. Greifeneder, F. E. Cellier, "Modeling Convective Flows Using Bond Graphs," *Simulation Series,* 2001.

[9] A. Zanj, F. He , "Conduction Model Compatible for Multi-Physical Domain Dynamic Investigations: Bond Graph Approach," *World Academy of Science, Engineering and Technology, International Journal of Mechanical, Aerospace, Industrial, Mechatronic and Manufact,* vol. 10, no. 3, pp. 524-535, 2016.

[10] P. C. Breedveld, Physical System Theory in Terms of Bond Graph, Enschede: University of Twente, 1984.

[11] P. C. Breedveld, J. J. Granada, F. E. Cellier , "Insight in Rigid Body Motion Stability Via an Alternative for the Eulerian Junction Structure," in *4th Bond graph modeling and simulation*, San Francisco, 1999.

CHAPTER 7: COUPLED AEROTHERMOVISCOELASTIC MODEL

Aim

The aim of this chapter is to connect the energy-based solid and fluid models generated in Chapters 5 and 6, respectively.

Description

To achieve this aim, owing to the domain-independency of the generated models, and since in the decomposition of these two fields a similar terminology has been employed, the generated power structures respectively for the two fields become continuously connectable. As a result, the total conservative power transactions between the two fields can be defined distinguishably from the power transactions of each corresponding physical subdomains of these two fields in the form of handshaking. To satisfy the compatibility conditions raised from the implementation of the different coordinate frames for the solid and fluid fields, a novel Variable Interface Dynamic Adaptation (VIDA) technique is developed to be implemented on the interface of the two fields. The outline of the presented study is organized as follows:

Results

The generated conservative power network of the system will make it possible to control and manage the system with respect to each physical subdomain individually, while allowing the influence of the other involving subdomains to be examined through explicitly-expressed embedded physical relations between the subdomains. The capabilities of the proposed physical model of the entire fluid-solid-interface system provide a novel feature into the system dynamic modeling that can, not only, broaden the valid range of the model but, more importantly, offer a unique opportunity for capturing and revealing the unknown phenomena of the system previously hidden using existing classical physical knowledge.

Conclusion

A novel fundamental framework for an integrated coupled-aerothermoviscoelastic model is generated with which the dynamics of the interactive solid-fluid system are generated with respect to the internal energetic interactions between the existing physical subdomains of each of the fields.

A NOVEL ENERGY-BASED AERTHERMOVISCOELASTIC MODELING FRAME FOR MULTIPLE-FIELD SYSTEM DYNAMIC INVESTIGATIONS, BOND GRAPH APPROACH

A. Zanj[1]*, F. He[2], P. C. Breedveld[3]

Abstract- In this study, a new fundamental framework for a coupled-aerothermoelastic model is proposed with which the dynamic of the system is generated with respect to its internal energetic interactions between the existing physical subdomains. To this aim, by means of the Bond Graph terminology, a domain-independent model is first developed for each of the fluid and solid fields that can demonstrate the reversible and irreversible energetic interactions within the field of concern. By considering the conservative power transactions between the two fields, the reversible and irreversible intra-connections is then generated. Owing to the domain-independency of the generated models, the total conservative power transactions between the two fields can be defined distinguishably from the power transactions of each corresponding physical subdomains of these two fields in the form of handshaking. This capability will broaden the physical insights of power transactions in fluid-structure-interactions (FSI) problems. In addition, the generated conservative power network of the system will make it possible to control and manage the system with respect to each physical subdomain individually, while allowing the influence of the other involving subdomains to be examined through explicitly-expressed embedded physical relations between the subdomains. In general, the added capabilities of the proposed physical model provide a novel feature into the system dynamic modeling that can, not only, broaden the valid range of the model but, more importantly, offer a unique opportunity for capturing and revealing the unknown phenomena of the system previously hidden using existing classical physical knowledge.

Keywords: *Bond Graph modeling, FSI problems, Dynamic system modeling, Convective flow, Viscoelasticity.*

1. Introduction

Modeling a correct aero-thermal load on a structure exposed to aerodynamic and thermodynamic conditions is one of the challenging areas in dynamic investigations of aerothermoelastic phenomena [1], as the magnitude of the aero-thermo load is entangled with the dynamics of both the fluid and solid sides of the interface instantaneously. Since the structural

[1] Research assistant in advanced control system group, School of science and engineering, Flinders University, Adelaide, Australia, email: amir.zanj@flinders.edu.au
[2] Associate Professor in School of science and engineering, Flinders University, Adelaide, Australia
[3] Associate Professor in robotics and mechatronics group, University of Twente, Enschede, Netherlands

deformation and thermal condition can change the thermodynamic characteristics of the surrounding fluid, and simultaneously the changes in the thermodynamic parameters of the fluid can generate different aero-thermo load for the structure, in order to generate a correct aero-thermo load, the systems respectively describing the fluid and solid fields are required to be dynamically coupled on the interface. However, there are two significant issues in coupling the fluid and solid fields together. The first issue is concerned with the conservation of power transmissions between the two fields, as the fluid power does not have an explicit character. The second issue relates to the translation of Lagrangian solid field's motion into the Eulerian fixed frame of the fluid field.

In earlier studies [2] [3], to address the above-described issues, slow-thermal-dynamics [4] and weak-connectivity [5] assumptions are commonly adopted. Through assumed decoupled-dynamics between the structure and the thermal domain, the former studies intend to decrease the degree of freedom of the system in order to generate an explicit transaction between the fluid and solid fields. In recent attempts [6] [7] [8], the weak-connectivity assumption is seen to be avoided by using numerical strategies to include the thermal impacts on each field's dynamics; however the slow-thermal-dynamics assumption on the interface is still firmly kept. In these studies, by employing the Helmholtz free energy in solid material model [9] and the Navier-Stokes equations for fluid field [10], the generated models for both the solid and fluid fields are domain-dependent [11] in nature. This feature of the modeling makes the dynamic coupling of the thermal subdomains of the two fields on the interface impossible to implement. Furthermore, the entropic interactions between the two fields remain ambiguous. Although the entropic interactions in comparison with other interactions may be negligible [5], the ignorance of this factor will put the conservation of power transaction between the two fields under question. Accordingly, the models thus generated, though capable of providing a clear picture of ongoing dynamics of the system, are seen to be unsuitable to provide a useful and unbroken root upon which the physical memory of the system underpinning the energy conservation law can be firmly established. In addition, the attained modeling accuracy relies heavily on mathematical constrains (filtration and stabilization [12]) employed and computational capacities required, which leads to the development of drastically high-order models valid only within a limited operational range. There is therefore a need to rethink the modeling technique and to create a new methodology that can be based on purely the intrinsic physical constrains of the system to generate valid models that naturally obey the energy conservation law and reveal the interconnected physical insights of the system dynamics truthfully.

The conservation of power transaction on the interface can be satisfied if isomorphic models of both the fluid and solid fields can be generated. In isomorphic models, for each portion of the power transportation (thermal, acoustic, or kinetic) in one field, there exists a specific gate in the other field with which a tractable transaction between the fields is attainable. However, because of the fundamental differences between the two fields (namely, the existence of mass flow in the fluid field), generating isomorphic models for each of the fields in a general form is not possible unless each field is decomposed into a set of alike subdomains where counterparts between the two fields become isomorphic. Knowing that an aerothermoelastic system is a multi-physical multiple-field (fluid and solid) system by nature, if one can generate a field-independent model (using physical states) of involving physical subdomains for each of the fields, the counterpart physical subdomains between the two fields (e.g., the thermal subdomain of the solid field and the thermal subdomain of the fluid field) will become isomorphic. Thus, the reversible and irreversible power transactions among the physical subdomains, regardless of the specific field, will become tractable.

In the current study, to develop the fundamentals for a conservative coupled-aerothermoelastic model, physical decomposition of the system is suggested [13] for the fluid and solid fields at the interface. Accordingly, since the physical (thermal, mass, kinetic, and potential) subdomains are alike in any field, generating isomorphic models for the physical subdomains regardless of the field becomes possible [14]. To this aim, by means of the port-based approach (known as the Bond graph approach) [15] [16] [17] [18], each field is first decomposed into its initial physical subdomains, and the dynamics of the field are generated from the reversible and irreversible interactions of the energetic components of the physical subdomains. Based on power continuity between the two fields, through connecting the counterpart pairs of the physical subdomains of the two fields with respect to the possible connections of their energetic components on the interface, the conservative coupled-aerothermoelastic model of the system can then be generated *if and only if* the compatibility issue between the fixed Eulerian frame of the fluid field and the moving Lagrangian frame of the solid field can be addressed satisfactorily.

To address the compatibility issue, the virtual interface dynamic adaptation (VIDA) technique [19] is employed. According to the VIDA technique, the likely motions of the Lagrangian solid frame is virtually translated into a reversible volumetric flow for the fixed Eulerian fluid frame. Accordingly, the compatibility of the two frames is satisfied and the required information of the

contact surface is refined at any instant in time to keep the power transactions at the interface continuous.

In overall, by using the proposed methodology, an energetic network of the system will be generated that can illustrate continuous reversible and irreversible power transactions (including power transformation and power transportation) among the various subdomains and between the two fields. The dynamics obtained from such a model will include more details in relation to the memory and physical characteristics of the system, which can in turn provide a desirable basis for analyzing the complex multi-physical multiple-field behaviors of the system. As the model is developed without the slow-thermal-dynamics and weak-connectivity assumptions and with no additional mathematical constrains, the model is valid in an extended range principally much wider than its conventional counterparts. Undoubtedly, the proposed energetic network of the system can be a useful tool for developing control strategies and energy management of the system.

To illustrate the development of the proposed model, the reminder of this paper is organized as follows. In Section 2, a simple multiple-field system is defined as an example to be physically decomposed. The energy-based model of the solid and fluid fields of the chosen system is then developed correspondingly in Sections 3 and 4. In Section 5, by implementing the VIDA technique, the conservative coupling between the two fields is generated to form a coupled-aerothermoviscoelastic model. In Section 6, via simulating several scenarios of the chosen system, the capability of the proposed model in capturing ongoing dynamic behavior of the system is examined. Finally, the capability of the proposed model in capturing the complex behavior of the system from the energetic interactions of the physical subdomains described in a discrete configuration is concluded in Section 7.

2. Physical system

To develop an energy-based aerothermoviscoelastic model avoiding complexity, a simple 1D multiple-field system given in Fig. 1 is considered for which the procedure for extracting the system model will be explained. As illustrated in Fig. 1, the system consists of a flexible duct containing compressible fluid in the form of a closed system where mechanical energy and thermal energy transfer between the solid and fluid fields. For simplicity, only the axial deformation of the flexible duct is considered together with the axial dynamics of the confined gas. As so, the

mechanical power transactions between the fluid and solid fields will occur only at both ends of the duct while the heat transfer between the two fields will occur alongside the system.

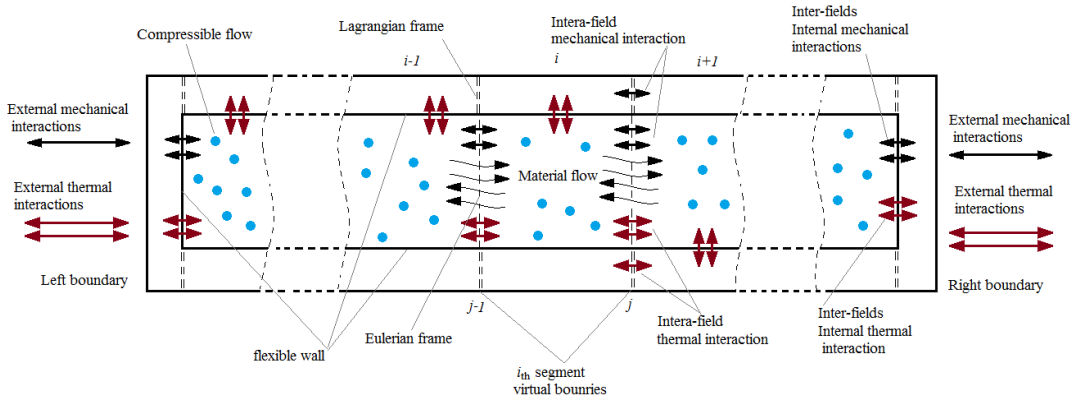

Fig.1 1D flexible duct structure

For the chosen system, two energy-based models resulting from the physical decompositions of the fluid and solid fields are first derived individually. By developing the handshake connections between the physical subdomains of the obtained models of the two fields, a conservative aerothermoviscoelastic model of the system is then generated. It should be mentioned that the choice of a 1D system in this study is just for the purpose of clarifying the procedure for generating the energetic network of the system. Since the considered states for both the fluid and solid fields are standard extensive physical states, the extension of the generated model for higher-dimension systems is systematically attainable.

3. Decomposed domain-independent thermo-viscoelastic model

To generate a physically-decomposed model of the solid field, the energy-based modeling technique proposed in [20] is employed. According to this method, a domain-independent dispersive model for each of the three physical (kinetic, potential, and thermal) subdomains is first developed using the Bond graph (BG) approach that can separately describe the energetic interactions within each of the subdomains. The possible reversible and irreversible energetic couplings between the subdomains are then installed inside the model to form an integrated decomposed thermo-viscoelastic model. Finally, the interactive modulations including deformation-modulated conductivity and temperature-modulated mechanical resistivity are added to the model. The obtained model will provide a clear dynamic map of the solid filed for the considered system's energy propagation.

3.1. Dissipative elastic domain BG model

To generate a distributed dispersive elastic model (including potential and kinetic subdomains of the solid field) for the considered 1D system shown in Fig. 1, an energy-based Maxwell discrete model suggested in [21] is employed. In this model, a resistor is placed inside each element in series with the storage component. Fig. 2 shows a discrete Maxwell structure for a finite number of elements. Since this reticulated space is indeed a continuous system, the adjacent boundaries of each two consecutive elements are bonded to move together. Therefore, one can consider the above discretization as a junction-element where the elements are the representative of the potential subdomain, and the junctions are the representative of the kinetic subdomain of the solid field.

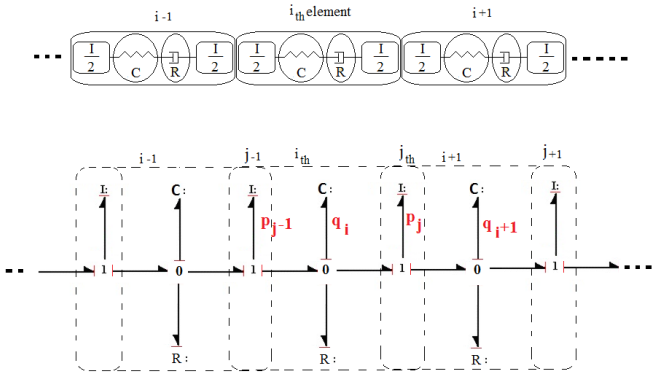

Fig.2 Maxwell model BG representation

For the BG representation shown in Fig. 2, considering the state variables for the i_{th} element and j_{th} junction as q_i and p_j which denote the deformation and momentum, respectively, the state equations for each junction-element are derived as:

$$\dot{p}_i = \frac{q_{j-1}}{C_{j-1}} - \frac{q_j}{C_j} \tag{1}$$

$$\dot{q}_i = \frac{p_{j-1}}{I_{j-1}} - \frac{p_j}{I_j} - \frac{q_i}{\tau_i} \tag{2}$$

$$\tau_i = R_i C_i \tag{3}$$

$$I_j = \frac{m_i}{2} + \frac{m_{i+1}}{2} \tag{4}$$

$$C_i = \frac{L_{0_i}}{A_i E_i} \tag{5}$$

where I_j is the boundary inertance defined as a function of the adjacent elements' masses; C_i

represents the capacitance of the element as a function of the element's geometrical and material parameters; L_{0_i}, A_i and E_i are the initial length, contact surface, and Young modulus of the element, respectively; R_i indicates the element's resistant coefficient obtained from the viscosity of the material. Using the geometrical and material parameters of the solid field, the presented model is able to generate the axial dispersive elasto-dynamics of the solid field of the chosen system.

3.2. Thermal domain BG model

An energy-based conduction model presented in [25] is employed to generate a thermal subdomain model of the solid field with its geometry reticulation and BG representation given in Fig. 3. The energy propagation within the model is described by a chain of dissipative (R) and capacitive (C) energy components placed interlaced [23]. It is assumed that thermal energy is stored in C components and dissipated while passing through R components.

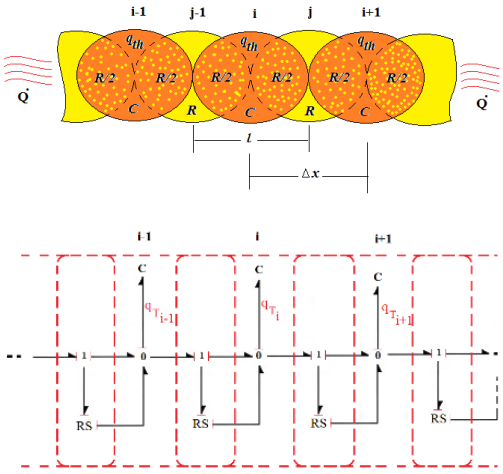

Fig.3 1D heat conduction schematic

Based on the obtained thermal BG integrative causality, the state equation of the thermal subdomain is derived by defining all the entropy flow to the storage component:

$$\dot{q}_{th_i} = \dot{s}_{j-1} - \dot{s}_j + \dot{S}_i^{gen} \tag{6}$$

where q_{th_i} denotes the amount of stored entropy, s, of the i_{th} element; $\dot{s}_{j-1}$, $\dot{s}_j$ and $\dot{S}_i^{gen}$ are the amounts of reversible inlet and outlet entropy flows, and the entropy generation rate, respectively. Considering the resistive constitutive equation of the thermal subdomain, the internal flow crossing the j_{th} boundary of the segment can be derived as:

$$\dot{s}_j = \frac{1}{R_j}(\psi_i(q_{th_i}) - \psi_{i+1}(q_{th_{i+1}})) \tag{7}$$

where R_j is the resistant coefficient of the j_{th} *RS* component, and $\psi_i(q_{th_i})$ is the i_{th} constitutive equation of the thermal subdomain. Assuming that the capacity of a long well-insulated rod is proportional to the temperature gradient [23], R_j is then presented as:

$$R_j = \frac{\Delta x_j T_j}{k_j A_j} \tag{8}$$

where k_j and A_j are specific thermal conductance coefficient and cross-section area of the j_{th} junction, respectively; Δx_j is the generalized length of the j_{th} resistive energy component.

To define $\psi_i(q_{th_i})$, use the constant-volume capacitive law:

$$Q = \rho V c \frac{dT}{dt} \tag{9}$$

where c, ρ and V are the specific heat, density, and volume of the element, respectively. Considering the relation between the conjugate variables of the thermal subdomain:

$$Q = T\dot{q}_{th} \tag{10}$$

the functionality of $\psi_i(q_{th_i})$ can be derived as:

$$T_i = \psi_i(q_{th_i}) = T_0 e^{\frac{1}{\rho_i V_i c_i}(q_{th_i} - s_0)} \tag{11}$$

where l_i is the length of the i_{th} storage component; T_0 and s_0 are respectively the reference temperature and entropy for the i_{th} element. To define the generated entropy rate, $\dot{S}_i^{gen}$, in Eq. (6), considering the continuous power transmission of a two-port *RS*-component and the junction's resistive constitutive equation:

$$\dot{S}_i^{gen} T_i = \dot{s}_{j-1}(T_{i-1} - T_i) \tag{12}$$

$$\dot{s}_j R_j = (T_i - T_{i+1}) \tag{13}$$

the generated entropy rate of the element is derived as:

$$\dot{S}_i^{gen} = \frac{1}{R_{j-1}} T_0 e^{\frac{1}{\rho_i V_i c_i}(q_{th_i} - s_0)} (e^{\frac{1}{\rho_i V_i c_i}(q_{th_i} - q_{th_{i-1}})} - 1)^2 \tag{14}$$

Accordingly, the governing equations for the thermal subdomain of the solid field are closed.

Since the generated thermal and elastic models are to be coupled to form the integrated thermo-

viscoelastic model, the geometrical compatibility conditions of their corresponding energy components must be satisfied. Accordingly, similar to the elastic model, the memory and resistivity characteristics of the thermal model are located at the center and the two sides of the element, respectively. To form the resistive component in the suggested configuration, using the same functionality in the elastic subdomain for junction elements:

$$R_j = \frac{T_0}{2}\left(\frac{l_i e^{\frac{1}{\rho V c}\left(q_{th_i} - s_0\right)}}{k_i A_i} + \frac{l_{i+1} e^{\frac{1}{\rho_{i+1} V_{i+1} c_{i+1}}\left(q_{th_{i+1}} - s_0\right)}}{k_{i+1} A_{i+1}}\right) \tag{15}$$

It is clear that by substituting Eqs. (7), (11), (14) and (15) into (6), the rate of the change in the entropy of the element will be dependent on the spatial material and geometrical characteristics of the element. This exclusive feature of the proposed model makes the thermal element compatible with elements of any other subdomains that have the same spatial references, and leads to the appropriateness of the thermal model for multi-physical domain dynamic investigations.

3.3. Thermo-elastic reversible and irreversible energetic coupling

The generated dispersive elastic and thermal models provide two separate power lines that individually illustrate the power transactions in each of the subdomains (It should be mentioned that the elastic energy line contains the transaction relating to the potential and kinetic subdomains; however for simplicity in the following this combination is considered as the elastic subdomain). The reversible and irreversible connections among the subdomains need to be added to the overall model to clarify the continuous power transformation between them. For this purpose, the respective memories (stored in *C*) of these subdomains, as well as the resistivity of the system, are required to be coupled. To achieve this, the storage components of both subdomains are replaced by the multiport storage [11], and the dissipated energy from the elastic to thermal subdomains is transferred via the mechanical *RS*-element as shown in Fig. 4.

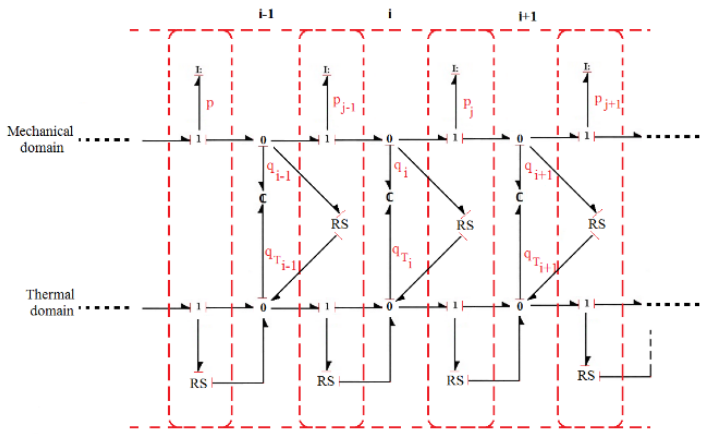

Fig.4 Coupled thermo-viscoelastic model

The replacement of the storage components mathematically means the change of the constitutive relation of each subdomain with two-dimensional constitutive equations that are reciprocal together. To extract the new constitutive equations for each subdomain, let's assume that the total energy stored inside this two-port storage is a function of the extensive states of both thermal and elastic subdomains:

$$U = U(q_m, S) \tag{16}$$

where q_m presents the deformation and S is the entropy of each element. Considering energy as a 1st-order homogenous function, the energy change in the field can be expressed as:

$$dU = \frac{\partial U}{\partial q_m} dq_m + \frac{\partial U}{\partial S} dS \tag{17}$$

where by definition the constitutive equations for the elastic and thermal subdomains are:

$$F(q_m, S) = \left(\frac{\partial U}{\partial q_m}\right)_S, \; T(q_m, S) = \left(\frac{\partial U}{\partial S}\right)_{q_m} \tag{18}$$

where F and T are defined earlier as the efforts (potentials) of the elastic and thermal ports, respectively. The deferential form of the constitutive equation for both subdomains with respect to the new variables can be presented as follows:

$$dT = \left(\frac{\partial T}{\partial q_m}\right)_S dq_m + \left(\frac{\partial T}{\partial S}\right)_{q_m} dS \tag{19}$$

$$dF = \left(\frac{\partial F}{\partial q_m}\right)_S dq_m + \left(\frac{\partial F}{\partial S}\right)_{q_m} dS \tag{20}$$

To start with the thermal subdomain constitutive relation, for the 2nd term of the right-hand side of Eq. (19), given the thermal energy Q at constant volume,

$$\partial Q = T\partial s = C_v dT \tag{21}$$

and considering the constant specific heat C_v, one can conclude:

$$\left(\frac{\partial T}{\partial S}\right)_{q_m} = \frac{T}{C_v} \tag{22}$$

To define the 1st term of Eq. (19), by taking the advantage of the reciprocity of the two constitutive equations and considering the Hook's law for 1D geometry, one has:

$$\left(\frac{\partial T}{\partial q_m}\right)_S = \left(\frac{\partial F}{\partial S}\right)_{q_m} \tag{23}$$

$$F = AE\frac{q_m}{L} + \alpha AE(T - T_0) \tag{24}$$

Taking the partial derivative of Eq. (24) with respect to entropy and comparing it with (23) yield:

$$\left(\frac{\partial T}{\partial q_m}\right)_S = \alpha AE\left(\frac{\partial T}{\partial S}\right)_{q_m} = \alpha AE\frac{T}{C_v} \tag{25}$$

Substituting Eqs. (22) and (25) into (19) and integrating yield:

$$T = T_0 e^{\frac{\alpha AE}{C_v}q_m} e^{\frac{(S-S_0)}{C_v}} \tag{26}$$

The elastic subdomain constitutive equation can be obtained by using Eq. (26) to change the causality of Eq. (24), resulting in:

$$F = AE\frac{q_m}{L} + \alpha AET_0(e^{\frac{\alpha AE}{C_v}q_m} e^{\frac{(S-S_0)}{C_v}} - 1) \tag{27}$$

The nonlinear multiport constitutive equations of the thermal and elastic subdomain are seen to contain a contribution related to the displacement/strain and a contribution related to the entropy, thus showing the reversible effect of thermo-elasticity on both subdomains.

To irreversibly connect the elastic and thermal subdomains, a non-return two-port energy transducer introduced in [21] is required to be installed inside the system. This new connection is presented in Fig. 4 as the *RS*-component connecting the elastic and thermal subdomains. Assuming that the energy stays conservative while transferring between the subdomains, and according to the allocated conjugate variables of each subdomain, one can write:

$$\dot{q}_m F = \dot{S}_{gen_m} T \tag{28}$$

For the i_{th} element, considering the constitutive equation of the resistive component, the introduced entropy rate to the thermal subdomain can be calculated as:

$$\dot{S}_{gen_{m_i}} = \frac{\left(\frac{A_i E_i}{L_i} q_{m_i}\right)^2}{R_{m_i} T_{0_i} e^{\frac{\alpha_i A_i E_i}{C_{v_i}} q_{m_i}} e^{\frac{\left(q_{th_i} - S_{0_i}\right)}{C_{v_i}}}} \tag{29}$$

Accordingly, the total generated entropy is obtained as:

$$\dot{S}_{th_i}^{gen} = \frac{T_{0_i} e^{\frac{\alpha_i A_i E_i}{C_{v_i}} q_{m_i}} e^{\frac{\left(q_{th_i} - S_{0_i}\right)}{C_{v_i}}}}{R_{th_{j-1}}} \left(\frac{T_{0_{i-1}} e^{\frac{\alpha_{i-1} A_{i-1} E_{i-1}}{C_{v_{i-1}}} q_{m_{i-1}}} e^{\frac{\left(q_{th_{i-1}} - S_{0_{i-1}}\right)}{C_{v_{i-1}}}}}{T_{0_i} e^{\frac{\alpha_i A_i E_i}{C_{v_i}} q_{m_i}} e^{\frac{\left(q_{th_i} - S_{0_i}\right)}{C_{v_i}}}} - 1 \right)^2 \tag{30}$$

$$R_{th_j} = \frac{1}{2} \left(\frac{L_i T_{0_i} e^{\frac{\alpha_i A_i E_i}{C_{v_i}} q_{m_i}} e^{\frac{\left(q_{th_i} - S_{0_i}\right)}{C_{v_i}}}}{k_i A_i} + \frac{L_{i+1} T_{0_{i+1}} e^{\frac{\alpha_{i+1} A_i{+1} E_{i+1}}{C_{v_{i+1}}} q_{m_{i+1}}} e^{\frac{\left(q_{th_{i+1}} - S_{0_{i+1}}\right)}{C_{v_{i+1}}}}}{k_{i+1} A_{i+1}} \right) \tag{31}$$

Eq. (30) demonstrates the amount of irreversibility occurring in the thermal subdomain. It can be seen that the mechanical resistive parameter now interferes with the entropy rate of the system according to an irreversible process. It is clear that this equation satisfies the second thermodynamic law as the amount of the generated entropy is always greater than zero.

3.4. Thermo-elastic interactive modulations

In addition to the energetic connections between the thermal and elastic subdomains, presented via energy ports, there exist information transformations between the non-memory components (resistors) of the system. Modulations of these parameters are thus required, which will provide the deformation-modulated conductivity and temperature-modulated viscoelasticity of the model and physically extend the capability of the model to a wider range of thermo-mechanical loading.

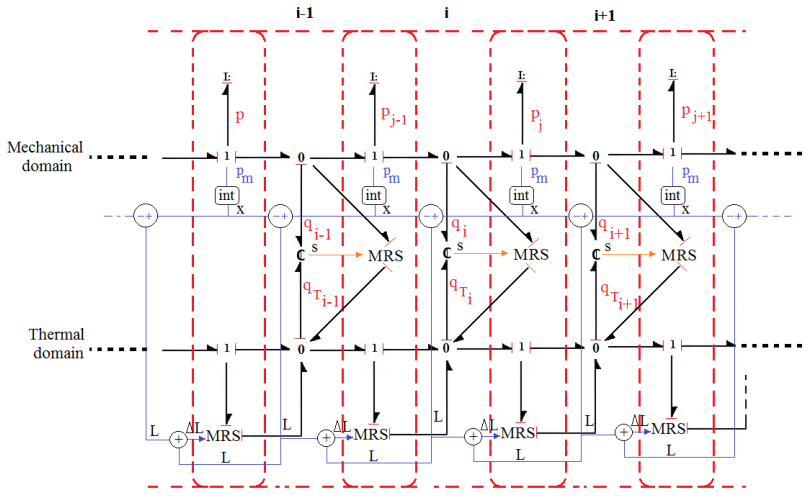

Fig.5 Final thermo-viscoelastic BG model

The modulations are presented in Fig. 5. Considering Eq. (8), the thermal resistance of each

element is proportional to the length of the adjacent element. This parameter of the system will vary under mechanical loading, leading to the change in the conductivity of the system. As shown in Fig. 5, via replacing the thermal *RS*-component with a deformation-modulated resistivity, *MRS*, the desired impact can be included as:

$$MR_{th_j} = \frac{1}{2}\left(\frac{ML_i T_{0_i} e^{\frac{\alpha_i A_i E_i}{C_{v_i}} q_{m_i}} e^{\frac{\left(q_{th_i} - S_{0_i}\right)}{C_{v_i}}}}{k_i A_i} + \frac{ML_{i+1} T_{0_{i+1}} e^{\frac{\alpha_{i+1} A_{i+1} E_{i+1}}{C_{v_{i+1}}} q_{m_{i+1}}} e^{\frac{\left(q_{th_{i+1}} - S_{0_{i+1}}\right)}{C_{v_{i+1}}}}}{k_{i+1} A_{i+1}}\right) \tag{32}$$

$$ML_i = x_{0_j} + \int \frac{p_{m_j}}{I_{m_j}} dt - x_{0_{j-1}} - \int \frac{p_{m_{j-1}}}{I_{m_{j-1}}} dt \tag{33}$$

where x_0 is the initial location of each boundary (node) in the global axis.

To modulate the mechanical resistance R_m, as shown in Fig. 5 the mechanical *RS*-components are replaced by the *MRS*-component as:

$$MR_{m_i} = R_{m_{0_i}} - B_i T_{0_i}\left(e^{\frac{\alpha_i A_i E_i}{C_{v_i}} q_{m_i}} e^{\frac{\left(q_{th_i} - S_{0_i}\right)}{C_{v_i}}} - 1\right) \tag{34}$$

where R_{m_0} is the related viscosity parameter at room temperature, and B_i is the correlative function of temperature.

3.5. Thermo-viscoelastic final model

By incorporating the proposed reversible and irreversible interactions together with the presented modulations shown in Fig. 5, the final state equations of the system are extracted as:

$$\begin{aligned} \dot{p}_{m_j} = A_i E_i \frac{q_{m_i}}{L_i} - A_{i+1} E_{i+1} \frac{q_{m_{i+1}}}{L_{i+1}} + \alpha_i A_i E_i T_{0_i}\left(e^{\frac{\alpha_i A_i E_i}{C_{v_i}} q_{m_i}} e^{\frac{\left(q_{th_i} - S_{0_i}\right)}{C_{v_i}}} - 1\right) - \\ \alpha_{i+1} A_{i+1} E_{i+1} T_{0_{i+1}}\left(e^{\frac{\alpha_{i+1} A_i{}^{+1} E_{i+1}}{C_{v_{i+1}}} q_{m_{i+1}}} e^{\frac{\left(q_{th_{i+1}} - S_{0_{i+1}}\right)}{C_{v_{i+1}}}} - 1\right) \end{aligned} \tag{35}$$

$$\dot{q}_{m_i} = \frac{p_{m_{j-1}}}{I_{m_{j-1}}} - \frac{p_{m_j}}{I_{m_j}} - \frac{A_i E_i q_{m_i}}{MR_{m_i} L_i} \tag{36}$$

$$\begin{aligned} \dot{q}_{th_i} = \frac{1}{MR_{th_{j-1}}}\left(T_{0_{i-1}} e^{\frac{\alpha_{i-1} A_{i-1} E_{i-1}}{C_{v_{i-1}}} q_{m_{i-1}}} e^{\frac{\left(q_{th_{i-1}} - S_{0_{i-1}}\right)}{C_{v_{i-1}}}} - T_{0_i} e^{\frac{\alpha_i A_i E_i}{C_{v_i}} q_{m_i}} e^{\frac{\left(q_{th_i} - S_{0_i}\right)}{C_{v_i}}}\right) - \\ \frac{1}{MR_{th_j}}\left(T_{0_i} e^{\frac{\alpha_i A_i E_i}{C_{v_i}} q_{m_i}} e^{\frac{\left(q_{th_i} - S_{0_i}\right)}{C_{v_i}}} - T_{0_{i+1}} e^{\frac{\alpha_{i+1} A_i{}^{+1} E_{i+1}}{C_{v_{i+1}}} q_{m_{i+1}}} e^{\frac{\left(q_{th_{i+1}} - S_{0_{i+1}}\right)}{C_{v_{i+1}}}}\right) + \end{aligned} \tag{37}$$

$$\frac{T_{0_i} e^{\frac{\alpha_i A_i E_i}{C_{v_i}} q_{m_i}} e^{\frac{\left(q_{th_i} - S_{0_i}\right)}{C_{v_i}}}}{MR_{th_{j-1}}} \left(\frac{T_{0_{i-1}} e^{\frac{\alpha_{i-1} A_{i-1} E_{i-1}}{C_{v_{i-1}}} q_{m_{i-1}}} e^{\frac{\left(q_{th_{i-1}} - S_{0_{i-1}}\right)}{C_{v_{i-1}}}}}{T_{0_i} e^{\frac{\alpha_i A_i E_i}{C_{v_i}} q_{m_i}} e^{\frac{\left(q_{th_i} - S_{0_i}\right)}{C_{v_i}}}} - 1 \right)^2 + \frac{\left(\frac{A_i E_i}{L_i} q_{m_i}\right)^2}{MR_{m_i} T_{0_i} e^{\frac{\alpha_i A_i E_i}{C_{v_i}} q_{m_i}} e^{\frac{\left(q_{th_i} - S_{0_i}\right)}{C_{v_i}}}}$$

where the indexes *m* and *th* are used to indicate the elastic and thermal parameters, respectively. Eqs. (35)-(37) form the final set of governing equations sufficient for describing the ongoing thermo-viscoelastic phenomena of the system based on energy conservation. As revealed in Eq. (35), the momentum rate of each element's boundary now reversibly (via q_{th}) depends on the temperature of the adjacent elements. Also, it is seen in Eq. (36) that the deformation rate of each element is irreversibly (via MR_m) dependent on the element temperature. Similar to the elastic subdomain, Eq. (37) reveals that the entropy rate of the system is reversibly (via q_m) and irreversibly (via MR_m and MR_{th}) related to the deformation of the system.

4. Energy-based convective flow model

To generate a physically-decomposed model of the fluid field, a simplified version of the energy-based modeling technique proposed in [25] is employed, with which the governing equations of a 1D compressible convective field are extracted for an ideal gas. Sequentially, the convective field is decomposed with respect to the general physical states, the decomposed power structure of the system is presented by means of the BG notation, the correctness of the generated BG model is checked via causality allocation, the state equations corresponding to the generated BG are extracted, and finally the potential functions together with the resistive and coupling coefficients are defined.

4.1. Physical decomposition of the fluid field

Consider the 1D discretized duct with flexible wall shown in Fig. 1 in which compressible air can transfer alongside the duct. Since the model is supposed to be used in multiple-field dynamic investigations, the domain-independency of the model is of interest. As so, the general physical states: mass m, entropy S, and volume V are selected with their corresponding potentials: mass potential μ, temperature T, and pressure P. Considering the selected conjugate variables, the flow field is physically decomposed to mass subdomain, potential subdomain (acoustic subdomain), and thermal subdomain, all of which can reversibly and irreversibly interact with each other. It should be mentioned that, in addition to the considered physical subdomains, there may exist the

velocity-momentum subdomain additional to the decomposed structure of the system [25]; however, since the main aim of this study is to clarify the entropic interaction of the interface via the BG method, this additional subdomain is omitted here to avoid unnecessary complexity.

Considering the chosen physical decomposition and the existing energetic component of the fluid field [25], the junction structure of the 1D flexible duct can be presented by Fig. 6. As can be seen, each segment (element) is the location of the energy storage component (capacitor) that provides the memory of the system. Each connecting junction is the location for the resistive components of which the parameters are a function of both material and geometrical parameters of the adjacent segments.

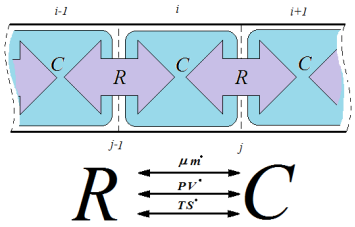

Fig.6 Decomposed 1D fluid field

Given that among the subdomains the reversible connections occur in the capacitors and the irreversible non-return interactions occur in the resistors, the general frame for the power structure of the system in the BG notation is depicted in Fig. 7. As can be seen, the total power of the system is decomposed into three separate power lines representing the energy flows of each of the subdomains individually. All the considered subdomains are reversibly connected via *C*-components, and the collective flow of each subdomain can be obtained from the corresponding *0*-junctions containing the divergence and coupling terms coming from the *1*-junctions (the boundaries of segment) and the flow source terms S_{f_i}, respectively. The physical subdomains are irreversibly connected via the *RS*-components which act as non-return power transformers to the thermal subdomain. The coupling transformers (MTF_{i-j}) of the energy transportation in the *1*-junctions provide the required convective information of each of the subdomains with respect to the natural dependency of the considered physical states of the system.

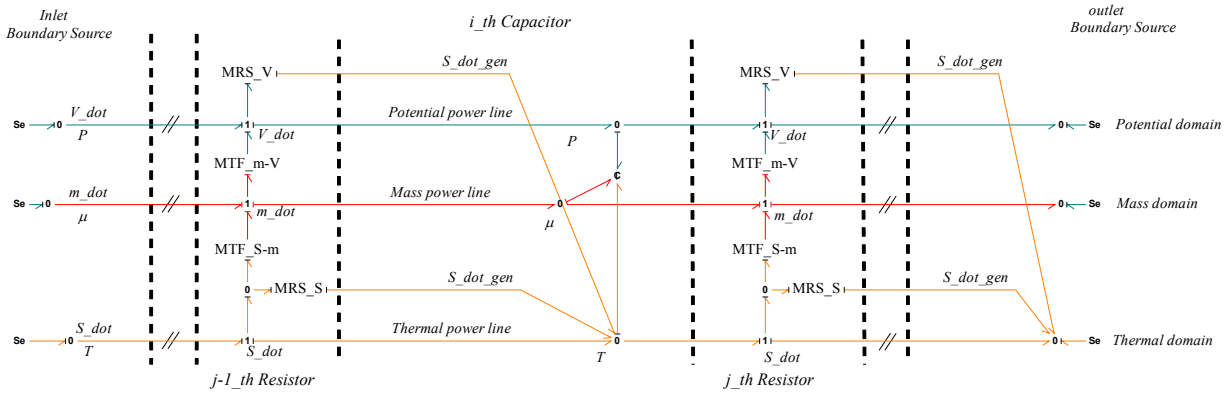

Fig.7 BG presentation of the general power structure of the fluid field of the system

The arrangement of the causality lines regarding the global conservation laws confirms the correctness of the proposed power structure. Thus, the well-posedness of the generated state equations from the obtained model is granted.

4.2. Fluid field state equations

The set of state equations corresponding to the generated power structure for the i_{th} segment can be presented as:

$$\dot{m}_i = \dot{m}_{j-1} - \dot{m}_j \tag{38}$$

$$\dot{S}_i = \dot{S}_{j-1} - \dot{S}_j + \dot{S}_{irr\ i}^{gen} \tag{39}$$

$$\dot{V}_i = \dot{V}_{j-1} - \dot{V}_j \tag{40}$$

where $\dot{x}_j$ $(x = m, V, S)$ corresponds to the introduced flow to the segment from the j_{th} spatial boundary, and $\dot{S}_{irr\ i}^{gen}$ denotes the collective generated entropy flow rate of the segment and is named as the irreversible flow. Condensing the coupling power and divergence power transported via unique flow, the flows crossing the j_{th} boundary of i_{th} segment are then defined as:

$$\dot{m}_j = \frac{1}{M_{TF_{m-V}\,j}} \frac{1}{R_{V\,j}} \left(P_i - P_{i+1} + \frac{1}{M_{TF_{m-V}\,j}} \left(\mu_i - \mu_{i+1} + M_{TF_{S-m}\,j} (T_i - T_{i+1}) \right) \right) \tag{41}$$

$$\dot{S}_j = \frac{T_i - T_{i+1}}{R_{S\,j}} + M_{TF_{S-m}\,j} \frac{1}{M_{TF_{m-V}\,j}} \frac{1}{R_{V\,j}} \left(P_i - P_{i+1} + \frac{1}{M_{TF_{m-V}\,j}} \left(\mu_i - \mu_{i+1} + M_{TF_{S-m}\,j} (T_i - T_{i+1}) \right) \right) \tag{42}$$

$$\dot{V}_j = \frac{1}{R_{V_j}}\left(P_i - P_{i+1} + \frac{1}{M_{TF_{m-V_j}}}\left(\mu_i - \mu_{i+1} + M_{TF_{S-m_j}}(T_i - T_{i+1})\right)\right) \tag{43}$$

Knowing that the dissipated power is transferred to the thermal subdomain via generated entropy rate of each subdomain, by considering the resistive components of each subdomain as an ideal non-return transducer, the irreversible flow to the thermal subdomain can be calculated as:

$$\dot{S}_{irr}^{gen}{}_i = \dot{S}_V^{gen}{}_i + \dot{S}_S^{gen}{}_i \tag{44}$$

where:

$$\dot{S}_V^{gen}{}_i = \frac{1}{T_i}\frac{(P_{i-1} - P_i)^2}{R_{V_{j-1}}} \tag{45}$$

$$\dot{S}_S^{gen}{}_i = \frac{1}{T_i}\frac{(T_{i-1} - T_i)^2}{R_{S_{j-1}}} \tag{46}$$

By defining the potentials, coupling factors, and dissipative coefficients as functions of the state variables ($x = m, p, V, S$), material parameters (P_m), and geometrical parameters (P_g), of the segment, the state equations of the system are closed.

4.3. Fluid field potential functions

To derive the potential functionalities, considering the internal energy $U(m, V, S)$ in a conservative field, the following relations can be presented for the potentials:

$$\left(\frac{\partial U}{\partial m}\right)_{V,S} = \mu(m, p, V, S) \tag{47}$$

$$\left(\frac{\partial U}{\partial V}\right)_{m,S} = P(m, V, S) \tag{48}$$

$$\left(\frac{\partial U}{\partial S}\right)_{m,V} = T(m, V, S) \tag{49}$$

To start with the thermal subdomain, considering Eq. (49), the differential form of the constitutive equation of the thermal subdomain can be presented as:

$$dT = \left(\frac{\partial T}{\partial m}\right)_{V,S} dm + \left(\frac{\partial T}{\partial V}\right)_{m,S} dV + \left(\frac{\partial T}{\partial S}\right)_{m,V} dS \tag{50}$$

Considering the energy law at constant volume and the thermal subdomain adjugate variables (T, S), the last term of Eq. (50) can be obtained as:

$$\left(\frac{\partial T}{\partial S}\right)_{m,V} = \frac{T}{mc_v} \tag{51}$$

where c_v is the specific heat in constant volume. Considering the first thermodynamics law for an ideal gas, the second term of Eq. (50) can be defined as:

$$\left(\frac{\partial T}{\partial V}\right)_{m,S} = -\frac{RT}{Vc_v} \tag{52}$$

Finally the first term of Eq. (50) with respect to the Gibbs equation for an ideal gas is presented as:

$$\left(\frac{\partial T}{\partial m}\right)_{V,S} = \frac{T}{c_v}\left(\frac{R}{m} - \frac{S}{m^2}\right) \tag{53}$$

By substituting Eqs. (51-(53) into Eq. (50) and integrating the obtained complete differential equation, the constitutive equation of the thermal subdomain for the i_{th} segment is obtained as:

$$T_i = T_{0_i}\left(\frac{V_{0_i} m_i}{m_{0_i} V_i}\right)^{\frac{R}{c_v}} e^{\frac{\left(\frac{S_i}{m_i} - \frac{S_{0_i}}{m_{0_i}}\right)}{c_v}} \tag{54}$$

where T_0, m_0, V_0, and S_0 are the reference temperature, mass, volume, and entropy, respectively.

Similar to the thermal subdomain, the differential form of the potential subdomain (P, V) constitutive equation can be written as:

$$dP = \left(\frac{\partial P}{\partial m}\right)_{V,S} dm + \left(\frac{\partial P}{\partial V}\right)_{m,S} dV + \left(\frac{\partial P}{\partial S}\right)_{m,V} dS \tag{55}$$

Given the reversible interactions between the subdomains in storage components and the fact that reciprocal relations do exist between the partial differential terms of the constitutive equations, one has:

$$\left(\frac{\partial P}{\partial S}\right)_{m,V} = \left(\frac{\partial T}{\partial V}\right)_{m,S} = -\frac{RT}{Vc_v} \tag{56}$$

$$\left(\frac{\partial P}{\partial V}\right)_{m,S} = \frac{P(R + c_v)}{Vc_v} \tag{57}$$

$$\left(\frac{\partial P}{\partial m}\right)_{V,S} = P\,\frac{1}{m}\left(\frac{S}{c_v m} - \frac{R}{c_v} - 1\right) \tag{58}$$

Substituting Eqs. (56)-(58) into Eq. (55) and integrating, the constitutive equation of the potential subdomain for the i_{th} segment is obtained as:

$$P_i = P_{0_i}\left(\frac{V_{0_i} m_i}{m_{0_i} V_i}\right)^{\frac{R-c_v}{c_v}} e^{\frac{\left(\frac{S_i}{m_i}-\frac{S_{0_i}}{m_{0_i}}\right)}{c_v}} \tag{59}$$

To define the mass potential, μ, considering the Gibbs-Duhem relation, $md\mu, = VdP - SdT$, the deferential form of the Gibbs free energy is presented as:

$$\begin{aligned} d\mu = &\left(\frac{V}{m}\left(\frac{\partial P}{\partial m}\right)_{V,S} - \frac{S}{m}\left(\frac{\partial T}{\partial m}\right)_{V,S}\right) dm + \left(\frac{V}{m}\left(\frac{\partial P}{\partial V}\right)_{m,S} - \frac{S}{m}\left(\frac{\partial T}{\partial V}\right)_{m,S}\right) dV \\ &+ \left(\frac{V}{m}\left(\frac{\partial P}{\partial S}\right)_{m,V} - \frac{S}{m}\left(\frac{\partial T}{\partial S}\right)_{m,V}\right) dS \end{aligned} \tag{60}$$

From an extensive but straightforward analysis with respect to the obtained partial derivatives, μ, is defined as:

$$\mu_i = \frac{\mu_{0_i}}{\left(R - \frac{S_{0_i}}{m_{0_i}}\right)}\left(\left(c_v - \frac{S_i}{m_i}\right)\left(\frac{V_{0_i} m_i}{m_{0_i} V_i}\right)^{\frac{R}{c_v}} e^{\frac{\left(\frac{S_i}{m_i}-\frac{S_{0_i}}{m_{0_i}}\right)}{c_v}} + c_v\right) \tag{61}$$

Collectively Eqs. (54), (59), and (61) form the constitutive equations of the fluid field with which the reversible interactions among the subdomains occur in each segment.

4.4. Fluid field coupling factors

To define the transformation coupling factors appearing in the state equations, using the Gibbs-Duhem equation to relate the potential gradient of the existing subdomain for adjacent boundaries of the neighboring segments (storages) [13], the transformation coupling factors can be obtained from the ratio of the reversible transportation flow of the subdomain to the flow of matter, which in principal are the weighted functions of the intensive form of the state variable of each subdomain. Considering the simple mean functionality, one has:

$$M_{TF_{m-V_j}} = \frac{1}{2}\left(\frac{V_i}{m_i} + \frac{V_{i+1}}{m_{i+1}}\right) \tag{62}$$

$$M_{TF_{S-m_j}} = \frac{1}{2}\left(\frac{S_i}{m_i} + \frac{S_{i+1}}{m_{i+1}}\right) \tag{63}$$

4.5. Fluid field dissipative mechanism

Finally, to close the state equations, the dissipative mechanisms of the field, namely, R_s and

R_V, need to be defined. Considering the Fourier conduction equation, for the chosen system, R_s can be presented as:

$$R_{s_j} = \frac{\Delta x_j \frac{T_i + T_{i+1}}{2}}{k_{T_j} A_j} \tag{64}$$

where Δx and k_T are the generalized length of the resistive component and conduction coefficient of the gas, respectively.

Since the dissipation of energy in the potential subdomain occurs as a result of geometrical changes (expansion or contraction) in the direction of the power flow, by considering a quadratic relation between the pressure difference and volumetric flow, $\Delta P = \rho \dot{V}^2 / 2A_d^2$, R_V can be defined as:

$$R_{V_j} = sign(\dot{V}_j) \frac{(m_i + m_{i+1})|\dot{V}_j|}{2A_{d_j}^2 (V_i + V_{i+1})} \tag{65}$$

where A_d is the actual cross section area and can be defined with respect to the geometry of the spatial boundary and the local pressure loss coefficient, ξ , as $A_d = \xi A$.

Accordingly, all the required coefficients appearing in the state equations of the fluid field of the system are defined using the material and geometrical parameters and the states of the system. In this model, the decomposed power trans*port*ation as well as the decomposed power trans*form*ation provide a distinctive power distribution of the fluid field with which the possible power connection gates to other physical subdomains are clarified.

5. Aerothermoviscoelastic model

The fluid and solid field models, using the arrangement of the energetic components of both fields, can be conservatively connected *if* the generated power gates (energy line) of the counterpart physical subdomains of both fields are connected on the interface. For the chosen system, there exist two different interfaces. The first interface is the boundary interface where both mechanical and thermal power can be exchanged. The second interface is the side interface where only thermal power can be transmitted between the fields. In the following, the continuous power connections for each of these two possible energy gates are developed.

5.1. Boundary-element interface energetic connections

For the chosen system, as depicted in Fig. 8, the energetic interactions between the two fields can occur on the interfaces of the left and right boundary elements, as well as the side interface of each segment (element). To define the energetic connections of the boundary elements, consider the generated BG models of the solid (Fig. 5) and fluid (Fig. 7) sides' of the interface. The conservative power connections of these two models can be achieved via, respectively, connecting the thermal and elastic energy lines of the solid model with the thermal and acoustic energy lines of the fluid model, as illustrated in Fig. 9.

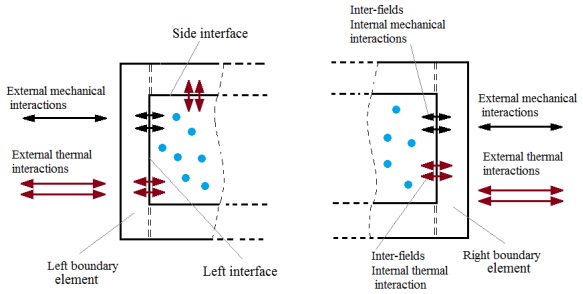

Fig.8 Interface energetic interactions

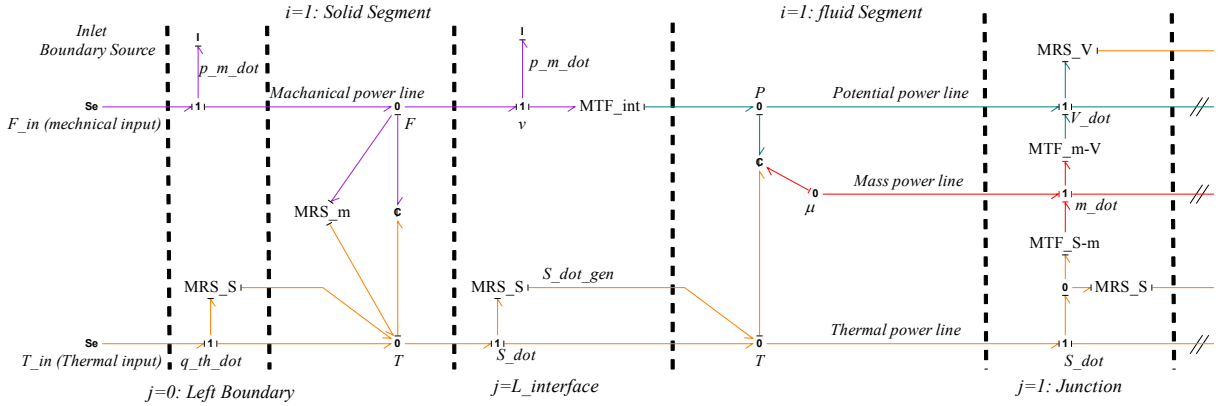

Fig.9 Left boundary element combined BG model

Considering the obtained BG model, the state equations for the boundary elements of each field are required to be refined with respect to the added connectivity of the model. For the solid field, since the left boundary interface of the chosen system is located at the second junction of the model and each junction is indexed after each segment in the junction structure (i-j-i+1-j+1), the refined boundary-element state equations are presented as:

$$\dot{p}_{m_1} = A_1 E_1 \frac{q_{m_1}}{L_1} + \alpha_1 A_1 E_1 T_{0_1} \left(e^{\frac{\alpha_i A_i E_i}{C_{v_i}} q_{m_i} e^{\frac{(q_{th_i} - S_{0_i})}{C_{v_i}}} - 1} \right) - M_{TF_{int}} P_{0_1} \left(\frac{V_{0_1} m_1}{m_{0_1} V_1} \right)^{\frac{R - C_v}{C_v}} e^{\frac{\left(\frac{S_1}{m_1} - \frac{S_{0_1}}{m_{0_1}}\right)}{C_v}} \quad (66)$$

$$\dot{q}_{m_1} = \frac{p_{m_0}}{I_{m_0}} - \frac{p_{m_1}}{I_{m_1}} - \frac{A_1 E_1 q_{m_1}}{M R_{m_1} L_1} \tag{67}$$

$$\dot{q}_{th_1} = \frac{1}{M R_{th_0}} \left(T_{in} - T_{0_1} e^{\frac{\alpha_1 A_1 E_1}{C_{v_1}} q_{m_1}} e^{\frac{\left(q_{th_1} - S_{0_1}\right)}{C_{v_1}}} \right) - \frac{1}{M R_{th_{int}}} \left(T_{0_1} e^{\frac{\alpha_1 A_1 E_1}{C_{v_1}} q_{m_1}} e^{\frac{\left(q_{th_1} - S_{0_1}\right)}{C_{v_1}}} - T_{0_{1_f}} \left(\frac{V_{0_1} m_1}{m_{0_1} V_1} \right)^{\frac{R}{c_v}} e^{\frac{\left(\frac{S_1}{m_1} - \frac{S_{0_1 f}}{m_{0_1}}\right)}{c_v}} \right) + \frac{T_{0_1} e^{\frac{\alpha_1 A_1 E_1}{C_{v_1}} q_{m_1}} e^{\frac{\left(q_{th_1} - S_{0_1}\right)}{C_{v_1}}}}{M R_{th_0}} \left(\frac{T_{in}}{T_{0_1} e^{\frac{\alpha_1 A_1 E_1}{C_{v_1}} q_{m_1}} e^{\frac{\left(q_{th_1} - S_{0_1}\right)}{C_{v_1}}}} - 1 \right)^2 + \frac{\left(A_1 E_1 \frac{q_{m_1}}{L_1}\right)^2}{M R_{m_1} T_{0_1} e^{\frac{\alpha_1 A_1 E_1}{C_{v_1}} q_{m_1}} e^{\frac{\left(q_{th_1} - S_{0_1}\right)}{C_{v_1}}}} \tag{68}$$

where the *f* and *int* indexes denote the fluid and interface variables, respectively.

For the fluid field, since the left interface is located at the left boundary of the first segment ($j = 0$), the terms to be refined in the state equations are the terms with the index $j = 0$. Therefore, the state equations of the left boundary are defined as:

$$\dot{m}_{i=1} = \dot{m}_{j=0} - \dot{m}_{j=1} \tag{69}$$

$$\dot{S}_{i=1} = \dot{S}_{j=0} - \dot{S}_{j=1} + \dot{S}^{gen}_{irr\ i=1} \tag{70}$$

$$\dot{V}_{j=1} = \dot{V}_{j=0} - \dot{V}_{j=1} \tag{71}$$

with the following collective flows coming from the interface:

$$\dot{m}_{j=0} = 0 \tag{72}$$

$$\dot{S}_{j=0} = \frac{T_{i=1_S} - T_{i=1_f}}{R_{S_{int}}} \tag{73}$$

$$\dot{V}_{j=0} = M_{TF_{int}} \frac{p_{m_{j=1}}}{I_{m_{j=1}}} \tag{74}$$

where $M_{TF_{int}}$ and $R_{S_{int}}$ are the interface reversible coupling factor (between the elastic and acoustic subdomains) and the interface resistive parameter, respectively; index *S* specify the temperature of the solid field. Considering the continuous power transformation between the elastic and acoustic subdomains, $M_{TF_{int}}$ for the chosen system is obtained as:

$$M_{TF_{int}} = A_{L-int} \tag{75}$$

where A_{L-int} is the left boundary element area touched by the fluid. Considering the mutual relevancy of the transported entropy to the resistive parameters of both fields as a weighted

function of the dissipated mechanisms of the adjacent elements connected via interface, using a simple functionality, $R_{S_{int}}$ can be obtained as:

$$R_{S_{int}} = \frac{1}{2}\frac{\Delta x_{j=1_S}}{k_{j=1_S} A_{L-int}}\frac{T_{i=1_S} + T_{i=1_f}}{2} + \frac{1}{2}\frac{\Delta x_{j=1_f}}{h\, A_{L-int}}\frac{T_{i=1_S} + T_{i=1_f}}{2} \tag{76}$$

where h is the convection coefficient of the fluid field. To calculate the terms related to the right boundary of the first segment ($j = 1$), Eqs. (41)-(43) are employed. For simplicity, consider the reversible mechanical interaction at the interface. The entropy generation rate of the first segment is defined as:

$$\dot{S}_{irr\ i=1}^{gen} = \frac{1}{T_{i=1_f}}\frac{\left(T_{i=1_S} - T_{i=1_f}\right)^2}{R_{S_{int}}} \tag{77}$$

Thus, the right spatial boundary of the first solid segment is energetically connected to the left spatial boundary of the first fluid segment.

For the right boundary interface, the connection scenario is the same. Via the generated connections, the distinctive mechanical power and thermal power exchanges between the two fields become possible. It should be mentioned that, in cases where the momentum subdomain of the fluid field needs to be considered, there will be more energetic connections between the subdomains of the two fields that can be defined using similar procedures. Since the aim of this paper is to introduce the proposed methodology, further connections to include the momentum subdomain following the demonstrated principles are omitted here for simplicity.

5.2. Side interface energetic connections and the VIDA method

By omitting the momentum subdomain of the fluid field, only the axial motion of the system is of concern. The energetic interactions of the side interface are then limited to the thermal power exchange via the side interface of each segment. The condition to generate this connectivity is the geometrical compatibility of the thermal resistive component [22] of both fields on the side interface. The mentioned compatibility is automatically satisfied for the boundary element interface, as the geometrical parameters of the resistive components of the fluid and solid thermal subdomains remain unchanged. However, for the side interface, the situation is different. As a result of the longitudinal elastic behavior of the solid field (resulted from, e.g., external mechanical

loads, or thermal expansion, or both), the side interface of the solid field can be variable. Since the side interface of each segment is the shared spatial boundary between the Lagrangian frame for the solid field and the Eulerian frame for the fluid field (as shown in Fig. 10), to generate a conservative energetic connection between the two fields, the motion of the Lagrangian frame has to be interpreted for the Eulerian frame.

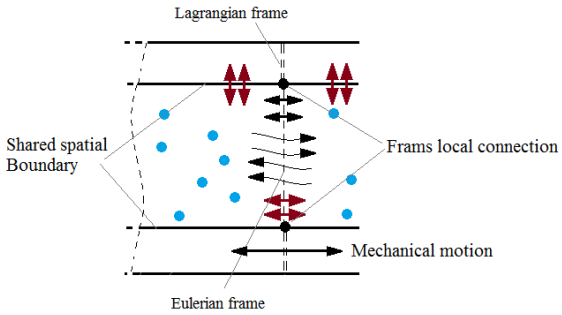

Fig.10 The connectivity of Lagrangian frame and Eulerian frame in the chosen system

To address this issue, the variable interface dynamic adaptation technique (VIDA) proposed in [19] is employed. In this method, separate convections of entropy and volume are considered in place of the only enthalpy convection proposed in [25]. By adding the capability of volume convection at each junction where motion of the attached boundary can occur, the Lagrangian frame's motion is translated into changes expressed in the Eulerian frame, as shown in Fig. 11.

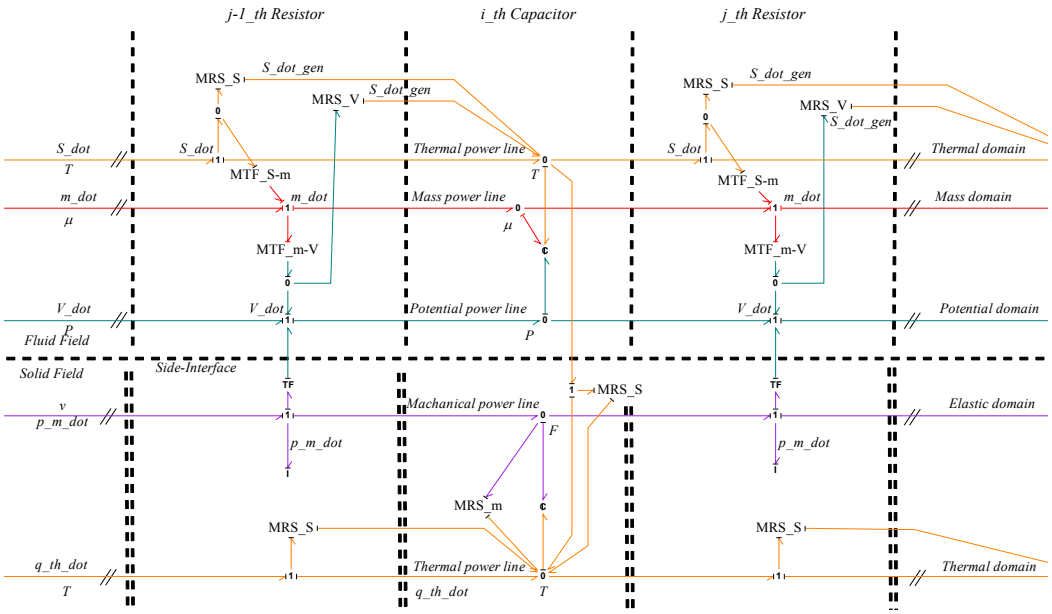

Fig.11 variable interface dynamic adaptation technique (VIDA) BG presentation

Accordingly, the motion of each junction leads to zero potential gradient matter exchange between the attached segments of the fluid field connected to that junction. As a result of this

adaptation, the geometry of the fluid filed is no longer fixed in the axial direction. As so, the shared side interface remains unique between the two fields, and the compatibility of the resistive components of the two fields on the side interface is satisfied.

By satisfying the compatibility issue, the continuous thermal power exchange between the two fields at the side interface can be simply realized by generating an energy branch between the two thermal subdomains, as shown in Fig. 11. Considering the generated thermal connection for each segment, the state equations of solid and fluid thermal subdomains are updated as follows:

$$\begin{aligned}\dot{q}_{th_i} = {} & \frac{1}{MR_{th_{j-1}}}\left(T_{0_{i-1}} e^{\frac{\alpha_{i-1}A_{i-1}E_{i-1}}{C_{v_{i-1}}} q_{m_{i-1}}} e^{\frac{(q_{th_{i-1}} - S_{0_{i-1}})}{C_{v_{i-1}}}} - T_{0_i} e^{\frac{\alpha_i A_i E_i}{C_{v_i}} q_{m_i}} e^{\frac{(q_{th_i} - S_{0_i})}{C_{v_i}}}\right) \\ & - \frac{1}{MR_{th_j}}\left(T_{0_i} e^{\frac{\alpha_i A_i E_i}{C_{v_i}} q_{m_i}} e^{\frac{(q_{th_i} - S_{0_i})}{C_{v_i}}} - T_{0_{i+1}} e^{\frac{\alpha_{i+1}A_i{+}1E_{i+1}}{C_{v_{i+1}}} q_{m_{i+1}}} e^{\frac{(q_{th_{i+1}} - S_{0_{i+1}})}{C_{v_{i+1}}}}\right) \\ & + \frac{T_{0_i} e^{\frac{\alpha_i A_i E_i}{C_{v_i}} q_{m_i}} e^{\frac{(q_{th_i} - S_{0_i})}{C_{v_i}}}}{MR_{th_{j-1}}}\left(\frac{T_{0_{i-1}} e^{\frac{\alpha_{i-1}A_{i-1}E_{i-1}}{C_{v_{i-1}}} q_{m_{i-1}}} e^{\frac{(q_{th_{i-1}} - S_{0_{i-1}})}{C_{v_{i-1}}}}}{T_{0_i} e^{\frac{\alpha_i A_i E_i}{C_{v_i}} q_{m_i}} e^{\frac{(q_{th_i} - S_{0_i})}{C_{v_i}}}} - 1\right)^2 \\ & + \frac{\left(\frac{A_i E_i}{L_i} q_{m_i}\right)^2}{MR_{m_i} T_{0_i} e^{\frac{\alpha_i A_i E_i}{C_{v_i}} q_{m_i}} e^{\frac{(q_{th_i} - S_{0_i})}{C_{v_i}}}} \\ & - \frac{1}{MR_{S-int_i}}\left(T_{0_i} e^{\frac{\alpha_i A_i E_i}{C_{v_i}} q_{m_i}} e^{\frac{(q_{th_i} - S_{0_i})}{C_{v_i}}} - T_{0_{i_f}} \left(\frac{V_{0_i} m_i}{m_{0_i} V_i}\right)^{\frac{R}{c_v}} e^{\frac{\left(\frac{S_i}{m_i} - \frac{S_{0_{i_f}}}{m_{0_i}}\right)}{c_v}}\right)\end{aligned} \tag{78}$$

$$\begin{aligned}\dot{S}_j = {} & \frac{T_i - T_{i+1}}{R_{S_j}} + M_{TF_{S-m_j}} \frac{1}{M_{TF_{m-V_j}}} \frac{1}{R_{V_j}}\left(P_i - P_{i+1} + \frac{1}{M_{TF_{m-V_j}}}\left(\mu_i - \mu_{i+1} + M_{TF_{S-m_j}}(T_i - T_{i+1})\right)\right) \\ & + \frac{1}{MR_{S-int_j}}\left(T_{0_{i_S}} e^{\frac{\alpha_i A_i E_i}{C_{v_i}} q_{m_i}} e^{\frac{\left(q_{th_i} - S_{0_{i_S}}\right)}{C_{v_i}}} - T_{0_i}\left(\frac{V_{0_i} m_i}{m_{0_i} V_i}\right)^{\frac{R}{c_v}} e^{\frac{\left(\frac{S_i}{m_i} - \frac{S_{0_i}}{m_{0_i}}\right)}{c_v}}\right) \\ & + \frac{\left(T_{0_{i_S}} e^{\frac{\alpha_i A_i E_i}{C_{v_i}} q_{m_i}} e^{\frac{\left(q_{th_i} - S_{0_{i_S}}\right)}{C_{v_i}}} - T_{0_i}\left(\frac{V_{0_i} m_i}{m_{0_i} V_i}\right)^{\frac{R}{c_v}} e^{\frac{\left(\frac{S_i}{m_i} - \frac{S_{0_i}}{m_{0_i}}\right)}{c_v}}\right)^2}{MR_{S-int_i} T_{0_i}\left(\frac{V_{0_i} m_i}{m_{0_i} V_i}\right)^{\frac{R}{c_v}} e^{\frac{\left(\frac{S_i}{m_i} - \frac{S_{0_i}}{m_{0_i}}\right)}{c_v}}}\end{aligned} \tag{79}$$

where MR_{S-int_i} is the modulated side interface resistivity defined as:

$$MR_{S-int_i} = \frac{\Delta y_i \frac{T_{i_s} + T_{i_f}}{2}}{h_i \, A_{S-int_i}} \tag{80}$$

where Δy is the generalized side resistor length, and A_{S-int} is the variable side interface obtainable from the instantaneous location difference of the junction boundaries of each segment as:

$$A_{S-int_i} = b_{S-int_i}(L_{0_i} + \int \left(\frac{p_{m_j}}{I_{m_j}} - \frac{p_{m_{j-1}}}{I_{m_{j-1}}}\right) dt) \tag{81}$$

with b_{S-int_i} denoting the width of the segment and *t* being the representative of time.

Collectively, for the chosen system, the side interface connections and the boundary interface connections form a conservative power exchange frame between the two fields, in which according to the considered situation all the internal energetic interactions are distinctively tractable.

6. Simulation and analysis

In this section, to highlight the capability of the generated model in demonstrating the interactive dynamics of the coupled fields, a simple vacuum injection is chosen to be investigated via simulating the transient behavior of the chosen system (shown in Fig. 1). For simplicity, it is considered that the chosen duct is uniformly discretized into 6 segments, and the axial dynamics for the lumped presentation of the system with the material and geometrical parameters listed in Table 1 is to be investigated. Also, it is assumed that initially the system is relaxed in room temperature.

Table 1. Geometrical and material properties of the convective duct

$\boldsymbol{l}$	Length	$\boldsymbol{2.1e^{-1}}$ $(\boldsymbol{m})$
$\boldsymbol{A}$	Cross section area	$1e^{-4}$ (m^2)
$\boldsymbol{n}$	Number of segments	6
$\boldsymbol{P_0}$	Initial pressure	101315 (pa)
$\boldsymbol{T_0}$	Initial temperature	298 (k)
$\boldsymbol{R}$	Individual gas constant	286.9 $(J/kg/K)$
$\boldsymbol{c_P}$	Specific heat capacity @ P_{cte}	1005 $(J/kg/K)$
$\boldsymbol{c_V}$	Specific heat capacity @ V_{cte}	718 $(J/kg/K)$
$\boldsymbol{k}$	Air conduction coefficient	$2.57e^{-2}$ $(J/m/K/s)$
$\boldsymbol{\mu_p}$	Air viscosity	$5.81e^{-5}$ $(kg/m/s)$
$\boldsymbol{k}$	Conduction coefficient	$(2.73e^2 J/m.K)$
$\boldsymbol{E}$	Young modulus	$6.9e^{10}$ (N/m^2)
$\boldsymbol{C_v}$	Specific heat	$8.97e^2(J/Kg.K)$
$\boldsymbol{\alpha}$	Linear expansion	$2.22e^{-5}(1/K)$
$\boldsymbol{S_0}$	Reference Entropy	$2.83e^1(J/Kg.K)$
$\boldsymbol{m}$	Beam mass	$5.67e^{-2}(Kg)$
$\boldsymbol{A}$	Cross section area	$1e^{-4}(m^2)$
$\boldsymbol{l}$	Length	$2.1e^{-1}(m)$
$\boldsymbol{M}$	Molar mass	$2.698e^{-2}(kg/mol)$

According to the considered scenario, the isolated fixed structure initially in equilibrium with its containing atmospheric gas is injected in a vacuum chamber under zero gravity situation. The expected behavior of the system, for the solid field, is the expansion accompanied by stress wave propagation and, for the fluid field, is the propagation of acoustic waves inside the system.

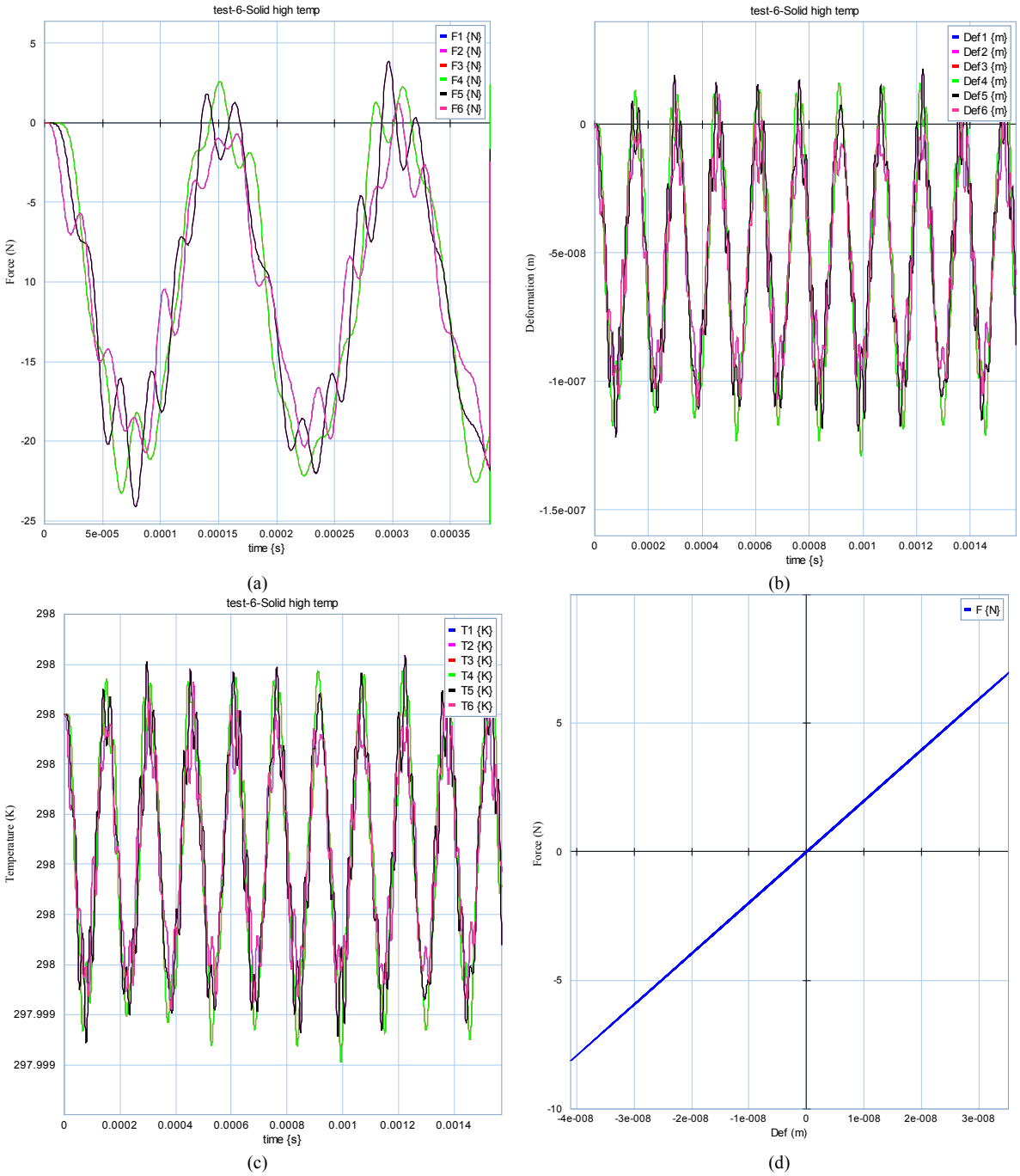

Fig.12 Internal dynamics of solid field

In Fig. 12 the resultant internal dynamics of the solid field is presented. Parts (a) and (b) demonstrate the internal deformation and the resultant tension of each solid element, respectively. Considering that the contraction of each element is positive, it is seen that each element responding to the existing pressure difference between the inside and outside of the duct tends to be expanded initially; however the generated tension returns the element to its initial size. A closer look into the profile of the generated internal tension indicates a generated stress wave inside the structure which is the result of the speed of the injection process. The corresponding temperature fluctuation of the solid field is presented in Part (c). One can see that the pattern of this fluctuation follows the pattern of behaviors of the elastic subdomain, which reflects the coupled thermoelastic dynamics of the solid field. In Part (d) the general energetic behavior of the system is presented. It is clear that for the considered material (aluminum-like material) this fluctuation remains in the elastic range. In general, one can see that in spite of the rough discretization, the physically-generated model for the solid field can demonstrate an acceptable presentation of the ongoing dynamics of the field.

In Fig. 13 the internal dynamics of the fluid field is presented. Parts (a) and (b) demonstrate the behavior of the potentials and extensive states of the fluid field. The expected acoustic wave propagation in the field is clearly shown. A closer look to the initial stages of the process highlights the propagation of a negative pressure and temperature wave responding to the initially expanded structure, which indicates the compatibility of the dynamic behavior between the two fields. In Part (c) the profile of the matter flow crossing the spatial boundary of the first and last segments of the fluid field is presented. Considering the positive direction to the right, the symmetry of the flow in the system at the initial time is clear shown, which indicates a symmetrical expansion of the system as expected; however, this trend dose not last long as a result of the existing nonlinearity of the system. In Part (d) the irreversible power transaction of the fluid field is presented. Since there is no significant external excitation to the system, the magnitude of the irreversibility of the system as compared with the other obtained values is seen to be negligible. However, simulation studies reveal that this presented irreversibility of the system in actual fact plays a critical role in stabilizing the model naturally, as ignoring this amount would lead to a complete failure of the simulation. In general, one can clearly see the capability of the generated model in capturing the complex dynamic behavior and ongoing phenomena of the fluid field regardless of the coarse discretization and simple functionalities used in the simulation.

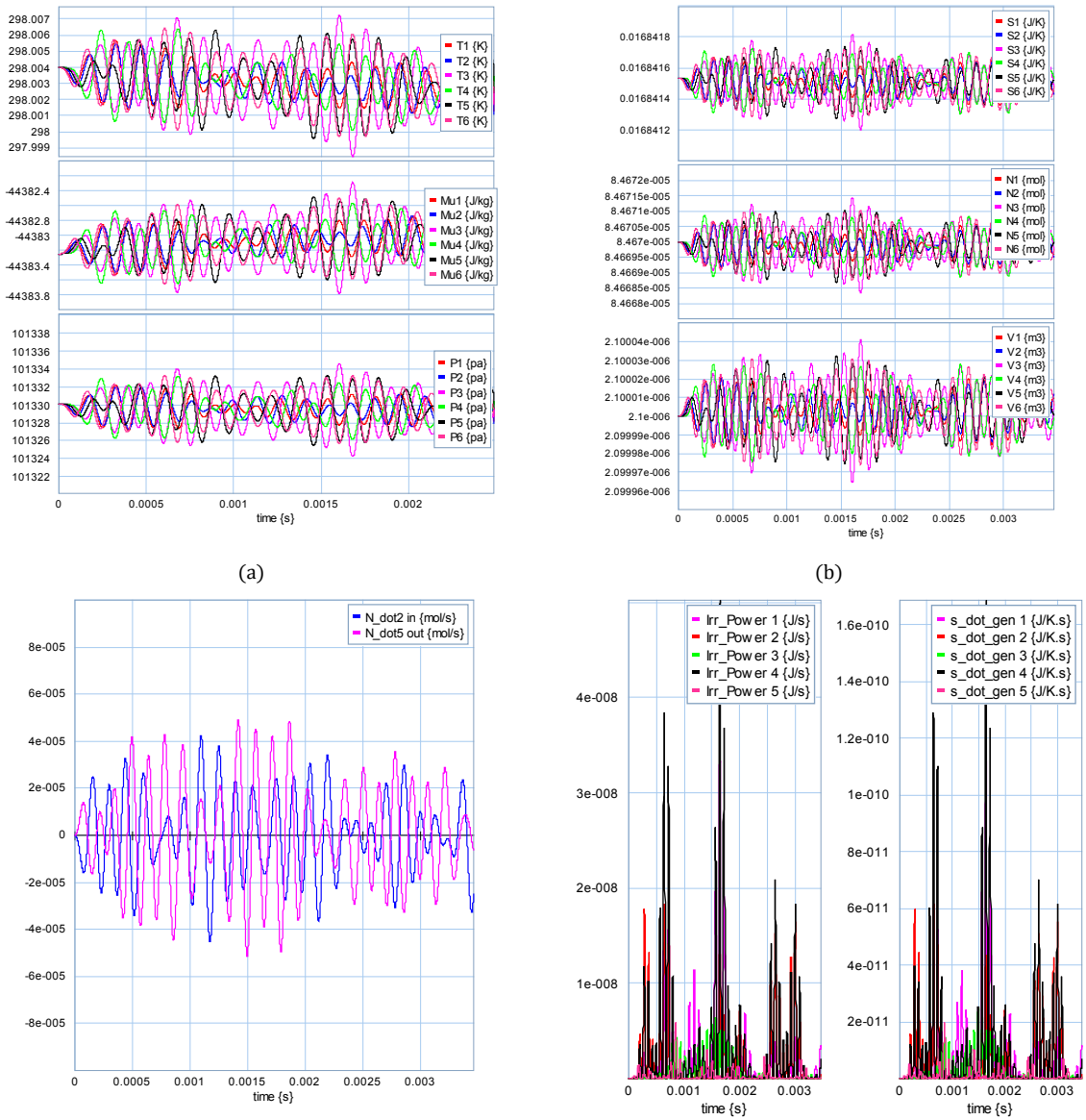

Fig.13 Internal dynamics of the fluid field

The results presented in Fig. 12 and Fig. 13 are the internal dynamics of the system as a result of the inter-field reversible and irreversible energetic interactions as well as the intra-field energetic interactions. The intra-field energetic interactions, which for the considered scenario is the main source for the excitation of the system, is presented in Fig. 14 that demonstrates the continuous power interactions between the fields. Part (a) shows the reversible and irreversible thermal power transportation between the thermal subdomain of the solid field and the thermal subdomain of the fluid field, considering the direction from solid to fluid being positive. Part (b) demonstrates the power transformation between the elastic subdomain of the solid field and the

acoustic subdomain of the fluid field, occurring at the left boundary element interface. A comparison between Part (a) and Part (b) reveals different transaction patterns between the thermal energy and the elastic energy. This indicates the different existing dynamics for the present subdomains. Although the amount of thermal power transaction between the two fields seems to be negligible in comparison with the amount of elastic-acoustic power transformation between the two fields, its impact on the general dynamics of the fluid field may not be ignored as it has a direct influence on the formation of acoustic interactive power. Given the highly-nonlinear nature of the fluid field, overlooking this amount of transferred energy may result in some unexplained behaviors of the system.

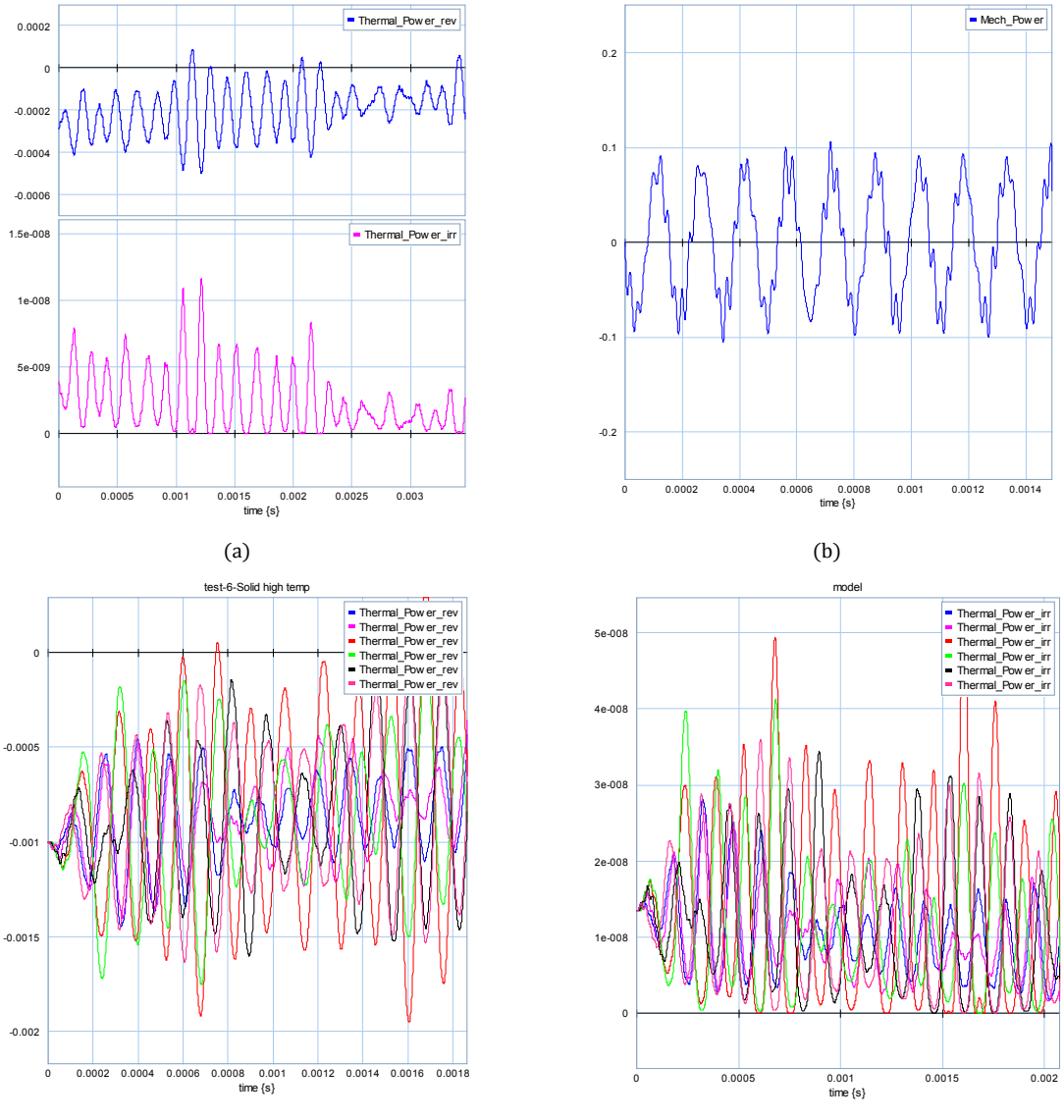

Fig.14 Interface dynamic power interactions

In Parts (c) and (d) the side-interface reversible and irreversible thermal interactions are presented, respectively. Since the system was initially in equilibrium, one can consider the different dynamic levels of the two fields as the main cause for the side-interface thermal power transactions. Given that the propagated stress wave in the solid field travels with a different speed than the acoustic and thermal waves in the fluid field, the temperature profiles for both of the fields alongside the duct are not analogous. Thus, temperature gradient is generated on the side interface causing the side-interface power transactions of the system.

7. Conclusion

In the current study, via physical decompositions of the fluid and solid fields, an energy-based coupled aerothermoviscoelastic model is proposed in which the general behavior of the system can be obtained on the basis of the energetic interactions of the present physical subdomains. This modeling technique can provide a conservative power network of the system with separate energy lines dedicated to each of the physical subdomains of the two fields, and clear identifications of reversible and irreversible power interactions within and between the fields.

The individual models of the fluid and solid fields are all domain-independent. This feature of modeling allows the development of a unique interface structure with which the power transformations between the two fields can be performed in a handshake manner. This capability of the proposed coupled model offers a greater physical insight into the system, thus a better explanation of the dynamic behavior of the system. It also provides a useful platform based on which control strategy development and energy management planning can be facilitated.

As the proposed methodology does not rely on imposed assumptions and mathematical constraints, the model thus generated would have a much wider valid range than those developed using more traditional means. The proposed strategy has the potential to be extended to modeling more complicated systems and to be used for discovering unknown phenomena previously hidden with existing classical physical knowledge.

References

[1] J. J. McNamara, P. P. Friedmann, "Aeroelastic and Aerothermoelastic Analysis of Hypersonic Vehicles: Current Status and Future Trends," in *48th AIAA/ASME/ASCE/AHS/ASC Structures, Structural Dynamics, and Materials Conference*, Honolulu, Hawaii, 23 - 26 April 2007.

[2] J. Bertin, Hypersonic Aerothermodynamics, AIAA, 1994.

[3] J. D. Anderson, Hypersonic and High Temperature Gas Dynamics, New York: McGraw-Hill, 1989.

[4] A. Frendi, "Coupling Between a Supersonic Turbulent Boundary Layer and a Flexible Structure," *AIAA Journal,* vol. 35, no. 1, pp. 28-66, 1997.

[5] W. R. Graham, "A comparison of models for the wavenumber–frequency spectrumof turbulent boundary layer pressures," *Journal of Sound and Vibration ,* vol. 206, p. 541–565, 1997.

[6] J. J. McNamara, P. P. Friedmann, K. G. Powell, B. J. Thuruthimattam, "Aeroelastic and Aerothermoelastic Behavior in Hypersonic Flow," *AIAA Journal,* vol. 46, no. 10, pp. 2591-2610, 2008.

[7] N. J. Falkiewicz, C. E. S. Cesnik, M. A. Bolender, D.B. Doman, "Thermoelastic Formulation of a Hypersonic Vehicle Control Surface for Control-Oriented Simulation," in *AIAA Guidance, Navigation, and Control Conference*, Chicago, Illinois, August, 2009.

[8] A. J. Culler, J. J. McNamara, "Fluid-Thermal-Structural Modeling and Analysis of Hypersonic Structures under Combined Loading," in *52nd AIAA/ASME/ASCE/AHS/ASC Structures, Structural Dynamics and Materials Conference*, Denver, Colorado, April 2011.

[9] W. K. Nowacki, "Progress in Thermoelasticity," *Warszawa: European Mechanics Colloquium,* 1967.

[10] L. Daun, M. M. Choudhari, M. Wu, "Numerical Study of Pressure Fluctuations due to High-Speed Turbulent Boundary Layers," in *42nd AIAA Fluid Dynamics Conference and Exhibit*, New Orleans, Louisiana, June, 2012.

[11] A. Zanj, P. C. Breedveld, F. He, "Domain-Independent Thermoelastic Coupling Suitable for Aerothermoelastic Modeling," in *23rd International Congress on Sound and Vibration*, Athens, Greece, July, 2016.

[12] D. Juvé, M. Berton, E. Salze, "Spectral Properties of Wall-Pressure Fluctuations and Their Estimation from Computational Fluid Dynamics," *Flinivia- Flow Induced Noise and Vibration Issues and Aspects, Switzerland,* pp. 27-46, 2015.

[13] P. Breedveld, Physical System Theory In Therms of Bond graphs, Enschede, Netherland: Univercity of Twente, 1984.

[14] P. C. Breedveld, "Thermodynamic Bond Graphs and the Problem of Thermal Inertance," *Journal of the Franklin Institute,* vol. 314, no. 1, pp. 15-40, 1982.

[15] J. Thoma, Simulation by Bond graph, Verlag, Gemany: Springer, 1990.

[16] A. Mukherjee, R. Karmakar, Modeling and Simulation of Engineering Systems through Bon dgraph, New Delhi, India: Narosa Publishing House, 2000.

[17] H. Afshari, A. Zanj, "Dynamic Analysis of a Nonlinear Pressure Regulator Using Bondgraph Simulation Technique," *Journal of Simulation Modeling Practice and Theory,* 2010.

[18] A. Zanj, F. He, "A Thermomechnical Enhanced Elastic Model: Bond Graph," in *23rd International Congress on Sound & Vibration*, Athens, Greece, July, 2016.

[19] P. C. Breedveld, A. Zanj, "Bond Graph Representation of Convection by Fluid Flow Alonf an Elastic Surface," in *12th international Conference on Bond Graph Modeling and Simulation*, Montreal,Quebec, Canada, July, 2016.

[20] A. Zanj, F. He, P. C. Breedveld, "Dynamic Analysis of Thermo-viscoelasticity in Multi-Physical Systems: A Bond Graph Approach," in *IEEE International Conferernce on Systems, Man, and Cybernetics*, Budapest, October, 2016.

[21] A. Zanj, P. C. Breedveld, F. He, "Domain Independent Viscoelastic Model: A Bond Graph Approach," *Sound and vibration,* 2016. (Under Revision).

[22] A. Zanj, F. He, "Conduction Model Compatible for Multi-Physical Domain Dynamic Investigations: Bond Graph Approach," *World Academy of Science, Engineering and Technology, International Journal of Mechanical, Aerospace, Industrial, Mechatronic and Manufacturing Engineering,* vol. 10, no. 3, pp. 524-535, 2016.

[23] F. Cellier, Continuous System Modeling, New York: Springer-Verlag, 1991.

[24] A. Zanj, P. C. Breedveld, F. He, "Domain-independent Thermoelastic Modeling: a Bond Graph Approach," p. (To be published), 216.

[25] A. Zanj, P. C. Breedveld, F. He, "Energy-Based Compressible Convective model Proper for Multiple field Dynamic Investigation: A Bond Graph Approach on FSI Problems," in *58th AIAA/ASCE/AHS/ASC Structures, Structural Dynamics, and Materials Conference*, Grapevine, Texas, January, 2017.

CHAPTER 8: SUMMARY AND CONCLUSION

As discussed in the literature the classical sequential approach (on the basis of the separation assumption broadly used in aeroelastic modeling) appears to be no longer an efficient solution for newly emerged aerothermoelastic problems. In Chapter 1 it was concluded that there exists a vicious circle in the existing literature, which may be a result of the implemented assumptions of the classical aerothermoelasticity. Also, it was mentioned that the portion of the physical flavor of the phenomena (e.g., the weak connectivity) that was removed in order to generate the sequential solution, in fact, eliminates the intrinsic ability of the classical approach to check the conservation of power transactions between the present fields. Therefore, to control the data transactions between the solvers, there remains no other generic means apart from mathematical constraints that lead to dramatically expensive solutions for the problems.

In this study, to generate continuous data transactions between the fields, reviving the conservation of power transactions between the fields is proposed, with which an intrinsic physical handle is added to the solution as a controlling tool in data transactions. To this end, the fundamental of a novel integrated energy-based modeling framework is designed to replace the classical sequential phenomenon-based framework of aerothermoelasticity.

To achieve this aim, given that the satisfaction of conservation in power transactions between the fields is due to the isomorphism of the power structure of each individual field, and that the generation of the isomorphic power structure for the fluid and solid fields is unfeasible using the traditional form due largely to the fundamental differences between them, an identical decomposition of each of the fields is suggested in order to attain the required isomorphism in the sub-structural level of each field. Since physical domains (e.g., kinetic, potential, thermal, etc.) are identical in any field, each field of interest is physically decomposed into its present physical subdomains. To include the fundamental differences between the counterpart subdomains of the fluid and solid fields while developing isomorphic models for them, a domain-independent modeling strategy is suggested. To generate such models, the port-based approach with Bond Graph (BG) notation is used, by means of which the general dynamics of each subdomain are attainable from the reversible and irreversible interactions between the energetic components (e.g., capacitance, inertance, resistance) of the subdomain. Since these components are identical in any

domains, and since the energetic interactions between the energetic components follow a similar pattern, the resultant models of the different physical subdomains generated in such a way become isomorphic with each other, and thus, the energetic transactions between them becomes tractable. Accordingly, the dynamic of each field is generated from the conservative interactions between the present subdomains of each field, and the general behavior of the multiple field system is defined with respect to the conservative power transactions between the fields at the interface.

In the present study, to generate the proposed integrated energy-based domain-independent modeling framework, the following steps are performed for a simple 1-D structure:

- First, the process of generating an energy-based model by means of the BG technique is clarified in Chapter 2, which provides a general sense of the implementation of the BG technique for the current purposes.
- Next, in Chapter 3, the solid field was first decomposed into its present physical subdomains, and the energy-based domain-independent model of each physical subdomain is developed.
- In Chapter 4, by reversibly coupling the solid field's present subdomains, the reversible thermoelastic model of the solid field is developed.
- Following the above, in Chapter 5, by adding the irreversible interactions between the subdomains, the general thermoviscoelastic model of the solid field is developed.
- In Chapter 6, the fluid field is first decomposed into a set of physical subdomains identical with the solid field, and then the general energy-based model of the fluid field is developed by reversibly and irreversibly coupling of the present subdomains.
- Finally, by defining a conserved coupling between the models of the solid and fluid fields, a conserved aerothermoviscoelastic model is generated in Chapter 7 in which the general behavior of the system is developed from the conservative interactions of the existing energetic components at the subdomain level.

The outcomes of each chapter are summarized as follows:

In Chapter 2, to introduce the fundamentals of the BG technique, and to evaluate the capability of this method in multi-physical multiple-field system dynamic investigations, the start period of hydro-mechanical control devices is investigated. A new multi-model BG approach is proposed

that can provide essential insights into the multi-physical dynamic behaviors of the system. The simulation results reveal a high-degree of complexity in the system's physical behaviors, which may otherwise be overlooked by other conventional modeling methods. The revealed physical behaviors are fully agreeable with the fundamental physics underpinning the multi-physical dynamics of the system, which confirms the integrity of the resulting nonlinear model of the system. It is this distinctive feature of the proposed approach that makes the modeling of the complex systems feasible, and thus, suitable for the current study.

In Chapter 3, firstly, in order to generate a domain-independent model of the elastic subdomain, an enhanced uncoupled thermoelastic model is developed for a beam structure of a control system (spool valve) that addresses the thermomechanical phenomena present in such systems. Using the concept of an equivalent thermal source, the structural expansion behavior of the system due to thermal loading is captured, and its impact on altering the system set-point is demonstrated. By examining the elastic domain energy function at the atomic level, the concept of a modulated capacitor that complies with the energy conservation principle is proposed. Using the modulated capacitor in the system's momentum equation, the material softening behavior of the system (induced by heating) is revealed and its effect on changing the system vibration modes is illustrated. The combined thermal-source and modulated-capacitor approach makes the modeling of the system's thermomechanical dynamics in a single elastic domain possible. The presented study explains the importance of unveiling the thermomechanical phenomena as a part of the dynamic examinations of the control devices under thermal loading.

The simulation results of this first part of Chapter 3 not only confirm the validity of the suggested thermomechanical-enhanced model of the system, but also demonstrated the potential benefits of the proposed approach in accessing the system's physical details during the transient and allowing each physical behavior of the system to be examined individually. It is this latter point that offers a unique feature within the proposed approach in providing a useful tool for conceptual design, fault detection, reliability assessment, and structural optimization of other similar macro-scale control devices.

In the second part of Chapter 3, to generate a domain-independent model of the thermal subdomain of the solid field and to investigate the dynamics of heat conduction in multi-physical phenomena, a new configuration of energy components is proposed to form a domain-independent

compatible thermal element. Using this configuration in a multi-physical domain setting, the impact of the thermal subdomain dynamics on the total dynamics of the system (and vice versa) can be examined. This method provides a useful tool for the management of the energy consumptions in multi-disciplinary systems where temperature control is an important issue.

The simulation results of the second part of Chapter 3 indicate the capability of the proposed model in capturing the dynamic behavior of the thermal subdomain. The obtained results also confirm the slow and relaxing behavior of the conduction process within the system and well-match the essential features of the thermal subdomain. The simulated thermoelastic results demonstrate that despite a weak connectivity between the elastic and thermal subdomains, the proposed model is able to capture the impact of the multi-physical phenomena on the thermal subdomain, and vice versa. Furthermore, the discrete nature of the proposed thermal model in Chapter 3 ideally matches the parallel computation platforms that can reduce the required computation time significantly. This advantage can increase the likelihood of employing the proposed model in developing real-time control strategies.

In Chapter 4, an energy-based, nonlinear, coupled thermoelastic model is generated which covers the reversible interactions of the present physical subdomains of the solid field. In this model, the reversible dynamic interactions between the elastic and thermal subdomains are considered using the proposed energy conservative coupling. The generated model is capable of not only describing the dynamic behavior of the system, but also providing a useful power frame within which the energy distribution of the system with respect to each of the involved subdomains is distinguishable.

The rational compatibility between the obtained results of Chapter 4 and the natural behavior of the system shows that the proposed model can unveil a high-degree of complexity (which are typically overlooked by other conventional models) in the system's internal dynamics under thermoelastic loading. In addition, the obtained separate energetic network of the proposed model offers a considerable potential for the development of more control-oriented strategies that can address the individual dynamics of each of the participating subdomains, instead of the total dynamics of the multi-physical system.

In Chapter 5, to include the impacts of energy dissipation on the general dynamics of the solid field, in the first part, an energy-based combined viscoelastic model, namely the CLS model, is

proposed based on the fusion of the conventional dispersive mechanisms. The comparison between the conventionally generated models and their BG representations indicates that the observable viscoelastic behavior of the system is in fact a direct result of two different dispersive mechanisms which act in two different subdomains of the system. Although both dispersive mechanisms result in energy dissipation, their impacts on the dynamics of the system are fundamentally different in different situations. Therefore, to describe the attenuation pattern of wave propagations in the system, both relaxation and retardation parameters are necessary for the whole range of frequencies. Furthermore, it is discovered that by employing the so-called relaxation time variable in the conventional viscoelastic models, the resistive and capacitive parameters of the system are combined in the system governing equations, which will limit the application of these models to a narrow range of fitted spectrum and single-domain dynamic investigations.

By relating the viscoelastic behavior of a mechanical domain to the dissipation of its subdomains, a four-parameter Combined Linear Solid (CLS) model is developed in the first part of Chapter 5. The comparison between the obtained results indicate that although the mathematical interpretations of both the proposed model and the conventional SLS model are the same, there exists a significant difference between the performances of these two models. This difference highlights that in the CLS model the dynamic level at which the viscoelastic behavior of the system is formed is lower than that in the conventional Standard Linear Solid (SLS) model. Thus, more detailed interactions between the various subdomains of the system can be revealed in the CLS model in contrast to its conventional counterparts. With the use of the energy-based modeling technique, generating a model, such as the CLS, at the level of subdomains is entirely feasible. This feature has allowed the proposed CLS model to sufficiently reveal the impacts of the subdomain interactions and specialized dissipation mechanisms on forming the comprehensive viscoelastic behavior of the system.

In the second part of Chapter 5, by including the physically generated dispersive mechanisms in the proposed coupled thermoelastic model generated in Chapter 4, a domain-independent thermoviscoelastic model is developed. This model reveals the irreversible thermo-mechanical behavior of the system on the basis of the energetic interactions of the existing physical subdomains. To derive this model, the reversible and irreversible dynamic interactions between

the elastic and thermal subdomains are generated together with the use of inter-domain modulations.

To clarify the impact of the internal energetic interactions on the general behavior of the system, different thermo-mechanical loading conditions are simulated in Chapter 5 for a chosen discrete structure. The obtained results in general demonstrate a good agreement with the natural behaviors of the system. Several thermo-mechanical phenomena including dilation, thermal stress, relaxation, vibrational heating, and material softening are successfully captured during the simulation. The effect of the deformation of the structure on the conductivity of the system is evidently tracked. On the basis of the attained physical insight of the system, it is clear that the changes in the viscosity of the system can be the main cause for the dynamic response changes of the system under temperature fluctuations.

The physically generated thermo-mechanical behavior illustrated in Chapter 5 clarifies that the general behavior of a system is in principal a combined result of different dynamics produced by different elements of the system, which can vary dynamically with regard to the location of the external sources applied to the system. Constructing the general dynamics of the system from its constructive elements with respect to the geometry of the system makes the proposed model suitable for controlled-structure dynamic examinations. The domain-independency of the model will also provide a desirable foundation upon which more complex multi-physical system dynamic investigations can be conducted. The physical nature of the proposed model allows it to become a suitable candidate for use in modeling different-scale dynamic systems.

In Chapter 6, a domain-independent energy-based nonlinear model, compatible with the proposed solid field's model, is developed for the fluid field. By means of the physical decomposition of the fluid field into thermal, mass, potential, and kinetic subdomains (identical to the solid field), the general complex dynamics of the system are developed on the basis of the conservative reversible and irreversible energetic interactions of the present physical subdomains. The dynamics of the system obtained in this way are directly connected to the physical memory of the system, and thus, provide the possibility of capturing the ongoing phenomena of the system including the energetic transactions between the mechanical and thermal subdomains.

The domain-independency of the model generated in Chapter 6 can be counted as a desirable feature for dynamic investigations of multi-disciplinary systems, as the complex power

transactions between the disciplines can be decomposed with respect to the present similar physical subdomains of different fields. Furthermore, the developed energetic network of the system provides a useful tool for control strategy development and energy management of the system.

The obtained relations among the existing subdomains discussed in the studies presented in Chapter 6 can also be used to define more appropriate relations for corresponding CFD modeling studies. The generated BG model of one segment can serve to generate the partial differential equations of the fluid field via a limited operation on the geometry of the segment, to provide a full freedom of choice for numerical-solution techniques.

In Chapter 7, finally, by combining the proposed solid and fluid models, an energy-based coupled aerothermoviscoelastic model is proposed in which the general behavior of the system can be obtained on the basis of the energetic interactions of the present physical subdomains. This modeling technique can provide a conservative power network of the system with separate energy lines dedicated to each of the physical subdomains of these two fields, as well as a clear identification of reversible and irreversible power interactions within and between the fields.

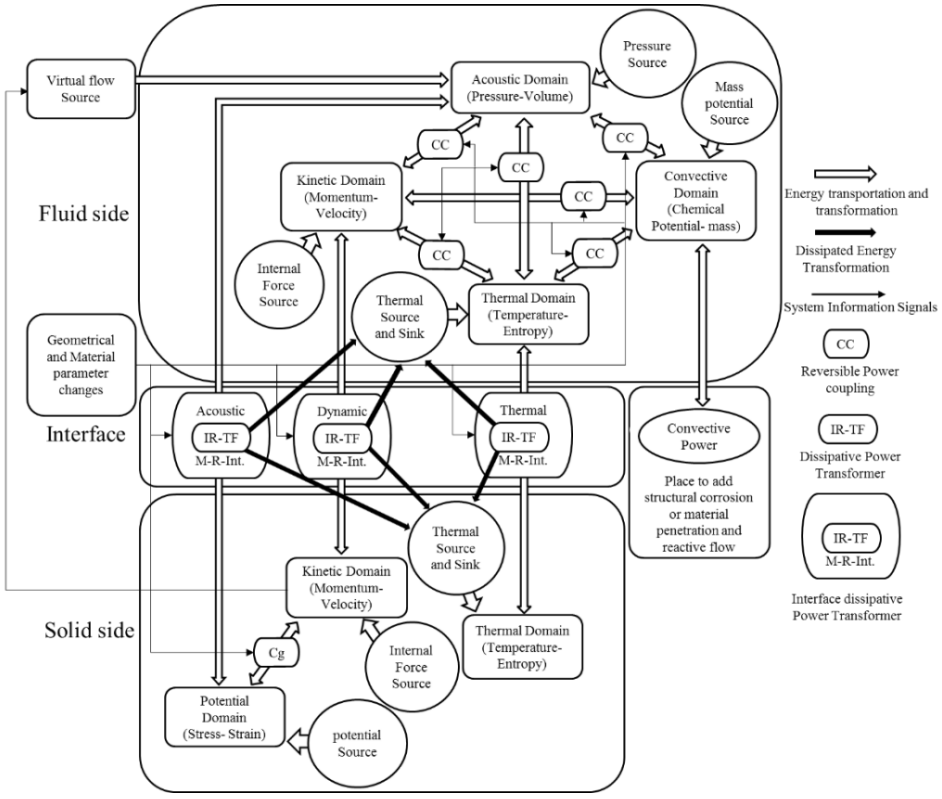

Fig. 8-1. Coupled fields energy structure

In the proposed coupled aerothermoviscoelastic model of Chapter 7, the individual models of the physical subdomains of the fluid and solid fields are all domain-independent. This feature of modeling allows the development of a unique interface structure shown in Fig. 8-1 with which the power transformations between the two fields can be performed in a handshake manner. This capability of the proposed coupled model offers a greater physical insight into the data transactions between the fields, thus a better explanation of the dynamic interactions of the two fields at the interface. It also provides a useful platform based on which control strategy development and energy management planning can be facilitated.

As the modeling techniques proposed in this thesis do not rely on imposed assumptions and mathematical constrains, the models generated using these methodologies will have a much wider valid range than those developed using more traditional means. The strategies proposed in this thesis possess the potentials to be extended to the modeling of more complex systems, and to the discovery of unknown phenomena previously inaccessible using existing classical physical knowledge.

APPENDIX: SUPPORTIVE CONFERENCE PUBLICATIONS ENSUING FROM THIS THESIS

A. Zanj*, F. He, P. C. Breedveld, " A Novel Energy-Based Aerthermoviscoelastic Modeling Frame for Multiple-field System Dynamic Investigations, A Bond Graph Approach," Submitted to the AIAA Science and Technology Forum and Exposition, Grapevine, Texas, January, 2017.

A. Zanj*, F. He, P. C. Breedveld, " Variable Interface Dynamic Adaptation (VIDA) Technique: A Novel Approach to Adjust Lagrangian Frame and Eulerian Frame at Flattering Interface," Submitted to the AIAA Science and Technology Forum and Exposition, Grapevine, Texas, January, 2017.

A. Zanj*, F. He, P. C. Breedveld, "Energy-Based Compressible Convective model Proper for Multiple field Dynamic Investigation: A Bond Graph Approach on FSI Problems," Submitted to the AIAA Science and Technology Forum and Exposition, Grapevine, Texas, January, 2017.

A. Zanj*, F. He, P. C. Breedveld, "Energy-Based Viscoelastic Model for Multi-Physical Systems: A Bond Graph Approach," To appear in the 2016 IEEE International Conference on Systems, man, and Cybernetics, Budapest Hungary, October, 2016.

A. Zanj*, F. He, P. C. Breedveld, "Dynamic analysis of Thermoviscoelasticity in Multi-Physical systems: A Bond Graph Approach," To appear in the 2016 IEEE International Conference on Systems, man, and Cybernetics, Budapest Hungary, October, 2016.

A. Zanj*, F. He, "Multi-Physical System Variable DOF Modeling: An Investigation on Hyro-Control Device Start Process," To appear in the 2016 IEEE International Conference on Systems, man, and Cybernetics, Budapest Hungary, October, 2016.

P. C. Breedveld, **A. Zanj***, "Bond Graph Representation of Convection by Fluid Flow Along an Elastic Surface," Published in the 12th International Conference on Bond Graph Modeling and Simulation, SCS international, Montreal, July 2016.

A. Zanj*, F. He, " Thermomechnical Enhanced Elastic Model: Bond Graph Approach," Published in the 23rd International Congress on Sound and Vibration, Athen, July, 2016.

A. Zanj[*], P. C. Breedveld, F. He, "Domain Independent Thermoelastic Coupling Suitable for Aerothermoelastic Modeling," Published in the 23rd International Congress on Sound and Vibration, Athens, July, 2016.

A. Zanj[*], F. He, "Conduction Model Compatible for Multi-Physical Domain Dynamic Investigations: Bond Graph Approach," Published in the 18th International Conference on Engineering Systems Modeling, Simulation and Analysis, Madrid, March, 2016.

BIBLIOGRAPHY

The following Bibliography is a sequential summary of the References sections of the chapters of the thesis.

L. E. Garrick, "Aeroelasticity-Frontiers and Beyond," *Journal of Aircraft,* vol. 13, no. 9, pp. 641-657, 1976.

H. Försching, "Prediction of the unsteady airloads on oscillating lifting systems and bodies for aeroelastic analyses," *Progress in Aerospace Sciences,* vol. 18, pp. 211-269, 1978.

F. L. Vosteen, "Effect of Temperature on Dynamic Modulus of Elasticity of Some Structural Alloys," NACA TN 4348, 1958.

L.E. Garrick, "A survey of Aerothermoelasticity," FIAS, NASA, Langley Research Centre, 1963.

R. L. Bisplinghoff, J. Dugundji, Influence of Aerodynamic Heating on Aeroelastic Phenomena, Pergamon Press, 1958, p. 288–312.

J. Hedgepeth, E. Widmayer, "Dynamic and Aeroelastic Problems of Lifting Re-Entry Bodies," *Aerospace Engineering,* p. 148–153, 1963.

W. R. Laidlaw, J. H. Wyker , "Potential Aerothermoelastic Problems Associated with Advanced Vehicle Design," *Aerospace Engineering,* p. 154–164, 1963.

R.L. Bisplinghoff, "Some Structural and Aeroelastic Considerations of High- Speed Flight," *Journal of the Aerospace Sciences,* vol. 23, no. 4, p. 289–329, 1956.

M. Rogers, "Aerothermoelasticity," *AeroSpace Engineering,* p. 34–43, 1958.

J. J. McNamara, "Aeroalastic and Aerothermoelastic Behavior of Two and Three Dimentional Lifting Surfaces in Hypersonic Flow," The Univercity of Michigan, 2005.

D. Raney, J. McMinn, A.Pototzky, C. Wooley, "Impact of Aeroelasticity on Propulsion and Longitudinal Flight Dynamics of an Air-Breathing Hypersonic Vehicle," in *34th*

AIAA/ASME/ASCE/AHS/ASC Structures, Structural Dynamics and Materials Conferences, La Jolla, April, 1993.

R. V. Doggett, R. H. Ricketts, T. E. Noll, J. B. Malone, "NASP Aeroservothermoelasticity Studies," NASA TM 104058, 1991.

M. D. Van Dyke, "A Study of Second-Order Supersonic Flow Theory," Tech. Rep. 1081, NACA, 1951.

H.G. Morgan, H.L. Runyan, V. Huckel, "Theoretical Considerations of Flutter at High Mach Numbers," *Journal of the Aeronautical Sciences,* vol. 25, no. 6, p. 371–381., 1958.

M. Lighthill, "Oscillating Airfoils at High Mach Numbers," *Journal of the Aeronautical Sciences,* vol. 20, no. 6, 1953.

C. Mei, C. Grey, "A Finite Element Method for Large-Amplitude, Two-Dimensional Panel Flutter at Hypersonic Speeds," in *30th AIAA/ASME/ASCE/AHS/ASC Structures, Structural Dynamics and Materials Conference* , April, 1989.

D.Y. Xue, C. Mei, "Finite Element Two-Dimensional Panel Flutter at High Supersonic Speeds and Elevated Temperature," in *31st AIAA/ASME/ASCE/AHS/ASC Structures, Structural Dynamics and Materials Conference*, 1990.

E.G. Gray, C. Mei "Large-Amplitude Finite Element Flutter Analysis of Composite Panels in Hypersonic Flow," in *33rd AIAA/ASME/ASCE/AHS/ASC Structures, Structural Dynamics and Materials Conference*, Dallas, TX, April 1992.

J.F. Abbas, R.A. Ibrahim, "Nonlinear Flutter of Orthotropic Composite Panel Under Aerodynamic Heating," *AIAA Journal,* vol. 31, no. 8, p. 1478– 1488., 1993.

C. Mei, K. Abdel-Motagly, R. Chen, "Review of Nonlinear Panel Flutter at Supersonic and Hypersonic Speeds," *Applied Mechanics Reviews,* 1988.

R. Ricketts, T. Noll, W. Whitlow, L. Huttsell, "An Overview of Aeroelasticity Studies for the National Aerospace Plane," in *34th AIAA/ASME/ASCE/AHS/ASC Structures, Structural Dynamics and Materials Conference*, La Jolla, CA, April, 1993.

I. Nydick, P. P. Friedmann, X. Zhong, "Hypersonic Panel Flutter Studies on Curved Panels," in *36th AIAA/ASME/ASCE/AHS/ASC Structures, Structural Dynamics and Materials Conference*, New Orleans, LA, April 1995.

J. Anderson, Hypersonic and High Temperature Gas Dynamics, New York: McGraw-Hill, 1989.

I. Nydick, "Studies in Hypersonic Aeroelasticity, Ph.D. thesis," University of California, Los Angeles, 2000.

J. Bertin, "Hypersonic Aerothermodynamics," *AIAA,* 1994.

M. Rasmussen, Hypersonic Flow,, New York: JohnWiley & Sons, 1994.

R.C. Scott, A.S. Pototzky, "A Method of Predicting Quasi-Steady Aerodynamics for Flutter Analysis of High Speed Vehicles Using Steady CFD Calculations," in *34th AIAA/ASME/ASCE/AHS/ASC Structures, Structural Dynamics and Materials Conference* , La Jolla, CA, April, 1993.

K.K. Gupta, L.S. Voelker, C. Bach, T. Doyle, E. Hahn, "CFD-Based Aeroelastic Analysis of the X-43 Hypersonic Flight Vehicle," in *39th Aerospace Sciences Meeting & Exhibit*, 2001, AIAA Paper No. 2001-0712..

S.L. Krist, R.T. Biedron, C.L. Rumsey, "CFL3D User's Manual (Version 5.0)," NASA TM 1998-208444, 1997.

E. Thornton, P. Dechaumphai, "Coupled Flow, Thermal, and Structural Analysis of Aerodynamically Heated Panels," *Journal of Aircraft,* vol. 25, no. 11, p. 1052 – 1058, 1988.

P. Dechaumphai, A. Wieting, A. Pandey, "Fluid-Thermal-Structural Interaction of Aerodynamically Heated Leading Edges," in *30th AIAA/ASME/ASCE/AHS/ASC Structures, Structural Dynamics and Materials Conference*, April 1989.

H. Tran, C. Farhat, "An Integrated Platform for the Simulation of Fluid-Structure-Thermal Interaction Problems," in *43rd AIAA/ASME/ASCE/AHS Structures, Structural Dynamics and Materials Conference*, Denver, CO, April 2002.

C. Farhat, M. Lesoinne, N. Maman, "Mixed Explicit/Implicit Time Integration of Coupled Aeroelastic Problems: Three-field Formulation, Geometric Conservation and Distributed Solution," *International Journal for Numerical Methods in Fluids,* vol. 21, pp. 807-835, 1995.

A. J. Culler, J. J. McNamara, "Fluid-Thermal-Structural Modeling and Analysis of Hypersonic Structures under Combined Loading," in *52nd AIAA/ASME/ASCE/AHS/ASC Structures, Structural Dynamics and Materials Conference*, Denver, Colorado, April 2011.

N. J. Falkiewicz, S. G. V. Frendreis, C. E. S. Cesnik, "Effect of Control Surface-Fuselage Inertial Coupling on Hypersonic Vehicle Flight Dynamics," in *AIAA Atmospheric Flight Mechanics Conference*, Portland, Oregon, August 2011.

L. Daun, M. M. Choudhari, M. Wu, "Numerical Study of Pressure Fluctuations due to High-Speed Turbulent Boundary Layers," in *42nd AIAA Fluid Dynamics Conference and Exhibit*, New Orleans, Louisiana, June, 2012.

W. K. Nowacki, "Progress in Thermoelasticity," *Warszawa: European Mechanics Colloquium,* 1967.

W. R. Graham, "A comparison of models for the wavenumber–frequency spectrumof turbulent boundary layer pressures," *Journal of Sound and Vibration ,* vol. 206, p. 541–565, 1997.

P. C. Breedveld, "Thermodynamic Bond Graphs and the Problem of Thermal Inertance," *Journal of the Franklin Institute,* vol. 314, no. 1, pp. 15-40, 1982.

J. Balino, "BG-CFD methodology for multicomponent solutions. Part I: Multivelocity model," in *International Conference on Bond Graph Modeling and Simulation*, 2003.

P. Breedveld, Physical System Theory In Therms of Bond graphs, Enschede, Netherland: Univercity of Twente, 1984.

S. Awodey, Category Theory, New York: Oxford University Press, 2006.

J. Thoma, Simulation by Bond graph, Verlag, Gemany: Springer, 1990.

A. Mukherjee, R. Karmakar, Modeling and Simulation of Engineering Systems through Bon dgraph, New Delhi, India: Narosa Publishing House, 2000.

H. Afshari, A. Zanj, "Dynamic Analysis of a Nonlinear Pressure Regulator Using Bondgraph Simulation Technique," *Journal of Simulation Modeling Practice and Theory,* 2010.

A. Zanj, F. He, "A Thermomechnical Enhanced Elastic Model: Bond Graph," in *23rd International Congress on Sound & Vibration*, Athens, Greece, July, 2016.

P. C. Breedveld, A. Zanj, "Bond Graph Representation of Convection by Fluid Flow Along an Elastic Surface," in *12th international Conference on Bond Graph Modeling and Simulation*, Montreal,Quebec, Canada, July, 2016.

H. Karimi, A. Nassirharand, A. Zanj, "Integration of modeling and simulation of warm pressurization and feed systems of liquid propulsion systems," *Acta Astronautica,* vol. 69, pp. 258-265, 2011.

H. Karimi, A. Zanj, A. Najafi, "Optimization of GG Pressurization System Performance of LPE Pressure Vessels," in *16th. annual International conference on Mechanical Engineering-ISME*, Kerman, 2004.

J. T. Odon, D. A. Kross, "Anallysis of general coupled thermoelasticity problems by the finite element method," Research Institute, Univ. of Alabama, Huntsville.

J. Watton, " The design of a single-stage relief valve with directional damping," *Journal of Fluid Control Including Fluidics Quarterly,* vol. 18, no. 2, p. 22–35, 1988.

C. Chin, "Static and dynamic characteristics of a two stage pilot relief valve," *ASME Dynamic Systems Measurements and Controls,* vol. 113 , p. 280–28, 1991.

D.C. Karnopp, R.C. Rosenburg, System Dynamics: A Unified Approach, Wiley Inter sciences, 1975.

W. Borutzky, Bond Graph Methodology: Development and Analysis of Multidisciplinary Dynamic System Models, Springer, 2010.

J. Amerongen, E. Coelingh , T. Vries , "Computer support for mechatronic control system design," *Robotics and Autonomous System,* vol. 30, 2000.

J. J. Granda, The role of bond graph modeling and simulation in mechatronics systems, An integrated software tool: CAMP-G, MATLAB-SIMULINK, Mechatronics, 2002.

P. C. Breedveld, "Thermodynamic Bondgraphs: a new synthesis," *Int. J. Modeling and simulation,* vol. 1, pp. 57-61, 1981.

A. Zanj, H. Karimi, A. J. Gholi, M. Shafiee, "Dynamic modeling of indirect hydro-control valve–Bondgraph approach," *Simulation Modeling Practice and Theory,* vol. 28, pp. 65-80, 2012.

A. Zanj, H. H. Afshari, "Dynamic analysis of a complex pneumatic valve using pseudobond graph modeling technique," *Journal of Dynamic Systems, Measurement, and Control ,* vol. 135, no. 3, 2013.

A. Mukherjee, A. K. Samantaray, Bond Graph In Modeling, Simulation And Fault Identification, I. K. International Pvt Ltd, 2006.

D. D. Reynolds, Engineering Principles in Acoustics, Boston: Allyn and Bacon Inc., 1981.

J. E. Lennard-Jones, "On the Determination of Molecular Fields," in *Proc. R. Soc. Lond.*, 1924.

M. I. Ojovan, "Configurons: thermodynamic parameters and symmetry changes at glass transition," *Entropy ,* vol. 10, no. 3, p. 334–364, 2008.

S. Volz, Microscale and Nanoscale Heat Transfer, Springer, 2010.

V. P. Carey, G. Chen, C. Grigoropoulos, M. Kaviany, A. Majumdar, "A Review of Heat Transfer Physics," *Nanoscale and Microscale Thermophysical Engineering,* vol. 12, no. 1, p. 1–60, 2008.

F. Cellier, Continuous System Modeling, New York, Verlag: Springer, 1991.

A. Zanj, F. He, "Conduction Model Compatible for Multi-Physical Domain Dynamic Investigations: Bond Graph," in *18th International Conference on Engineering Systems Modeling, Simulation and Analysis*, Madrid, Spain, 2016.

R. P. Starkey, D. D. Liu, P.C. Chen, A. Sengupta, K.T. Chang, "Integrated Aero-Servo-Thermo-Propulso-Elasticity (ASTPE) Methodology for Hypersonic Scramjet Vehicle Design/Analysis,"

in *48th AIAA Aerospace Sciences Meeting Including the New Horizons Forum and Aerospace Exposition*, Orlando, Florida, January, 2010.

J. U. Thoma, Simulation by Bondgraph, springer, 1990.

E. L. Wilson, Three-Dimensional Static and Dynamic Analysis of Structures, California: Conputers and Structures: Inc, Berkeley, 2002.

H. F. Brinson, L. C. Brinson, Stress and Strain Analysis and Measurement," in Polymer Engineering Science and Viscoelasticity an Introduction, Springer, 2008, pp. 16-53.

J. Peraire, P. O. Persson, "High-Order Discontinuous Galerkin Methods for CFD,In Adaptive High-Order Methods in Computational Fluid Dynamics," *World Scientific series in Advances in Computational Fluid Dynamics,* vol. 2, pp. 119-152, 2010.

J. M. O. Duhamel, "Second memoire sur lesphenomenes thermome'eaniques," *J. de l'Ecole Polytechn.,* vol. 15, pp. 1-15, 1837.

W. Voigt, Lehrbuck der Kristallphysik, Teubner, 1910.

H. Jeffreys, "The thermodynamics of an elastic solid," in *Proc. Camb. Phil. Soc., 26*, 1930.

M. A. Biot, "Thermoelasticity and irreversible thermodynamics," *J. Appl. Phys.,* vol. 27, 1956.

S. R. D. Groot, Thermodynamics of irreversible processes, Amsterdam,, 1952.

P. C. Breedveld, Physical System Theory In Therms of Bond graphs, Enschede: Univercity of Twente, 1984.

A. Mukherjee, R. Karmakar , Modeling and Simulation of Engineering Systems through Bon dgraph, New Delhi, India: Narosa Publishing House, 2000.

B. A. Boley, J. H. Weiner, Theory of thermal stresses, New York: John Wiley, 1960.

R. Courant, D. Hilbert, Methods of Mathematical Physics, Verlag: Willey-VCH, 2004.

H.P. Liu, D. L. Anderson, H. Kanamori, "Velocity dispersion due to anelasticity," *Geophys. J. Roy. Astr. Soc.,* pp. 41-58, 1967.

J. Ferry, Viscoelastic Properties of Polymers, N.Y.: J. Wiley, 1970.

R. Lakes, Viscoelastic Solid, N.Y.: CRC Press, 1999.

C. Friedrich, "Relaxation and retardation function of the Maxwell model with fractional derivatives," *Rheol. Acta,* vol. 30, 1991.

H. Schiessel, R. Metzler, A. Blumen, T.F. Nonnenmacher, "Generalized viscoelastic models: Their fractional equations with solutions," *J. Phys. A: Math. Gen.,* vol. 25, 1995.

T. Pritz, "Five-parameter fractional derivative model for polymetric damping materials," *J. Sound Vibration ,* vol. 265, pp. 935-952, 2003.

R. Metzler, T.F. Nonnenmacher, "Fractional relaxation processes and fractional rheological models for description of a class of viscoelastic materials," *Int. J. Plast.,* vol. 19, 2003.

J.G. Liu, M.Y. Xu, "Higher-order fractional constitutive equations of viscoelastic materials involving three different parameters and their relaxation and creep functions," *Mech. Time-Depend. Mater,* vol. 10, 2006.

P.C. Powell, A.J. Ingen Housz, Engineering with Polymers, Cheltingham: Stanley Thornes Publishers, 1998.

D. Hudgin, Polymer Viscoelasticity: Stress and Strain in Practice, N.Y.: Marcel Dekker, 2000.

L. Kari, "On the wave guide modeling of dynamic stiffness of cylindrical vibration isolations," *Journal of Sound and Vibration,* vol. 244, no. 2, pp. 211-257, 2001.

S.J. Zhu, X.T. Weng, G. Chen, "Modeling of the stiffness of elastic body," *Journal of Sound and Vibration,* vol. 262, p. 1–9, 2003.

R. M. Christensen, Theory of viscoelasticity - An introduction, Academic Press, Inc, 1982.

F. Riesz, "Sur les opérations fonctionnelles linéaires," *C. R. Acad. Sci. Paris,* vol. 149, p. 974–977, 1909.

D. Roylance, "Engineering Viscoelasticity," Massachusetts Institute of Technology, Cambridge, MA 02139, October, 2001.

A. Zanj, P. C. Breedveld, F. He, "Domain-Independent Thermoelastic Coupling Suitable for Aero-thermoelastic Modeling," in *23rd International Congress on Sound & Vibration*, Athens, Greece, July, 2016.

H. Hübel, "Basic conditions for material and structural ratcheting," *Nuclear Engineering and Design,* vol. 162, no. 1, pp. 55-65, March 1996.

J. McNamara, P. Friedmann, "Aeroelastic and Aerothermoelastic Analysis of Hypersonic Vehicles:Current Status and Future Trends," in *48th AIAA/ASME/ASCE/AHS/ASC Structures, Structural Dynamics, and Materials Conference*, Honolulu, Hawaii, 2013.

E. A. Ivanova, "Derivation of theory of thermoviscoelasticity by means of two-component medium," *Acta Mechanica,* vol. 215, no. 1, pp. 261-286, 2010.

A. D. Freed, A. I. Leonov, "A thermodynamic theory of solid viscoelasticity," NASA Technical Documents, 2002.

E. A. Ivanova, "On one Model of Generalized Continuum and its," in *Mechanics of Generalized Continua*, Berlin Heidelberg, Springer-Verlag, 2011, pp. 151-174.

C. Truesdell, "A first course in rational continuum mechanics," *Pure and Applied mathematics,* vol. 1, pp. 359-364, 1977.

R. M. Christensen, Theory of voscoelasticity, Dover Publications, 2003.

A. M. Freudental, H. Geiringer , The mathematical theories of the inelastic continuum, Berlin, Göttingen, Heidelberg: Springer-Verlag, 1958.

G. E. Mase, Theory and problems of continuum mechanics, McGray-Hill Book Company, 1970.

A. Zanj, P. C. Breedveld, F. He, "Domain Independent Viscoelastic Model: A Bond Graph Approach," *Sound and vibration,* 2016. (Under Revision).

A. Zanj, F. He, "Multi-Physical Domain Variable DOF Modeling: Bond Graph Approach," *Mechatronics, IEEE/ASME Transactions on,* p. (Under review), 2016.

D.C. Karnopp, D.L. Margolis, R.C. Rosenburg, System Dynamics–Modeling and Simulation of Mechatronic Systems, John Wiley & Sons, 2000.

G. A. Francfort, P. M. Suquet, "Homogenization and mechanical dissipation in thermoviscoelasticity," *Archive for Rational Mechanics and Analysis,* vol. 96, no. 3, pp. 265-293, 1986.

J. L. Balino, A.E. Larreteguy, E. F. Gandolfo Raso, "A general bond graph approach for computation fluid dynamics," *Simulation Modeling Practic and Theory,* vol. 14, pp. 884-908, 2006.

D. C. Karnopp, "Bond graph modeling philosophy for thermofluid systems," *ASME Trans., Journal of Daynamic System Measurment and Cntrol,* vol. 100, no. 1, pp. 70-75, 1978.

D. C. Karnopp, "States variables and pseudo Bond geaph for compressible thermofluid systems," *ASME Trans., Journal of Dynamic System Measurment and Control,* vol. 101, no. 3, pp. 201-204, 1979.

D. L. Magolis, "Modeling of two-stroke internal combustion engine dynamics using Bond graph technique," *ASME Trans.,,* pp. 2263-2275, 1976.

P. C. Breedveld, N. Hogan, "Energetically Proper Modeling of A Simple Trottling Process," in *IMACS l. MathMod, Technical University*, Vienna, Austria, Vol. 1, pp- 37- 40, 1994.

A. Zanj, P. C. Breedveld, F. He, "Variable Interface Dynamic Adaptation (VIDA) technique: A Novel Approach to adjust Lagrangian Frame and Eulerian Frame at Flattering Interface," in *AIAA Modeling and Simulation Technologies Conference*, Grapevine, Texas, January, 2017.

G. Hetsroni, Handbook of Multiphase Systems, Hemisphere Publishing Corporation, 1982, ISBN 0-07-028460-1.

J. Greifeneder, F. E. Cellier, "Modeling Convective Flows Using Bond Graphs," *Simulation Series,* 2001.

P. C. Breedveld, Physical System Theory in Terms of Bond Graph, Enschede: University of Twente, 1984.

J. Bertin, Hypersonic Aerothermodynamics, AIAA, 1994.

J. D. Anderson, Hypersonic and High Temperature Gas Dynamics, New York: McGraw-Hill, 1989.

A. Frendi, "Coupling Between a Supersonic Turbulent Boundary Layer and a Flexible Structure," *AIAA Journal,* vol. 35, no. 1, pp. 28-66, 1997.

J. J. McNamara, P. P. Friedmann, K. G. Powell, B. J. Thuruthimattam, "Aeroelastic and Aerothermoelastic Behavior in Hypersonic Flow," *AIAA Journal,* vol. 46, no. 10, pp. 2591-2610, 2008.

N. J. Falkiewicz, C. E. S. Cesnik, M. A. Bolender, D.B. Doman, "Thermoelastic Formulation of a Hypersonic Vehicle Control Surface for Control-Oriented Simulation," in *AIAA Guidance, Navigation, and Control Conference*, Chicago, Illinois, August, 2009.

D. Juvé, M. Berton, E. Salze, "Spectral Properties of Wall-Pressure Fluctuations and Their Estimation from Computational Fluid Dynamics," *Flinivia- Flow Induced Noise and Vibration Issues and Aspects, Switzerland,* pp. 27-46, 2015.

A. Zanj, F. He, P. C. Breedveld, "Dynamic Analysis of Thermo-viscoelasticity in Multi-Physical Systems: A Bond Graph Approach," in *IEEE International Conferernce on Systems, Man, and Cybernetics*, Budapest, October, 2016.

A. Zanj, P. C. Breedveld, F. He, "Energy-Based Compressible Convective model Proper for Multiple field Dynamic Investigation: A Bond Graph Approach on FSI Problems," in *58th AIAA/ASCE/AHS/ASC Structures, Structural Dynamics, and Materials Conference*, Grapevine, Texas, January, 2017.

P. C. Breedveld, J. J. Granada, F. E. Cellier , "Insight in Rigid Body Motion Stability Via an Alternative for the Eulerian Junction Structure," in *4th Bond graph modeling and simulation* , San Francisco, 1999.